UNIVERSITÀ DEGLI STUDI DI NAPOLI "FEDERICO II"

SCUOLA POLITECNICA E DELLE SCIENZE DI BASE

DOCTORATE IN EARTH, ENVIRONMENT AND RESOURCES SCIENCE

XXXII CYCLE

HIGH RESOLUTION INTEGRATED RECONSTRUCTION OF HOLOCENE CLIMATIC AND PALEOENVIRONMENTAL CHANGES IN THE SOUTHERN TYRRHENIAN SEA: A CODA APPROACH.

TUTORS   **PHD STUDENT**

Prof. Valentino Di Donato   Joanna Jamka

Prof. Marco Sacchi (CNR-ISMAR)

Prof. Josep A.Martin-Fernández (University of Girona, Spain)

PhD coordinator: Prof. Maurizio Fedi

Academic year: 2018/2019

Palaeoenvironmental reconstructions through compositional data analysis (Article)

Compositional regression-based methods for palaeoenvironmental reconstruction (Article)

References

1. Introduction

The field of this research is the reconstruction of paleoenvironmental changes used complex methods obtained by Compositional Data Analysis statistical methods (CoDA), so in the result to develop new transfer functions (mathematical methods to obtain data to reconstruct paleoenvironmental changes) due to which we can observe the paleoclimatic and paleoenvironmental changes and volcanic activities during The Late Glacial and Holocene in the Gulf of Naples and Gulf of Salerno (**fig.3**) in collaboration with IAMC (CNR) and University of Girona (statistical methods).

To obtain this we use quantitative analysis of planktonic and benthic Foraminifera, radiocarbon dating, stable isotope 13C and 18O, TOC (total organic carbon analysis), granulometric analysis and tephrostratigraphy, all analyzed by the innovative statistical CoDA method. As the results we obtained the calibrated radiocarbon age, correlation of the main tephra, planktonic and benthic Foraminifera compositional zones on the base of clustering algorithms, SST (sea surface temperatures) and relative abundance of each species of Foraminifera within the core. For the reference core form G. of Salerno GNS98 C106 (34Ky) has been published the results in Alpine and Mediterranean Quaternary with obtained SST, the errors for the closest modern analogues, and Aitchison distances obtained from isometric log-ratio coordinates of relative abundances. The number of analogues from which obtain the estimates was determined through leave-one-out verification of modern assemblages, mean distances and local outlier factor are considered to evaluate the quality of palaeoestimates. The method has been tested on Atlantic Ocean and Mediterranean planktonic foraminiferal assemblages to reconstruct SST, which is more precise than obtaining SST through raw data MAT. CoDa-MAT yields lower estimates of the W Mediterranean last glacial period SST than previously studied ones. The future development of the method is to obtain more precise data than through traditional methods.

Quantitative estimation of past environmental parameters is one of the most challenging engagements of palaeoclimatical and palaeoecological investigations. In palaeoceanographical studies quantitative palaeoclimatic reconstructions can be attained by means of geochemical methods, such as the analysis of long chain alkenones (Brassel et al., 1986) and the Mg/Ca ratio in foraminifera (Elderfield and Ganssen, 2000), or more strictly paleontological methods based of statistical analysis of census counts of assemblages. These methods, known as transfer function

methods, have been introduced to provide quantitative estimates from counts of fossils, including regression-based methods (Imbrie and Kipp, 1971), modern analogue techniques (MAT) (Hutson, 1979; Pflaumann et al., 1996; Waelbroeck et al., 1998) and artificial neural networks (Malmgren et al., 2001). The starting point of these methods is a modern dataset usually consisting of counts of modern assemblages and measured environmental parameters.

Gulf of Naples and Gulf of Salerno have been studied before, but still they are not well known, there are a lot of researches which should be done in this complicated area. Until now for the Holocene in the Gulf of Naples were studied global paleoclimatic changes and palaeoceanoceanographic evolution of Mediterranean Sea from foraminiferal assemblages from the marine cores (Cita et al., 1977; Blanc-Vernet et al., 1984; Violanti et al., 1987; Vergnaud-Grazzini et al., 1988; Flores et al., 1997; Kallel et al., 1997; Capotondi et al., 1999, Ariztegui et al., 2000; Cacho et al., 2001, Pérez-Folgado et al., 2003, 2004; Sprovieri et al. 2003; Amore et al., 2004). In this regard, high-resolution analysis of continuous and well-preserved sedimentary late-Quaternary records, collected from key areas of the Mediterranean Basin (e.g. Asioli et al., 2001; Rohling et al., 1998, 2002; Cacho et al., 2000, 2001, 2002; Pérez -Folgado et al., 2003, 2004; Sprovieri et al. 2003, 2006; Sbaffi et al., 2004, Geraga et al., 2005) suggested that the principal climatic events and oscillations of the Northern Hemisphere, documented by multi-proxy records of the Greenland GRIP and GISP ice cores, were faithfully recorded in its sedimentary marine archives.

In comparison with the Gulf of Naples, the Gulf of Salerno is by far better known, as characteristics and architecture of sediments along the continental shelf were reconstructed by means of seismic profiles, geomineralogical and sedimentological analyses (Buccheri et al., 2002; Naimo et al., 2005). Paleontological studies (planktonic forams, palynomorphs, nannofossils, ostarcods and pteropods) and researches focused on sea-level and climatic changes during the late Pleistocene-Holocene were carried out by – Buccheri at al., 2002; Ciampo, 2003; Buccianti and Esposito, 2004. Quantitative paleoclimatic reconstructions (on pollen and planktonic foraminifera) based on statistical CoDA methods were proposed by Di Donato et al. (2008) and Di Donato and Martin-Fernandez (2008). CoDA methods were also applied in this area on the base of planktonic and benthic foraminifera (Di Donato et al., 2009) and geochemistry (Vallefuoco, 2008).

Objective of the thesis

One of the main objectives of the thesis is to elaborate statistical methods under the framework of CoDa (Compositional data analysis: CoDa; Aitchison, 1986) to obtain the SST (sea surface temperatures) from counting of fossil assemblages. Two approaches were considered:

1) The modern analogue technique (CoDaMAT)– the revised method adopts the Aitchison distance, obtained from isometric log-ratio coordinates of relative abundances, as a natural measure of similarity among assemblages. The number of analogues from which obtain the estimates was determined through leave-one-out verification of modern assemblages. Mean distances and local outlier factor are considered to evaluate the quality of palaeoestimates. The method has been tested on Atlantic Ocean and Mediterranean planktonic foraminiferal assemblages to reconstruct past sea surface temperatures (SST). The MAT compares fossil assemblages with modern ones using a distance measure or a similarity coefficient. The palaeoenvironmental estimates are obtained from the environmental parameters measured at the location of the most similar modern assemblages. For each fossil samples the nearest modern ones are found by adopting an appropriate distance (d).

2) Regression-based methods - standard and robust Partial Least Squares Regression (PLSR) and Principal Component Regression (PCR), applied to the log-ratio coordinates of percentage data of Atlantic Ocean and Mediterranean Sea planktonic foraminifera assemblages. Due to the presence of groups, it was preferred to model separately high latitude and mid to low latitude assemblages. The application of the obtained transfer function involves cluster, MANOVA and discriminant analysis applied to the log-ratio transformed fossil assemblage's composition.

<u>Why this area of the research?</u>

The Mediterranean basin (**Fig.1**), is considered as one of the most complex marine environment on the Earth (Williams, 1998) for its hydrogeography and geographic extension. The Mediterranean is an example of an excellent 'natural laboratory', where processes can be studied in conveniently reduced spatial scales and short time, and with better signal to interferences than we can expect in the open ocean (Rohling, 2001).

Researchers are usually focused on the study of Late-Quaternary record to recognize the geological record, paleo-analogues to the modern climatic conditions and for understanding the evolution of the climate in the future. Anyhow, there are still some uncertainties concerning the resolution of the chronostratigraphic outline. The most important, and not so easy issue is to choose

and find a proper marine core, records and high-resolution proxies needed for the high-resolution paleoclimatic studies in a tens and hundreds of years scale. For this reason, the Mediterranean Sea is a specific and exceptional area to observe global and regional climate changes at high resolution time scale and to analyze continuous sedimentation series without high sedimentation rates and not disturbed ones.

Moreover, due to the complex geological structure of the region and the multitude of volcanoes in the area, for the short-time interval control and for a high-resolution integrated stratigraphy are very important independent tie-points such as tephra layers. During the late-Quaternary, several volcanoes such as Vesuvius, Campi Flegrei and volcanoes of Ischia and Procida Islands have been active in the Mediterranean area (Fig.1 and 3). For our paleo-studies the eruptive events can be considered as immediate geologic events, and then vitreous volcanic extrude, tephra, can be used as time-synchronous marker horizons at regional scale.
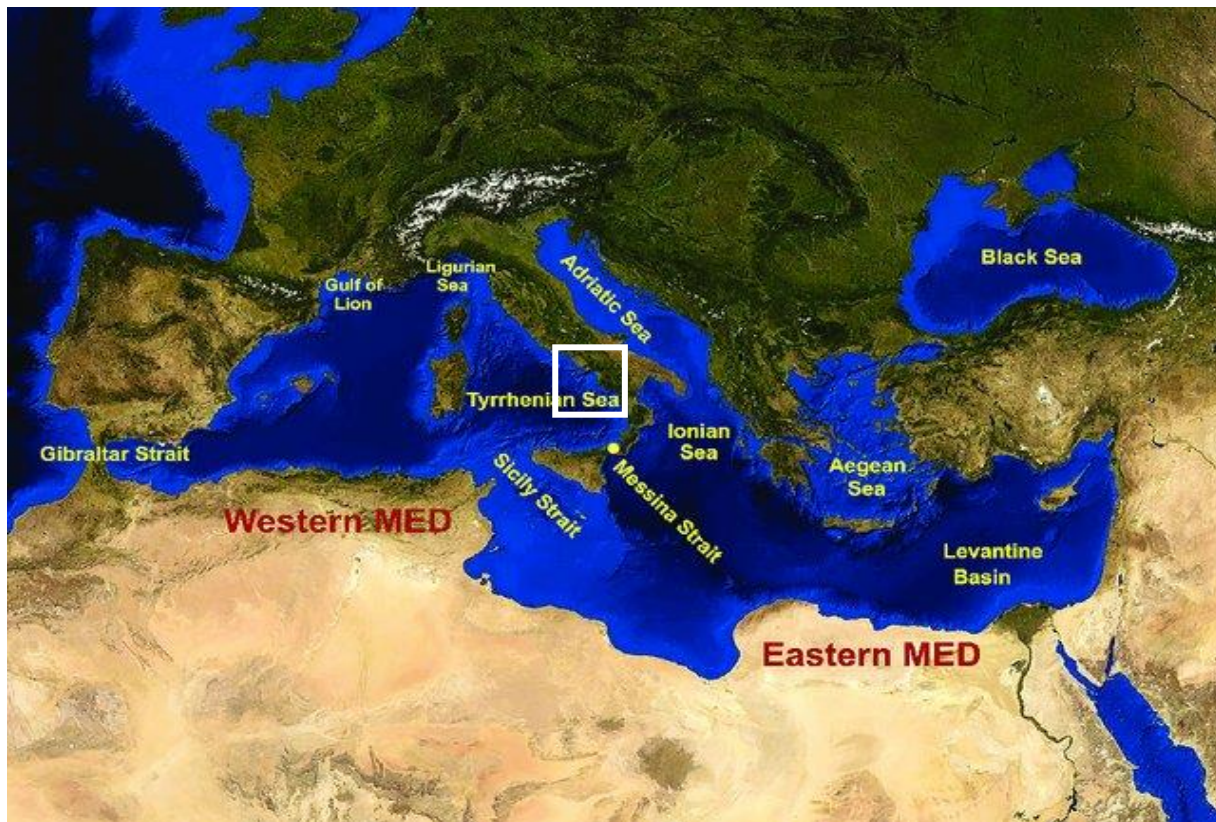

Figure 1 Mediterranean Sea map (Spanò and De Domenico, 2017) with the location of the studied area from Tyrrhenian Sea, South Italy, Western Mediterranean Sea (white square, see fig.3 for the details).

1.1. Holocene climatic changes in the Mediterranean Sea

The reconstruction of the climate for the Holocene is still controversial due to the different times and different event amplitudes in different areas of the Mediterranean basin. However, a clearer indication of the evolution of this period has recently emerged as the number of high-resolution marine and land records became available.

The beginning of the Holocene was characterized by a warm interval (Optimum climatic). The times of this maximum temperature range varied according to the different sub-regions, being 11.5 - 10.2 ka BP in the Gulf of Cadiz, 10 - 9 km BP in the Alboran sea (Cacho et al., 2001), 8, 9 - 8.4 ka BP in the Tyrrhenian Sea (Sbaffi et al., 2001) and 9.2 - 8.5 ka BP in the Aegean Sea (Rohling et al., 2002). This interval was characterized by warmer summers and colder winters today (Watts et al., 1996) due to the greater summer insolation in the northern hemisphere (Kutzbach and Webb, 1993). There is the evidence that precipitation (of a non-monsoon nature) has increased in the Mediterranean regions, along with monsoon rainfall and sapropel deposition (Toucanne et al., 2015, Quaternary Science Reviews; Wagner et al., 2019, Nature). At the same time, the eastern Mediterranean basin was affected by a strong stagnation of deep water responsible for the formation of the anoxic layer known as Sapropel 1 (Rossignol-Strick, 1985; Kallel et al., 1997; Rossignol-Strick, 1999; Ariztegui et al., 2000).

The middle Holocene (from about 7 to 5 ka BP) was globally characterized by strong climate changes (Steig, 1999). In the Mediterranean area, this time interval marked the beginning of a process of aridification connected with an orbital change that caused a weakening of the monsoon activity after 7 ka BP (Rossignol-Strick, 1985; Gasse and Van Campo, 1994; deMenocal et al., 2000).

The late Holocene (about 5 - 0 ka BP) shows a weak general tendency of simultaneous cooling to progressive aridification (Cacho et al., 2001; Sbaffi et al., 2001; Rohling et al., 2002).

Data from peri-Mediterranean continental speleothems indicate that the last part of the Holocene was characterized by a complex substructure with a decrease in temperature starting from 7.5 ka BP (McDermott et al., 1999). These long-term trends have been superimposed on a number of short events that led to significant decreases in sea and air surface temperatures.

The western Mediterranean Sea has undergone a brief cooling (lasting between 250 and 1500 years, Cacho et al., 2001) of greater intensity towards the east, ranging from 1.5 ° C in the Alboran Sea to 3 ° C in the Tyrrhenian Sea. The frequency of these events was calculated by Cacho et al. (2001) and is approximately 730 years old. The Aegean Sea record shows short-lived events caused by flows of winter air from the north. These events showed an intensity comparable to that of the western Mediterranean (2 - 4 ° C), but with a periodicity of about 2300 years (Rohling et al., 2002). During the last part of the Holocene, two intervals of increasing humidity were recorded in deep water cores from the eastern Mediterranean Sea to Israel (between 3.5 - 3 and 1.7 - 1 ka BP), suggesting a change of fresh water balance several times during this period (Schilman et al., 2001).

1.2. Southern Tyrrhenian Sea

The Southern Tyrrhenian Sea area, which contains the Gulf of Naples, the Gulf of Gaeta and the Gulf of Salerno, probably can be considered as one of the most complicated coastal environments of the Mediterranean Sea. The Gulf of Naples (figs. 2 and 3) is located between the Ischia and Procida Island and Phlegrean Fields in the northwest and Capri Island and Sorrento Peninsula in the south (Sgarrella, 1993). The Gulf of Naples is surrounded by the two main volcanic complexes of Mount Somma-Vesuvius and Phlegrean Fields. It is an approximately rectangular marginal basin, NW oriented with an area of about 900 km^2 which is a part of the Campanian Volcanic Province (CVP) (Passaro et al., 2016). The Gulf of Naples belongs to the volcano-tectonic Phlegrean Fields system. The geology in this region is very dynamic and is related to quite recent and intensive volcanic activity to which are associated with bradyseismic movements and also gas emissions on land and underwater (Bergamin et al., 2005).

The area has around 150km^3 with quite deep mean depth about 170m. Connection with the Tyrrhenian Sea in the major place is SW oriented and up to 9,5km^2 (Sgarrella and Moncharmont-Zei 1993). Gulf of Naples is connected with the Tyrrhenian Sea by the two openings: the Bocca Piccola, a small opening between Punta Campanella (Sorrento Peninsula) and Capri Island, and the Bocca Grande between two islands – Capri and Ischia. There are also two more openings connecting Gulf of Naples with the Gulf of Gaeta in the north – the Procida Channel with shallow threshold of 12m between Procida Island and the coast and the Ischia Channel with the threshold of 24m separating two islands Ischia and Procida (de Ruggiero, 2013; Sgarrella and Moncharmont-Zei 1993).

The Tyrrhenian Sea is the result of extension, from Miocene up to Quaternary, contemporary with the eastward accretion and anticlockwise rotation of the Apenninic fold and thrust belt in the time of the roll-back of the subducting Adria plate (Milia and Torrente, 1999; Bruno et al., 2003; Sacchi et al., 2005; Insinga et al., 2008; Wang et al., 2015). The Gulf of Naples and The Campanian Plain with the Gulf of Salerno and the Sele Plain are parts of half-graben basins, which are developed along the eastern Tyrrhenian margin (Sacchi et al., 2015). The Campanian Plain extends from NW to SE starting from Roccamonfina and Aurunci Mountains to the Sorrento Peninsula. Caserta Mountains are the evident subsidence that has been started during the Late Quaternary (Branaccio et al., 1991; Insinga et al., 2008) and got filled up with 3km of Pliocene-Pleistocene deposits discovered by seismic profiles (multichannel reflection) and bore data (Ippolito et al., 1973; Finetti and Morelli, 1974; Mariani and Prato, 1988; Brocchini et al., 2001). The sedimentary succession consists of siliciclastic deposits interbedded with volcanoclastic rocks and lavas mostly from Campi Flegrei, Procida island, Ischia island and Mount Somma-Vesuvius (Insinga et al., 2008).
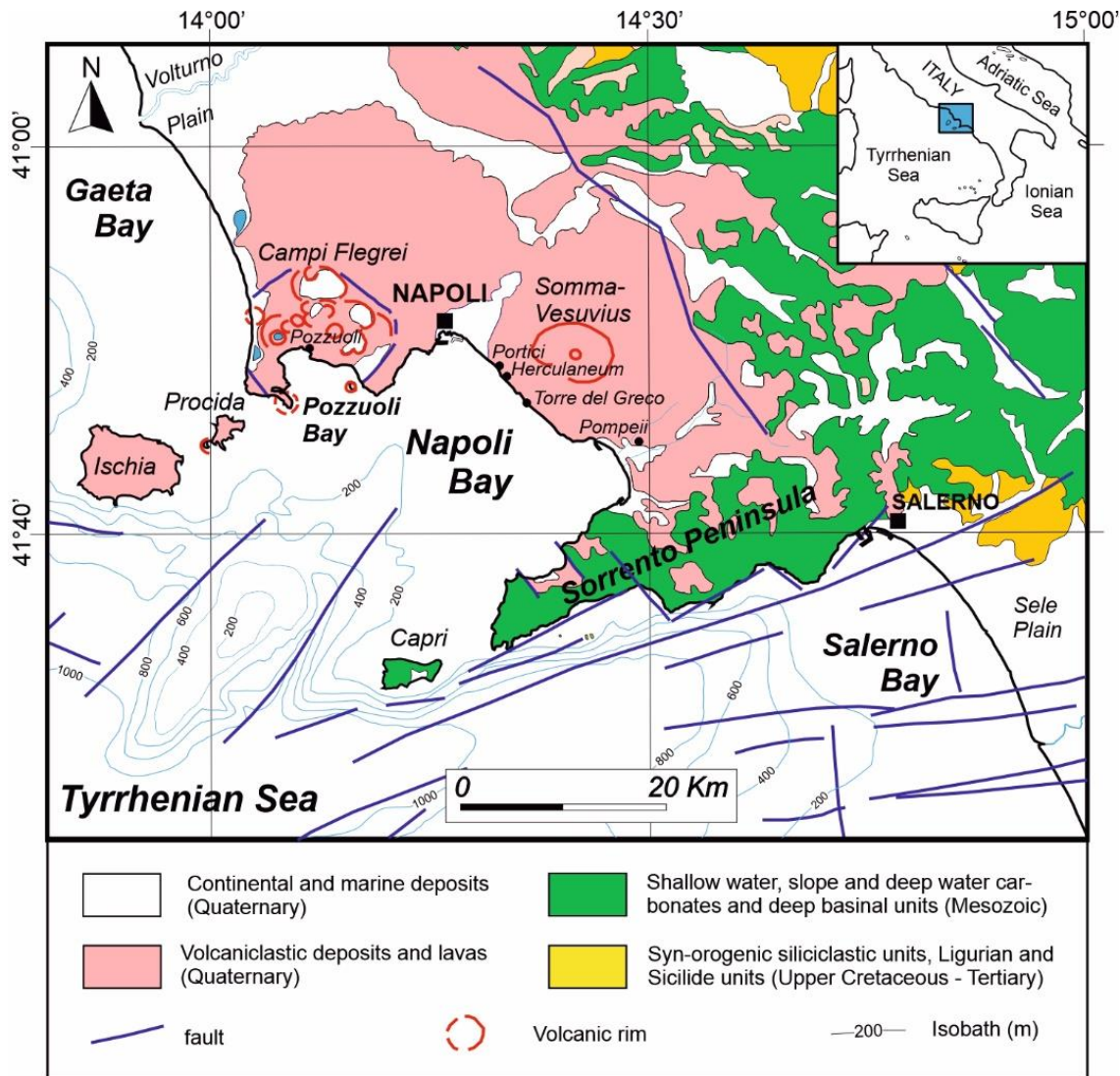
Figure 2 Geological sketch of the studied area – Southern Tyrrhenian Sea (G. of Naples, G. of Salerno and G. of Gaeta) (from D'Argenio et al., 2004, modified).

The sea bottom of the Gulf of Naples and Gulf of Salerno is covered by Pleistocene-Quaternary sedimentary and from pyroclastic fall deposits (Bruno et al., 2003). They are two peri-Tyrrhenian basins situated in the eastern part of the Tyrrhenian Sea (Mariani and Prato, 1988), which represent the offshore equivalent of the Campania and Sele coastal plains. Those basins are the effect of a large-scale Late Neogene to Pleistocene distensive tectonics (Insinga et al, 2008). The volcanism in the area has a potassic affinity with the emission of lava flows, domes, and pyroclastics related to strombolian eruptions and lava fountain and caldera-forming plinian eruptions. It was developed since about 300-360 ka and is currently active, dated on the basis of the oldest found rocks in deep wells (Orsi et al., 2004). The last eruptions in Gulf of Naples

occurred at Ischia Island in 1302 CE (Vezzoli et al., 1988), Phlegrean Fields in 1538 AD (Di Vito et al., 1987) and Mt. Somma-Vesuvius in 1944 CE (Santacroce et al., 2008). These three active volcanoes are aligned along a WNW–ESE strike (e.g. Acocella and Funiciello, 2006; Berrino et al., 2008). Submarine volcanic vents (e.g. Nisida, Miseno, Penta Palummo banks) are developed offshore the Phlegrean Fields, within and around in Pozzuoli Bay (De Pippo et al., 1984; Ferraro and Molisso, 2000), which are represented by monogenic volcanic centers that mostly formed in shallow marine environments and were active at different phases during the last 200 kyr (Milia, 2010; Sacchi et al., 2014). The Ammontatura and Dohrn channels are the main sedimentary structures in the area (D'Argenio et al., 2004).

The Sele Plain, jointly with on-shore Salerno basin, is a quite deep basin, which was developed during the Pliocene-Pleistocene situated between the Sorrento Peninsula to the north and the Cilento Promontory to the south. Data from the boreholes (AGIP, 1977) and seismic profiles (Sacchi et al., 1994) point to maximum thickness more than 1,7km of the post-Miocene infilling in the Gulf of Salerno, and due to that progressing subsidence until middle-upper Pleistocene (Budillon et al., 1994) with average sedimentation rates of 24cm/1ky (Sacchi et al., 1994).

1.2.1 Late Quaternary evolution of the Campania Plain–Naples Bay basin

The Campania Plain is characterized by the evident subsidence during the Late Quaternary (Branaccio et al., 1991). The beginning of the last glaciation between 125 ka and 18 ka occurred together with decreasing sea level and resulted in a seaward shift of the shoreline, parallel with the forced regression of paralic-shallow marine depositional systems (Milia,1996, 1999a,b, 2000; Cinque, 1999; Conforti, 2003). When the base level was low, all continental margin of Campania was uncovered and in consequence modern submarine canyon system of the Gulf of Naples (Dohrn and Magnaghi canyons) quickly evolved across the old continental slope. Major role in creating morphology of the coastal landscape and continental shelf had widespread volcanic activity and formation of a number of volcanic centers in the coastal zone of Campania (Vesuvius and Campi Flegrei) (Sacchi et al.2005).

Further volcanic activity of the Phlegrean Fields occurred with the eruption of Neapolitan Yellow Tuff ~15ka (Insinga, 2003; Deino et al., 2004) and also formation of numerous submarine

and subaerial vents (tuff rings and tuff cones) across the Campi Flegrei coastal plain and the Gulf of Pozzuoli continental shelf between 10ka and 1538 CE.

The reconstruction of the extent of the Holocene (Flandrian) transgression on the Sarno river plain (Cinque, 1999) was possible to obtain due to radiocarbon dating, geomorphologic evidence on land and subsurface data. During the Latest Pleistocene-Early Holocene (~15-6 ka) rising sea level systematically flooded the lower part of the Plain and lead to progressive expanding of the inner shelf by cutting into Upper Pleistocene alluvial fans. Late Early Holocene erosional terraces are possible to find on the water depth from 20 up to 13m. The ending of the transgressive phase had place about 6 ka ago and meant significant landmark within the coastline migration trend and the beginning of the Late Holocene progradation (Barra et al., 1989; Conforti, 2003). During the last 5 ka lower delta plain together with the delta system have changed sites of deposition, which was accompanied by a general seaward migration of the shoreline in the range of 3-6km (Cinque et al., 1997), however the area was still subsiding with rates about 2mm/year. Beach deposits of the age 5,6-4,5 ka occur from 3,5 to 10m below nowadays sea level and beach deposits from the Roman Age are found 4m below the present sea level (Sacchi et al., 2005).

1.2.2 Physiography of the Gulf of Naples

The southeastern Gulf of Naples is characterized by a range of 10 to 15 km wide continental shelf, cut in its distal part by two branches of the Dohrn canyon. The general physiography of the Gulf is affected by the interplay of volcanism and sedimentary processes during the Late Quaternary (Milia, 1999a,b; Milia and Torrente, 2000, 2003; Aiello et al., 2001). The zone is characterized by a wide continental shelf spreads up to 100-180m water depths (Milia, 1999b). The shelf width ranges from a maximum of ~20km in the middle part of the Gulf to about 2,5km off the Capri and Procida islands. The northern shelf area is characterized by an irregular morphology due to the occurrence of numerous submarine volcanoes, with a shelf break lying at the 70-150 m water depth. The inner shelf depositional system of the eastern Gulf of Naples is controlled by the occurrence of two small coalescent deltas, namely formed by the Sarno and Sebeto rivers, which are partially separated by an irregular relief on the south of Vesuvius, down to a depth of 100 m, associated with around 18ka old volcanic debris avalanche (Milia et al., 2003b). The southeastern sector of the Gulf of Naples continental shelf inclines from the Sorrento Peninsula toward the northwest. The morphology of this area is the result of the erosion and depositional features created

by sea level fluctuations over the past 39 ka (Milia, 1996, 1999b). Offshore the Sarno river mouth, the occurrence of extensive seafloor instability of Upper Holocene deposits has also been registered (Aiello et al., 2001; Conforti, 2003; Sacchi et al. 2005).

1.2.3 Physiography of the Gulf of Salerno

The physiography of the Gulf of Salerno has a significant control by the tectonic setting of the coastal zone and the high sediment supply. The width of the continental shelf varies greatly along of Gulf. In the Sele delta, southern sector, the shelf break is located around 15-25km away from the coast (Insinga et al., 2008).

Detailed seismostratigraphic studies (Bartole et al., 1984; Sacchi et al., 1994; Budillon et al., 1994; Conforti, 2003) distinguished a thick Pleistocene clinostratified succession, which is prograding to the south and west part of the Gulf. The top of that succession is cut by a sharp erosive surface related to the last sea level fall and low stand culminated during the Last Glacial Maximum (~18ka). The sea level during that period was at ~120m. The lates Pleistocene-Holocene deposits progress above that surface and can arrive at maximum offshore thickness of 35m in Vietri and Maiori (Conforti, 2003; Budillon et al., 2005). High resolution stratigraphy, petrophysical and paleomagnetic measurements point out important variations in the average sedimentation rate throughout the Holocene in the northern part of the Gulf (Buccheri et al., 2002; Iorio et al., 2004).
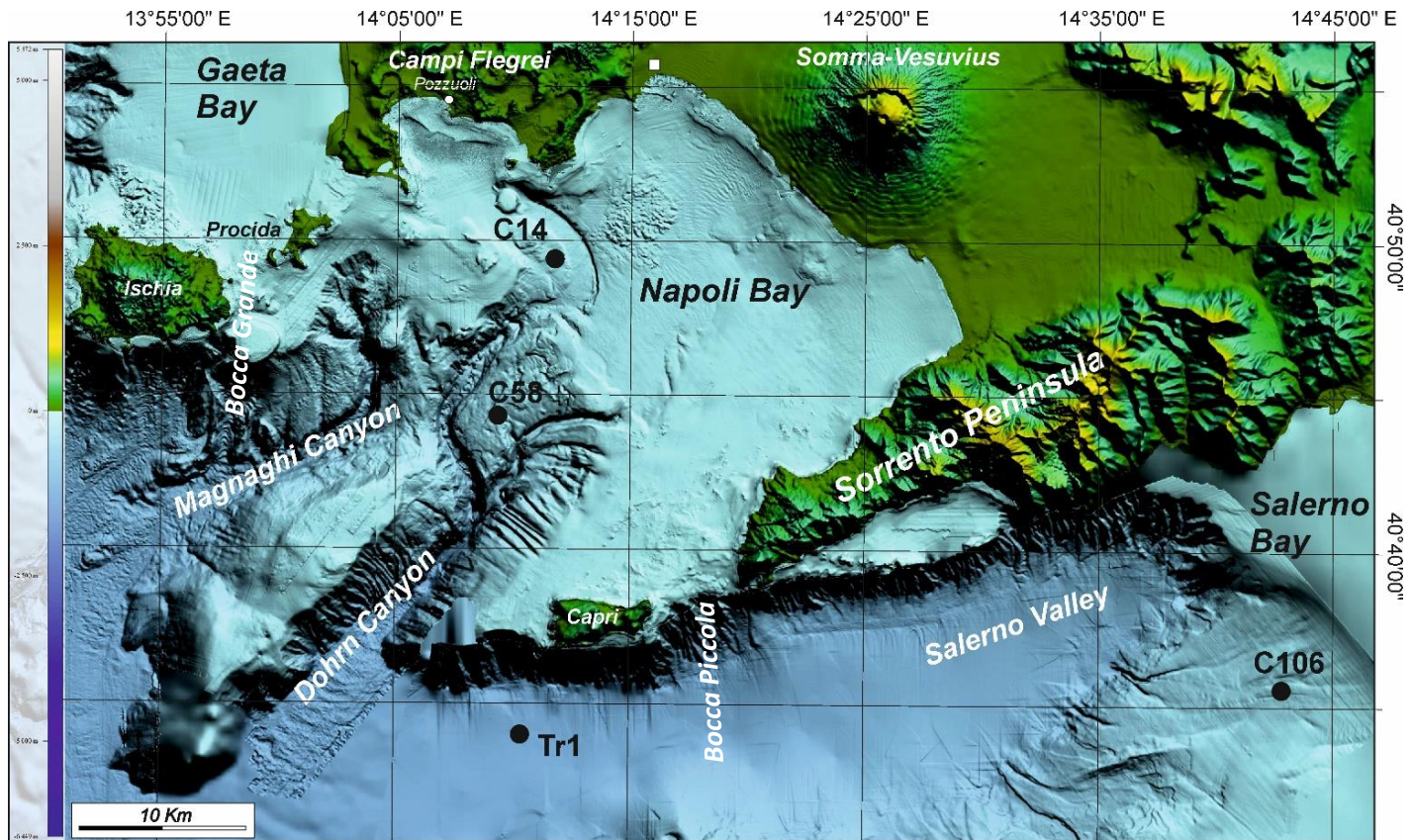
Figure 3 Base map with the location of the cores: GMS_98-01 C14, GMS_98-01 C58, GMS_84 C106, Transect_2017 TR1.

1.3. Mediterranean Sea hydrography

The Mediterranean Sea is characterized by the presence of thresholds that separate the basin in a series of sub-basins. The Strait of Gibraltar, a threshold with a depth of 284 m (**Fig. 4**) (Bryden and Kinder, 1991) controls the exchange of Atlantic and Mediterranean waters, has an important role to play in the circulation and productivity of the Mediterranean Sea. The Strait of Sicily divides the Mediterranean into the main western and eastern basins, while several satellite basins and definite entities may be distinguished in more detail, such as the Ligurian, Tyrrhenian, Alboran, Balearic, Adriatic, Ionian and Aegean Seas (Vallefuoco 2008).

Figure 4 West - East cross-section showing water mass circulation in the Mediterranean Sea during winter (after Wüst, 1961). Isolines indicate salinity values and arrows indicate the direction of water circulation in the Mediterranean Sea (Rohling et al., 2008).
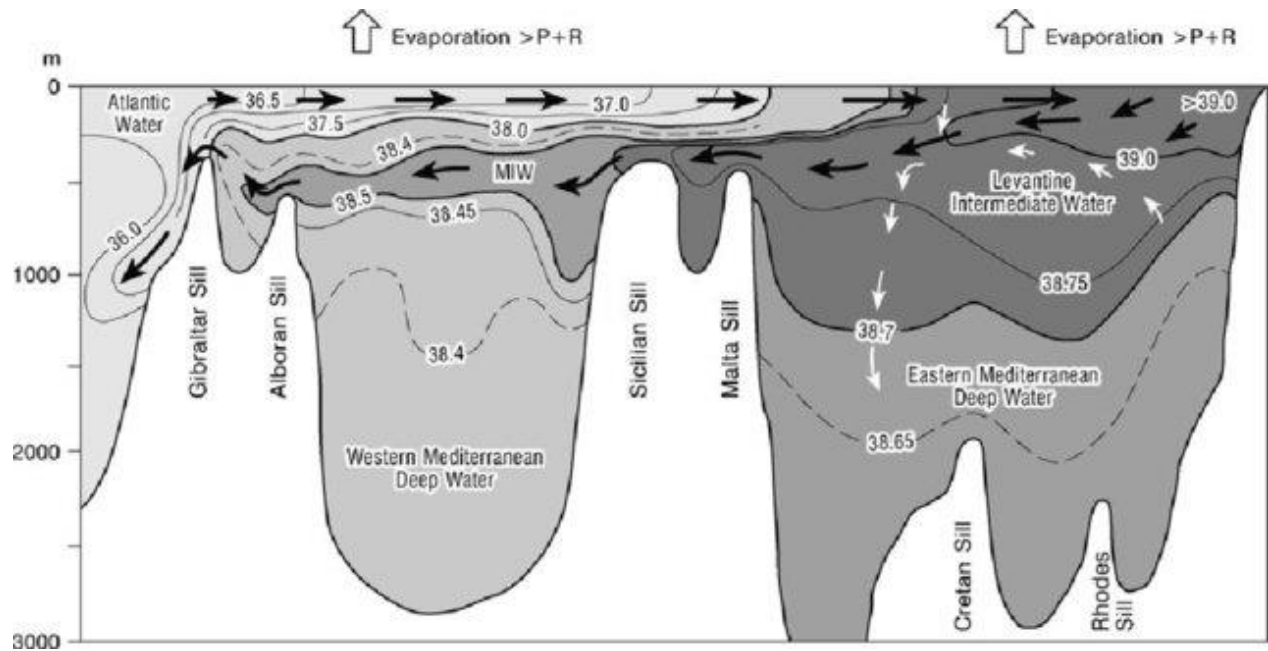
The Mediterranean Sea anti-estuarine circulation pattern is driven by the negative hydrological balance and the density gradient with the Atlantic Ocean (Robinson and Golnaraghi, 1994). The Mediterranean Circulation is driven also by water exchange through the various straits, wind stress, and thermohaline fluxes, with the latter depending on the basin's freshwater and heat budgets (Robinson et al., 2001). In the northern sector of the basin the surface water circulation pattern is dominated by cyclonic gyres. In the southern sectors surface waters derived from the Atlantic Ocean flow eastwards through currents, jets (Western basin) and anticyclonic gyres (Eastern basin) (Pinardi and Masetti, 2000). The Mediterranean Sea is defined a concentration basin, with an excess of evaporation over freshwater input resulting in strong temperature and salinity gradients in surface waters from West to East (Wüst, 1961; Béthoux, 1979; Garrett, 1996; Gilman and Garrett, 1994), despite the high freshwater input from rain or rivers in the region. The vertical distribution of the Mediterranean water masses includes the surface waters (0-200 m), the intermediate waters (200-600 m), and the deep waters (> 600 m) (Pinardi and Masetti, 2000; Tsimplis et al., 2006) (**Fig. 4**). Atlantic water (AW, 0-200 m) interacts and mixes with upwelled

Levantine Intermediate Water (LIW) (Hayes, 1999). Modified Atlantic Water (MAW) has nutrient levels higher than in resident waters and they favor the phytoplankton bloom in the western Mediterranean (Alboran, Balearic Seas), even in the Sicilian Channel (Rinaldi et al., 2014, Continental Shelf research).

In the Southern Tyrrhenian Sea, for example in Gulf of Naples, the two water masses: Modified Atlantic Water (MAW) and the Levantine Intermediate Water (LIW) are representative of the surface and intermediate branches of the so-called Mediterranean conveyor belt (Malanotte-Rizzoli, 2001; Robinson et al., 2001). Water of Atlantic origin (AW, e.g. Atlantic Water) get into the surface through the Strait of Gibraltar, mainly along the southern boundary, leaving the Algerian Basin and flowing along the northern coast of Sicily (Astraldi et al., 2002; Poulain and Zambianchi, 2007) and circulates eastwards and in this way replenish the upper layer of the entire Mediterranean, then mixing with the ambient waters and so modifying its original characteristics (therefore the definition of MAW). The LIW forms in the Levantine basin at subsurface levels, as the very salty water mass (e.g. in the Rhodes gyre), where intensive winds cause strong evaporation, what provides the huge increase of surface salinity (more than 39.0 psu, see e.g. Lascaratos, 1993). The constantly increasing density causes that this water sink and settle at intermediate depths. The LIW flows westwards between 200 and 500m, circulating in the eastern sub-basin and entering the western Mediterranean through the Straits of Sicily thresholds (Sparnocchia et al., 1999).

Moreover, during its passage eastward, AW nutrients are further reduced by phytoplankton (Béthoux et al., 1997), while climatic factors such as evaporation have resulted in its salinity increasing by up to 10% (Milliman et al., 1992) (**Fig. 4, 5a**). Consequently, the Atlantic Water (AW) that eastward up inflow in the Mediterranean Sea is currently referred to as the Modified Atlantic Water (MAW) (Heburn and La Violette, 1990; Milliman et al., 1992; Millot, 1999). During winter occasional outbreaks of cold and dry air masses above the northern Levantine basin cool the sea surface, what leads to vertical convection of the cold, dense and salty surface waters and form the Levantine Intermediate water (LIW, 200-600 m) in the Rhodes Gyre (**Fig. 5b**) (Malanotte-Rizzoli and Hecht, 1988; Georgopoulos et al., 1989; Buongiorno Nardelli and Salusti, 2000). This water mass afterwards settles between 200 and 600 m and spreads out in the entire Mediterranean basins and eventually enters the Atlantic Ocean, by Gibraltar Strait (Parrilla et al., 1986; Richez and Gascard, 1986; Marino, 2008) (**Fig. 5b**). The interaction of the LIW with cold

surface waters in the northern basins of the Mediterranean (the Gulf of Lions and the Adriatic Sea) governs deep water formation processes (**Fig. 5b**), which is responsible for the deep-sea ventilation (Pinardi and Masetti, 2000). Sites of deep-water formation are the Gulf of Lions for the western basin (Western Mediterranean Deep Waters, WMDW), while the sources of the Eastern Mediterranean Deep Water (EMDW) are the Adriatic and Aegean Seas (Schlitzer et al., 1991) (**Fig. 5c**).

The incoming Atlantic water is lighter and flow above water out of the Mediterranean, Levantine Intermediate Water (LIW) and the Mediterranean Deep Water (MDW) (**Fig. 5b**).

The East-West gradient in ocean productivity exists (Turley et al., 2000) because of important for life nutrients such as nitrogen and phosphorus (Krom et al., 1991). Because of this conditions the marine climate of the Mediterranean Sea is characterized by relatively warm, salty and poor in nutrients waters. Nowadays it is believed that the gradients are thought to exert the main control on present day planktonic foraminiferal distribution patterns (e.g. Thunell, 1978; Pujol and Vergnaud-Grazzini, 1995). Probably it can be expected that temporary variations in the temperature and salinity gradients would be expressed by changes in the planktonic foraminiferal assemblage records, for example from the sediment cores.
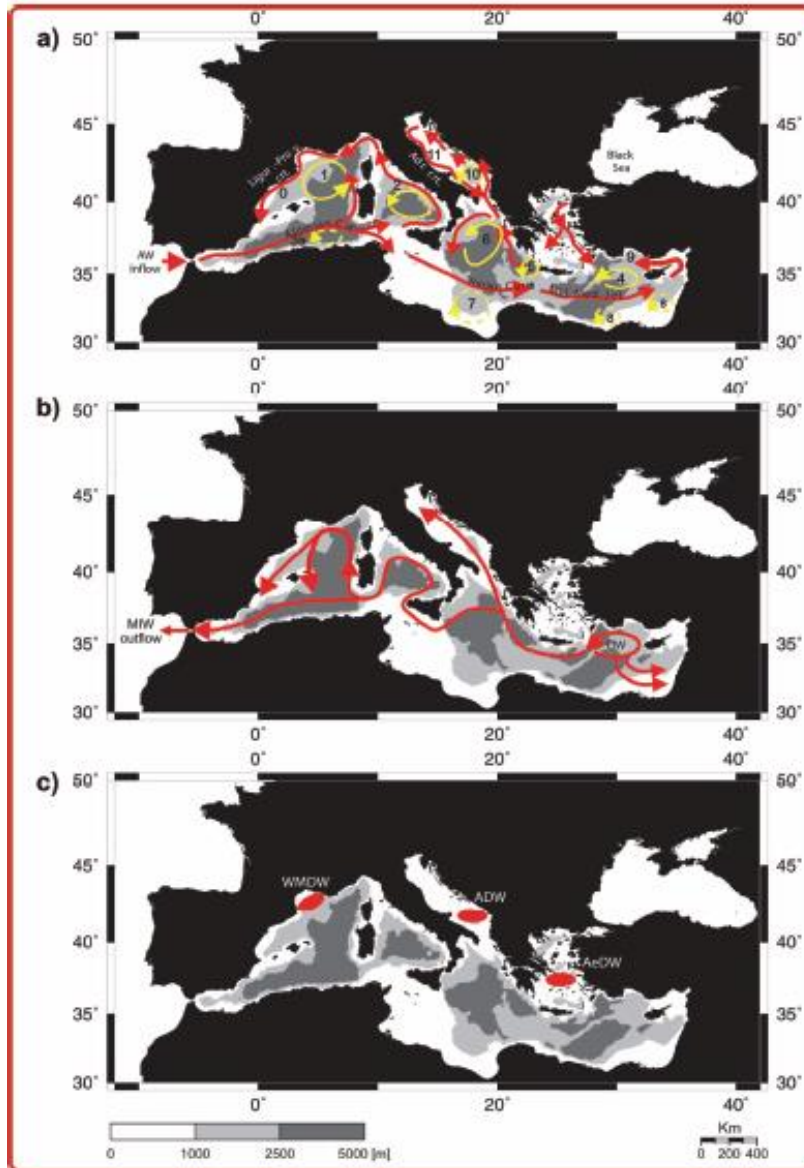
Figure 5 Water mass circulation in the Mediterranean Sea (**a**) The schematic of major basin current and gyres systems. **0** Ligurian-Provencal current; **1** Lion Gyre; **2** Tyrrhenian cyclonic circulation; **3** Algerian current; **4** Rhodes Gyre; **5** Western Cretan Gyre; **6** Western Ionian Gyre; **7** Anticyclone in the Gulf of Syrte; **8** Shikmona and Mers a-Matruh gyres system; **9** Cilican and asia Minor current; **10** Southern Adriatic gyre; **11** Western Adriatic Coastal current. Ligur. - Prov. crt. = Ligurian-Provencal current; Adr. crt. = Adriatic current; Mid Med. Jet = Mid Mediterranean Jet. (**b**) **LIW** dispersal pathways. (**c**) Sites of deep-water overturning. **WMDW** (western Mediterranean Deep Waters); **ADW** (Adriatic Deep Waters); **AeDW** (Aegean Deep Waters). (after Pinardi and Masetti, 2000; Vallefuoco 2008 and Schlitzer, 2018).

1.3.1 Hydrology of the Gulf of Naples

Hydrology of the Gulf of Naples was studied in the past by several authors among others: Hapgood, 1960; De Maio, 1959; Düing, 1965; De Maio and Moretti, 1973; Carrada et al., 1980. They indicated the exact relationship between the water masses and circulation within the Gulf (Sgarrella and Moncharmont-Zei 1993). To achieve more current data from 1977 to 1981 it was created a monitoring program performed by the Institute of Meteorology and Oceanography of the Istituto Universitario Navale of Naples (currently Department of Environmental Sciences of the "Parthenope" University by De Maio et al., 1978-1979a, 1978-1979b, 1980-1981, 1983). Marine currents were measured at 11 fixed sites along the coast of Gulf of Naples. That studies have provided for longer time the only information on the oceanography of the Gulf. More recent research in modelling of the wind-driven circulation of the Tyrrhenian Sea (Gravili et al.,2001; Grieco et al., 2005) analyzed the barotropic dynamical features and the dispersion of reactive/passive tracers in the Gulf of Naples. All these researches emphasized the spatio-temporal complexity of the dynamics in that coastal area. There is a strict relationship between the circulation and water masses within the gulf, which is part of the Tyrrhenian Sea. With specific reference to the hydrological features the Gulf of Naples is characterized by the presence of two main water masses (De Maio et al., 1978-1979a and 1978-1979b): the Modified Atlantic Water (MAW) and the Levantine Intermediate Water (LIW).

Modified surface waters of Atlantic origin (AW) typically lies in the upper 100-200m of the water column Millot, 1987; Astraldi et al., 1996; Millot, 1999; Fusco et al., 2003; Budillon et al., 2009). These waters are identified by a subsurface salinity minimum (S<37.4) and a seasonally variable temperature value. The MAW shows a constant temperature around 14°C during the winter period due to the intensive mixing of the water column.

The LIW enters the lower layers of the Tyrrhenian Sea (~400-500m) through the Straits of Sicily. It appears in the Gulf of Naples at the deepest measure sites close to the Bocca Grande and is located below 300m during the winter and 200m during the summer. Typical hydrological values of the LIW in the Gulf of Naples are T = 14.2°C, S = 38.65 psu (De Maio et al., 1978-1979a and 1978-1979b).

Also, other water masses can be present in the Gulf of Naples, depending on the season (Carrada et al., 1980). Winter mixing favors the formation of the Tyrrhenian Intermediate Water

(TIW), which is present in the homogeneous water column at the depth ~150m (e.g. Düning, 1965, Carrada et al., 1980). The thermocline is located in the surface layers during spring and deepens up to 20-30m with the end of the summer (Düning, 1965). A coastal currents flows SE during the summer with values up to 7500 m^3/s and in the opposite direction during the fall up to 40000 m^3/s through the Ischia and Bocca Piccola Channels (Düning, 1965). TIW is characterized by the temperature around 14 °C and salinity around 38.1 psu. Due to the summer warming and freshening the TIW rises in the water column above 75m, where it is changing for Tyrrhenian Surface Water (TSW) with the typical temperature 25 °C and salinity 38.3 psu (Hopkins et al., 1994). The Coastal Surface Water (CSW) is strongly affected by the river discharges and by the industrial and urban sewages as well, which in result causes an eutrophic coastal subsystem near the coast in opposite to the oligotrophic subsystem present in the open sea with a water warmer and fresher than the TSW (Sgarrella and Moncharmont-Zei 1993; Cianelli et al., 2012).

The hydrology in the Gulf of Naples shows a seasonal pattern featured by the summer stratification of the water column, which determines a formation of a surface mixed layer 30-40m dense. By the other hand, the intensive winter mixing affects the entire water column, which is homogenous down up to 150m (Carrada et al., 1980).

2. Ecological and palaeoceanographic meaning of benthic foraminifera

Benthic foraminifera are often considered fundamental not only in biostratigraphic studies, but also in paleoenvironmental studies, they are abundant in the geological record and from their appearance they form the majority of the microfauna and meiofauna of the ocean floor. Usually there are no single species present but different peculiar assemblages of benthic foraminifera distributed mainly according to latitudes, temperature and salinity gradients.

Foraminifera are perfectly suitable for environmental studies, because they record the environmental changes due to their wide distribution over all marine environments. A large number of physical and chemical parameters, such as temperature, salinity, depth, sediment, oxygen, food availability, influence the distribution of benthic foraminifera, and make them a useful tool for them useful tools for ecological and environmental interpretations.

Benthic foraminifera are widely used in ecological and palaeoceanographic studies of different marine environments. In shallow-water habitats, they can be influenced by a variety of parameters as oxygen, gradients in light, temperature, salinity, organic matter, substrate, as well as velocity and turbulence of surface water currents (Culver and Buzas 1986; Sen Gupta 2003). These microfaunas commonly show a high number of specimens, variable diversity and a dominance of epifaunal and shallow infaunal taxa (e.g. Semeniuk 2000; Murray 2006). In the Mediterranean Sea, the distribution of shelf benthic foraminifera is well documented in various regional studies (e.g., Jorissen 1987; Cimerman and Langer 1991; Sgarrella and Moncharmont-Zei 1993; Frezza and Carboni 2009; Mojtahid et al. 2009). These studies show significant spatial contrasts in the composition of shelf faunas. In fine grained sediments of the Adriatic Sea and of the Gulf of Lions, benthic foraminifera assemblages are influenced by food availability, oxygen penetration into the sediment and distinct microhabitat zonation (Barmawidjaja et al. 1992; Jorissen et al. 1992; Schmiedl et al. 2000). In other regions is observed a strong correlation between the diversity and abundance of symbiont-bearing shallow-water foraminifera and water column illumination (Langer 1988). In the last decades, several authors have investigated on the distribution of benthic foraminiferal assemblages from the southern Tyrrhenian Sea mainly focused on restricted sectors of the Campania continental shelf (Sgarrella and Barra 1984; Sgarrella et al. 1983; Coppa et al. 1994; Coppa and Di Tuoro 1995; Ferraro et al. 1997; Ferraro and Lirer 2006). The Campania continental shelf encompasses a variety of coastal marine habitats, as inner parts of continental

shelves, delta areas, outer shelf and seagrass areas, which are usually areas of high environmental variability, in which benthic foraminiferal species and their distribution are mainly controlled and/or related to several parameters as water depth, substratum type, food availability, nutrient fluxes, salinity and water currents.

2.1 Arrangement of benthic foraminifera in the sediment

Benthic foraminifera are commonly used as a tool in the reconstruction of seabed paleoenvironments and their changes in time and space (Tab.1). We use here a close relationship between the morphology of individual groups of benthic foraminifera and their requirements for specific environmental parameters (Gooday, 2003). The explanation of the pattern of benthic foraminifera arrangement requires consideration of many different environmental factors. It cannot be expected that every accumulation of foraminifera can be explained in terms of only a few factors, such as the availability of oxygen or the supply of organic matter, as this would be too simplistic (Murray, 2001). However, in deeper sea or ocean waters, where a number of environmental factors show lack or little spatial or temporal variability, several main factors can be indicated that have the greatest impact on the distribution of the foraminifera in the sediment (Murray, 2001). Such major factors seem to be the degree of oxygenation of the sediment and the amount of delivery of organic matter to the bottom of the basin. In muddy/silt sediments, the redox boundary in the sediment is separating oxygenated waters from waters containing hydrogen sulfide (Wilkin et al., 1996) and usually occurs at the level of a few centimeters below the level of the seabed. Due to the fact that in most of silty environments the access of oxygen in the sediment is limited, benthic foraminifera are usually located no deeper than 1cm. As a result, epifaunal and infaunal species appear relatively close to each other. Thus, assemblages found in marl sediments may consist of diverse microenvironments. This is well reflected by the foraminiferal oxygen indicator proposed by Kaiho (1994) - see below. In any paleoecological interpretation, the presence of fauna living in environments with a limited amount of oxygen should not be automatically interpreted as evidence of the low-oxygen toxicity of the seabed. In fact, such conditions are where disoxia or anoxia extend down to the bottom of the water column (Murray, 2001).

Proxy of	Purpose
Oxygenation	• Reconstruction of biogeochemical cycling • Ocean circulation history • Organic pollution assessment • Estimating preservation-potential of organic matter
Depth	• Geohistory analysis of sedimentary basins
Organic flux	• Reconstruction of Bioproduction (CO_2 research) • Quality and quantity of organic matter (hydrocarbon generation)

Table 1. Overview of the most important fields in which benthic foraminifera are applied as proxies (from Van der Zwaan, 1999).

Jorissen et al. (1995) summarized the earlier research of Corliss and Emerson (1990) regarding the distribution of benthic foraminifera in the sediment as a function of the inflow of organic matter to the bottom and oxygenation of the sediment. This model was called TROX (Fig. 6) model - trophic conditions and oxygen concentrations (Jorissen et al., 1995). This model uses the assumption that the depth to which organisms can live is determined by the availability of oxygen and its presence in the sediment, for infaunal forms. The authors suggest that benthic foraminifera have certain requirements for the critical amount of oxygen and food necessary for life (quantity and quality of nutrients) and they differ between different species. In the model, the depth of life of benthic foraminifera is limited by the critical value of nutrient levels in oligotrophic environments, while for eutrophic environments this limitation will be the critical oxygen content (Jorissen et al., 1995). In relatively shallow environments, where the supply of marine organic matter is quite high, oxygen consumption is high and, as a consequence, penetration of the infauna is shallow because the redox zone is also at a shallow depth (Jorissen et al., 1995, Van der Zwaan et al., 1991). The oxygen content of pore water decreases because oxygen is used by bacteria to dissolve organic matter (Peryt, 2003). In much deeper or more oligotrophic environments, penetration of the fauna occurs deeper due to less absorption of oxygen by decomposing organic matter, consequently the boundary of the redox zone is also deeper. The inflow of organic matter to the deepest parts of the ocean is the smallest. The redox border is deep and not related to limiting

the distribution of the fauna. In this case, the supply of organic matter is so small that the amount of organic matter can be a parameter limiting the occurrence of deep infauna due to lack of food in the deeper layers of the sediment. The second parameter limiting the presence of foraminifera in the discussed model is the availability of organic matter (food). The largest number of foraminifera is always in the upper centimeters of sediment, which is associated with a large amount of organic matter in the sediment. Benthic foraminifera are also found very deep in the sediment, even in the deep sea, suggesting that at least some of them are able to survive in such conditions. As the water depth increases and the organic supply decreases, the main strategy for feeding benthic foraminifera changes. In such deep-sea environments, the dominant nutritional strategy, in contrast to shallow-water environments, where a significant amount of epifauna and infauna feed on the detritus occurring in the sediment, is filtration. There is a change from bands dominated by burrowing forms to bands living on the water/sediment boundary (Van der Zwaan and Jorissen, 1991; Jorissen et al., 1995) and which are very characteristic for very deep environments (above 1000m deep).
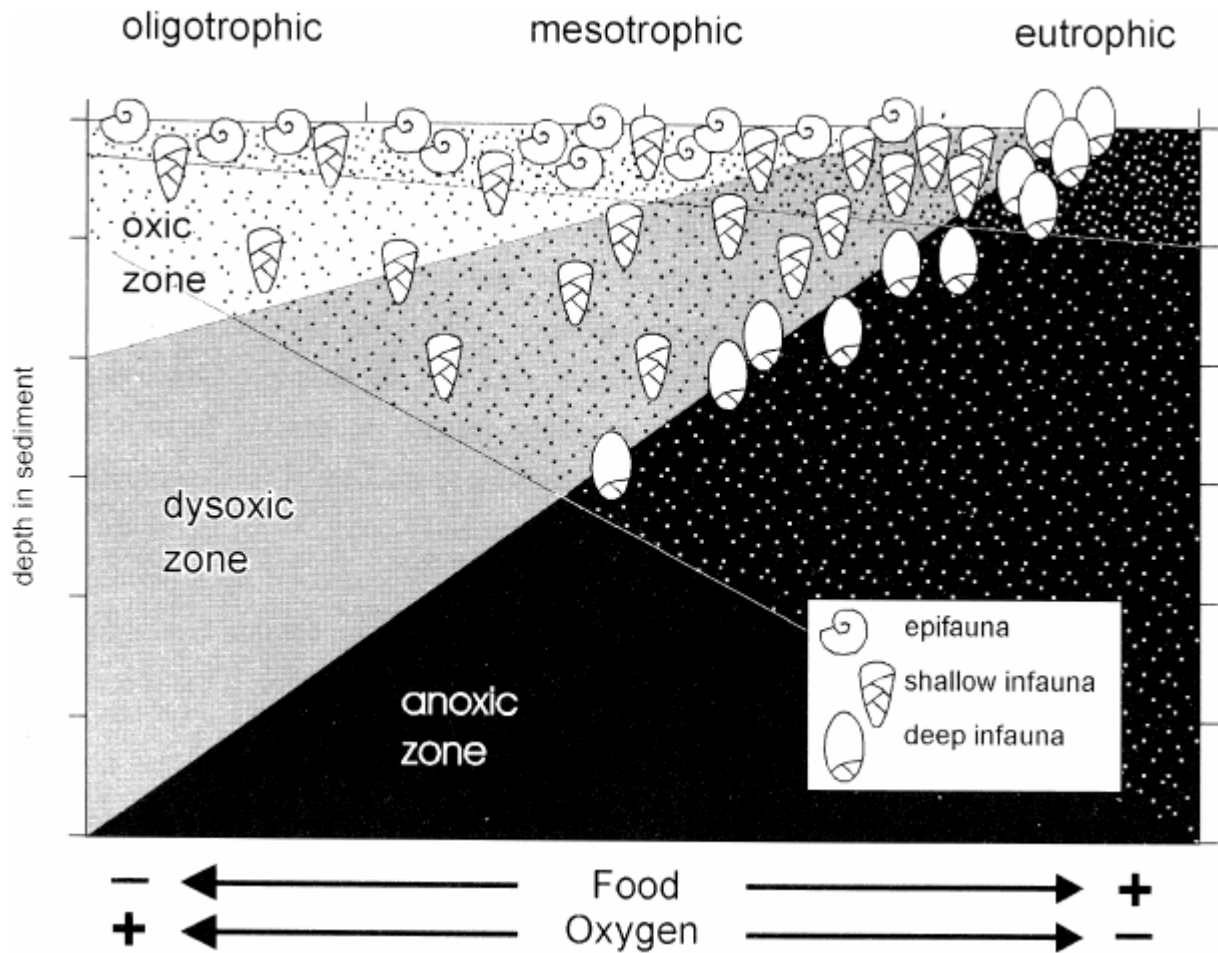
Figure 6 TROX model (from Jorissen et al., 1995).

The differences in the amount of oxygen at the water/sediment boundary significantly affect the occurrence and taxonomic/morphologic composition of benthic foraminifera assemblages. These changes may be visible in the size, thickness or porosity of the foraminifera shell. These morphological and taxonomic differences were defined as the foraminiferal oxygenation indicator for sediment (Kaiho, 1994).

High oxygen environment indicators:

- epifaunal forms with thick and large walls (> 350 μm)

- epifauna living under high-oxygen bottom water conditions, and which are absent in low oxygen environments.

- flat-biconvex, biconvex, round trochospiral and spherical test shapes (e.g. *Cibicidoides* spp*., Gavelinella* spp*., Nuttallides* spp*., Stensioina* spp. and *Globocassidulin*a spp.) and large, thick-walled millolides (Kaiho, 1994).

Indicators of suboxic environments (medium oxygenation) are divided into three groups:

A. Small species, smaller than 350 µm, are indicators of average oxygenation, since small individuals can live in conditions with reduced oxygen content, as mentioned earlier.

B. Between the niche occupied by morphotypes characteristic of aerobic and dysoxic environments there is a taxonomic group B. These include *Lenticulina* spp*., Dentalina* spp., large *Nodosaria* spp., large ornamented species – *Bulimina* spp.; rounded planispiral, flat-oval and spherical forms (Kaiho, 1994); small and / or thin-walled, flat-convex and biconvex forms, as well as *Uvigerina* spp. and 4 taxa related with low oxygen content: *Gyroidinoides* spp*., Gyroidina* spp*., Hoeglundina* spp. or *Oridorsalis* spp.. Group B species include both infauna and epifauna inhabiting the well-oxygenated bottom zone, as well as epifauna living in the poorly oxygenated zone.

C. The last group consists of foraminifera that have thin walls but occupy micro-environments between the dysoxic and those occupied by group B. These are *Bulimina aculeata, Nonionella* spp and *Elphidium excavatum*.

Indicators of low oxygen (dysoxic) environment:

The most characteristic feature of foraminifera from low oxygen microenvironments have a thin shell, e.g. *Bolivina* spp., *Chilostomella* spp., *Fursenkoina* spp., and *Globobulimina* spp.. The thin shell wall can be associated with a limited calcium carbonate precipitation in dysoxic environments (Kaiho, 1994).

- Most of benthic foraminifera are small in size (the diameter of the spiral molds is usually less than 200µm (at constant temperature, oxygen consumption increases significantly for individuals larger than 250µm), while the length of the elongated molds does not exceed 500µm (Kaiho, 1994);

- Foraminifera with unornamented and highly perforated shells, longitudinal and conical, are also typical for these environments. The high surface area to volume ratio of such morphotypes, small shell sizes and high porosity, can provide better oxygen capture.

- The high porosity of the shells may also indicate difficulties associated with calcium carbonate precipitation in dysoxic environments.

In addition to the above-mentioned characteristics of low oxygen foraminiferal assemblages, it is worth to emphasize that the same infaunal morphotypes occurring deep (down to several cm) in a sediment in a well-oxygenated environment can live very shallowly as epifauna or a shallow infauna (shallow infauna) in a poorly oxygenated environment, with the low content of dissolved oxygen in the surface sediment.

Based on analysis of modern and fossil species, Bernhard (1986) presented a summary of taxa and morphotypes of benthic bore holes of low-oxygen and organic-rich environments. Such benthic foraminifera include, among others:

1. Forms with a flattened shell. The author speculates that such a flattened shell having a larger surface of the shell in relation to its volume than in more isometric, convex forms, can maximize oxygen uptake and further minimize sinking in the sediment with even lower oxygen concentration. These observations suggest that while small, low-density, foraminifera prefer low-oxygen environments, those with larger-weight foraminifera can more easily adapt to underlying anaerobic deposits (Bernhard, 1986).

2. Calcareous foraminifera with small-sized shells that also maximize relative surface area. The tendency for small sizes with a spherical shape is observed in anaerobic syndromes. Convex, unfolded youngest chambers, observed in lenticulinides, may also provide additional surface area in relation to volume.

3. Foraminifera with elongated, convex chambers including *Bolivina* spp.*, Bulimina* spp..

4. Generally, anaerobic environments are dominated by unornamented, perforated, thin-walled shells, which may be associated with difficulties in the precipitation of calcium carbonate in these environments (Bernhard, 1986). The reason for the reduction of carbonate organisms in these environments is the acidic environment and/or low calcium water. Paradoxically, if these foraminifera need to maximize the surface area to volume ratio to increase oxygen uptake or reduce

sinking in sediment, then calcium carbonate precipitation will need to be increased. The solution can be thinning of walls with maximum surface area, many pores and a thin, unornamented shell, and this is what foraminifera from anaerobic units look like (Bernhard, 1986).

Corliss (1985) also stated that morphologically dominant deep-infaunal foraminifera (tolerating less oxygen than epifaunal forms) are those with a large surface area to volume ratio and numerous pores, while epifaunal foraminifera have fewer pores and a smaller surface area to volume ratio (Bernhard, 1986). These infaunal deep foraminifera, found at a depth of 15cm below the seabed, can occur in an environment with very low oxygen content. The most characteristic species of foraminifera for dysoxic environments are, as in the case of anoxic environments, those with a thin wall, including *Bolivina* spp. or *Globulimina* spp. (Kaiho, 1994). Most species found in such environmental conditions have a problem with calcium carbonate precipitation, so they are small in size (the diameter of the spiral forms is less than 200 μm, and the length of elongated, flat forms are less than 500 μm; after Kaiho, 1994). Dominant morphogroups in anaerobic syndromes are similar to infaunal forms (after Bernhard, 1986).

The second way to deal with insufficient calcium carbonate precipitation may be to produce agglutinated shells using organic cement. Some agglutinating foraminifera occur in anaerobic environments, but are not the dominant group (e.g., *Textularia*) (Bernhard, 1986).

2.2 Ecological features of selected benthic foraminifera *taxa*

Angulogerina angulosa: it is a semi-infaunal species omnivorous and euhaline. It lives in substrates formed by coarse sediments, generally sandy, in waters with temperatures of 16 - 0 ° C and salinity around 34 p.s.u. (Rögl, 1998). In the Mediterranean, it lives in circalittoral and bathyal depths. In the Tyrrhenian Sea it was found at 2860 m (Sgarrella and Moncharmont Zei, 1993).

Amphycorina scalaris: is a species commonly found in a circalittoral zone, but more abundant in a bathyal environment (Blanc-Vernet, 1969; Sgarrella and Barra, 1984; Sgarrella and Moncharmont Zei, 1993).

Bolivina aenariensis: it is an infaunal species, from shallow to deep, of mesotrophic / eutrophic environments, possibly in combination with hypoxic conditions (Corliss, 1991; Gooday,

1994; De Stigter et al., 1998; Schmiedl et al., 2000; Melki et al., 2010). It lives at depth from neritic to batial. It is considered a cold climate marker.

Bolivina albatrossi: it is found in sediments with high organic carbon content and reduced oxygen concentrations, in bathyal muds (Sgarrella and Moncharmont Zei, 1993). In the Mediterranean Sea it is more abundant during the last glacial period than in the Holocene.

Bolivina dilatata: it is an infaunal species, from shallow to deep, of mesotrophic / eutrophic environments, possibly in combination with hypoxic conditions (Corliss, 1991; Gooday, 1994; De Stigter et al., 1998; Schmiedl et al., 2000; Melki et al., 2010). It is associated with a high input of organic matter. Its habitat extends from the inner platform to the bathy plain.

Bolivina spathulata: it is a potential infaunal opportunistic species. The species of Bolivina (*B. alata, B. spathulata* and *B. dilatata*) are shallow or deep infaunal taxa, which are commonly found in a wide range of mesotrophic and eutrophic conditions, possibly in combination with hypoxic conditions. It tolerates low amounts of oxygen (Stefanelli, 2004), lives at infralittoral and circalittoral and bathyal muds (Sgarrella and Moncharmont Zei, 1993).

Bulimina aculeata: it is found at depth from infralittoral to batial, commonly at circalittoral depths (40 - 130 m) (Jorissen, 1988; Avnaim-Katav et al., 2013). It is an opportunistic infaunal species that tolerates low amounts of oxygen and high amounts of organic matter (Schmiedl et al., 2000). It is abundant in areas of high productivity where the flow of organic matter is high, often combined with non-toxic or sub-toxic conditions of the bottom or pore waters (Schmiedl et al., 2000). It lives in fine-grained sediments, in water masses with temperatures> 0.5 ° C.

Bulimina marginata: it is an opportunistic species that lives in superficial infaunal environments with high organic input associated with nutrient-rich waters (Abu-Zied et al., 2008; Frezza and Carboni, 2009). It tolerates low oxygenation levels (Sen Gupta et al., 2009b; Davidsson, 2014) and prefers temperate-cold waters. It is commonly found in in environments with eutrophic conditions. It lives at depths from neritic to lower bathyal.

Bulimina costata-inflata: it is an opportunistic infaunal species from low to intermediate. It lives in highly productive areas with low oxygenation conditions at the sea bottom (Miller and Lohmann 1982, Lutze and Coulbourn 1984).

Cassidulina crassa: it is an opportunistic infaunal species that prefers high concentrations of oxygen. It lives in eutrophic conditions at a shallow water. It is frequent from circalittoral to bathyal muds (Sgarrella and Moncharmont Zei, 1993).

Cassidulina carinata: it is an opportunistic infaunal species and not very resistant to sub-toxic conditions, present in temperate-cold waters. It adopts an opportunistic life strategy in order to profit from organic matter pulses (Jorissen et al., 1998; Schmiedl et al., 2000; De rijk et al., 2000; Morigi et al., 2001). It is found in the circalittoral and bathyal muds (Sgarrella and Moncharmont Zei, 1993).

Cibicidoides pachyderma: it is an epifaunal and opportunistic species, but in some cases specimens have been found at different depths within the sediment according to their ontogenetic stage: the youngest at greater depths (1.5 - 6 cm) than adults (0 - 1 cm) (Rathburn and Corliss 1994). It mainly prefers the upper bathyal area (200 - 1000 m). It lives in well-oxygenated environments with stable physico-chemical conditions (Van der Zwaan, 1982).

Gyroidina spp.: it is an opportunistic species typical of oligotrophic and well-oxygenated environments. They tolerate small inputs of organic carbon, low primary production. *Gyroidina Neosoldanii* (or *G. orbicularis)* is a characteristic species of deep and abyssal bathymetry (Wenger, 1987), it is more common at depths greater than 550 m (Dieci, 1959).

Hoeglundina elegans: it is an oligotrophic, epifaunal or surface water species. It is found in well-oxygenated environments (Corliss and Emerson, 1990; Cacho et al., 2001; Geslin et al., 2004). It is typical of areas with small input of organic carbon and low primary production. It is found at depth from neritic to bathyal.

Hyalinea Baltica: it is a shallow opportunistic or intermediate opportunistic species, slightly resistant to low oxygen content. It is essentially a circalittoral and especially epibathyal muds in Mediterranean Sea (Sgarrella and Moncharmont Zei, 1993). In the current ocean, *H. baltica* is more abundant in the cold waters of the North Atlantic (van Morkhoven et al., 1986).

Melonis barleeanum: it is an intermediate and deep infaunal species. It is abundant in areas of high productivity, with large flows of organic matter, in non-toxic or sub-toxic conditions, in bottom waters or pore waters (Schmiedl et al., 2000).

Miliolidae*:* miliolids are characteristic of well-oxygenated oligotrophic and mesotrophic environments. They are abundant in shallow waters, along the coast and also present at great depths.

Sigmoilopsis schlumbergeri: lives in environments with an influence of a river delta, at depths from the muddy circalittoral and bathyal bottoms. They seem to have a preference for nutrient-rich levels (Sgarrella and Moncharmont Zei, 1993).

Sphaeroidina bulloides: it is a mesotrophic epifaunal species (Linke and Lutze, 1993, Loubere and Fariduddin, 1999; Altenbach et al., 1999). It does not tolerate stress related low level of oxygenation. In the Mediterranean Sea this species lives in the circalittoral and bathyal muds, below 1300 m depth. (Sgarrella and Moncharmont Zei, 1993).

Uvigerina mediterranea: it is a shallow infaunal and opportunistic species. It lives from circalittoral to bathyal muds (Sgarrella and Moncharmont Zei, 1993) in Mediterranean Sea, but in the Eastern Mediterranean only in epibathyal zone, what is probably related to the scarce ventilation of the deep waters.

Uvigerina peregrina: it is a shallow infaunal and opportunistic species, abundant in regions with a high supply of organic matter and in areas affected by river discharge. It only tolerates a moderate lack of oxygen and avoids anoxic areas (Schmiedl et al., 1997). It lives in eutrophic to mesotrophic conditions but prefers mesotrophic environments. It is commonly found down to 3000 m water depth.

Valvulineria bradyana: it is an opportunistic species and prefers environments rich in organic matter and low oxygenation such as VTC (coastal terrigenous muds) bottoms (Blanc-Vernet, 1969; Sgarrella and Moncharmont Zei, 1993) from circalittoral and epibathyal muds.

2.3 Planktonic foraminifera biogeography and life strategy.

Planktonic foraminifera are an important component of marine plankton. They appeared in the Middle Jurassic, but the peak of their development occurs on the Late Cretaceous period, for which they are one of the main orthostratigraphic fossils. Planktonic foraminifera are largely used in paleoenvironmental and paleoceanographic reconstructions (Hemleben et al., 1989).
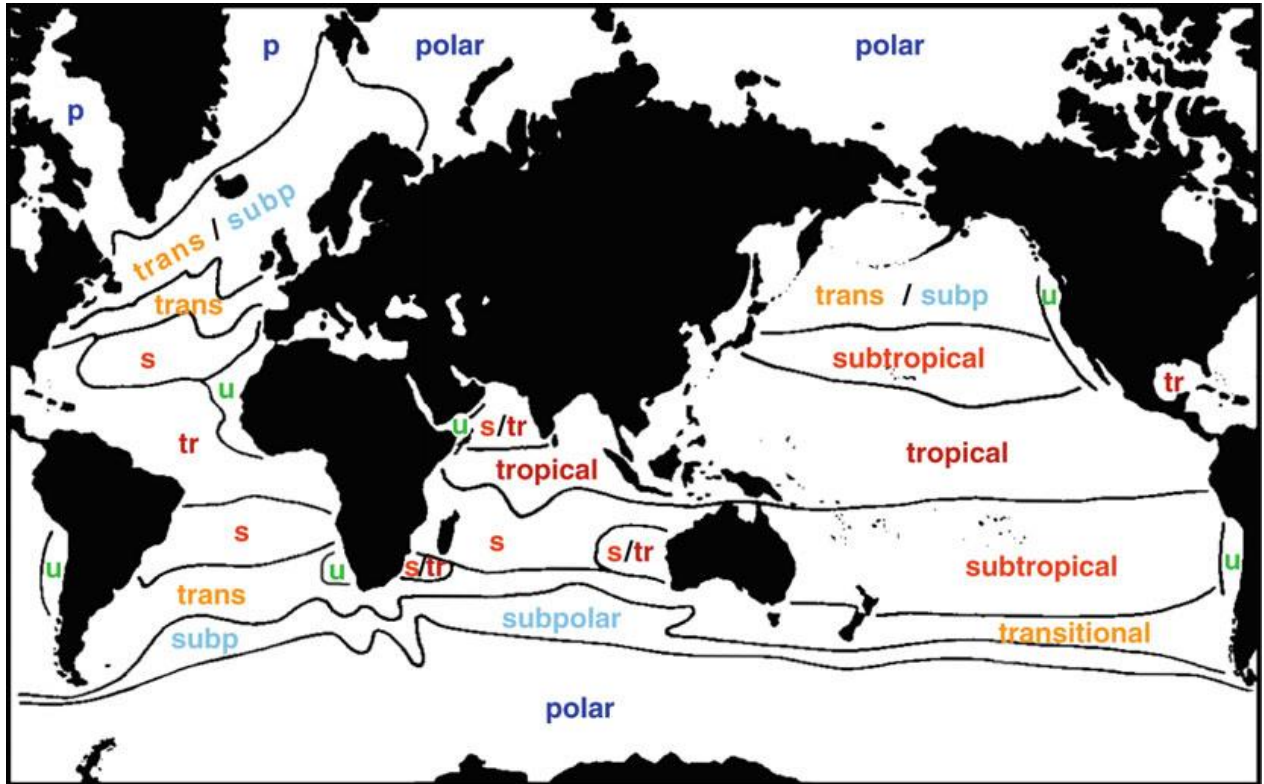
Figure 7 Planktonic foraminifera bioprovinces according to data from plankton tows and sediment samples (Hemleben et al. 1989, and references therein). Latitudinal provinces are polar (p), subpolar (subp), transitional (trans), subtropical (s), and tropical (tr). A sixth province is characterized by upwelling (u) and eutrophic conditions.

The horizontal and vertical distribution and the number of planktonic foraminifera specimens is determined by various biotic and abiotic factors. These include temperature, salinity and depth of the basin; sea current system; reproductive potential; presence/absence of symbionts; primary oceanic productivity and the associated supply of nutrients (Hemleben et al., 1989; Premoli Silva and Slitter, 1995). Modern planktonic foraminifera are limited to the open sea environment with normal sea salinity and transparent water (Leckie, 1987). They occur most frequently in the euphotic zone, although the environmental conditions for specific species are different. The distribution of planktonic foraminifera in the water column reflects the depth stratification closely related to the morphology of their shells: Most of spinose planktonic foraminifera are symbiont-bearing species and are limited into the photic zone (Schiebel and Hemleben, 2017).

In today's oceans, five planktonic foraminifera bioprovinces are identified: tropical, subtropical, transient, subpolar, polar (Hemleben et al., 1989). Different planktonic foraminifera assemblages in each bioprovinces reflect species preference for different oceanographic settings, among other water column configuration, surface ocean streams activity and oceanic fronts (Fig. 7).
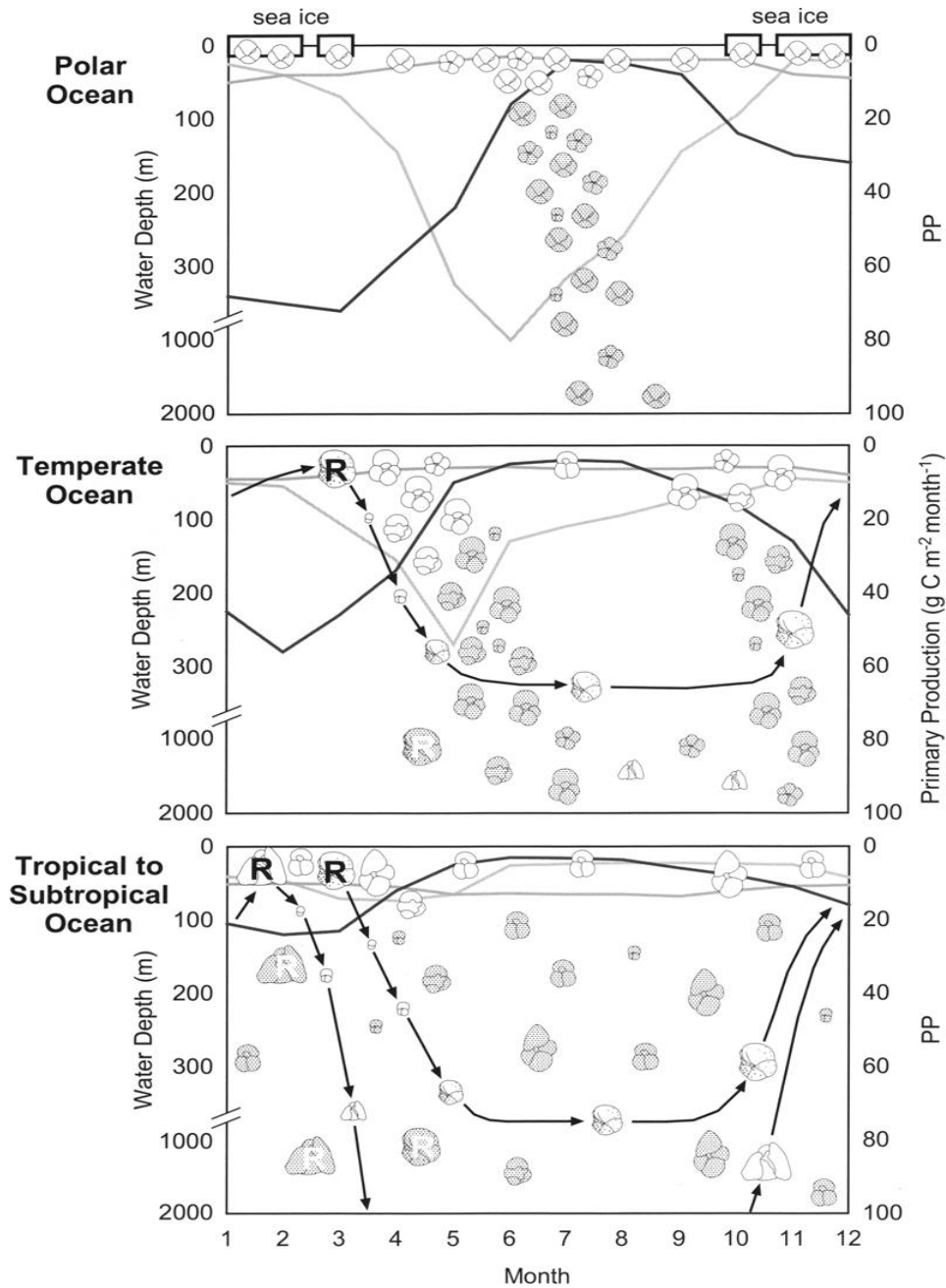

Figure 8 Relationship between planktonic foraminifera life strategists and primary productivity at different latitude (from Schiebel, 2005).
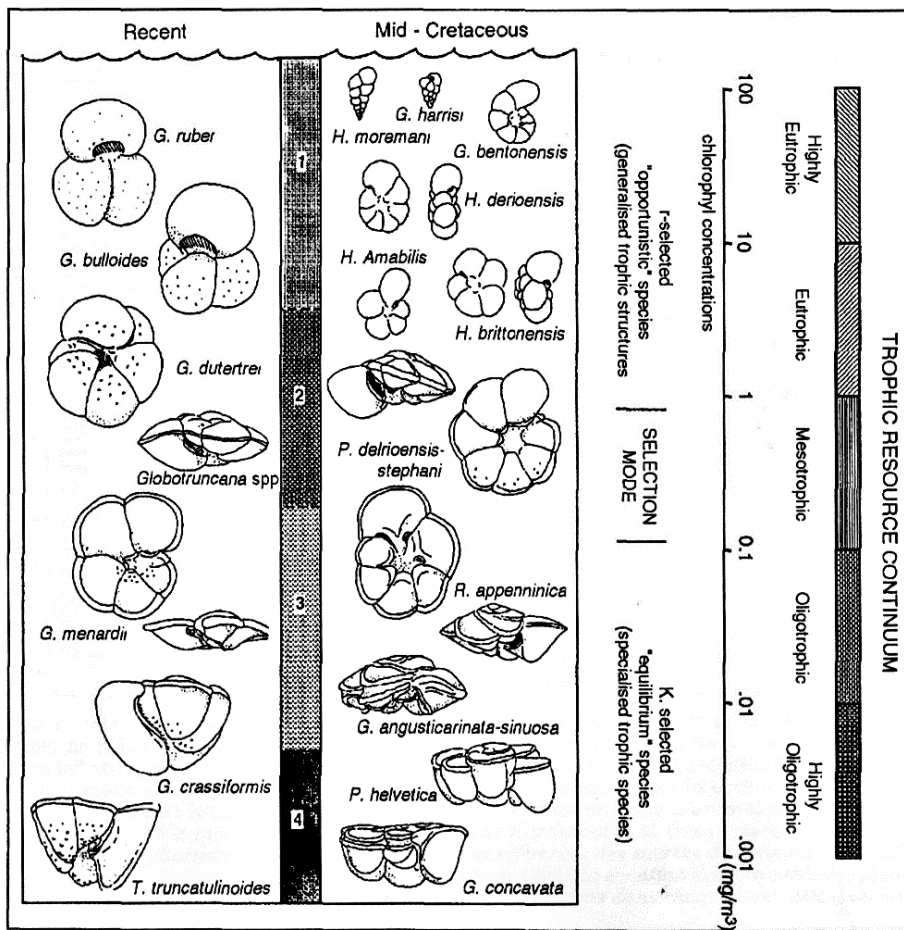
Figure 9 Planktonic foraminifera water depth preference (middle cretaceous vs. present) and their relationship to environmental trophism (from Hart and Bailey, 1978).

The different preference of planktonic foraminifera species is illustrated in Figure 9. In Figure 10, it is instead illustrated the reproductive strategy followed by different species. Planktonic foraminifera reproduce at species-specific depths (fig.8), possibly close to the pycnocline (separates water masses with different densities), thereby increasing the chances of successful fertilization and ensuring optimal living conditions for the offspring (Schiebel, 2005).
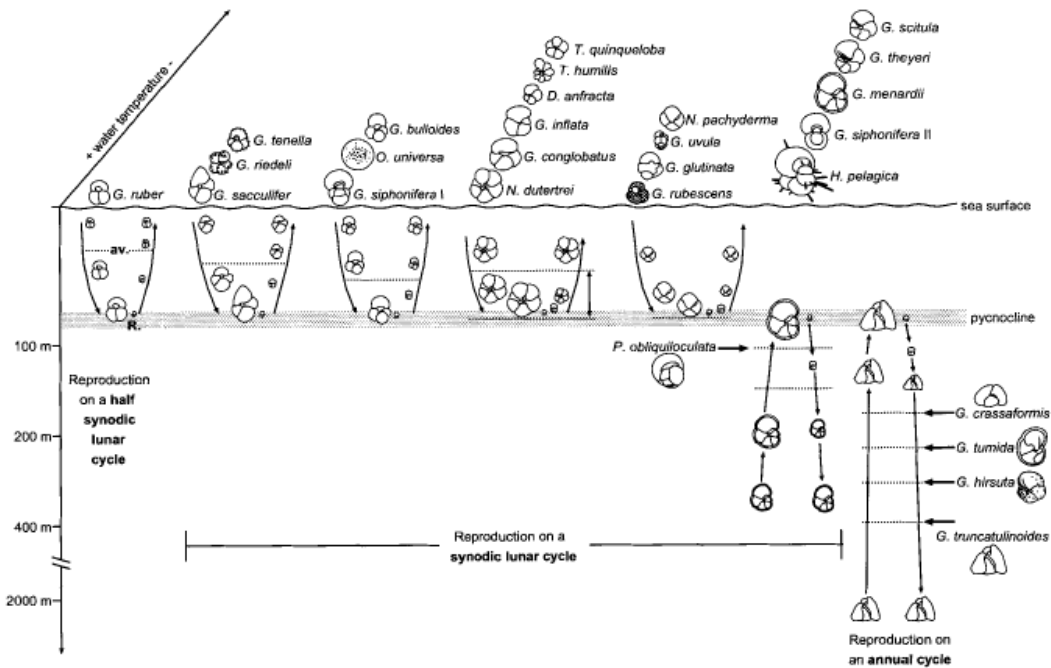
Figure 10 Planktonic foraminifera species and their reproduction strategy from Schiebel (2005).

Foraminifera with a short and shallow life cycle are characterized by a simple shell structure and small size. They reach maturity quickly, have a high reproductive potential and low requirements. These are called r-strategists. In contrast, foraminifera with longer and deeper life cycles reach the adult stage ready for reproduction only after achieving a large morphological change in the shell (fig.11) (after Caron and Homewood, 1983).

Life-cycles and depth-stratification.

Figure 11 Life cycle of planktonic foraminifera and water depth migration (Caron and Homewood, 1983).
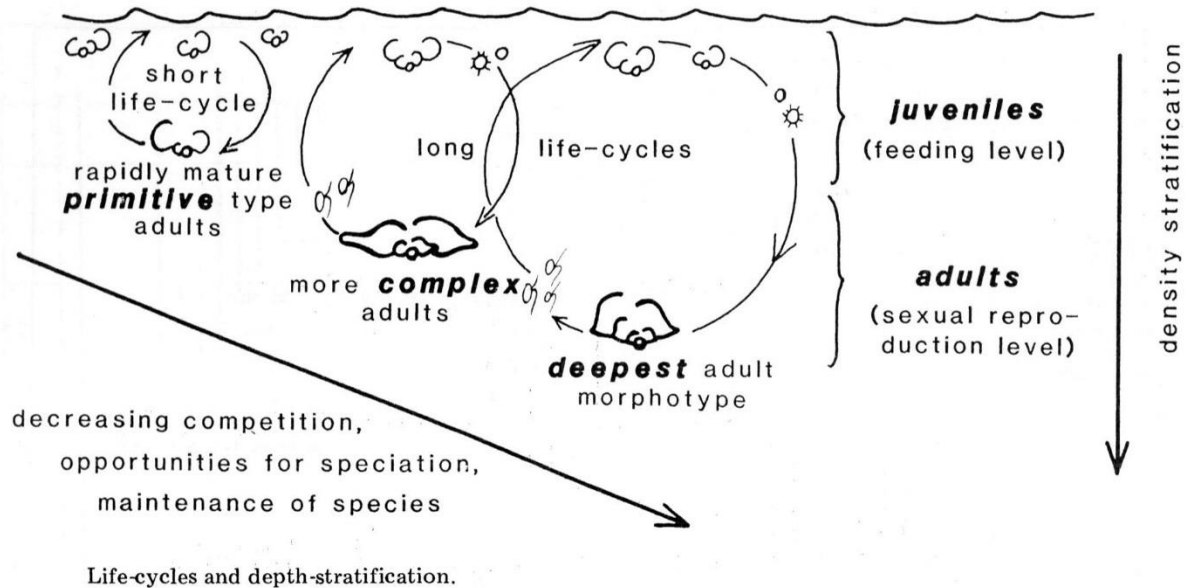
The variety of life strategies of planktonic foraminifera is closely related to food access (Fig.8), reproductive potential and size. There are three life strategies for planktonic foraminifera (Petrizzo, 2002; Tab. 2):

R-strategists - opportunists. They live in nutrient-rich environments and allow the release of numerous offspring. They are capable of rapid population growth through rapid reproduction and adhering to small sizes. They prefer eutrophic conditions and are associated with instability of environmental conditions.

K-strategists - highly specialized forms. They live in poor-nutrient water. They are characterized by long individual life and low reproductive potential, and generally larger sizes. They are associated with oligotrophic environments that guarantee stable environmental conditions.

In the center are the so-called **R/K-strategists** (intermediate forms) living in a mesotrophic environment (Petrizzo, 2002). They can be either more K-strategists or more R-strategists. This subgroup is more widespread than more R-strategists (Petrizzo, 2002; Nederbragt et al., 1998).

r-strategists	r/k-intermediates		k-strategists
	more r-selected	more k-selected	
Simple morphotypes, small-sized	Low to medium trochospiral morphotypes with subglobular chambers without keels	Trochospiral morphotypes with hemispherical chambers and marginal keel(s)	Complex morphotypes with single or double keels
Opportunistic taxa			Specialist taxa

Tab.2 Life strategy and morphology of planktonic foraminifera (from Petrizzo, 2002).

2.4 Ecological preference of planktonic foraminifera species.

In the Mediterranean Sea the temperature, salinity, presence of eddies and gyres and nutrients gradients between Western to Eastern part of the basin have the main control on modern planktonic foraminiferal distribution patterns (e.g. Thunell, 1978; Pujol and Vergnaud-Grazzini, 1995). Because of this planktonic foraminifera fossil assemblages can be considered a perfect proxies for paleoclimatic and paleoceanographic researches.

The anoxic or dysoxic sedimentation during periods of sapropel deposition prevents bioturbation, hence allowing highly resolved reconstructions of planktonic foraminiferal changes in the time domain. It provides important information on planktonic foraminiferal palaeoecological features (e.g. Thunell et al., 1978; Thunell and Williams, 1983; Ganssen and Troelstra, 1987; Tang and Stott, 1993; Rohling et al., 1997, Hayes, 1999).

Globigerinoides ruber (d'Orbigny 1839)

Globigerinoides ruber is the most frequent species in tropical to subtropical waters
of the global ocean (e.g., Bé 1977; Schiebel and Hemleben, 2017). *Globigerinoides ruber* bears dinoflagellate symbionts similar to those occurring in other *Globigerinoides* species and O. universa (Hemleben et al. 1989).
Both pink and white varieties appear to range among the shallowest dwelling planktonic foraminifera out of all modern species (e.g., Bé 1977). *Globigerinoides ruber* is thought to be a tolerant species to low sea surface salinity (SSS), caused by continental fresh water runoff into the ocean (Deuser et al. 1988; Guptha et al. 1997; Ufkes et al. 1998; Schmuker 2000; Schmuker and Schiebel 2002; Rohling et al. 2004).

Although this species is able to tolerate a broad range of temperatures and salinities, it usually thrive in the warm, nutrient-poor waters of the summer mixed layer well above the thermocline and nutricline (Hemleben et al., 1989). In the Mediterranean, the highest frequencies are found at the end of summer. At that time, it occurs all over the Mediterranean, but maximal densities are recorded east of the Sicilian Strait and in the Ionian basin at in the 50-100 m water-depth (Pujol and Vergnaud Grazzini 1995).

Globigerinoides sacculifer (Brady 1877)

Ecology: *Globigerinoides sacculifer* is an abundant tropical to subtropical surface dweller (e.g., Bé 1977; Schmuker and Schiebel 2002, Schiebel and Hemleben, 2017). It is one of the most investigated planktonic foraminifera species in laboratory culture, and a large amount of experimental ecological data are available for this species (e.g., Hemleben et al. 1977; Spero and Lea 1993). *Globigerinoides sacculifer* bears dinoflagellate symbionts, feeds mostly on calanoid copepods, and reproduces on a synodic lunar cycle (Hemleben et al. 1989; Bijma et al. 1990a; Erez et al. 1991). *Globigerinoides sacculifer* is a euryhaline species tolerating salinities between 24 and 47 PSU, and temperatures ranging from 14 to 32 °C (Bijma et al. 1990b). *Globigerinoides sacculifer* is one of the most frequent species in oligotrophic surface waters (e.g., Naidu and Malmgren 1996a; Conan and Brummer 2000; Schiebel et al. 2004). In the northwestern Mediterranean Sea, data collected over ten years in sediment traps show that this species increases in abundance in late summer/early fall (Rigual-Hernández et al., 2012).

Globigerina bulloides (d'Orbigny 1826)

Globigerina bulloides mainly dwells above the thermocline within the upper 60 m of the water column, and is a non-symbiotic species usually associated with temperate to sub-polar water masses, as well as upwelling (Schiebel and Hemleben, 2017). *Globigerina bulloides* is equally characteristic of upwelling environments in lower latitudes (e.g., Thiede 1975; Bé and Hutson 1977; Kroon and Ganssen 1988; Naidu and Malmgren 1996a, b; Conan and Brummer 2000; Seears et al. 2012), as of seasonally enhanced primary production at mid and high latitudes (e.g., Bé and Tolderlund 1971; Bé 1977; Ottens 1992; Schiebel and Hemleben 2000; Chapman 2010). Moreover, in the Mediterranean Sea this species occurs in significant abundances in winter and

spring (Pujol and Vergnaud-Grazzini, 1995; Rigual-Hernández et al., 2012). High frequencies are observed between 50 and 200 m water depth in the western Mediterranean (Pujol and Vergnaud-Grazzini 1995). In contrast to most spinose species, an important part of the diet of *G. bulloides* consists of algae, as indicated by the olive green to brownish coloration of its cytoplasm in freshly collected specimens and shown by transmission electron microscopy.

Orbulina universa (d'Orbigny 183*9)*

Orbulina universa tolerates a wide range of temperature and salinity values and is abundant from tropical to temperate waters (e.g., Hemleben et al. 1989 and references therein; Bijma et al. 1990b; De Vargas et al. 1999; Chapman 2010). This taxon lives in the mixed layer (Bé et al., 1985; Vergnaud-Grazzini et al., 1986; Thunell and Reynolds, 1984) and deeper waters (Fairbanks et al., 1982; Almogi-Labin, 1984; Bé et al., 1985). It generally prefers surface waters with temperatures between 13°C and 19°C. Its symbiont activity may also partly control its distribution (Spero and Parker, 1985). In the Mediterranean, *O. universa* is more prolific at the end of summer in the 50-100 m depth interval along the North African coast and around the Balearic Isles (Pujol and Vergnaud-Grazzini 1995). *Orbulina universa* is mostly carnivorous, particularly during its spherical adult ontogenetic stage. Pre-adult stages may prefer herbivorous diet (Anderson et al. 1979).

Turborotalita quinqueloba (Natland 1938)

Turborotalita quinqueloba is one of dominant species in the modern ocean.
Standing stocks of *T. quinqueloba* in the Arctic Ocean reach up to several hundreds of specimens (>63 μm) per cubic meter at the sea-ice margin (Carstens et al. 1997), following an overall enhanced primary production and food availability (Volkmann 2000a). *T. quinqueloba* is a eurythermal (shallow dweller) species that increases production during diatom blooms (in spring) (Sautter and Thunell, 1991). The temperature range for this taxon is 2.2°C - 16°C, with optimum between 4.6°C and 10.8°C (Tolderlund and Bé, 1971). It reaches the highest concentrations in upwelling regions or in areas of vigorous mixing in water column (Reynolds and Thunell 1985) where high phytoplankton productivity prevails.

***Neogloboquadrina dutertrei* (d'Orbigny 1839)**

Neogloboquadrina dutertrei is frequent in tropical to subtropical waters and may be present in temperate waters during summer (e.g., Bé 1977; Kemle-von-Mücke and Hemleben 1999; Schiebel and Hemleben 2000). In the eastern tropical Atlantic, *N. dutertrei* occurred at maximum standing stocks at the Deep Chlorophyll Maximum (DCM) (Ravelo et al. 1990). Along hydrographic fronts of the nutrient rich Congo River fresh water plume, and in the western Caribbean Sea (Amazon/Orinoco River discharge), *N. dutertrei* occurred at increased numbers in surface to thermocline waters, possible displaying an opportunistic behavior to increased food availability at DCM depths (Ufkes et al. 1998; Schmuker and Schiebel 2002). *Neogloboquadrina dutertrei* tolerates salinities and temperatures between 25 and 46 PSU, and 13 °C to 33 °C, respectively, under laboratory conditions (Bijma et al. 1990b).

Neogloboquadrina incompta* (Cifelli 1961) – *Neogloboquadrina pachyderma dx is mostly represented by *N. incompta* type specimens, however due to the large morphological variability we preferred not to count separately *N. pachyderma* dx and *N. incompta. Neogloboquadrina incompta/pachyderma* dx is a typical surface-dwelling species of the temperate ocean (e.g., Cifelli 1961; Fairbanks and Wiebe 1980; Ottens 1991; Kemle-von-Mücke and Hemleben 1999; Kuroyanagi and Kawahata 2004). It is characteristic of subpolar and transitional waters (Bé and Tolderlund, 1971; Cifelli, 1973) that reproduces on a synodic cycle (Schiebel and Hemleben, 2005) that could well live at or below the thermocline (Bé, 1960, 1977; Bé and Ericson, 1963). The distribution in the Mediterranean is almost restricted to the Northern Basin (core top database of Kallel et al.,1997), where it reaches high concentrations in surface waters and at mesopelagic depth during winter (Pujol and Vergnaud Grazzini, 1995). Pujol and Vergnaud Grazzini (1995) suggested that the distribution of this species in the Mediterranean would mainly be controlled by temperature, only being present in those areas where annual SST reach temperatures below 13 °C (Rigual-Hernández et al., 2012). In NW Mediterranean the maximum annual fluxes of *N.pachyderma* dx occur during March in sediment traps, with the period with maximum phytoplankton productivity (Rigual-Hernández et al., 2012). Peaks of maximal abundance of this species are usually found at the depth of maximum chlorophyll biomass when the upper part of the water column is isothermal and cold, what suggests that it feeds on material concentrated at the

DCM level (Pujol and Vergnaud Grazzini, 1995). It can partly explain its increased production when fertility levels are high

Globorotalia inflata (d'Orbigny 1839)

Globorotalia inflata is most abundant in the subtropical to the subpolar ocean. Due to its regionally high standing stocks, and its high fossilization potential, *G. inflata* is of considerable interest as a proxy in paleoceanography (e.g., Dittert et al. 1999; Niebler et al. 1999; Lončarić et al. 2006). *Globorotalia inflata* prefers cool and well-mixed waters with intermediate to high nutrient levels (Pujol and Vergnaud-Grazzini, 1995). It prefers cooling and/or increased seasonal contrast, with vertical mixing during winter. The absence of this species has been observed in many Late Quaternary sapropel layers and this pattern is interpreted as the response to a lack of mixing of the water column, with year-round stratification (Capotondi et al., 2000; Ariztegui et al., 2000; Principato et al., 2003). *G.inflata* has often been found to occur in the vicinity of hydrologic fronts and eddies, in mesotrophic conditions (Lončarić et al. 2007; Storz et al. 2009; Chapman 2010; Retailleau et al. 2011). Is a species that can live in deep levels of the water column because it migrates vertically during its life cycle. During enhanced phytoplankton production in the spring, the cytoplasm has often been found to be greenish due to consumed chrysophytes, or orange in case of diatom prey (Hemleben et al. 1989). In addition to its abundance in pelagic waters, *G. inflata* may dominate the planktic foraminifer fauna at surface (0–40 m) or subsurface (40–100 m) water depths in neritic waters of enhanced food availability, caused by weak topographically driven upwelling over a submarine canyon head in the SE Bay of Biscay (Retailleau et al. 2012).

Globorotalia scitula (Brady 1882)

Globorotalia scitula is a cosmopolitan species most frequent at mid-latitude temperate regions during spring and fall, i.e. during times of increased primary productivity (Schiebel and Hemleben 2000; Schiebel et al. 2002; Chapman 2010; Schiebel and Hemleben, 2017). From mid latitudes towards low and high latitudes, *G. scitula* decreases in abundance (Schiebel et al. 2002). In pelagic waters, *G. scitula* dwells at subsurface waters below the thermocline to 200–300 m depth (Ottens

1992; Schmuker and Schiebel 2002; Retailleau et al. 2011). Itou et al. (2001) propose *a G. scitula-to-N. dutertrei* ratio as a proxy of the mixed layer depth at the Kuroshio-Oyashio confluence off NE Japan. *Globorotalia scitula* may be present in high standing stocks in neritic waters following time-intervals of enhanced primary productivity (Retailleau et al. 2012). In neritic waters <200 m waters depth, *G. scitula* may be most frequent in the surface water column (Retailleau et al. 2011). *Globorotalia scitula* co-occurs with *G. hexagonus* in the upper Oxygen Minimum Zone (100–200 m depth) of the central Arabian Sea, which may possibly indicate a preference in diet than low-oxygen conditions (cf. Baumfalk et al. 1987). In the western Arabian Sea off Somalia, *G. scitula* increases in number during the late phase of SW monsoonal upwelling (Conan and Brummer 2000).

Globorotalia truncatulinoides (d'Orbigny 1839)

G. truncatulinoides is a very deep dwelling species (Tolderlund and Bé, 1971; Hutson, 1977; Hemleben and Spindler, 1983; Vergnaud-Grazzini et al, 1986; Hemleben et al.,1989) that live between 15.4°C to 22°C (Tolderlund and Bé, 1971; Brummer and Kroon, 1988; Hemleben et al., 1989). In the Mediterranean, this non-spinose taxon prevails during winter in deep waters of the western basin. It seems that the primary factor controlling the distribution of this species within the Mediterranean is the winter convection and vertical mixing whereas food availability and temperature are secondary limiting factors (Pujol and Vergnaud-Grazzini 1995). *Globorotalia truncatulinoides* probably populates the deepest habitat of all extant species, having been sampled alive from the water column below 2000 m water depth (Schiebel and Hemleben 2005). *Globorotalia truncatulinoides* was found to reproduce once per year, i.e. in late winter in surface waters at different regions at the poleward margin of the subtropical gyres (Bé and Hutson 1977: Indian Ocean; Weyl 1978: North Atlantic; Hemleben et al. 1985: Bermuda; Kemle-von-Mücke and Hemleben 1999: South Atlantic; Schiebel et al. 2002: Azores), and this is probably true for the Pacific Ocean (cf. Bé 1977). It is speculated that *G. truncatulinoides* generally reproduces in surface waters to provide sufficient food for offspring (compared to deeper waters), and to avoid competition or predation. In the subtropical ocean towards higher latitudes, *G. truncatulinoides* dwells at decreasing water depths, possibly driven by the availability of food. A similar shoaling

of habitat towards the poles has been observed in other subsurface dwelling globorotalid species like *G. crassaformis* (Hemleben et al. 1985).

Globorotalia truncatulinoides may enter marginal basins like the Mediterranean Sea and the Caribbean Sea through shallow and narrow passages and occurs at some distance from the passage at subsurface depth (e.g., Schmuker and Schiebel 2002). Globorotalia truncatulinoides is absent from the modern Red Sea and Arabian Sea (e.g., Ivanova et al. 2003). In the Arabian Sea, *G. truncatulinoides* was present in low standing stocks during the past glacials, possibly imported by currents from the southern Indian Ocean (e.g., Auras-Schudnagies et al. 1989; Ivanova et al. 2003).

Globigerinita glutinata **(Egger 1893)**

Globigerinita glutinata is possibly the most ubiquitous planktonic foraminifera species in the modern ocean. *Globigerinita glutinata* is most abundant in subtropical to temperate waters, and decreases in frequency towards high latitudes (cf. Ottens 1992; Schiebel and Hemleben 2000; Volkmann 2000a; Schmuker and Schiebel 2002). In the NE Atlantic, G. glutinata is present in surface waters throughout the year and constitutes up to 20 % of the live fauna during spring, following enhanced phytoplankton production in surface waters (Schiebel et al. 1995; Schiebel and Hemleben 2000; Chapman 2010). A second seasonal maximum of *G. glutinata* in the NE Atlantic occurs in fall, when wind-driven nutrient entrainment into surface waters triggers phytoplankton production at the nutricline (Schiebel et al. 2001). Similarly, the occurrence of *G. glutinata* in the Gulf of Aden is related to nutrient entrainment into surface waters during the NE monsoon (Ivanova et al. 2003). With up to 35 individuals per cubic meter, *G. glutinata* is the second most frequent species in the Caribbean Sea after *G. ruber* and may be related to eddy-driven nutrient entrainment into surface waters, and phytoplankton production (Schmuker and Schiebel 2002). Calcification depths of *G. glutinata* tests range from surface waters down to thermocline depths (Lončarić et al. 2006; Friedrich et al. 2012).

3. Materials, site setting and the Oceanographic Cruise Transect_17

During the first phase of the research was important to select few cores belonging to CNR-ISMAR (Istituto delle Scienze Marine, Naples) and given for usage of that research. It is important

to choose the cores which are in appropriate distance from the coast, so far from the anthropogenic pollution, major river and volcanoclastic inputs, in order to avoid too strong dilution of fossil assemblages due to very high sedimentation rates. The best cores are that with normal marine sedimentation. To understand it was needed to study geomorphological maps of the sea bottom and in some cases deciding after opening the core to control, if the sediment is not too sandy or too clayey, which would be a difficulty with finding the proper number of the Foraminifera.

Three cores were selected for this study, among those stored in the Naples CNR-ISMAR archive. These cores were recovered in the Gulf of Naples (GMS_98-01 C14, GMS_91-01 C58 and Transect_2017 TR1). Moreover, additional data were obtained fom the core GNS84-C106, recovered in the Gulf of Salerno (Buccheri et al., 2002) **(Fig.12)**.
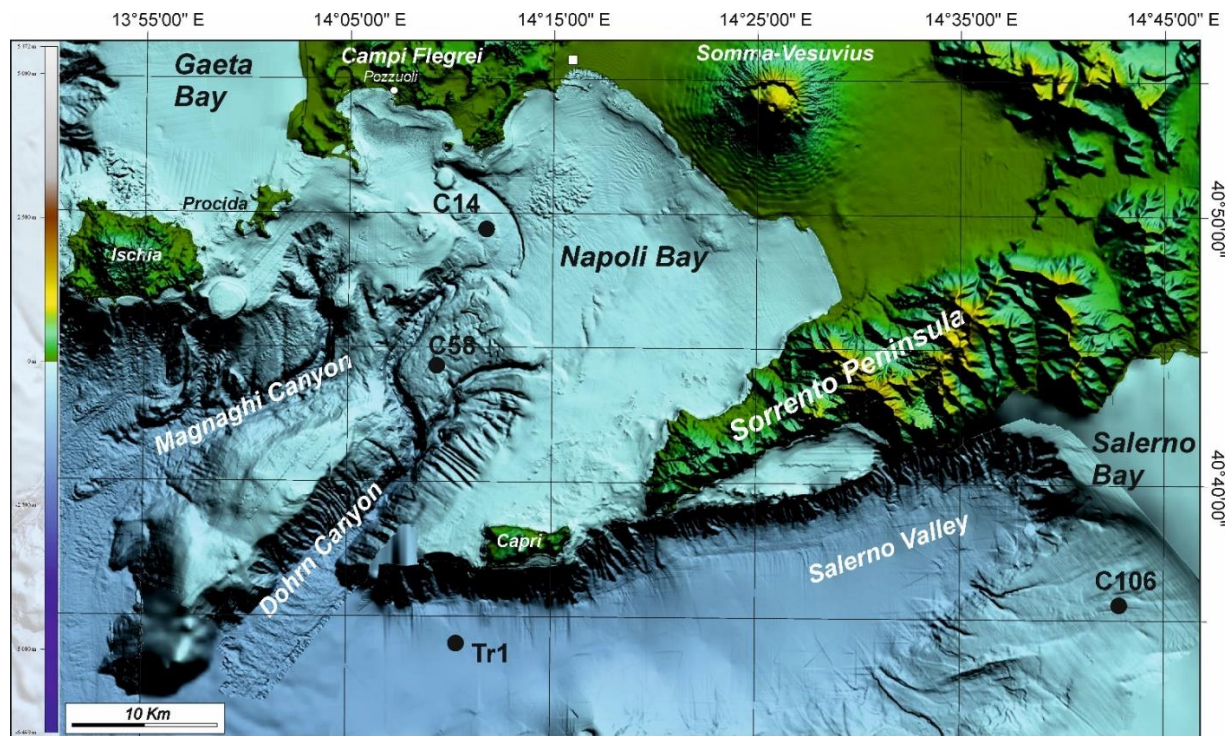

Figure 12 Base map with the location of all the cores: GMS_98-01 C14, GMS_98-01 C58, GMS_84 C106, Transect_2017 TR1.

The Oceanographic Cruise Transect_17

Aims of the Oceanographic cruise

The Cruise had place from 6th of October till 17th of October 2017, during which was possible to take the new cores from nearby of Capri island and make seismic profiles of that area.

The Oceanographic Cruise Transect_17 stems from the collaboration between ISMAR-CNR Naples, University of Palermo, University of Catania, University of Naples, INGV-Roma1 and private companies (Geo Marine Survey Systems (Rotterdam, The Netherlands) and GeoSurveys (Aveiro, Portugal)). The aim of the study was to understand tectonics and active geodynamic processes in the marine and coastal areas, and the recognition and mapping of shallow structures associated with active tectonic and volcano-tectonic deformations of selected areas of the Italian continental margin. Another aim of the Oceanographic Cruise was to obtain with a gravity corer (fig.13) three cores near the Capri island (tables 3-4), in specific South Capri, Banco Di Fuori and Alto Sele plus a fourth core in the Offshore Licosa, on the base which will be received paleoecological, sedimentological and stratigraphic view for that areas.

The survey area included a transect across the eastern Tyrrhenian margin, with especial reference to the underwater volcanic submerge of the Phlegrean Fields and the Campania continental margin between Palinuro Seamount and P.ta Licosa. In that areas have been acquired:

1. High resolution reflection multichannel seismic tomography (3D) with two 2kJ sparker sources with two 2 kJ sparker sources and four 48-channel streamers, sub-bottom Chirp, multibeam bathymetry and gravity cores (Pozzuoli and Naples Bay);

2. Single-channel 1.5 kJ sparker reflection seismic profiles, sub-bottom Chirp, multibeam bathymetry, magnetometry and gravity cores (morpho-structural high between Palinuro Seamount and P.ta Licosa).

Technical parameters of the vessel Minerva Uno

The vessel Minerva Uno is about 41m long operated by the company SO.PRO.MAR. on behalf of CNR. The vessel is used for geological, geophysical, biological research in the Mediterranean and in the neighboring areas, included the Black Sea. Minerva Uno is equipped with DGPS and SEAPATH (satellite linking system FURGO), single beam and multibeam echo sounds, and another instrumentation for the sampling of deep sea and water columns, and as well for the acquisition of geophysical and oceanographic data (as for example ADCP, CHIRP SBP and another sonar sensors).

Parameters of the core TR1 taken during the Oceanographic Cruise:

Istituto	CNR - ISMAR	Data:	10/12/2017	Strumento:	Gravity corer
		Ora:	18:30		
Campagna:	TRANSECT_2017	Lat (° ')	40° 29.31' N	Nome:	**TR1**
		Lat (° ' ")	40° 29' 18.6000" N		
Nave:	MINERVA UNO	Long (° ')	14° 10.39' E	Operatore:	Joanna Jamka
		Long (° ' ")	14° 10' 23.4000" E		
Zona:	Capri Sud	Lung. Camp.:	5.195 m	Prof. (m):	1055.0

Table 3. Gravity core TR_1, Location: Capri Sud

N. spez./camp.	Lung. Liner (m)
A	1.000
B	1.000
C	1.000
D	1.000
E	1.000
F	0.195

Table 4. The length of the core. Sample taken from the top: Dark grayish clayey silt.

Methodology of taking the core with the gravity corer:

Gravity Corer is a simple and reliable instrument for collecting sediment cores from coastal and deep water sites for sample analysis. The corer uses the pull of gravity to penetrate the seabed with its carbon steel core barrel, which can collect samples of up to six meters in length. The entire corer is made from carbon steel and is fitted with stabilizing fins to ensure that the corer penetrates the seabed in a straight line. A replaceable core liner is housed within the carbon steel barrel to ensure

that it is simple to remove the collected sample. The barrel is fitted with a sharpened replaceable carbon steel core cutter to ensure minimal disturbance. Sample loss on retrieval is minimized by a core catcher fitted inside the end of the barrel.
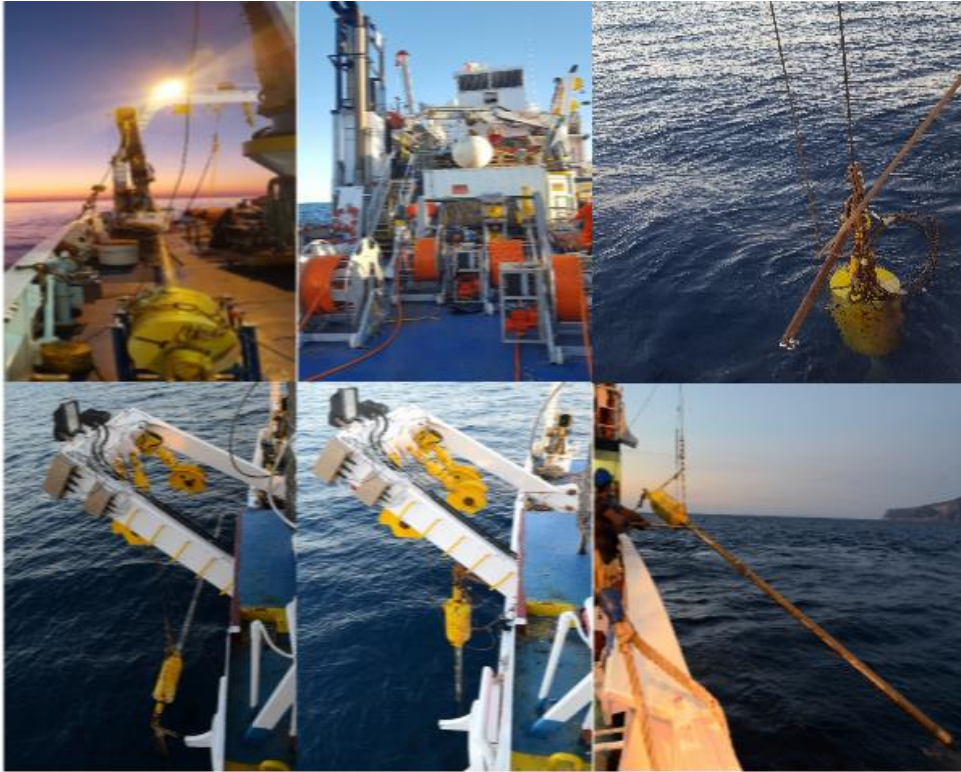

Figure 13 Gravity corer and operation of taking the cores, and geoseismic instrumentations on the board of the vessel Minerva Uno.

3.1. Cores description and analysis.

The data presented in this table include 4 marine cores (Table 5).

Core	Location	Depth	Length
GNS84-C106*	14°42.40' E; 40°28.87' N	292 m	617 cm
TRANSECT_2017 TR1	14°10.39' E; 40°29.31' N	1055m	516 cm
GMS_98-01 C14	14°11.30' E; 40°44.47' N	186.5m	521 cm
GMS_98-01 C58	14°09.17' E; 40°39.20' N	335 m	366 cm

*see Buccheri et al., 2002;

Table 5. The four studied cores with their location, depth and length.

Core Transect_2017 TR1

The gravity core TR1 (fig. 14 and 15) is located close to the southern part of Capri Island, in the Gulf of Naples (40° 29.31' N, 14° 10.39' E, eastern Tyrrhenian), at a water depth of 1055m and with a the length 5.16 m.

Fig.14 Snapshot of the gravity core Transect_2017 TR1, from the Capri Island offshore (grants to Monica Capodanno, CNR-ISMAR).
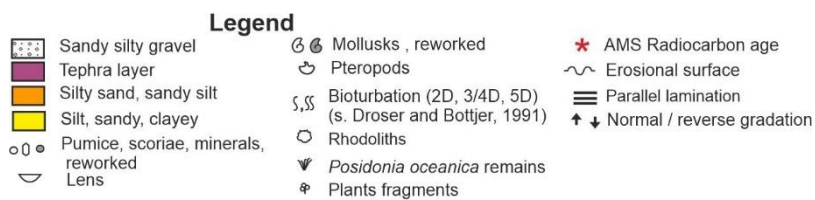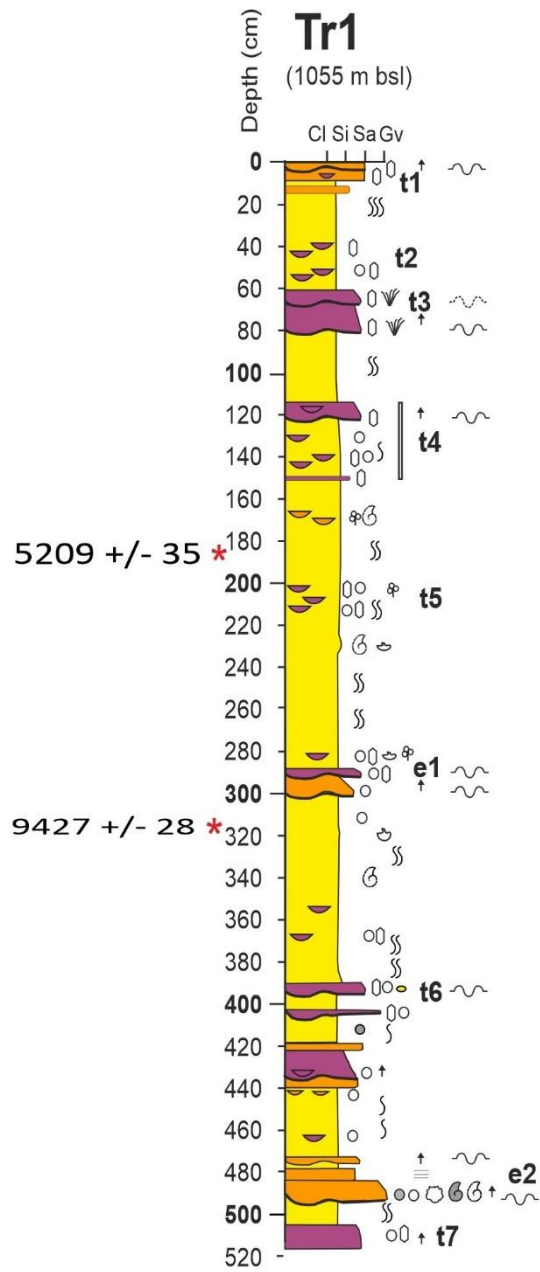
Figure 15 Log of the core Transect_2017 TR1 with calibrated radiocarbon age points.

The core is represented mostly by sandy, clayey silt with sandy events, mostly tephra layers or tephra lenses from the eruptions of Vesuvius, Campi Flegrei and Ischia. The core can be divided on three facies.

Facies **a** (319-516 cm below sea floor (cmbsf)) consists mostly of silty clayey sand and sandy clayey silt interrupted by a number of tephra layers (real tephra and reworked ones) and shows some erosive layers, parallel lamination, normal gradation and bioturbated. From the 504-516cmbsf is very fine clayey silty sand: tephra layer (Neapolitan Yellow Tuff, identified by Prof. Petrosino and Prof. Insinga); reworked tephra from 473-494cmbsf with grey and white pumices, rhodoliths and a lot of mollusks; 466-467cmbsf: tephra lens; 419-441cmbsf dark grey volcanic sand with white pumices and scoria; 408-419cmbsf olive grey clayey silt (volcanic with bioclasts and with white sharp pumice, scoria and sanidine; 391-396cmbsf very dark grey tephra layer (Pomici Principali) (medium/coarse sand, good sorting, white and dark pumices, scoria and sanidine and lithoclasts from Vesuvius, and borrowing. All of that layers inside of hemipelagic sediment, olive grey clayey sandy silt with some bioclasts.

Facies **b** (150-319cmbsf) – consists of olive grey clayey sandy silt hemipelagic with bioclasts (foraminifera, gastropods, bivalves, radiolaria, ostracoda, big pteropods and plants fragments). The sediment is bioturbated and shows distinctive erosive surfaces and wo tephra layers were identified. From 287-293cmbsf (tephra lens Vesuviane) very dark grey fine silty sand and 201-208cmbsf, there are tephra lens (Piano Liguori) that consist of dark grey silty medium/coarse sand with obsidian, mica, pyroxene, augite and sanidine.

Facies **c** (0-150cmbsf) – consists mostly of olive grey clayey sandy silt with bioclasts. It has normal gradation, big bioturbation and erosive surfaces. The sediment is mixed with volcanic sand from the tephra layers. There are abundant tephra lenses and also reworked tephra with *Posidonia* accompanying the eruption of Vesuvius 79CE. The main tephra events are: 127-144cmbsf the range with tephra lenses from eruptions of AP with very dark grey and white, quite sharp pumices and sanidine; 60-80cmbsf Somma-Vesuvius eruption 79CE with a lot of *Posidonia.* It is characterized by a very fine sandy silty with sanidine and good sorting; 28-47cmbsf: range with tephra lenses from Pollena eruption; 7-8cmbsf 1631+medieval eruption characterized by a dark grey tephra lens with quite sharp black pumices. Sedimentation rate in this facies is much lower than in others.
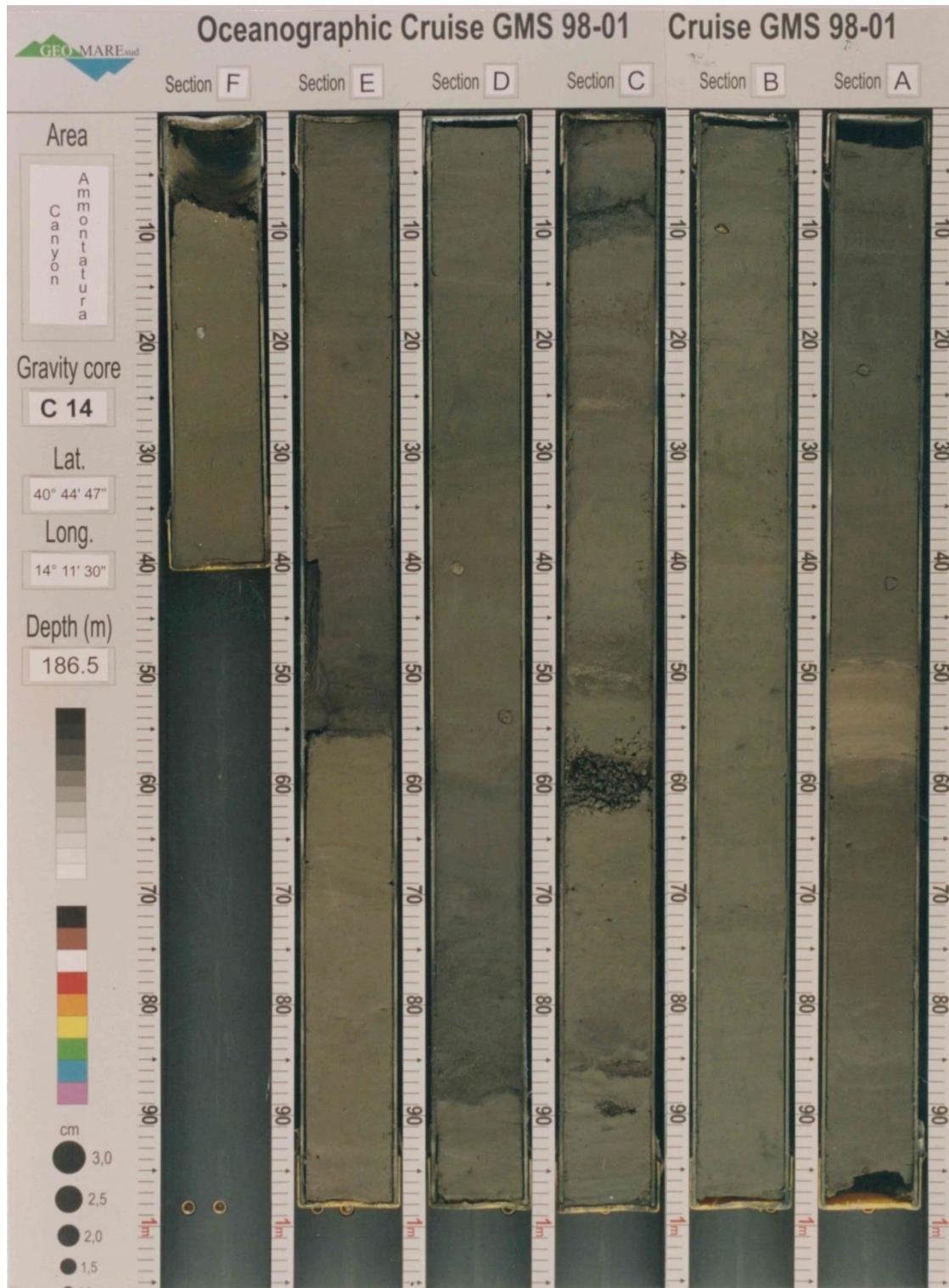
Core GMS_98-01 C14.

Figure 16 Snapshot of the core GMS_98-01 C14, located in the Ammontatura Canyon (Grants to Monica Capodanno, CNR-ISMAR).

The gravity core C14 (fig. 16 and 17) is located in Ammontature Canyon in the Gulf of Naples (40° 44.47' N, 14° 11.30' E), next to the Gulf of Pozzuoli (eastern Tyrrhenian) and was recovered at 186.5 m depth with a recovery of 521 cm of sediments. Mostly the sediment in the core is hemipelagic clayey silt interrupted by the tephra events or tephra lenses. The tephra were identified by Prof. Petrosino and Prof. Insinga.
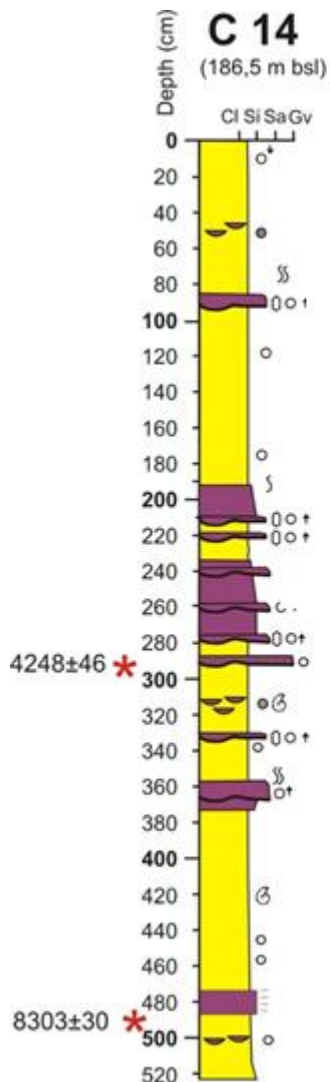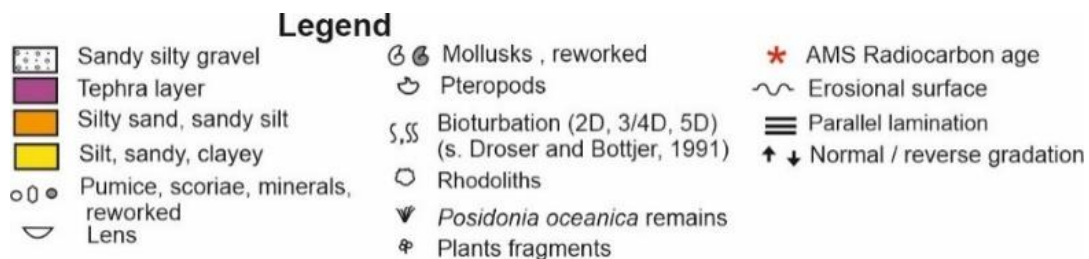

Figure 17 The log of the core GMS_98-01 C14 with dated tephra (Petrosino et al., 2018) and the calibrated radiocarbon ages.

In the following, there is a short description of lithological and sedimentological features.

488–521cmbsf – sandy clayey silt with tephra lenses (500cmbsf) with pumices.

474-488cmbsf – tephra layer (Mercato + Fondi di Baia).

370-474cmbsf – clayey silt with pumices and mollusks.

358-370cmbsf- tephra layer with pumices and normal gradation.

336-358cmbsf - clayey silt strongly bioturbated with some white pumices.

332-336cmbsf - tephra layer with pumices, some dark minerals and normal gradation.

294-332cmbsf - clayey silt with tephra lenses (310cmbsf) with reworked pumices and Mollusks.

290-294cmbsf – tephra layer (Averno2).

280-290cmbsf – clayey silt.

236-280cmbsf – tephra layer with some dark minerals and pumices and normal gradation (Miseno).

222-236cmbsf – clayey silt.

218-222cmbsf – tephra layer with some dark minerals and pumices.

215-218cmbsf – clayey silt.

192-215cmbsf – tephra layer with pumices, some dark minerals and normal gradation (Astroni).

94-192cmbsf – clayey silt slightly bioturbated and with pumices.

84-94cmbsf – tephra layer with some dark minerals, pumices and normal gradation.

0-84cmbsf – clayey silt strongly bioturbated with pumices and reverse gradation with tephra lenses (50cmbsf) with reworked pumices.

Core GMS_98-01 C58

The gravity core C58 (fig. 18 and 19) is located in the Dohrn Canyon in the Gulf of Naples (40° 39.20' N, 14° 09.17' E eastern Tyrrhenian), at 335 m water depth, with a recovery of 366 cm of sediments. In comparison with the nearest core C14, the C58 has much more silty sand, less hemipelagic sandy silt interrupted with tephra events and tephra lenses.

In the following, there is a short description of lithological and sedimentological features.

342–366cmbsf – sandy silt with tephra lenses (350cmbsf) with pumices and some minerals.

300-342cmbsf – silty sand (m/c) with mollusks very strong bioturbation, with tephra lenses (at 340cmbsf and reworked from 330cmbsf) with some dark minerals, pumices and reworked pumices.

294-300cmbsf – tephra layer with erosive surface, reworked pumices, some dark minerals, pumices and normal gradation.

274-294cmbsf- silty sand (m) with mollusks and rhodoliths.

270-274cmbsf – tephra layer with erosive surface and reworked pumices.

250-270cmbsf – silty sand (f/m).

244-250cmbsf - tephra layer with erosive surface, pumices, reworked pumices and normal gradation.

212-244cmbsf - sandy silt with mollusks and tephra lenses (240 and 220cmbsf).

210-212cmbsf – tephra layer with erosive surface and some dark minerals.

200-210cmbsf – clayey silt.

198-200cmbsf – tephra layer with erosive surface and some dark minerals.

141-198cmbsf – clayey silt with quite strong bioturbation.

137-141cmbsf – tephra layer with erosive surface and normal gradation.

132-137cmbsf – silty clayey silt.

120-132cmbsf – tephra layer with erosive surface, pumices, normal gradation and tephra lenses.

80-120cmbsf – sandy clayey silt with quite strong bioturbation and pumices.

76-80cmbsf – tephra layer with some dark minerals, erosive surface and quite strong bioturbation.

46-76cmbsf – clayey silt with quite strong bioturbation.

40-46cmbsf – tephra layer with erosive surface, some dark minerals and pumices.

0-40cmbsf –sandy clayey silt with tephra lens (20cmbsf) with reworked pumices.
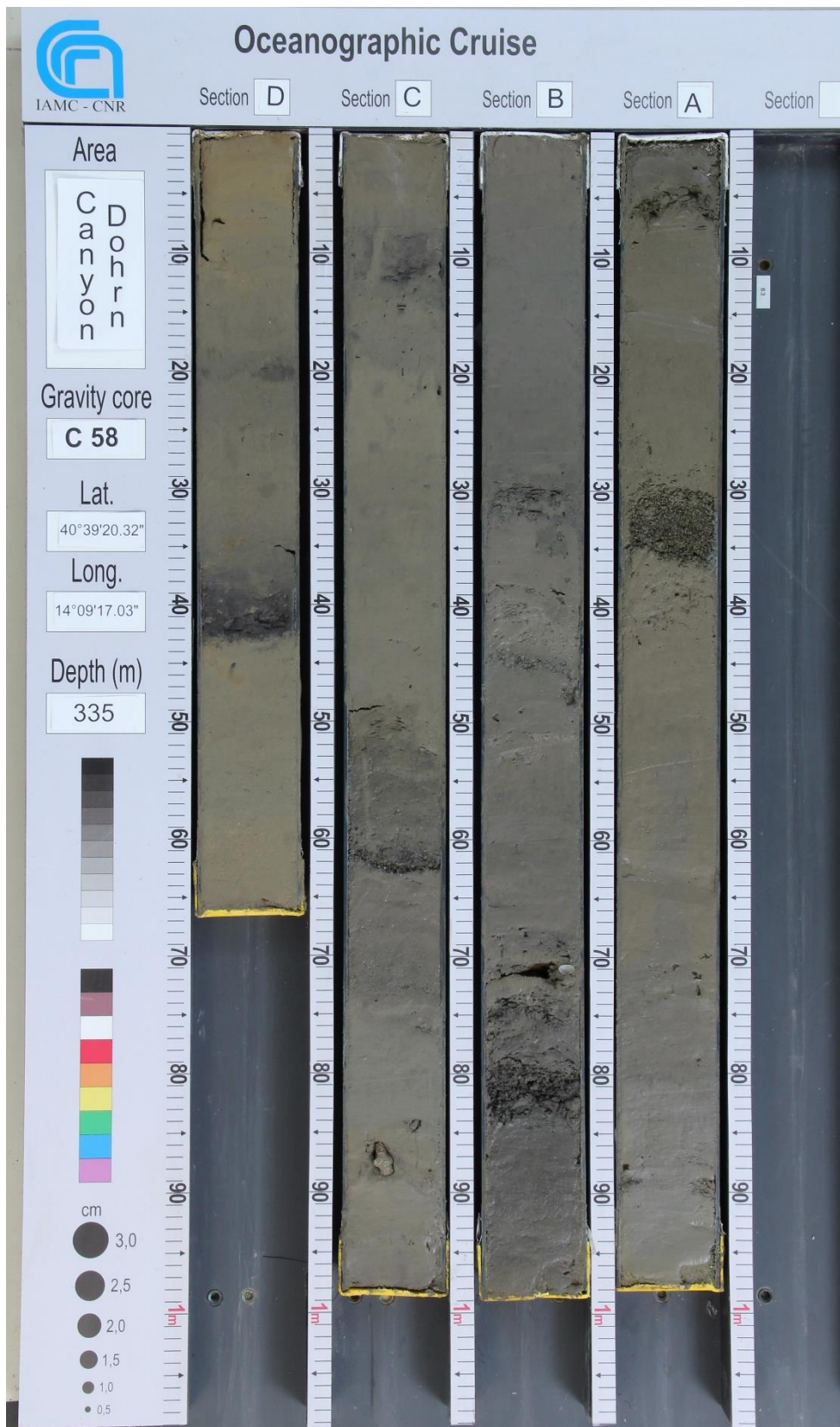
Figure 18 Snapshot of the core GMS_98-01 C58 located in the Canyon Dohrn (Grants to Monica Capodanno, CNR-ISMAR).

Figure 19 The log of the core GMS_98-01 C58 with dated tephra (Petrosino et al., 2018) and the calibrated radiocarbon age.

Core GNS84-C106.

Figure 20 Stratigraphy and sedimentology of core C106. Legend: (a) sandy silt; (b) silt, clayey silt and/or silty clay; (c) pumice level; (d) sharp contact; (e) erosional contact. In figure: C=clay; S=silt; G=gravel; SkI =inclusive graphic skewness; KG =graphic kurtosis; Md =median diameter. (From Buccheri et al., 2002)

The gravity core C106 (fig. 20) from the Gulf of Salerno is 6.17 m long, was collected off the Sele River mouth (40º28'N,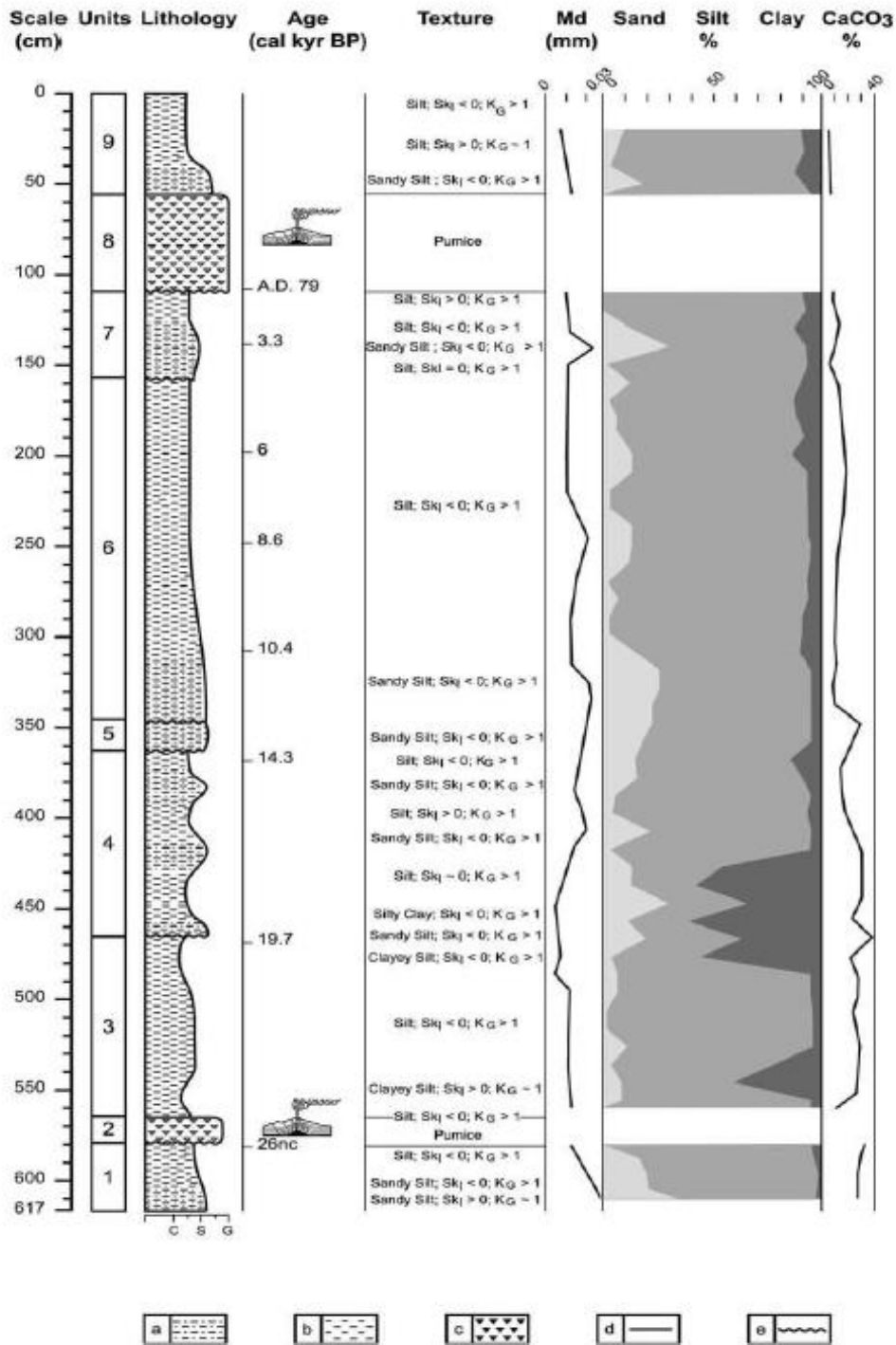 14º42' E) at a depth of 292 m, beyond the continental shelf break, in a basin on the continental slope (Buccheri et al., 2002) and already studied before and described in previously published papers. Previous studies on this core were aiming at reconstructing characteristics and architecture of sediments along the continental shelf based on seismic profiles, geomineralogical and sedimentological analyses (Buccheri et al., 2002; Naimo et al., 2005). Paleontological studies (planktonic foraminifera, palynomorphs, nannofossils, ostracods and pteropods) provided paleoclimatic trends, in agreement with changes in the isotopic composition of oxygen.

That core was included within this research because it had very good record, is already well dated (the bottom is 34 ky old) with the volcano event – 79CE Vesuvio represented by a 50 cm thick pumice layer. In the current research, more benthic and planktonic foraminifera data were kindly provided by Prof. Valentino Di Donato).

In Buccheri et al. (2002), the Core GNS84-C106 was divided on 9 units on the basis of lithology and sedimentology (Fig. 20):

1 unit (617 – 579-6cmbsf): olive grey sandy silt and dark grey silt at the top of the unit. Inside the sediment are numerous fragments of bioclasts and fine sand lenses. The calcium carbonate ranges from 30 to 35%. That unit was dated for 28-29 ka.

2 unit (579 – 565 cmbsf): light grey to olive grey colour sub-rounded pumices and ashes. The lower part rests on an erosive contact. This is the level of tephra Y3 of the Campi Flegrei, dated at 26 ka BP (Keller, 1981).

3 unit (565 – 465 cmbsf): alternating silty clay and silt, from gray to olive gray, with rounded pumice and unidentifiable fragments of shells. The sediment is moderately sorted at the bottom and very little sorted at the top. From 550 to 493 cmbsf there is a black silt lens. The amount of calcium carbonate ranges from 24.5% to 40%. This unit is dated 26- 19.5 ka.

4 unit (465 – 363 cmbsf): alternating sandy silt, from gray to olive gray, little sorted, loosely sorted silty clay, moderately sorted silt rich in fragments of shells (molluscs, briozoa, worm tubes). The basal contact is of the erosional type. The calcium carbonate content ranges from 14.5 to 34%. This unit is dated 19.5 - 13.9 ka.

5 unit (363- 346 cmbsf): bad sorted olive gray sandy silt with bioclasts. The contacts at the bottom and at the top are erosional. The calcium carbonate content ranges from 28.5% to 32.5%. It is dated 13.9 - 12.8 ka.

6 unit (346 – 157 cmbsf): bad sorted sandy silt, with colors ranging from dark gray to dark olive gray, grading towards the top with moderately sorted silt, rich in fragments of shells (molluscs) and a low content of organic matter; presence of pumice rounded to the bottom. Carbonate ranges from 12.5 to 23.5%. This unit is dated 12.8 - 4 ka.

7 unit (157 – 110 cmbsf): moderately sorted silt: black, olive gray and olive at the bottom, with a sandy silt bad sorted at about 140 cmbsf and moderately sorted at the top. The upper and lower contacts are erosive. The carbonate content ranges from 10 to 17.5%. It has been dated from 4 ka to 79 CE.

8 unit (110 – 55.5 cmbsf): at the bottom there are sub-rounded light gray pumices (110 - 88.5 cmbsf), sub rounded gray pumices (88.5 - 61 cmbsf) and black ashes with gray top pumice (61 - 55 cmbsf); This unit has been identified as a fall deposit of the eruption of Vesuvius in 79 CE (called Pumices of Pompei).

9 unit (55.5 – 0 cmbsf): sandy silt bad sorted at the bottom from olive to dark olive gray and silt quite bad sorted at the top; the silt consists mainly of volcanic ash and sand of millimetric pumice.

The core GMS_98-01 C14 was sampled every 1cm and the core GMS_98-01 C58 each 2cm and the core Transect_17 TR1 each 1cm, only bigger tephra layers each 2cm. Every sample then is closed in the plastic bags with the name of the core, which section and from which cm of the core was taken.

3.2 Processing the samples in the laboratory.

All the samples were processed in the same way. Each wet sample of ~20g was dried in 105°C and washed over sieves with mesh-width size of 63 microns. Afterwards to dissolve organic matter was made two times washing with H_2O_2 and then once with H_2O. Sediment minor than 63microns is needed for granulometric analysis. Samples were sieved with the following size mesh: 2000, 1000, 500, 250, 125, 63, <63microns and weighed.

Processing and preparation of all the samples has been done in the sedimentological laboratories of CNR- ISMAR (Naples).

Fig. 21 Snapshots on different activities carried out on the studied cores, including benthic and planktonic foraminifera analysis, lithological description, sediment sampling and TOC analysis.

3.3 Quantitative analysis of planktonic and benthic foraminifera.

Samples for quantitative micropaleontological analyses were taken every 5 cm, sometimes if needed more often or each 10cm, depends on a sedimentological feature of the studied core. At least 300 specimens of planktonic foraminifera were analysed on both 106- and 150-micron size

fractions. The 150-micron size fraction was used to perform quantitative SST reconstructions, according to the modern core top assemblages reference dataset (Prell et al., 1999; Hayes et al., 2004; Kucera et al., 2004). However, the analysis of this size fraction may bias the relative abundance of small sized species, such as *T. quinqueloba.* In order to better highlight trend of these species, the >106-micron size fraction seem to be more suitable (Di Donato et al., 2015). More than 300 specimens were analyzed for benthic foraminifera assemblages, in the size fraction > 106 microns. For the quantitative analysis was used a microscope Olympus SZX12.

3.4 TOC – Total Organic Carbon method.

Total Organic Carbon analyses from 65 samples from the core Transect_2017 TR1 were kindly performed by Dott. Paola Rumolo et the CNR-ISMAR of Naples. Sediments were treated with 1 M HCl. This process was repeated three/four times in order to completely remove carbonates. Samples were then dried (60 ℃) in an oven and weighed (15–20 mg) in silver capsules. Total organic carbon (TOC) and total nitrogen (TN) were measured on freeze-dried powdered samples by a Thermo Electron Flash Elemental Analyzer (EA 1112) with combustion and reduction temperatures of ~1020℃ and 680 ℃, respectively (Verardo et al., 1990). The external standard was acetanilide (C8H9ON, elemental composition: 71.09% carbon and 10.36% nitrogen). Samples were run with blank cups and known acetanilide standards in order to correct the C and N associated with tin/silver cups and calibrate for elemental analysis. Detection limits for TOC and TN are 0.07% and 0.01%, respectively.

C/N ratio (carbon/nitrogen) = TOC/TN

3.5 Granulometric analysis – diffractometer and sedimentological features.

Grain-size analyses (fig. 22 and 24), performed at ISMAR in Naples, followed wet-sieving of samples which minimizes pumice breakage and facilitates the separation of fine ash coatings from larger clasts. The sandy fraction was separated with wet sieving using a sieve >125 μm and successively dry sieved by hand. Grain-size distributions were determined using sieves with mesh sizes spaced at one-phi interval between −2Φ and 3Φ and a Helos/KF/ Quixel Sympatec grain size laser analyzer for the fine fraction (b125 μm). Sedimentological analysis conducted along the split

cores were carried out at cm-scale using both a 10× hand lens and microscope observations of dried-sieved sand and silt (N3 µm) after the wet separation between the coarse and fine fractions.

Measurements in micrometers were converted into the phi (Φ) equivalent value (Krumbein, 1938). Principal statistical parameters were calculated using graphic expressions (Mz,σI) after Folk and Ward (1957). The sedimentological nomenclature used in the classification for grain size of the pyroclastic deposits is from Sohn and Cough (1989) and for the mixed marine portion from Wentworth (1922). The colour of the deposits is determined using a Munsell Soil Color Charts (1994) and the grade of bioturbation according to Droser and Bottjer (1991).
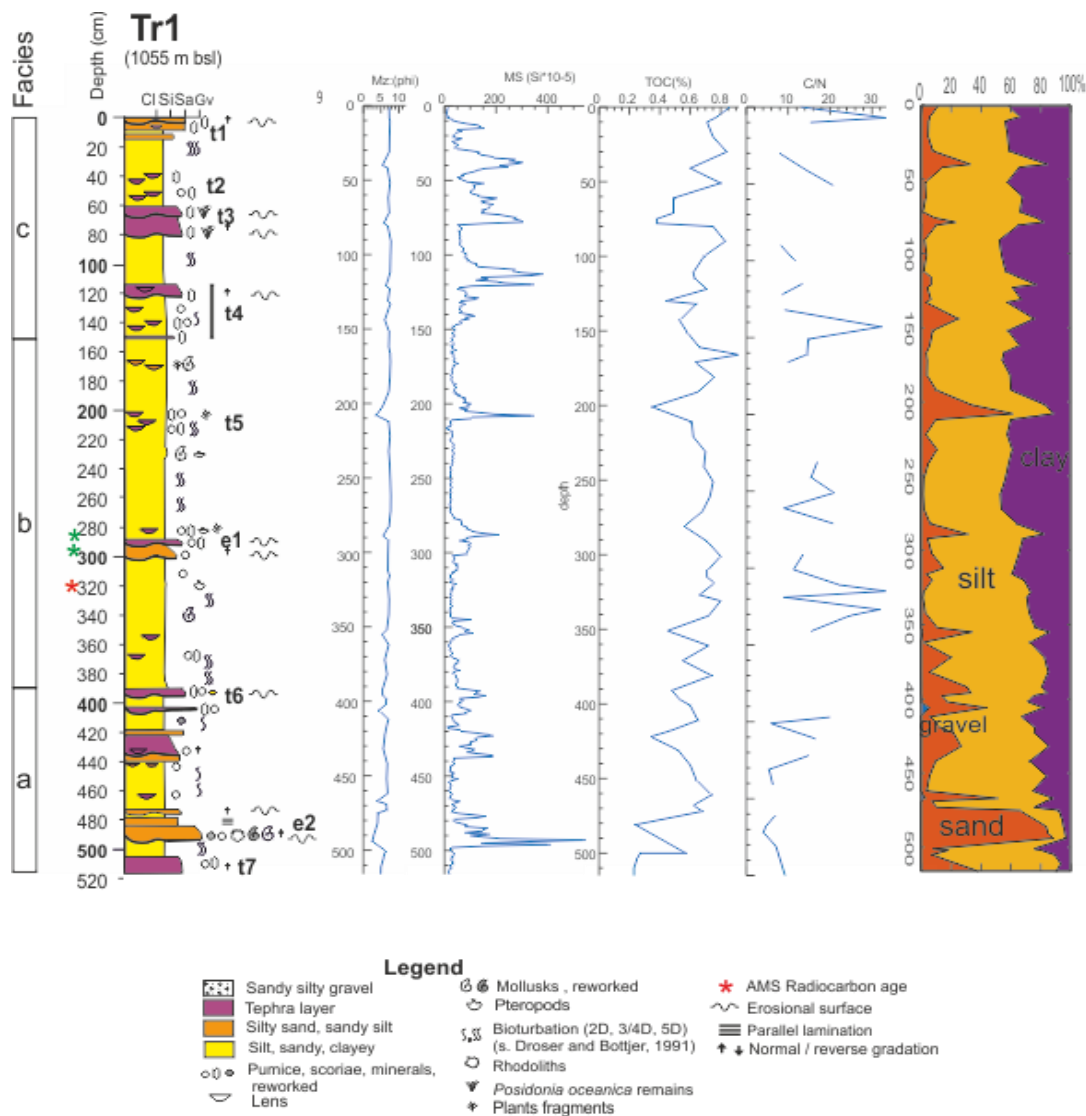

Figure 22 Integrated log of gravity core TR1: a) facies b) Mz: Mean-grain size; c) MS Magnetic susceptibility; d) C/N; e) TOC: Total Organic Carbon: Carbon/Nitrogen.

4. Statistical methods – Compositional Data Analysis (CoDa).

A row vector, x = [x₁, x₂, . . ., xₐ], is defined as a D-part composition when all its components are strictly positive real numbers and they carry only relative information. Indeed, that compositional information is implicitly stated in the units, as they are always parts of a whole, like weight or volume percent, ppm, ppb, or molar proportions. The most common examples have a constant sum κ and are known in the geological literature as closed data (Chayes, 1971). Frequently, κ = 1, which means that measurements have been made in, or transformed into, parts per unit, or κ = 100, for measurements in percent. Other units are possible, like ppm or ppb, which are typical examples for compositional data where only a part of the composition has been recorded; or, as recent studies have shown, even concentration units (mg/L, meq/L, molarities and molalities), where no constant sum can be feasibly defined (Buccianti and Pawlowsky-Glahn, 2005; Otero et al., 2005).

Compositional data are data where the elements of the composition are non-negative and sum to unity. While the data can be generated directly (e.g. probabilities), they often arise from non-negative data (such as counts, area, volume, weights, expenditures) that have been scaled by the total of the components. Geometrically, compositional data with *D* components has a sample space of the regular unit *D*-simplex, *SD*. The key question is whether standard multivariate analysis, which assumes that the sample space is R*D*, is appropriate for data from this restricted sample space and if not, what is the appropriate analysis? Ironically, most multivariate data are non-negative and hence already have a sample space with a restriction to R*D* + (Pawlowsky-Glahn and Buccianti, 2011).

4.1. Sample space.

The sample space of compositional data is the simplex, defined as

$$
\mathcal{S}^D = \left\{ \mathbf{x} = [x_1, x_2, \ldots, x_D] \,\middle|\, x_i > 0, i = 1, 2, \ldots, D; \sum_{i=1}^{D} x_i = \kappa \right\} .
$$

The components of a vector in *SD* are called parts to remark their compositional character (Pawlowsky-Glahn et al., 2011).

In any statistical analysis of data, it is important to recognize the sample space within which one's data lie. It is taken for granted that most data are represented by variables free to vary from -∞ to +∞ within Euclidian space and that classical statistical techniques provide a rich set of tools to deal with these sorts of data. However, compositional data occupy a restricted space where variables can vary only from 0 to 100, or any other given constant. Such a restricted space is known formally as a simplex. In the following discussion, only full compositional vectors are considered, including a residual part if necessary, and a compositional (row) vector of D parts, $x = [X_l, X_{2,}, . . . , X_D]$, will always be a vector of strictly positive components summing to a constant. Zero components are not considered here, as they require a particular approach, as discussed by Martin-Fernández & Thi6-Henestrosa (2006) in the third section of this volume. The D-part simplex, S^D, is a subset of D dimensional real space. For D = 2, it can be represented as a line segment; for D = 3, as a triangle (the ubiquitous ternary diagram) and for D = 4, as a tetrahedron. Clearly, no graphical representations of simplices are possible beyond D = 4. Therefore, discussion is restricted to numerical examples with D < 4 parts. However, the definitions, operations and interpretations are valid for any number of parts. At this juncture, it is important to emphasize that data in which the components do not sum exactly to a constant are not free from the constant sum constraint. The fact that there is commonly not an exact constant sum merely reflects measurement error and/or unanalyzed components - particularly a feature of geochemical data. Recall that the problems of spurious correlation affect pairs of measurement: correlation coefficients, computed using the traditional Pearson product-moment correlation coefficient, will not change if a residual part is added to the vector of measurements (Pawlowsky-Glahn and Egozcue, 2006).

A final comment on units is important. Besides the above-mentioned units, there are other types of units that do not close to a constant, such as molar or molal composition. They are a particular type of compositional data that can be handled with the same log-ratio methods (Buccianti and Pawlowsky-Glahn 2005). The strategy is simple: convert the data to weight percent, compute the results, then convert them back into the desired units.

4.2. Perturbation and powering.

The classical algebraic/geometric operations (addition/translation, product/scaling, scalar product/orthogonal projection, Euclidean distance) used to deal with conventional real vectors are neither subcompositionally coherent nor scaling invariant. As an alternative, Aitchison (1986)

introduced a set of operations to replace these conventional ones in compositional geometry. Perturbation plays the role of sum or translation and is a closed component-wise product of the compositions involved:

$$\mathbf{z} = \mathbf{x} \oplus \mathbf{y} = \mathscr{C}[x_1 \cdot y_1, \ldots, x_D \cdot y_D].$$

With "compositions", one can perturb a pair of compositions in two ways: by using the command perturbe (x,y) or by adding or subtracting two vectors of class.

Powering or power transformation replaces the product of a vector by a scalar (geometrically, this is equivalent to scaling) and is defined as the closed powering of the components by a given scalar:

$$\mathbf{z} = \lambda \odot \mathbf{x} = \mathscr{C}[x_1^\lambda, \ldots, x_D^\lambda].$$

(van den Boogaart and Tolosana-Delgado, 2013).

For an illustration of the effect of perturbation and powering on a set of compositions, see Figure 23.
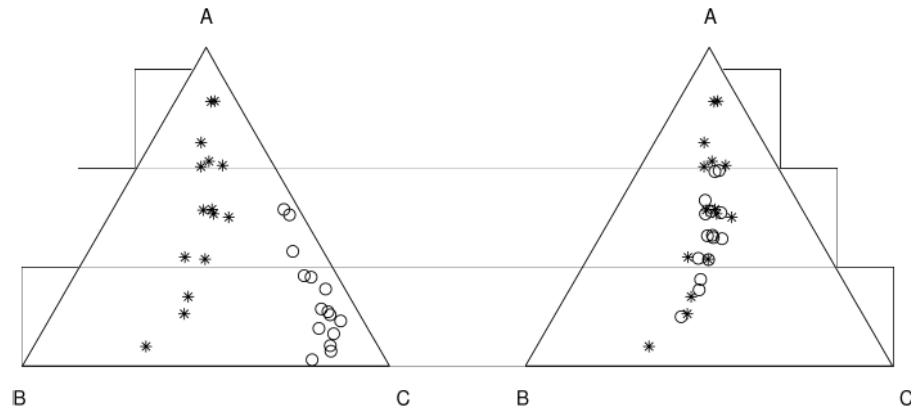

Figure 23. Left: Perturbation of initial compositions (∘) by p = [0:1; 0:1; 0:8] resulting in compositions (∗). Right: Powering of compositions (∗) by α= 0:2 resulting in compositions (∘) (Pawlowsky-Glahn et al., 2011).

4.3. Aitchison geometry: clr and ilr.

Aitchison (1986) used the fact that for compositional data size is irrelevant as interest lies in relative proportions of the components measured to introduce transformations based on ratios, the essential ones being the additive log-ratio transformation (alr) and the centered log-ratio transformation (clr). Then, he applied classical statistical analysis to the transformed observations, using the alr transformation for modelling, and the clr transformation for those techniques based on a metric. The underlying reason was, that the alr transformation does not preserve distances, whereas the clr transformation preserves distances but leads to a singular covariance matrix. In mathematical terms, we say that the alr transformation is an isomorphism, but not an isometry, while the clr transformation is an isometry, and thus also an isomorphism, but between S^D and a subspace of RD, leading to degenerate distributions. Thus, Aitchison's approach opened up a rigorous strategy, but care had to be applied when using either of both transformations. Using the Euclidean vector space structure, it is possible to give an algebraic geometric foundation to his approach, and it is possible to go even a step further. Within this framework, a transformation of coefficients is equivalent to express observations in a different coordinate system. We are used to work in an orthogonal system, known as a Cartesian coordinate system; we know how to change coordinates within this system and how to rotate axis. But neither the clr nor the alr transformations can be directly associated with an orthogonal coordinate system in the simplex, a fact that lead Egozcue et al. (2003) to define a new transformation, called ilr (for isometric logratio) transformation, which is an isometry between SD and RD−1, thus avoiding the drawbacks of both the alr and the clr. The ilr stands actually for the association of coordinates with compositions in an orthonormal system in general, and this is the framework we are going to present here, together with a particular kind of coordinates, named balances, because of their usefulness for modelling and interpretation (Pawlowsky et al., 2007).

The centered logratio transformation denoted by clr is the one-to-one function from the compositional space C^{D-1} to the subspace

$$V = \{\mathbf{z} = (z_1, \ldots, z_D)' \in \mathbb{R}^D : z_1 + \ldots + z_D = 0\}$$

of $\mathbb{R}^D$, defined by

$$\text{clr } \underline{\mathbf{w}} = \log \frac{\mathbf{w}}{g(\mathbf{w})} \qquad (\underline{\mathbf{w}} \in \mathcal{C}^{D-1}).$$

The inverse transformation, from V to C^{D-1}, is given by

$$\text{clr}^{-1} \mathbf{z} = \text{ccl} (\exp \mathbf{z}) \quad (\mathbf{z} \in V).$$

The logarithmic and the exponential transformations establish a one-to-one correspondence between the simplex SD and the hyperplan V in $\mathbb{R}^D$.

Ilr – isometric logratio

Let $\mathcal{V} = \{\mathbf{v}_1, \ldots, \mathbf{v}_{D-1}\}$ an orthonormal basis of the subspace

$$V = \{\mathbf{z} = (z_1, \ldots, z_D)' \in \mathbb{R}^D : z_1 + \ldots + z_D = 0\}.$$

Then, since $\text{clr } \underline{\mathbf{w}} \in V$, it will be always possible to write

$$\text{clr } \underline{\mathbf{w}} = u_1 \mathbf{v}_1 + \ldots + u_{D-1} \mathbf{v}_{D-1},$$

for any $\underline{\mathbf{w}} \in \mathcal{C}^{D-1}$.

The isometric logratio transformation |denoted by ilrV | is the one-to-one function from the compositional space C^{D-1} to $\mathbb{R}^{D-1}$ defined by

$$\text{ilr}_{\mathcal{V}} \underline{\mathbf{w}} = (u_1, \ldots, u_{D-1})' \qquad (\underline{\mathbf{w}} \in \mathcal{C}^{D-1}).$$

Like clr , the transformation ilrV is an isomorphism between the vector spaces

$$(\mathcal{C}^{D-1}, \oplus, \otimes) \text{ and } (\mathbb{R}^{D-1}, +, .).$$

(Barceló Vidal et al., 2019).

4.4. Stats:

a) Geomean - expected value.

In a compositional context, totals have no meaning. If we want to add cases, we have to go back to the original amounts. For the geometric mean composition on the contrary, the result is the same, whether the amounts are averaged first and then an average composition is computed, or whether the geometric mean of the compositions is computed directly. The D-part composition giving the closed arithmetic mean of amounts and closed geometric mean estimators are, respectively

$$\bar{p}_{am}(S) = \frac{1}{\sum_{i \in U} w_i t_i z_i(S)} \sum_{k \in U} w_k t_k z_k(S) \, \boldsymbol{p}_k,$$

$$\bar{p}_{gm}(S) = \frac{1}{\sum_{i \in U} w_i z_i(S)} \odot \prod_{k \in U} [w_k z_k(S)] \odot \boldsymbol{p}_k.$$

In second equation, the product is computed component wise. We can notice that only the closed geometric mean is compatible with Aitchison's geometry (Pawlowsky-Glahn and Egozcue 2002). On the other hand, when a data set is created, the compositions of interest are frequently obtained from closed sums of amounts. For example, household incomes are sums of the incomes of individual household members. It is necessary to go back to the individual data in order to compute the sampling variability at the household level (Pawlowsky-Glahn and Buccianti, 2011)

The geometric means are central values of the parts in each group of parts; its ratio measures the relative weight of each group; the logarithm provides the appropriate scale; and the square root coefficient is a normalizing constant which allows to compare numerically different balances. A positive balance means that, in (geometric) mean, the group of parts in the numerator has more weight in the composition than the group in the denominator (and conversely for negative balances) (Pawlowsky-Glahn et al., 2007).

b) Variation array.

A typical way to present estimations of the centre and the variability is the variation array (Aitchison 1986).

Aitchison (1986) has pioneered methods for compositional data analysis, founded upon log-ratios of components. Among other things, this approach provides a sound alternative to the analysis of covariance in compositions by using the compositional variation array (Aitchison 1986)

4.5. Data analysis methods.

4.5.1 Constrained cluster analysis.

The constrained cluster analysis (CCA; Grimm, 1987) is a zonation technique based on Ward's clustering algorithm. For CoDa it can be computed (Di Donato et al., 2009) from a matrix of Aitchison distances between observations. It is worth noting that the Aitchison distance is equivalent to the Euclidean distance between log-centered observations. CCA was applied to both micropaleontological and granulometrical data to obtain compositional zones for the analyzed cores.

Cluster analysis, or group analysis, is a multivariate data analysis technique through which it is possible to group homogeneous elements into a set of data. Clustering techniques are based on measures relating to the similarity between the elements. In many approaches this similarity (or dissimilarity) is conceived in terms of distance in a multidimensional space. The validity of the analyzes obtained by the clustering algorithms depends very much on the choice of the size, and therefore on how the distance is calculated.

Considering a set X of points in a space with p dimensions, a distance is a function that associates to each pair of points a real number:

d= X × X → R

so that for every choice of points xik, xjk, xkk in X we have:

(i)   d (xik, xjk) ≥ 0 and (xik, xjk) = 0 if and only if xik = xjk

(ii)   (ii) d (xik, xjk) = d (xik, xjk)

(iii)   (iii) d (xik, xjk) ≤ d (xik, xkk) + d (xjk, xkk) (triangular relation)

There are various choices for the function d, the most common being the Euclidean distance, which for two objects i and j in a p-dimensional space is given by:

$$d_{ij} = \sqrt{\sum_{k=1}^{p} (x_{ik} - x_{jk})^2}$$

The clustering algorithms group the elements on the basis of their mutual distance, and therefore the belonging or not to a whole depends on how much the element taken into consideration is distant from the same whole. The hierarchical cluster groups the data on different scales represented by a dendrogram, or a tree cluster. The latter is not a single data partition, but rather a multilevel hierarchy, where the clusters of a level can be joined as clusters to the next level. This allows you to decide the level or scale of the clustering most appropriate for your application. Each branch of the diagram corresponds to a cluster, while the connecting line of two or more branches identifies the distance level. In the dendrograms that will be illustrated, the distances are shown on the abscissa axis and the individual elements are shown on the ordinate axis. Clustering techniques can be based on aggregative or divisive methods. For this work, an aggregative method is used where in principle all the data are considered clusters by itself and the algorithm joins the nearest clusters. The algorithm continues to join elements to the cluster until a predetermined number of clusters is obtained, or until the minimum distance between the clusters does not exceed a certain value, or again in relation to a given statistical predetermined criterion.

In the constrained Cluster Analysis (CCA) (Grimm, 1987), the analysis is constrained so that the order of the objects remains unchanged. Consequently, the dendrogram reflects the similarity between successive observations. This is obviously very useful in stratigraphic studies as a method of zoning, that is as a method of subdivision of the sequences on the basis of the

analyzed characteristics. In the constrained grouping only the adjacent data or clusters are analyzed, so the dendrogram keeps the objects in the initial order.

The CCA was calculated with an Aitchison distance matrix between the elements. Aitchison's distance is equivalent to the Euclidean distance between log-centered data. The log-centered transformation (clr) can be described as follows:

$$clr(x) = z\left(\ln\frac{x_1}{g(x)}; \ln\frac{x_2}{g(x)}; ...; \ln\frac{x_d}{g(x)}\right)$$

With $g(x) = (\Pi_{i=1}^{d}x_i)^{1/d}$ that is, the geometric mean of the composition.

This transformation requires the zero-substitution procedure with very small values so as not to significantly influence the results.

The matrix of Euclidean distances between log-centered observations was used to calculate the CCA based on the Ward method, whose aggregation index is based on a square Euclidean distance. Based on the distances of Aitchison (Aitchison, 1986), defined as:

$$\Delta(x,y) = \left[\sum_{i<j}^{D}\left\{\log\frac{x_i}{x_j} - \log\frac{y_i}{y_j}\right\}^2\right]^{1/2} = \left[\sum_{i=1}^{D}\left\{\log\frac{x_i}{g(x)} - \log\frac{y_i}{g(y)}\right\}^2\right]^{1/2} (x,y \in S^D)$$

the intervals obtained can be defined as compositional zones. The compositional zones, in some cases, have been further subdivided into subzones.

4.5.2 Relative Variation Biplot.

A biplot is a graphical display of the rows and columns of a rectangular $n \times p$ data matrix **X**, where the rows are often individuals or other sample units and the columns are variables. In almost all applications, biplot analysis starts with performing some transformation on **X**, depending on the nature of the data, to obtain a transformed matrix **Z** which is the matrix that is actually

displayed. Examples of transformations are centring with respect to the overall mean, centring with respect to variable means, normalization of variables, square root and logarithmic transforms. Suppose that the transformed data matrix $\mathbf{Z}$ has rank r. Then $\mathbf{Z}$ can be factorized as the product

$$\mathbf{Z} = \mathbf{F}\mathbf{G}^{\mathrm{T}},$$

where $\mathbf{F}$ is $n \times r$ and $\mathbf{G}$ is $p \times r$. The rows of $\mathbf{F}$ and the rows of $\mathbf{G}$ provide the co-ordinates of n points for the rows and p points for the columns in an r-dimensional Euclidean space, called the full space since it has as many dimensions as the rank of $\mathbf{Z}$. This joint plot of the two sets of points can be referred to as the exact biplot in the full space. There are an infinite number of ways to choose $\mathbf{F}$ and $\mathbf{G}$, and certain choices favor the display of the rows; others the display of the columns. For any particular choice, however, the biplot in r dimensions has the property that the scalar product between the ith row point and jth column point with respect to the origin is equal to the (i; j) th element z_{ij} of $\mathbf{Z}$. We are mainly interested in low dimensional biplots of $\mathbf{Z}$, especially in two dimensions, and these can be conveniently achieved by using the singular value decomposition (SVD) of $\mathbf{Z}$:

$$\mathbf{Z} = \mathbf{U}\boldsymbol{\Gamma}\mathbf{V}^{\mathrm{T}},$$

where U and V are the matrices of left and right singular vectors, each with r orthonormal columns, and Γ is the diagonal matrix of positive singular values in decreasing order of magnitude: $\gamma 1 \geq \ldots \geq \gamma\, r > 0$. The Eckart–Young theorem (Eckart and Young, 1936) states that if one calculates the n $\times$ p matrix $\hat{\mathbf{Z}}$ using the first r* singular values and corresponding singular vectors, e.g. for r* = 2,

$$\hat{\mathbf{Z}} = (\mathbf{u}_1 \quad \mathbf{u}_2) \begin{pmatrix} \gamma_1 & 0 \\ 0 & \gamma_2 \end{pmatrix} (\mathbf{v}_1 \quad \mathbf{v}_2)^{\mathrm{T}}$$

then $\hat{\mathbf{Z}}$ is the least squares rank r* matrix approximation of $\mathbf{Z}$, i.e. $\hat{\mathbf{Z}}$ minimizes the fit criterion

$$\|\mathbf{Z} - \mathbf{Y}\|^2 = \sum_i \sum_j (z_{ij} - y_{ij})^2$$

over all possible matrices $\mathbf{Y}$ of rank r*, where $\|\cdots\|$ denotes the Frobenius matrix norm. It is this approximate matrix $\hat{\mathbf{Z}}$ which is biplotted in the lower r*-dimensional space, called the *reduced*

space. This biplot will be as accurate as is the approximation of $\hat{\mathbf{Z}}$ to $\mathbf{Z}$. The sum of squares of

$\mathbf{Z}$ decomposes into two parts: $\|\mathbf{Z}\|^2 = \|\hat{\mathbf{Z}}\|^2 + \|\mathbf{Z} - \hat{\mathbf{Z}}\|^2$, where $\|\hat{\mathbf{Z}}\|^2 = \gamma_1^2 + \cdots \gamma_{r*}^2$

and

$$\|\mathbf{Z} - \hat{\mathbf{Z}}\|^2 = {}$$
$$(\gamma^2{}_{r}* + 1 + \ldots + \gamma_r{}^2)$$

and the goodness of fit is measured by the proportion of explained sum of squares $(\gamma_1{}^2 + \ldots + \gamma^2{}_{r*}) / (\gamma^2{}_1 + \ldots + \gamma^2{}_r)$, usually expressed as a percentage.

The SVD also provides a decomposition which is a natural choice for the biplot. For example, from equation (3) in two dimensions. $\hat{\mathbf{Z}} = \mathbf{F}\mathbf{G}^T$ with

$$\mathbf{F} = (\, \gamma_1^{\alpha}\mathbf{u}_1 \quad \gamma_2^{\alpha}\mathbf{u}_2 \,),$$
$$\mathbf{G} = (\, \gamma_1^{1-\alpha}\mathbf{v}_1 \quad \gamma_2^{1-\alpha}\mathbf{v}_2 \,)$$

for some constant α. The most common choices of α are the values 1 or 0, when the singular values are assigned entirely either to the left singular vectors of U or to the right singular vectors of V respectively, or 0.5 when the square roots of the singular values are split equally between left and right singular vectors. Each choice, while giving exactly the same matrix approximation, will highlight a different aspect of the data matrix. The term principal co-ordinates refer to the singular vectors scaled by the singular values (e.g. F with $\alpha = 1$ or G with $\alpha = 0$), whereas standard co-ordinates are the unscaled singular vectors (Greenacre, 1984). In the CoDA framework, biplots can be computed on clr data (Aitchison and Greenacre, 2002), the so-called Relative Variation Biplots can be evaluated by focusing links between column (variable) points instead of rays, in practice:

- Short links between two parts indicate that they are proportional;
- 3 separate, very long rays define a high-variance subcomposition;
- collinear links: indicate subcompositions showing a onedimensional;
- orthogonal links: indicate that two subcompositions are uncorrelated.

In order to compute RVB for foraminiferal assemblages, data must be strictly positive. This procedure requires a zero substitution. In order to reduce the number of zero values to be substituted, analysis was only performed on the most abundant taxa. Moreover, less abundant taxa were amalgamated into informal taxonomic groups. With regard to planktonic foraminifera, it can also be noted that *Neogloboquadrina incompta* refers to right-coiled specimens, *N. pachyderma* left-coiled ones being recorded sporadically throughout the core. The planktonic foraminifera amalgamated warm species group (PFAWS) includes *Orbulina universa, Globoturborotalita tenella, Globoturborotalita rubescens* and *Globigerinella siphoniphera*. This group, with the exception of *Globigerinoides sacculifer* which was not included within it, corresponds to the SPRUDT group of Jorissen et al. (1993). Within benthic foraminiferal assemblages *Bulimina costata* and *Bulimina inflata* were put together; Miliolids includes deep water species belonging to this groups; Arenaceous includes all the agglutinant species (mostly *Textularia* spp., *Bigenerina* spp., *Clavulina* spp.). *Deep infauna* includes oxygen-resistant species such as *Globobulimina* spp., *Chilostomella* spp., *Cassidulinoides bradyi;* shallow water (such as *Ammonia* spp. and *Elphidium* spp.) and epiphytes taxa (mostly *Rosalina* spp., *Cibicides lobatulus*) were also considered as groups.

5. Results
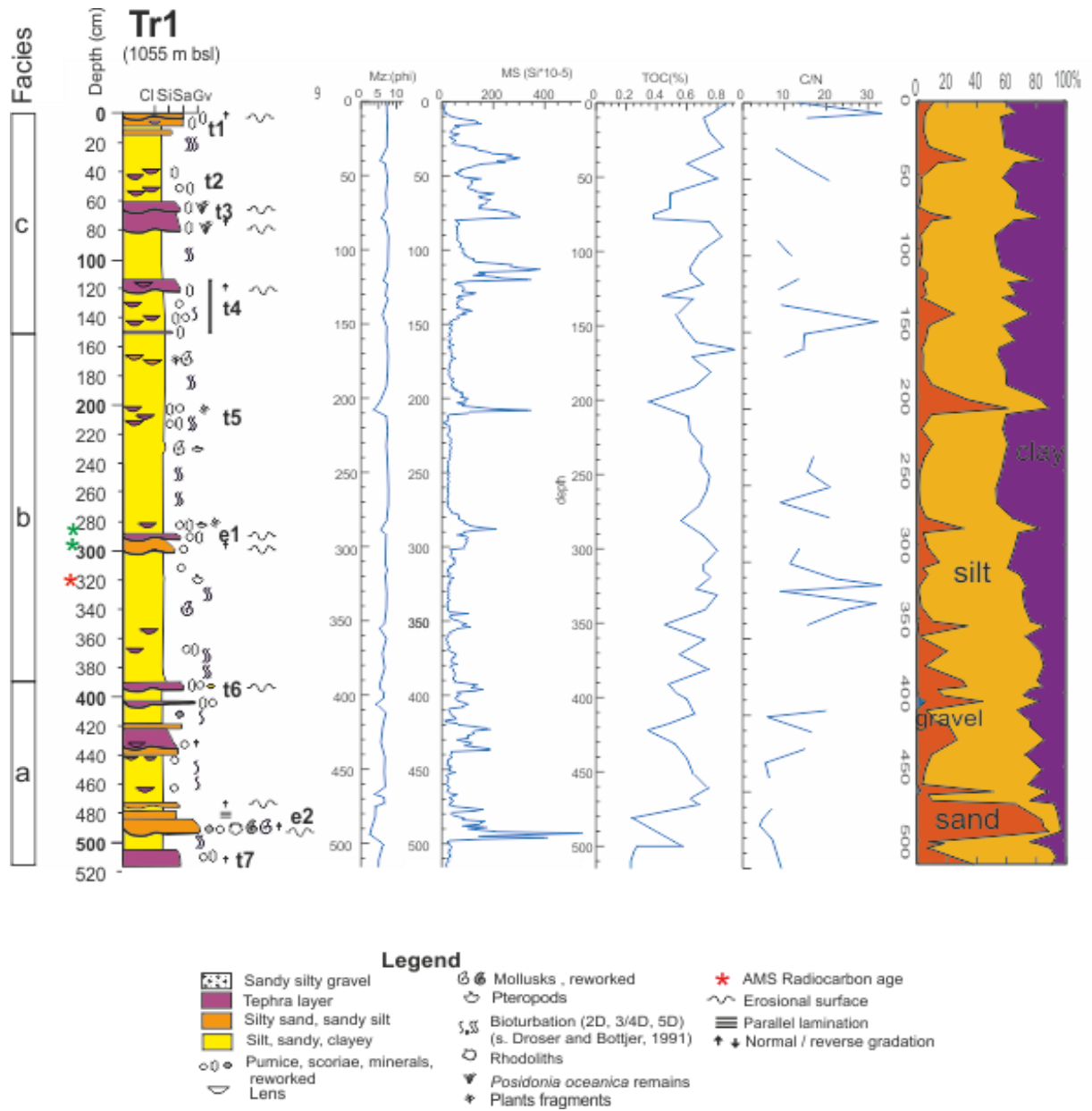
5.1 Granulometric and TOC analysis

Figure 24 Integrated log of the gravity core TR1: a) facies b) Mz: Mean-grain size; c) MS Magnetic susceptibility; d) C/N; e) TOC: Total Organic Carbon: Carbon/Nitrogen.

Granulometric data (fig. 24 and 25) are summarized into a ternary diagram (Shepard, 1954) in which sands, silt and clay are considered as parts of the composition. By means by CCA 5 intervals were identified.
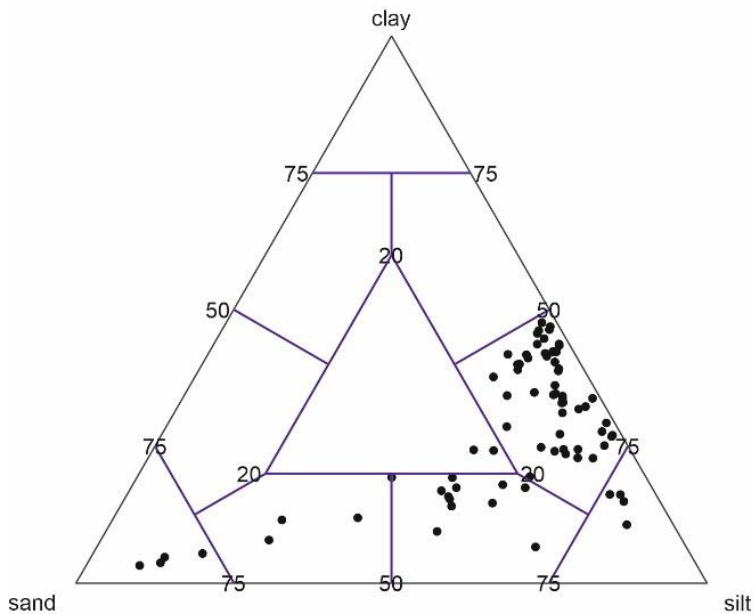

Figure 25 Ternary diagrams of granulometric data from the core TR1: **a)** ternary diagram (Shepard, 1954) in which sands, silt and clay are considered as parts of the composition.

In the core TR1 was made TOC analysis (fig.24). The results of the ratio C/N from 4 to 10 means marine origin of the carbon and values >15 means terrestrial origin (terrestrial plants end so on) (Gray and Biddlestone, 1973). The higher TOC is the higher TN we have. In the core TR1 we have a higher amount of terrestrial origin carbon such as at 490 cmbsf, 340 cmbsf and 2 cmbsf of depth.

5.2 Age model.

The age model of all the cores (Fig.26-29) was obtained by the interpolation between the dated levels using the program MATLAB "interpol" written by prof. Valentino Di Donato which allow to use different methods of the interpolation. In this case it was adopted a monotonic spline (Piecewise Cubic Hermite Interpolating Polynomial) (de Boor, 1978).

The Age model is based on a mixed approach including radiocarbon dating, tephro- and eco-stratigraphy. Radiocarbon datings of Core GNS84-C106 refer to Bucheri et al. (2002) and Di Donato e al., (2009). The tie-points for the analysed cores are reported in table 6. Radiocarbon datings were provided for the cores GMS_98-01 C58 (one sample) and Transect_2017 TR1 (two samples). For the cores GMS_98-01 C14 and GNS84-C106 C14 radiocarbon datings were already done.

At least 30 mg of the bioclasts: foraminifera and pteropods in fraction bigger than 250 μm were picked for: 2 samples from TR1 (74mg (319-320cm) and 36.6mg (181-182cm)) and 1 sample from C58 (32mg (110-112cm)). The analysis was carried out at the Centre for Isotopic Research on Cultural and Environmental Heritage (CIRCE) radiocarbon laboratory, Caserta, (Italy). The CIRCE Accelerator Mass Spectrometry (AMS) system, based on the 3MV 9SDH-2 Pelletron accelerator provides a mean overall precision of 0.63% (Terrasi et. al, 2007). All radiocarbon dates were corrected using a reservoir age of 48 +/- 21 yr (a mean DR value calculated among six of the Tyrrhenian Sea) and calibrated using the marine data base and the CALIB 7.1 Program of Stuiver and Reimer (1993).

Radiocarbon ages were calibrated by means in the programm CALIB 7.1. The ecostratigraphic approach was applied within the considered dataset, i.e. some events identified in the Core GNS84-C106, were correlated to other cores. Since the study was conducted at a sub-basin scale, we considered as negligible diachronicities that may have characterised the distribution of planktonic assemblages at a full Mediterranean basin scale. Tephrostratigraphical data were kindly provided by Prof. Paola Petrosino and Prof. Donatella Insinga.

Core	Depht (cm)	Event (eruptions, foraminiferal peaks)	Radiocarbon age	Cal ka
GNS84-C106	2	1944		0.006
GNS84-C106	4	1790		0.128
GNS84-C106	6	1631		0.319
GNS84-C106	8	1631		1.14
GNS84-C106	32	II medioeval		1.44
GNS84-C106	36	472 CE		1.478
GNS84-C106	46	150 CE		1.8
GNS84-C106	56-119	79 CE		1.871
GNS84-C106	132	AP6		3.484

GNS84-C106	140		3.47+/-40	3.351
GNS84-C106	146	AP3		3.588
GNS84-C106	148	AP2		3.62
GNS84-C106	172	Astroni		4.197
GNS84-C106	176	Averno 2		4.269
GNS84-C106	188	Agnano montespina		4.553
GNS84-C106	200		5.66+/-40	6.064
GNS84-C106	206	Piano Liguori		5.577
GNS84-C106	214	Piano Liguori		5.577
GNS84-C106	250		8.16+/-70	8.656
GNS84-C106	274	Pigna S.Nicola		
GNS84-C106	276		9.314+/-41	10.162
GNS84-C106	310		9.87+/-100	10.823
GNS84-C106	318	Pomici principali		
GNS84-C106	338	Soccavo 1		
GNS84-C106	338	Soccavo 2		12.644+-0.709
GNS84-C106	370		12.87+/-100	14.625
GNS84-C106	392	PRA		
GNS84-C106	414	Biancavilla		17.584+-0.741
GNS84-C106	416	Ischia Sant'Angelo		17.780+-30
GNS84-C106	470		17.11+/-60	20.152
GNS84-C106	478	Pomici di base		21.670+-0224
GNS84-C106	514	solchiaro		23.624+-0.330
GNS84-C106	514	solchiaro		
GNS84-C106	532	ecozona simona 8/9		
GNS84-C106	583		26.03+/-150	29.777
GNS84-C106	616	Codola		32.869+-767
TRANSECT_2017 TR1	7	Vesuvio medievale		0.319
TRANSECT_2017 TR1	43	Pollena		1.478
TRANSECT_2017 TR1	51	Cretaio		1.8
TRANSECT_2017 TR1	79	Vesuvio		1.871
TRANSECT_2017 TR1	116	*G sacculifer* peak		3.174 (Core GNS84-C106)
TRANSECT_2017 TR1	161	*G. truncatulinoides* ds peak		4.343 (Core GNS84-C106)
TRANSECT_2017 TR1	181		5209 +/- 35	5.573 (5.473 – 5.643)
TRANSECT_2017 TR1	226	*Neogloboquadrina* ds peak		7.48 (Core GNS84-C106)
TRANSECT_2017 TR1	319		9427 +/- 28	10.254 (10.187 – 10.364)
TRANSECT_2017 TR1	386	Base Holocene		11.653
TRANSECT_2017 TR1	395	Pomici Principali		12.036

TRANSECT_2017 TR1	405	Soccavo		12.318
TRANSECT_2017 TR1	467	Ischia island tephra		14
TRANSECT_2017 TR1	515	Neapolitan yellow tuff		15.1
GMS_98-01-C58	64	*G sacculifer* peak		3.174 (Core GNS84-C106)
GMS_98-01-C58	90	*G. truncatulinoides* ds peak		4.343 (Core GNS84-C106)
GMS_98-01-C58	110		5198 +/- 25	5.565 (5.475 – 5.617)
GMS_98-01-C58	148	*N. pachyderma* ds peak		7.48 (Core GNS84-C106)
GMS_98-01-C58	240	Base Holocene		11.6
GMS_98-01-C58	294			12.846
GMS_98-01 C14	79	Vesuvio		1.871
GMS_98-01 C14	190	Astroni		4.249
GMS_98-01 C14	240	Miseno		3.90
GMS_98-01 C14	290	Averno 2		4.2835
GMS_98-01 C14	298		4248 +/- 46	4.352 (4.216-4.496)
GMS_98-01 C14	303	*G. truncatulinoides* ds peak		4.343 (Core GNS84-C106)
GMS_98-01 C14	395	*Neogloboquadrina* ds peak		7.48 (Core GNS84-C106)
GMS_98-01 C14	473	Mercato		8.90
GMS_98-01 C14	486		8303+/- 30	8.873 (8.736-8.981)

*for radiocarbon ages, the numbers in parenthesis represent the 2-sigma (95.4%) range.

Table 6. List of the tie-points used for the age model assessment of the selected cores. The depth, the age (kyr BP) and the nature of these tie-points are also indicated.

Based on the available dating points, the age models (Figs. 26-29) were built by means of monotonic cubic splines.
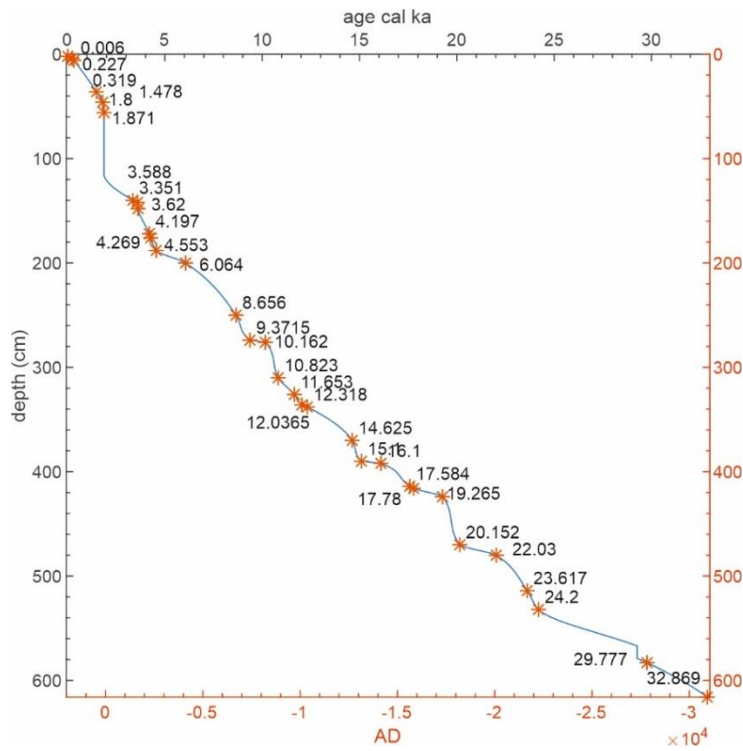
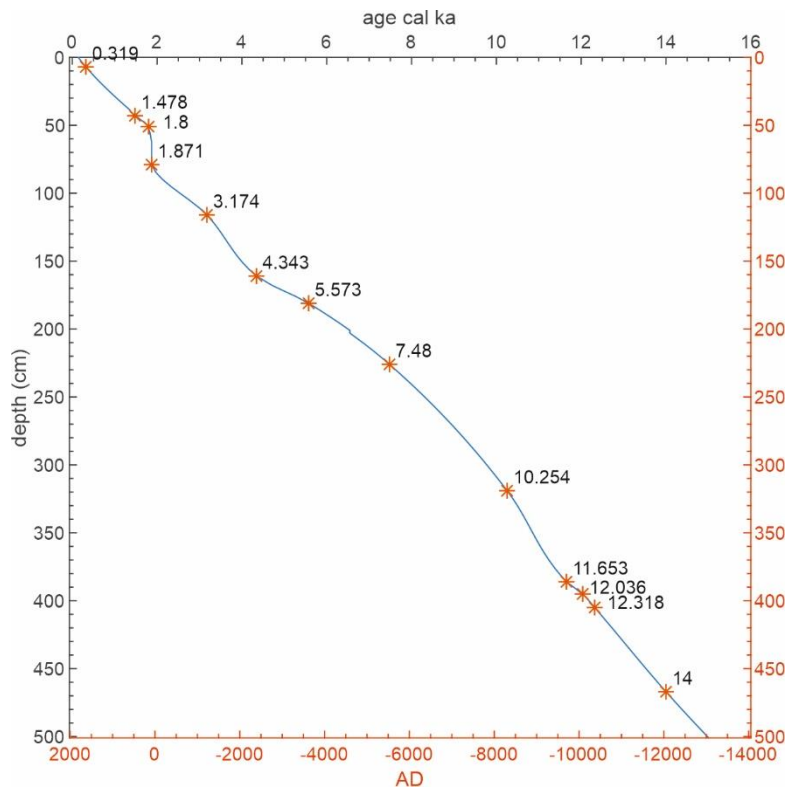*Figure 26- Age model for Core GNS84-C106*
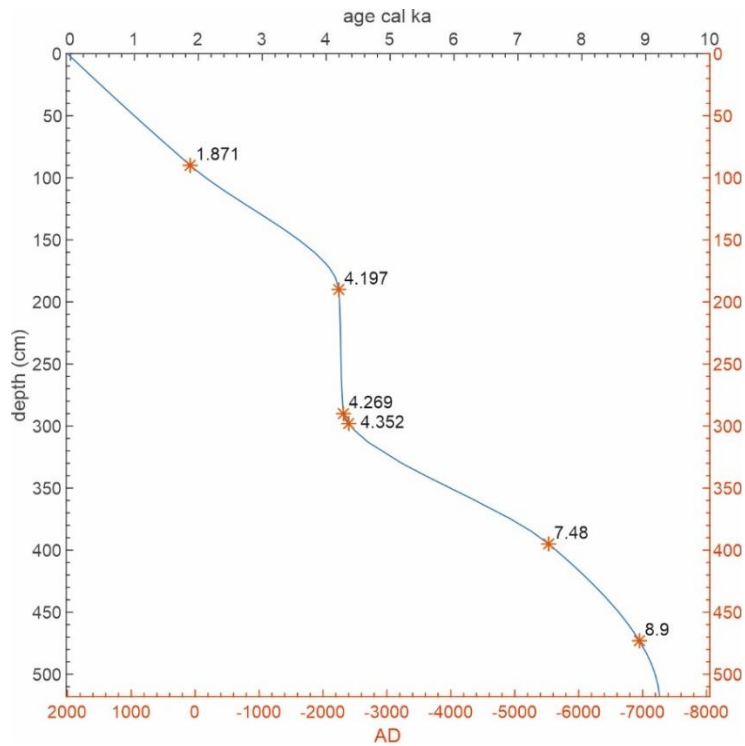

Figure 27 Age model for Core Transect2017_TR1

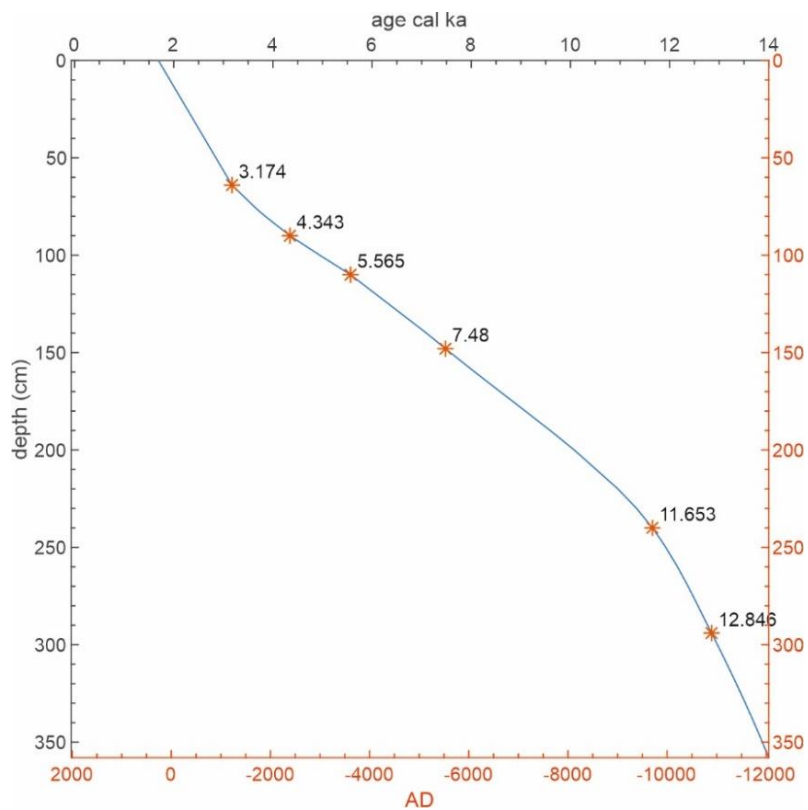81

Figure 28 - Age model for GMS_98-01 C14

Figure 29 Age model for the Core GMS_98-01 C58

5.3 Planktonic foraminifera Zonation of the Cores.

The distribution of planktonic foraminifera in the analysed cores is shown in figures 30 to 33.

Compositional zones for each of the studied cores were obtained by means of Constrained cluster analysis (Ward method on clr coordinates) (Grimm 1987; Di Donato et al., 2008) (Figures 30-33). By integrating the zonation of the two most detailed records of Core GNS84-C106 and Transect2017_TR1, an ecozonation scheme for the last 33 ka of the Tyrrhenian Sea was obtained (Figure 41 and 42). The scheme is constituted by three main intervals, each of which divided in subzones. The description of these subzones is provided below:

STPFCZ3c (33-24.1 cal ka) - In these subzones dominant species are *G. bulloides, G. ruber alba, G. glutinata, N. incompta, T. quinqueloba and G. scitula.* Common species are *N. pachyderma sx, G. inflata, G. siphonifera Globoturborotalita* and *O. universa*. Some species are rare as *G. ruber rosea, G. sacculifer, G. truncatulinoides sx, G. truncatulinoides dx.* The most visible trends in that subzone are decreasing percentage values of *G. ruber alba* and increasing percentage values of *N. incompta, G. scitula, G. glutinata and G. bulloides* till the end of the 24.1ka and exactly at the end of the interval those species are decreasing drastically.

STPFCZ3b (24.1-19.4 cal ka) - In this subzone dominant species are *G. ruber alba, G. bulloides, G. glutinata, N. incompta, G. scitula and T. quinqueloba.* Common species are *N. pachyderma sx, G. inflata, G. siphonifera, Globoturborotalita* and *O. universa*. Some species are rare as *G. ruber rosea, G. sacculifer, G. truncatulinoides sx* and *G. truncatulinoides dx.* The most visible trends in that subzone are large increasing percentage values of *G. ruber alba* with decreasing percentage values at the end of the subzone. *G. bulloides, G. glutinata, G. scitula, T. quinqueloba* and *N. incompta* in comparison with PFCZ3c percentage values are slightly increasing again.

STPFCZ3a (19.4-14.4 cal ka) - In this subzone dominant species are *G. bulloides, G. glutinata, T. quinqueloba N. incompta, G. scitula* and less abundant *G. ruber alba*. Common species are *N. pachyderma sx, G. inflata, G. siphonifera, Globoturborotalita* and *O. universa*. Some species are rare as *G. ruber rosea, G.sacculifer, G. truncatulinoides sx* and *G. truncatulinoides dx.* The most visible trends in that subzone are very big decreasing of

Figure 30 Distribution pattern of planktonic foraminifera in the Core GNS-84 C106 (>150 micron size fraction)
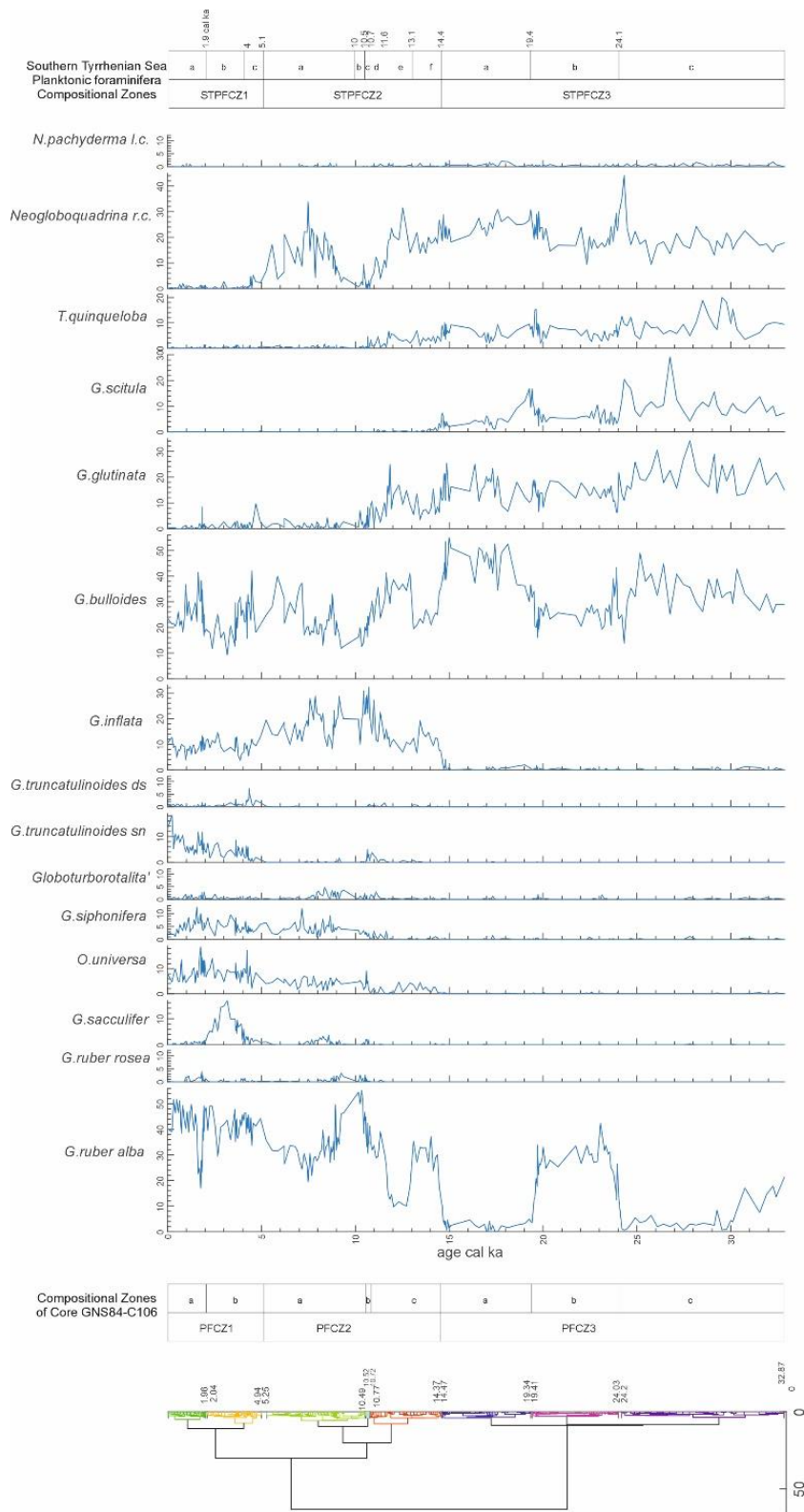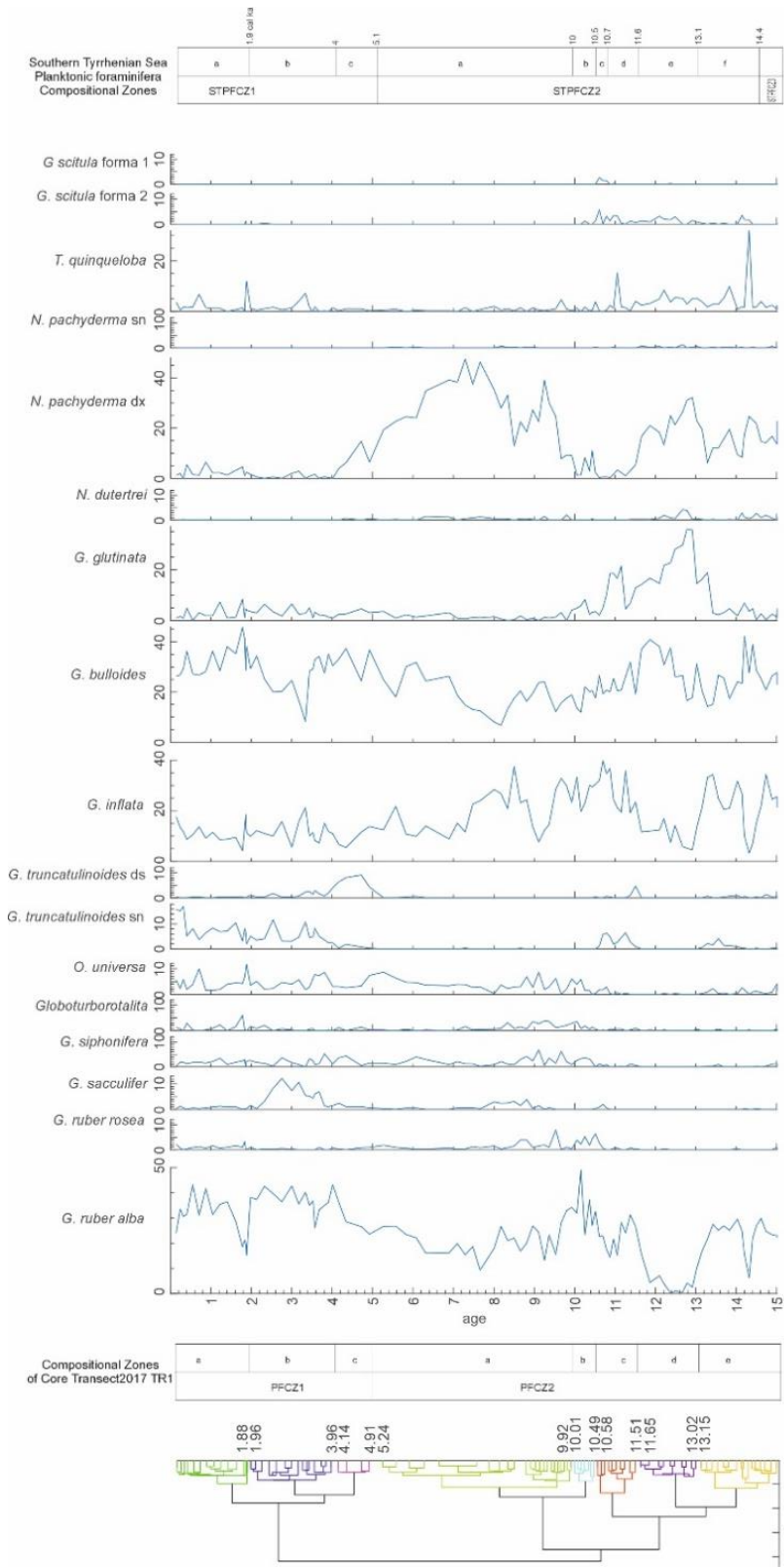
Figure 31 **Distribution pattern** *of planktonic foraminifera in the Core Transect2017_TR1 (>150 micron size fraction)*
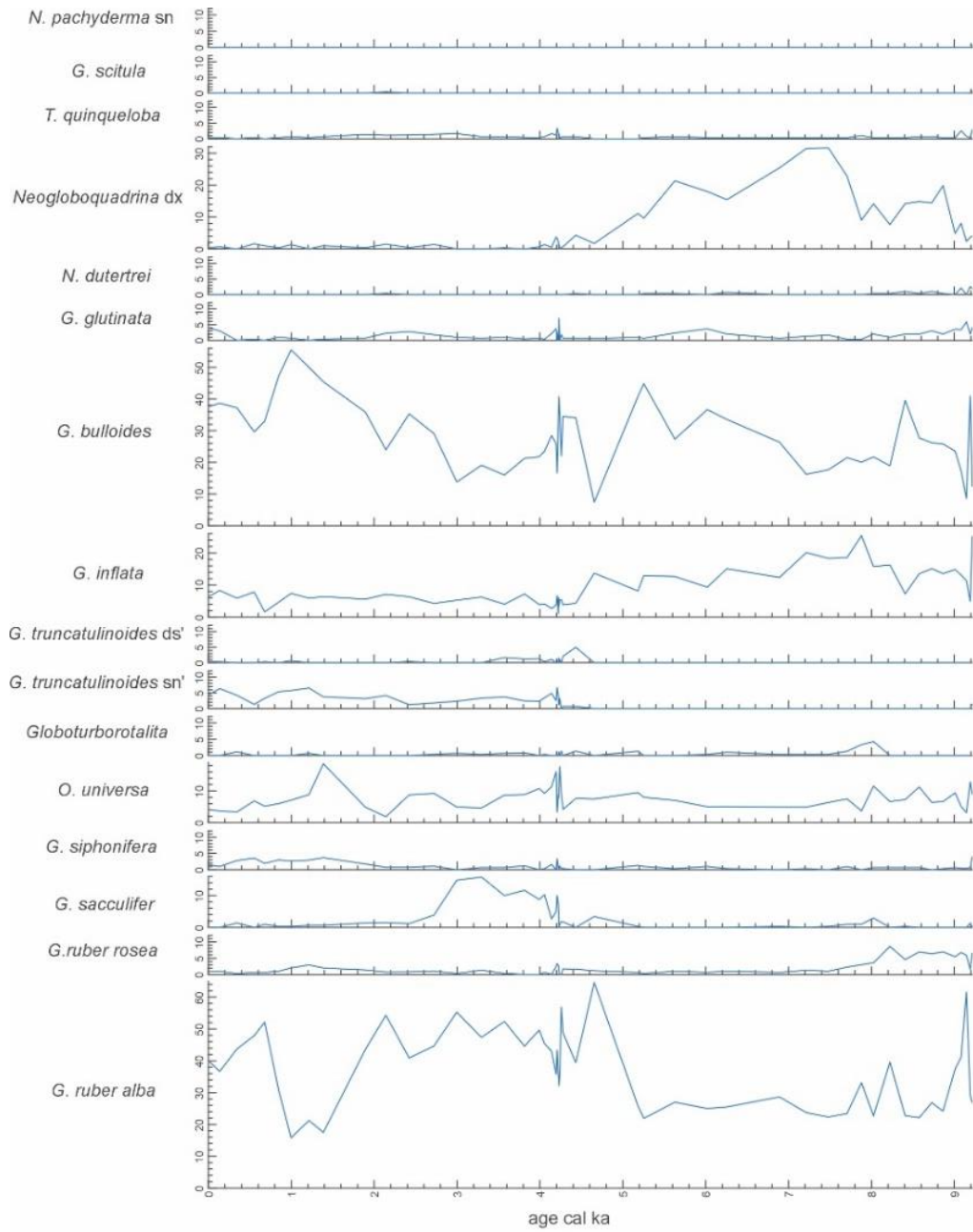
Figure 32 Distribution pattern distribution of planktonic foraminifera in the GMS_98-01 C14 (>150 micron size fraction)
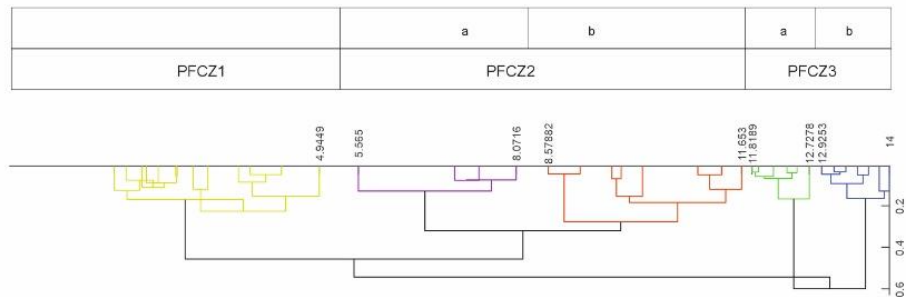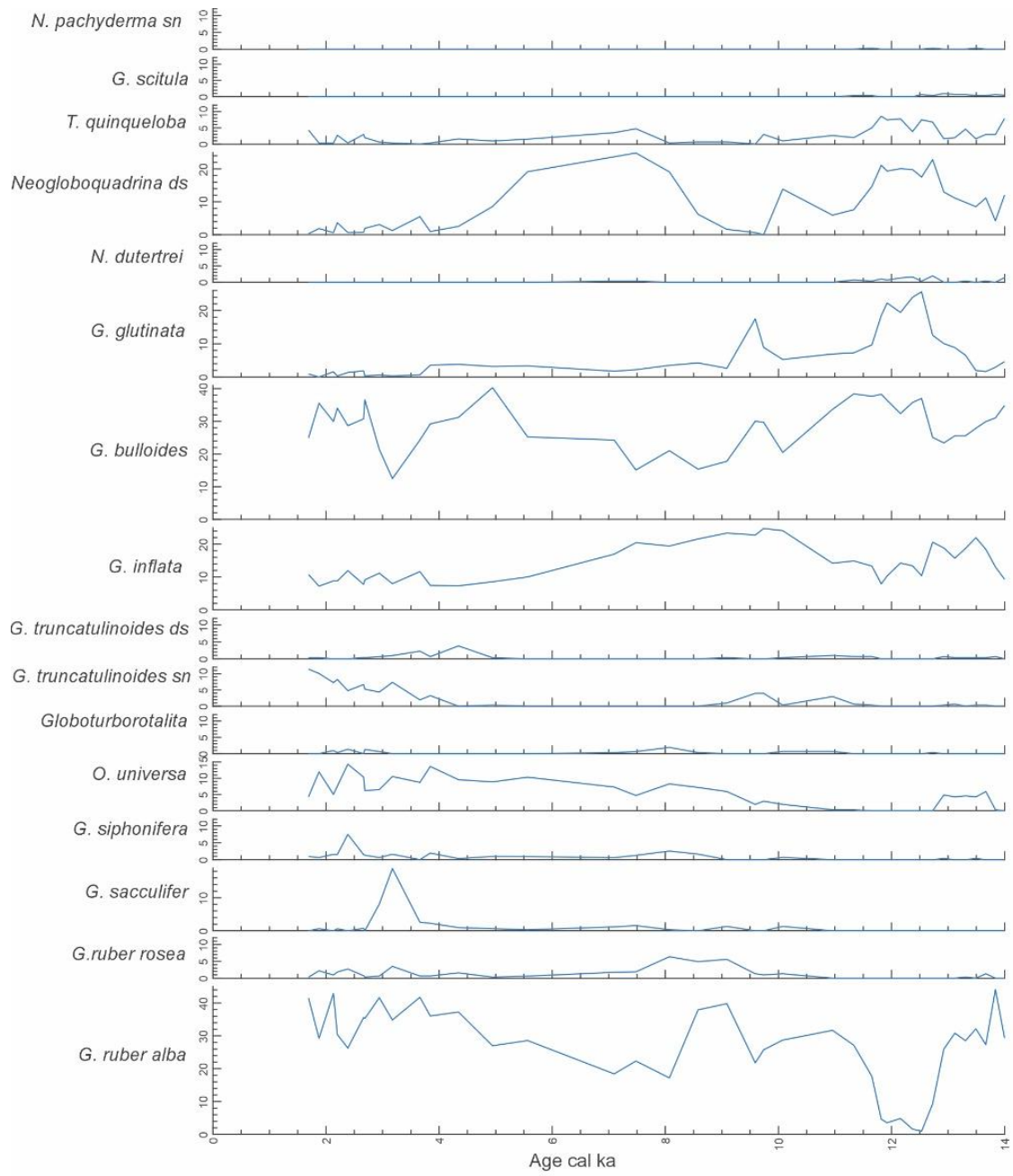
86

Figure 33 Distribution pattern of planctonic foraminifera in the GMS_98-01 C58 (>150 micron size fraction)

G. ruber alba, disappearance of *G. inflata* with the end of the subzone, the offspring of *G. bulloides, N. incompta* and slightly decrease of *G. scitula* and peak around 15ky first decreasing percentage values and then immediately increasing percentage values of *G. ruber alba, G. bulloides, G. glutinata, G. scitula, T. quinqueloba, N. incompta* and *N. pachyderma sx.*

STPFCZ2f (14.4-13.1 cal ka) - In this subzone dominant species are *G.bulloides, G.ruber alba, G. inflata, N. incompta, G. scitula, G. glutinata and T. quinqueloba.* Common species are *G. siphonifera, G. truncatulinoides sx G. truncatulinoides dx Globoturborotalita, G. scitula* forma 2 (two types of *G. scitula* described in Sgarrella 1988), *N. dutertrei* and *O. universa.* Some species are rare as *G. ruber rosea, N. pachyderma sx, G. sacculifer,* and *G. scitula* forma 1 (Sgarrella 1988). The most visible trends in that subzone are increasing percentage values and then decreasing percentage values of *G. ruber alba,* increasing percentage values and then decreasing percentage values of *G. inflata* with the end of the subzone, increasing of *G. glutinata,* the high peak of *T. quinqueloba* and small peak of *G. scitula* forma 2 and the appearance of *G. truncatulinoides sx.*

STPFCZ2e (13.1-11.6 cal ka) - In this subzone dominant species are *G. bulloides, G. glutinata, G. inflata, N. incompta,* less abundant *G. ruber alba* and *T. quinqueloba.* Common species are *N. dutertrei, G. ruber rosa, O. universa, N. pachyderma sx* and *G. scitula* forma 2. Some species are rare as *G. siphonifera, G. sacculifer, Globoturborotalita, G. truncatulinoides dx* and *sx* and *G. scitula* forma 1. The most visible trends in that subzone are increasing percentage values almost up to disappearance of *G. ruber alba* and then its increasing, decreasing percentage values and then increasing percentage values of G. inflata, big peak of *G. glutinata* and *N. incompta, s*mall peak of *G. scitula* forma 2 and the disappearance of *G. truncatulinoides sx* and *dx, G. siphonifera, Globoturborotalita* and *O. universa.*

STPFCZ2d (11.6-10.7 cal ka) - In this subzone dominant species are *G. bulloides, G. ruber alba, G. inflata, G. glutinata, T. quinqueloba* and *G. truncaatulinoides sx.* Common species are *G. ruber rosea, G. sacculifer, G. siphonifera, G. truncatulinoides dx, N. dutertrei, N. pachyderma sx, Globoturborotalita, G. scitula* forma 2 and *O. universa.* The only rare species is *G. scitula* forma 1. The most visible trends in that subzone are appearance of *G. truncatulinoides dx* and *G. truncatulinoides sx,* increasing percentage values of *G.inflata* with the end of the subzone, very big decreasing percentage values of *G.glutinata, N. incompta,* the high peak of *T. quinqueloba* and

small peak of *G.ruber rosea, G.scitula* forma 2 and appearance of *G.scitula* forma 1 and also *G.truncatulinoides* sx and *G.truncatulinoides sx.*

STPFCZ2c (10.7-10.5 cal ka) - In this subzone dominant species are *G.bulloides, G.ruber alba, G.inflata, G.glutinata, N. incompta, G. siphonifera, O.universa and G. truncatulinoides sx.* Common species are *T. quinqueloba, G. ruber rosea, G. sacculifer, G. truncatulinoides dx, G. truncatulinoides sx, Globoturborotalita* and *N. pachyderma sx*. Rare species are *G. scitula* and *N. pachyderma sx*. The most visible trends in that subzone are decreasing percentage values of *G. ruber alba* and *G. bulloides,* increasing percentage values of *G. inflata*, almost disappearance of *N. incompta* and *T. quinqueloba.*

STPFCZ2b (10.5-10.0 cal ka) - In this subzone dominant species are *G. bulloides, G. ruber alba, G. inflata, G. glutinata,* less abundant *N. incompta, O.universa, Globoturborotalita, G. siphonifera* and *G. ruber rosea.* Common species are *N. dutertrei* and *G. scitula* forma 2. Rare species are *G. sacculifer, N. pachyderma sx, G. scitula* forma 1, *G. truncatulinoides dx* and *G. truncatulinoides sx*. The most visible trends in that subzone are appearance of *G. ruber rosea,* disappearance *of G. sacculifer, G. scitula* forma 1 *and G. truncatulinoides sx,* increasing percentage values of *G. ruber alba, G. siphonifera, Globoturborotalita, O.universa and N. incompta.*

STPFCZ2a (10.0-5.1 cal ka) - In this subzone dominant species are *G. bulloides, G. ruber alba, G.* inflata and N. *incompta.* Common species are *G. ruber rosea, G. sacculifer, G. siphonifera, O.universa, T. quinqueloba, N. dutertrei, G. glutinata, N. pachyderma sx* and *Globoturborotalita*. Rare species are *G. scitula* forma 1 and forma 2, *G. truncatulinoides sx* and *dx*. The most visible trends in that subzone are appearance of *N. dutertrei*, disappearance *of G. scitula* both forms, increasing percentage values of *G. bulloides* and *O.universa*, decreasing percentage values of *G. ruber alba G. ruber rosea, N. incompta* and the high peak of *N. incompta.*

STPFCZ1c (5.1-4.0 cal ka) - In this subzone dominant species are *G. bulloides, G. ruber alba, G. inflata, N. incompta, O. universa* and *G. truncatulinoides dx.* Common species are *G. ruber rosea, G. sacculifer, G. siphonifera, G. truncatulinoides sx, N. dutertrei, T. quinqueloba* and *Globoturborotalita.* Rare species are both forms of *G. scitula* and *N. pachyderma sx*. The most visible trends in that subzone are appearance of *G. truncatulinoides sx* and high peak of *G. truncatulinoides dx,* increasing percentage values of *G. bulloides* and very big decreasing percentage values of *N. incompta.*

STPFCZ1b (4.0-1.9 cal ka) - In this subzone dominant species are *G. bulloides, G. ruber alba, G. inflata, G. sacculifer, O. universa, G. glutinata, T. quinqueloba* and *G. truncaatulinoides sx.* Common species are *G. ruber rosea, G. siphonifera, G. truncatulinoides dx, N. incompta* and *Globoturborotalita*. Rare species are *N. dutertrei, G. scitula* both forms and *N. pachyderma sx*. The most visible trends in that subzone are the high peak of *G. sacculifer,* decreasing percentage values of *N. incompta, G. truncatulinoides dx* and *G. bulloides* and then around 4ka decreasing percentage values of *G. truncatulinoides dx* followed by the 3.4ka decreasing percentage values of *G. bulloides* and decreasing percentage values on the end of the subzone of *G. ruber alba*.

STPFCZ1a (1.9 cal ka-present) - In this subzone dominant species are *G. bulloides, G. ruber alba, G. inflata, G. truncaatulinoides sx. G. glutinata, T. quinqueloba, O.universa* and *N. incompta.* Common species are *G. ruber rosea, G. sacculifer, G. siphonifera, G. truncatulinoides dx, G. scitula* forma 2 and *Globoturborotalita*. Rare species are *N. dutertrei, N. pachyderma sx* and *G. scitula* forma 1. The most visible trends in that subzone are increasing percentage values of *G. ruber alba, G. ruber rosea, Globoturborotalita, O. universa, G. inflata, N. incompta* and *T. quinqueloba* around 1.8ky, decreasing percentage values of *G. sacculifer* and *G. truncatulinoides dx.*

In figure 34, this new ecozonation scheme is compared with previous schemes proposed for the Tyrrhenian Sea.
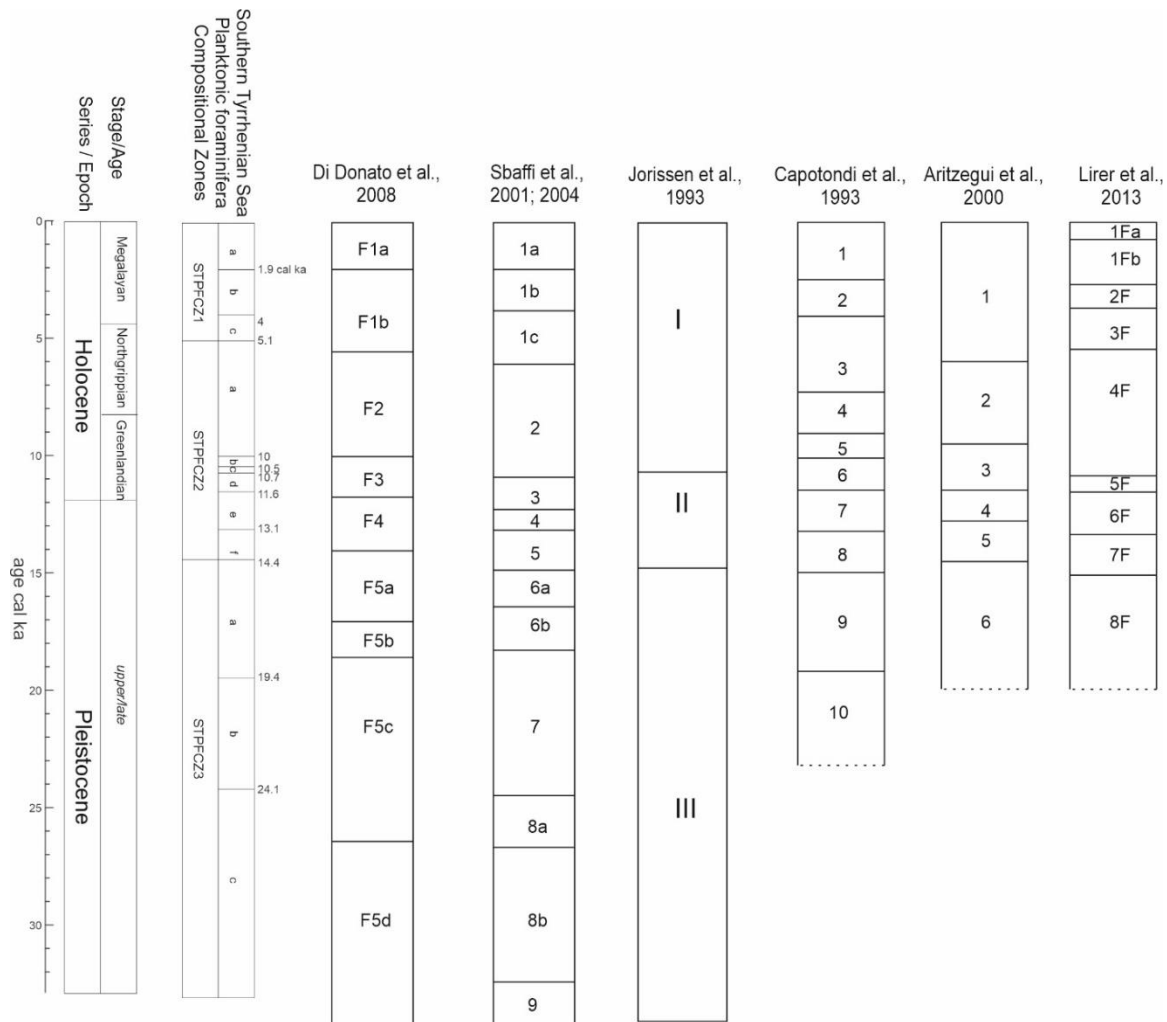
Figure 34 The new planktonic foraminifera ecozonation scheme is compared with previous schemes proposed for the Tyrrhenian Sea.

5.4 SST reconstructions

SST reconstructions from planktonic foraminiferal assemblages were obtained by means of CoDa-MAT and Coda-PLS. Details on these methods can be found in (Di Donato et al., 2018a; Di Donato et al., 2018b; Di Donato et al., 2019 in press.). The modern calibration dataset required by these methods consists of 1253 Atlantic and Mediterranean core top assemblages (Prell et al., 1999; Hayes et al., 2004; Kucera et al., 2004). The Mediterranean subset is represented by 156 core top assemblages. The oceanographic parameters were extracted from the World Ocean Atlas 2009 (Antonov e al., 2010; Locarnini et al., 2010) by means of Ocean Data View 4.5.1 (Schlitzer, 2018),

and are referred to a depth of 10 m (Kucera et al., 2005). The analyses were made by expressly written Matlab codes.

The SST reconstructions for the studied cores are shown in figures 35-40.

Figure 35-CodaMat reconstruction for Core GNS-84 C106. The error bars show the standard deviation obtained for each reconstructed value. The mean distance graph shows the mean Aitchison distance of each fossil assemblages from the closest modern analogues. The squared mahalanobis graph shows the squared mahalanobis for the centre of the cloud of the modern assemblages. Values beyond the blue line are atypical at an alpha level of 0.001

The core GNS-84 C106 SST is reconstructed for the last 33ka. The magnitude for the summer between the lowest and highest temperatures is 13°C. The lowest T for the summer is 11°C around 30ka, 28ka and 27.5ka and the highest T is 24°C for the last 5ka (Fig. 35). For the winter the magnitude between the lowest and highest temperatures is 8°C. The lowest T for the winter is 7°C around 30ka and 28ka and the highest T is 15°C for the 4ka and for 7-9ka. The base of the

record shows SST of 17°C in the summer and 12°C in the winter and around 30ka decreased to 11°C in summer, 7°C in the winter during the period of Heinrich event 3 (H3). These SST fluctuations show only small fluctuations up to 24.5 ka. The most important fluctuation appears between 24 ka and 19 ka (Heinrich event 2- H2), when SST increased to 20°C in summer and 15°C in winter. Between 19 ka and 15 ka SST decreased to 12°C in the summer and 8°C in the winter. Between 15 ka and 12ka SST increases to 24°C in summer and 15°C in winter with strong decreasing of SST from 13 ka. From 12 ka till now the SST are quite stable with the values 20-24°C for the summer and 13-15°C for the winter.
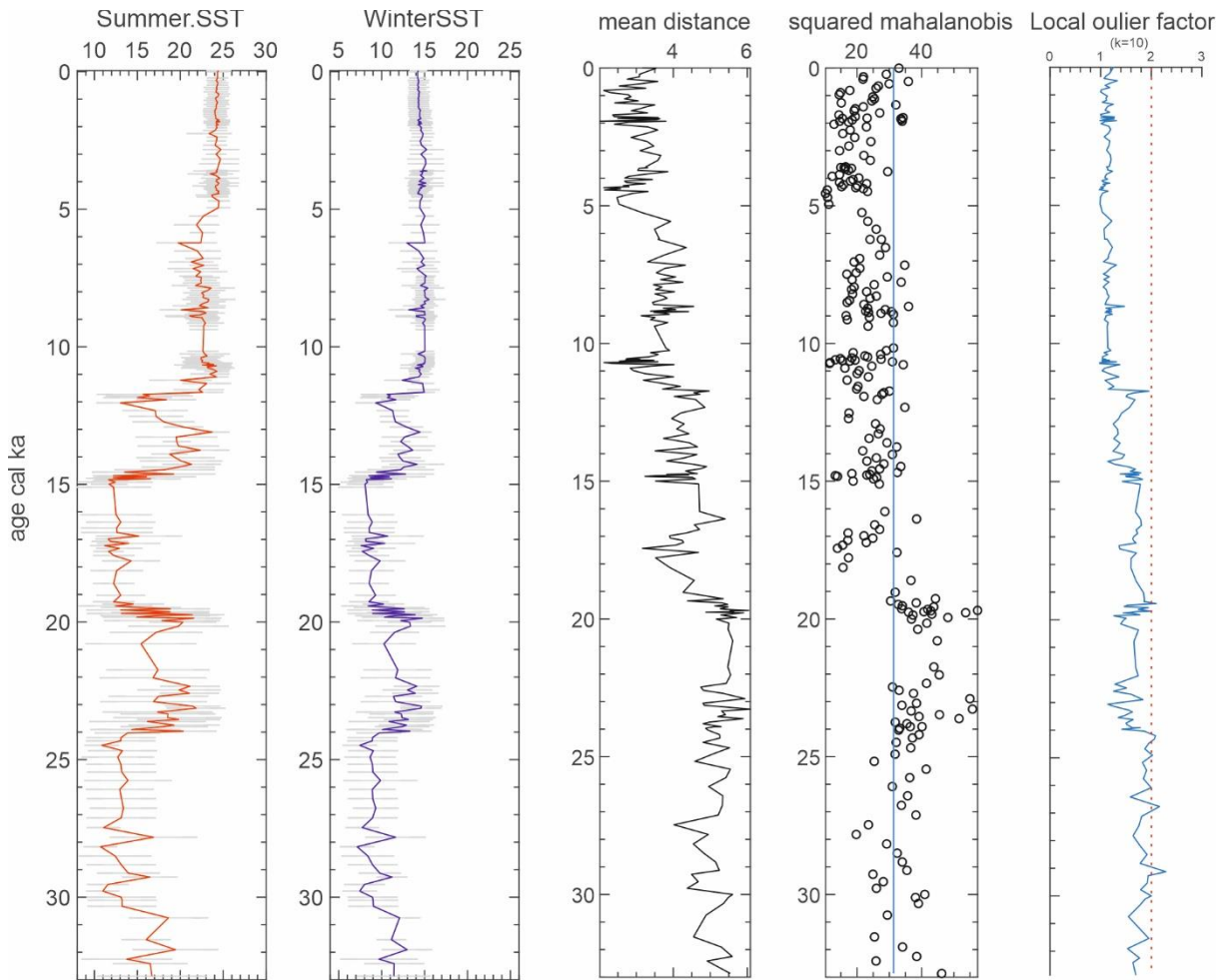

Figura 36 - CodaMat SST reconstruction for Core TRansect2017_TR1. The error bars show the standard deviation obtained for each reconstructed value. The mean distance graph shows the mean Aitchison distance of each fossil assemblages from the closest modern analogues. The squared mahalanobis graph shows the squared mahalanobis for the centre of the cloud of the modern assemblages. Values beyond the blue line are atypical at an alpha level of 0.001

The core Transect_2017 TR1 SST is reconstructed for the last 15 ka, as the base of the core is marked by the Neapolitan Yellow Tuff eruption. For the summer the magnitude between the

lowest and the highest SST is 13°C (fig.36). The lowest summer SST is 12°C around 13 ka and the highest SST is 25°C for 5 ka. For the winter SST range between the lowest and highest values is 7°C. The lowest winter SST is 8°C around 13 ka and the highest SST is 15°C for the range 8-9 ka. 15 ka started with values 19°C in summer and 13°C in winter. Then around 13ka SST decreased to 12°C in the summer and decreased to 8°C in the winter from the beginning of Younger Dryas till the end of YD 11.7 ka, which is the most important fluctuation appeared in the core. Then from 11.7 ka SST increases and decreases around 11ka again with summer SST 18°C and 13°C in winter. From 11 ka till recent values increases and with some smaller fluctuations stays in the range of SST 20-25°C in summer and 13-15°C in winter.
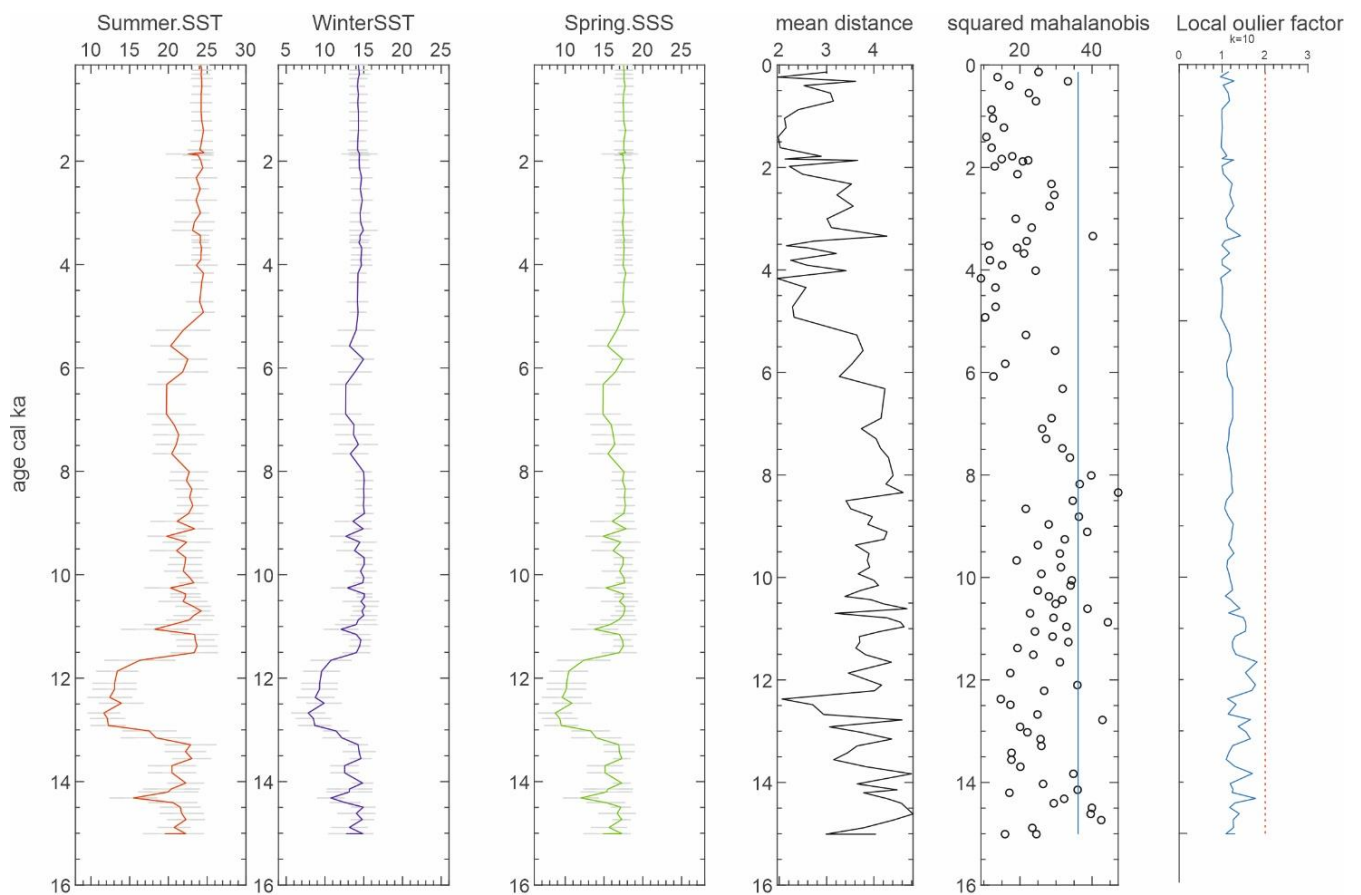

Figura 37-CodaMat reconstruction for Core GMS_98-01-C58. The error bars show the standard deviation obtained for each reconstructed value. The mean distance graph shows the mean Aitchison distance of each fossil assemblages from the closest modern analogues. The squared mahalanobis graph shows the squared mahalanobis for the centre of the cloud of the modern assemblages. Values beyond the blue line are atypical at an alpha level of 0.001.

The core GMS_98-01-C58 SST is reconstructed from 13.5 ka to 1 ka, because very likely the top core was lost during the recovery. The magnitude for the summer between the lowest and highest temperatures is 11°C. The lowest summer SST is 12°C around 12.5ka (YD) and the highest SST value is 23°C for 8-6 ka and for 3.5 ka. The magnitude between the lowest and highest winter SST is 9°C. The lowest winter SST value is 8°C around 13 ka (beginning of YD) and the highest SST value is 17°C for the 3.5-3 ka and 1.5 ka (fig. 37). 13.5 ka started with summer SST values 18°C and winter SST values 14°C. Then around 12.5ka SST decreased to 12°C in summer and 8°C in the winter and SST values increased around 10.5 ka to 22°C in the summer and 17°C in the winter. From 10.5 ka SST increased and decreased with some smaller fluctuations in SST values in the range 20-23°C in summer and 15-17°C in winter.
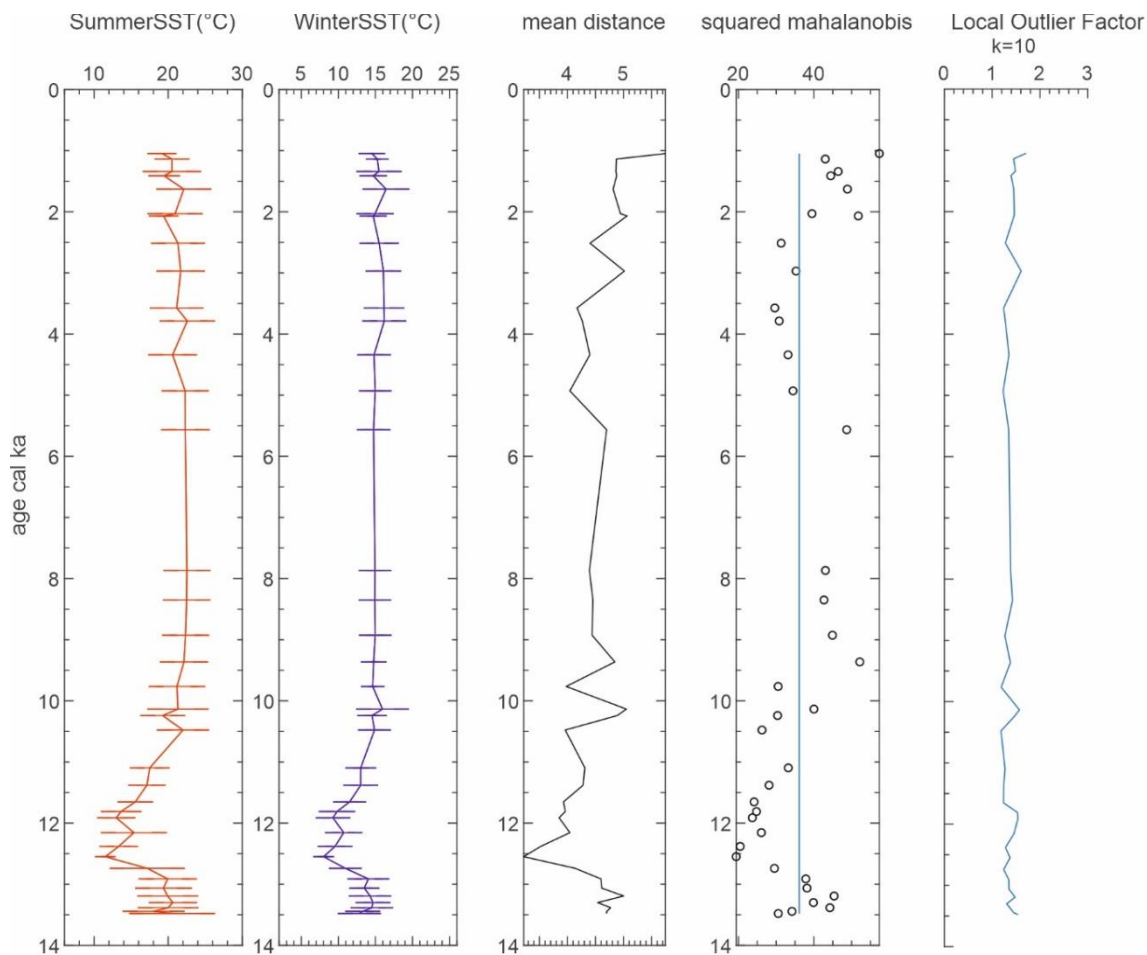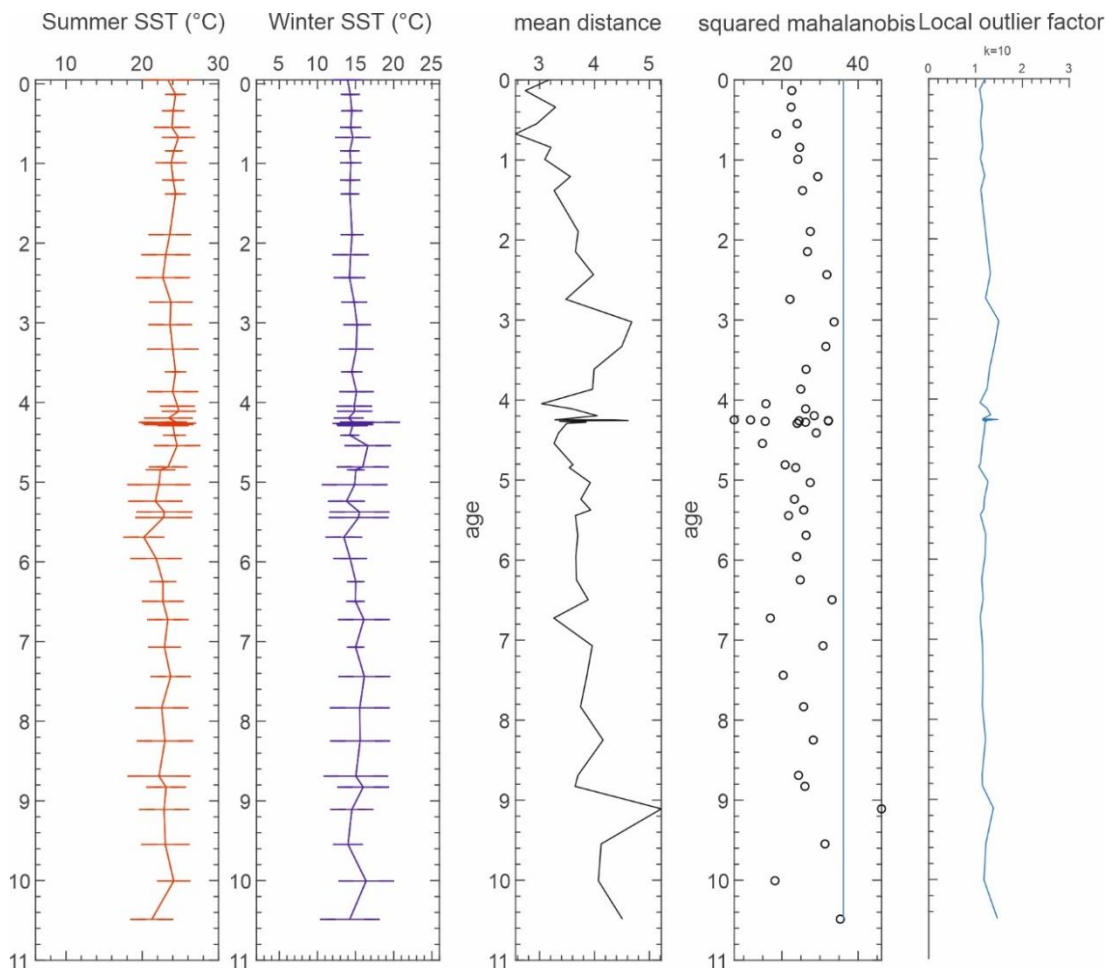

Figure 38 - CodaMat reconstruction for Core GMS_98-01-C14. The error bars show the standard deviation obtained for each reconstructed value. The mean distance graph shows the mean Aitchison distance of each fossil assemblages from the closest modern analogues. The squared mahalanobis graph shows the squared mahalanobis for the centre of the cloud of the modern assemblages. Values beyond the blue line are atypical at an alpha level of 0.001.

The core GMS_98-01-C14 SST is reconstructed from 10.5 ka. The magnitude for the summer between the lowest and highest temperatures is 5°C. The lowest summer SST value is 20°C around 5.5 ka and the highest SST is 25°C from 4 ka to 1ka (Fig. 38). The magnitude between the lowest and highest winter SST values is 3°C. The lowest winter SST value is 14°C around 9 ka and 5.7 ka. The highest winter SST is 17°C for the 4.5 ka. In the core the fluctuations are small without visible trends, increasing slightly after 5.5 ka.
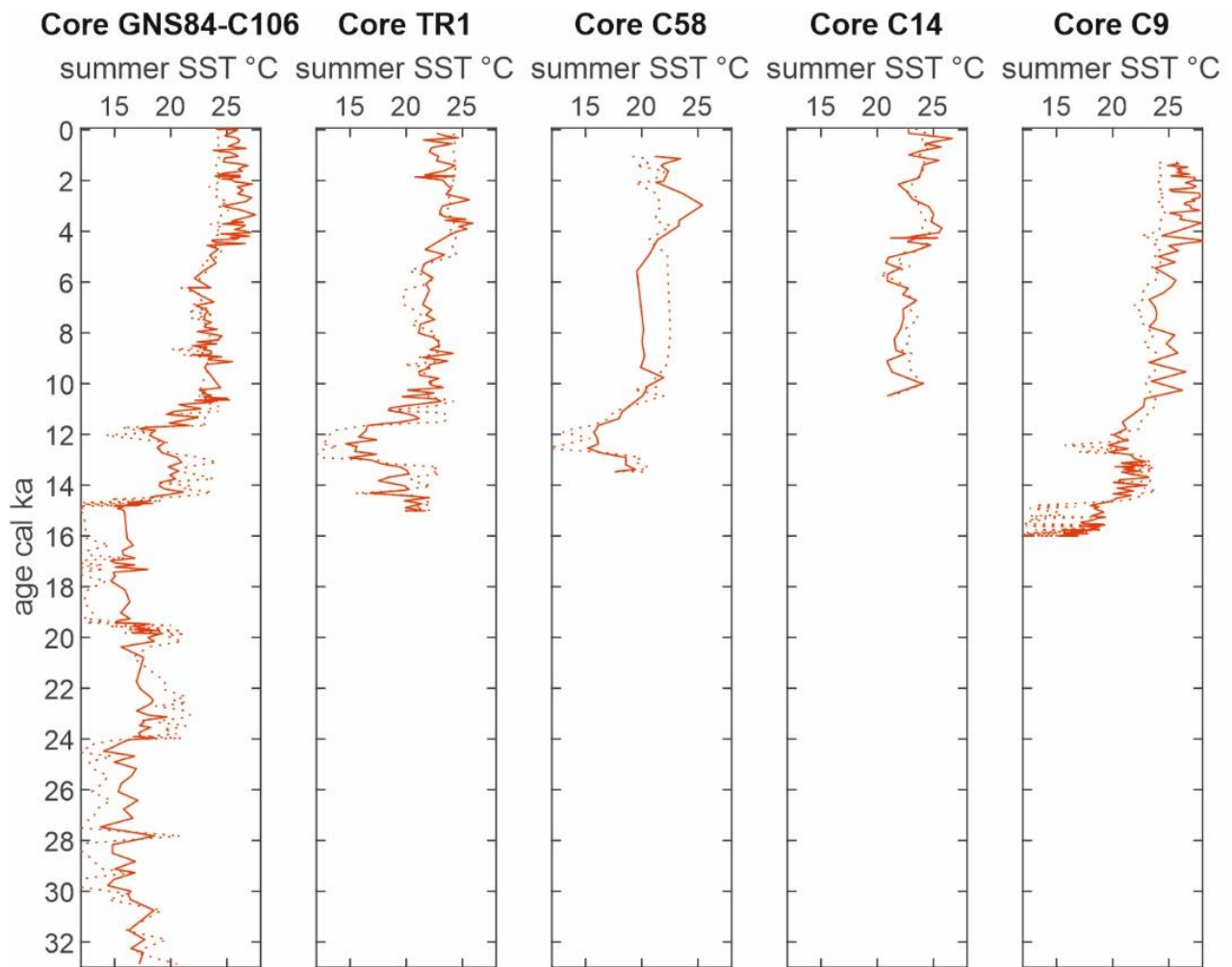
Figure 39- Comparison between Coda-PLS (full line) and Codamat summer SST (dotted line) reconstructions. In the figure are also reported the results obtained from the Core G93-C9 (unpublished data, kindly provided by Prof. Valentino Di Donato)
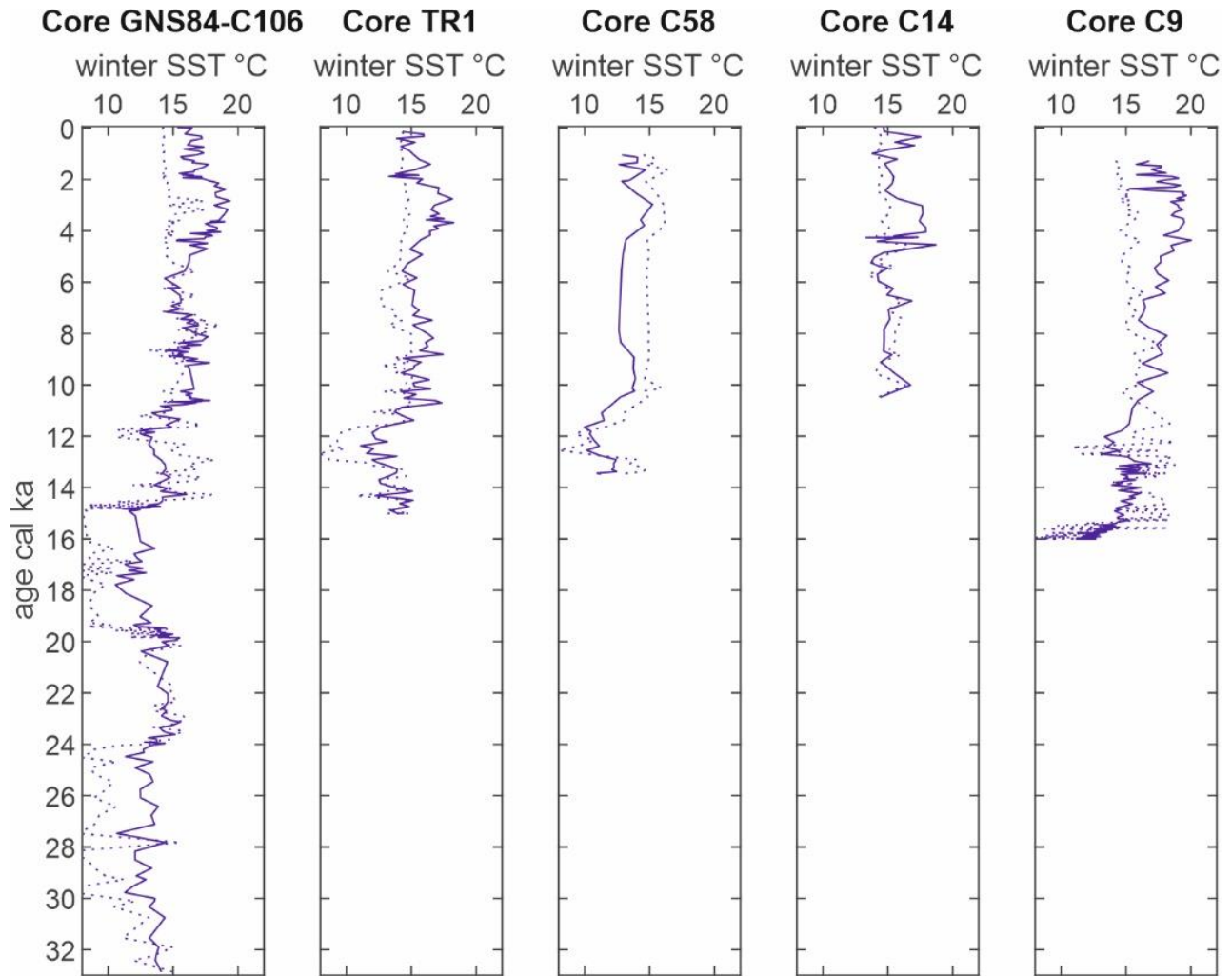
Figure 40-Comparison between Coda-PLS (full line) and Codamat winter SST (dotted line) reconstructions. In the figure are also reported the results obtained from the Core G93-C9 (unpublished data, kindly provided by Prof. Valentino Di Donato)

On the basis of the CoDa methods applied to planktonic foraminifera assemblages it was obtained: the CoDa regression Partial Least Squares (full line; finds linear regression by projecting the predicted variables from core top assemblages) and CoDaMAT modern analogue techniques (dotted line; mean of temperature and standard deviation). The figures 39 and 40 are the comparison of the summer and winter SST in five cores from western Mediterranean Sea: C106 (G. of Salerno), TR1 (Capri Sud), C58 and C14 (Gulf of Naples) and G93-C9 (Gulf of Gaeta – unpublished data provided by Prof. Valentino Di Donato).

5.5 Benthic foraminifera Zonation of the cores.

The distribution of benthic foraminifera in the cores Transect2017_TR1 and GNS84-C106 is shown in figures 41 and 42. For the GNS84-C106, the record improves the previously published data by strongly increasing the chronological resolution.

The Zonation of the Cores is shown in figures 41 and 42. It can be noted that two compositional changes around 14.2 and 11 ka, at the beginning of the Bølling-Allerød and the Holocene, respectively, are recorded in both cores. Within the Holocene, two compositional changes are evident for the Core GNS84-C106: the first at 8.7 ka approximates the end of the ORL1 interval, while the second, at 4.6 ka, follows the end of the Sapropel S1 event. In the Transect2017_TR1, a compositional change was recorded at 7.6 ka, between the end of the ORL1 interval and the end of the Sapropel S1 event. The main compositional changes recorded in the cores are not synchronous. However, due the depth of recovery of these two cores, the Core Transect2017_TR1 could be expected to record changes in the WMDW dynamics, while the record of the Core GNS84-C106 could be more related to the dynamic of surface to intermediate water masses.

Figure 41 Distribution of benthic foraminifera in the Core Transect2017_TR1. Benthic foraminifera are compared with the Greenland ice core record. The extension of the ORL1 and Sapropel S1 is also reported to the right.
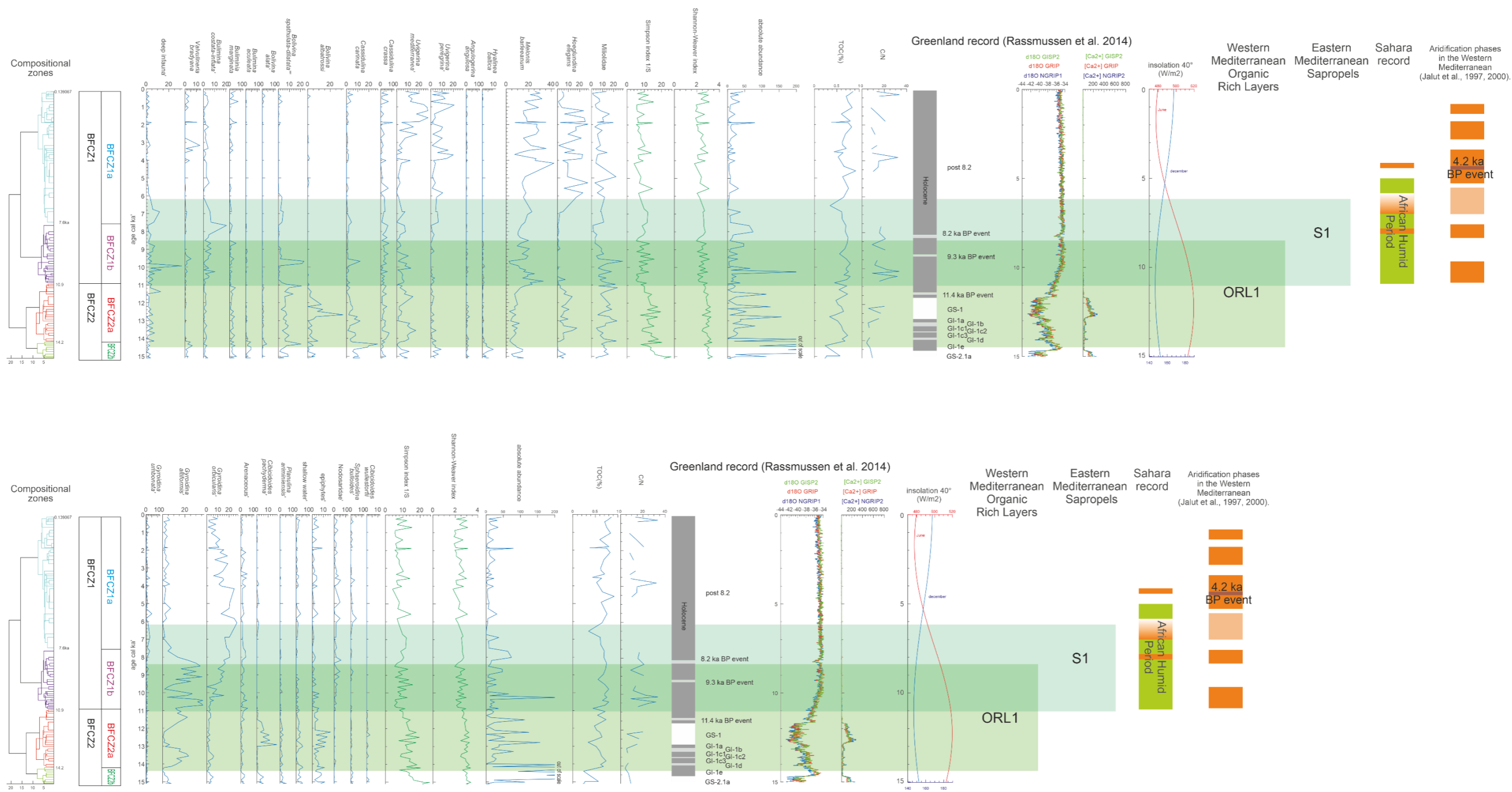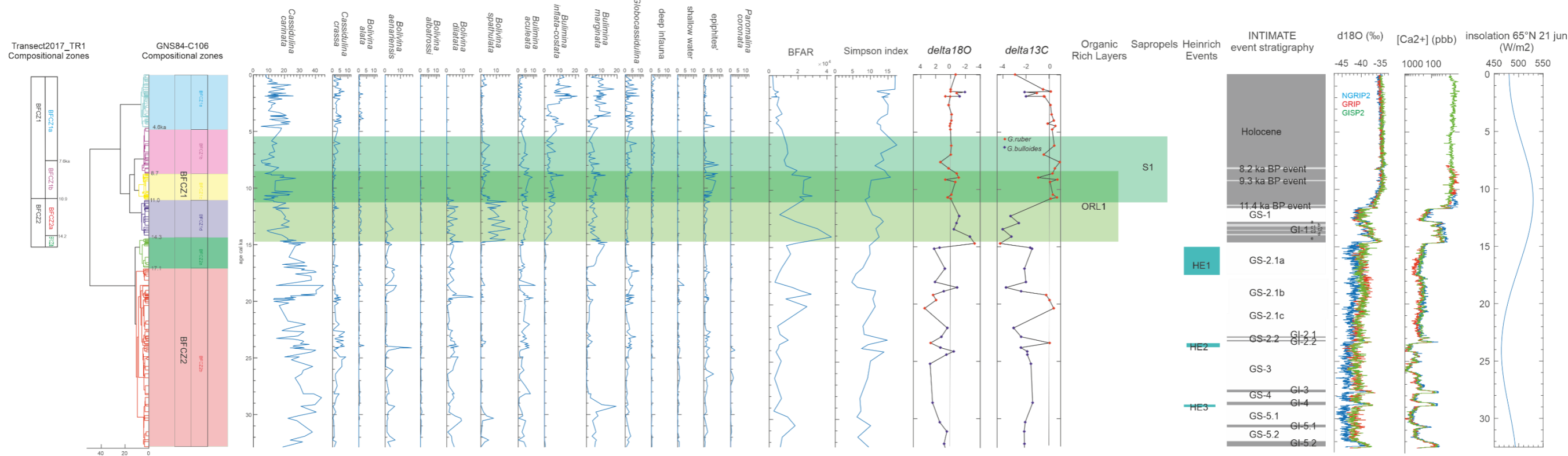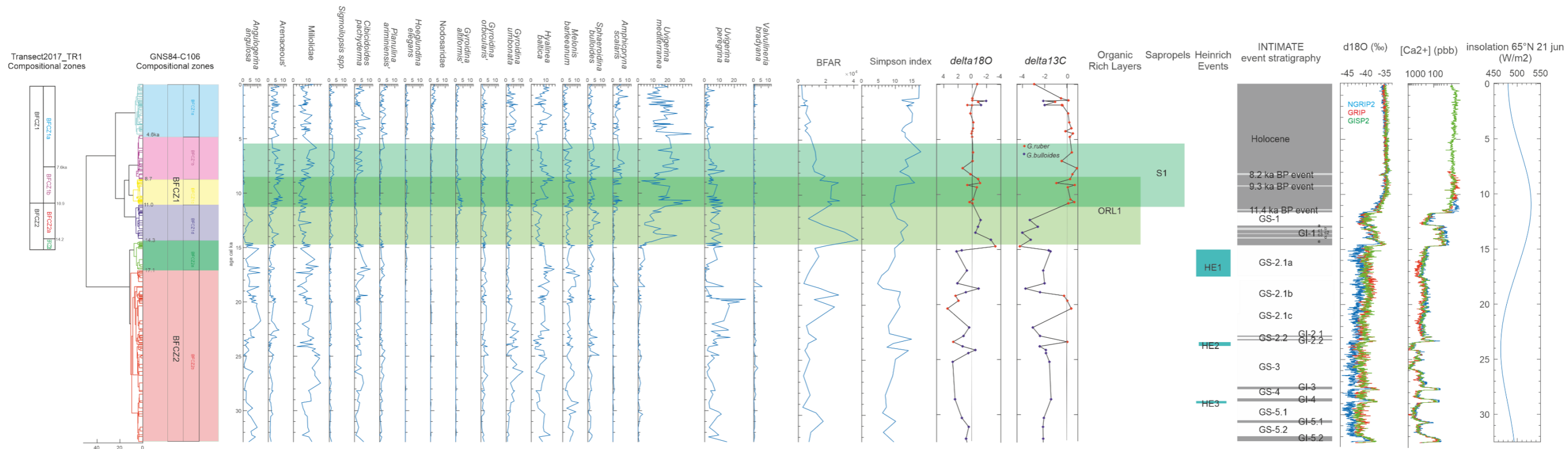
Figure 42 Distribution of benthic foraminifera in the Core GNS84-C106. Benthic foraminifera are compared with the Greenland ice core record. The extension of the ORL1 and Sapropel S1 is also reported to

Fig. 43 Distribution of benthic foraminifera in the Core GMS_98-01-C58.
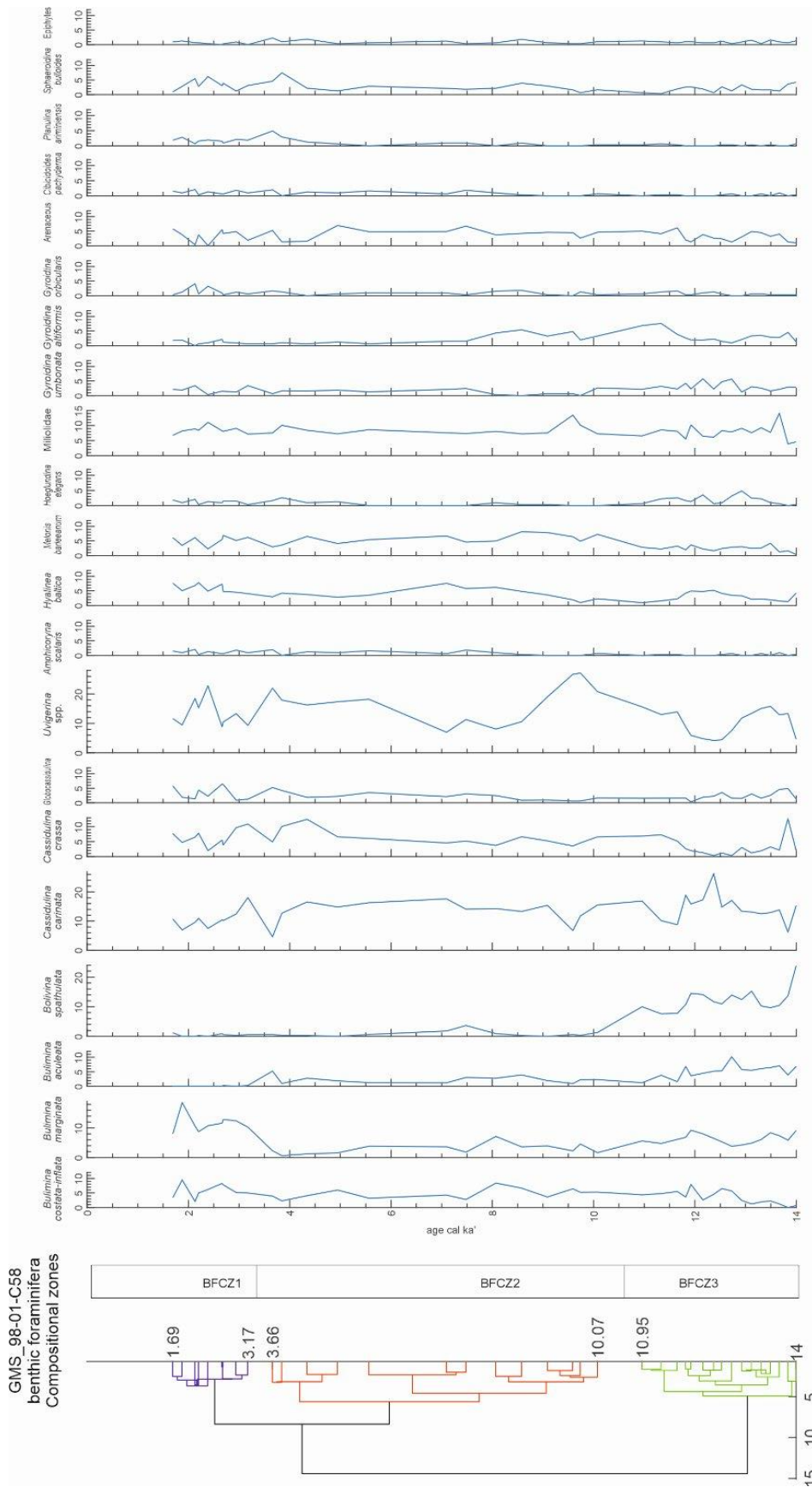
Fig. 44 Distribution of benthic foraminifera in the Core GMS_98-01-C14.

Benthic Foraminifera Compositional zones

The compositional benthic zones are below described for cores TR1, C106, C58 and C14.

In core Transect2017_TR1 two main zones with the four subzones were identified:

STBFCZ2b (15 – 14.2 cal ka) - In this subzone abundance of the Foraminifera is the highest from all subzones. Dominant species are *B. spathulata-dilatata, C. carinata, C. crassa, Miliolidae U. peregrina, U. mediterranea, M. barleanum, H. baltica* and *H. elegans.* Less abundant are *B. marginata, B. aculeata, C. pachyderma, G. altiformis, epiphyties G. orbicularis, shallow water species* and *B. albatrossi* Some species are rare or are very few in comparison to another subzones: *V. brayana, A. angulosa, P. ariminensis* and *B. inflata-costata.* The most visible trends in that subzone are increasing values respectively to other groups such *B. spathulata-dilatata, C. carinata, abundance of C. wullestorfii, B. albatrossi and H. baltica.*

STBFCZ2a (14.2- 10.9 cal ka) - In this subzone on the beginning of ORL1 dominant species are *C. carinata, B. albatrossi, B. spathulata-dilatata, U. mediterranea, C. crassa, M. barleanum, Miliolidae, G. altiformis, B. marginata, C. pachyderma* and *H. elegans*. Some species are quite abundant respectively to another subzones: *H. elegans* and *B. albatrossi.* The main trends are increasing percentage values of *G. altiformis,* Arenaceous species*, C. pachyderma* (from the middle of the subzone)*, B. albatrossi* and *B. spathulata-dilatata* is very abundant in comparison with other subzones. Another characteristic change is decreasing percentage values of V. *bradyana B. aculeata, U. peregrina* and *H. baltica*.

STBFCZ1b (10.9– 7.6 cal ka) - In this subzone till the end of the ORL1 and correspondence with the Sapropel S1, dominant species are deep infaunal species*, M. barleanum, B. costata-inflata, U. mediterranea, Miliolidae, G. altiformis, G. orbicularis C. crassa* and *C. carinata.* Some species are specifically abundant in comparison to the another subzones: deep infaunal species, *B. spathulata-dilatata,,* very high peak of *G. altiformis, G. orbicularis* and *B. inflata-costata,.*The most visible trends in that subzone are decreased values of *B. albatrossi, Milioolidae, H. elegans,* epiphytes *a*nd *C. pachyderma.* It can be noticed also increasing percentage values of *Sphaerodina. Bulloides, G. umbonata* and *Nodosaridae.*

STBFCZ1a (7.6 - present) - In this subzone corresponding to the end of Sapropel S1 (until ~6ka), dominant species are *U. mediterranea, U. peregrina, Miliolidae, M. barleanum, H. elegans, G. orbicularis* and *B. marginata.* Some species are typically abundant in comparison to another subzones: *H. elegans*, *U. mediterranea, U. peregrina, V. bradyana* and *B. marginata.* The most visible trends in that subzone are decreased values of deep infaunal species, *B. spathulata-dilatata, C. pachyderma, C. carinata, P. ariminensis* slightly *Miliolidae,* B. *inflata – costata,* Areanaceous species and slightly *G. orbicularis.*

In core GNS_84-C106 two zones and six subzones were identified:

STBFCZ2b (33 – 17.1 cal ka) - In this subzone dominant species are *C. carinata, U. peregrina, Miliolidae* and *B. marginata.* Common species are *A. amgulosa, C. pachyderma, G. orbicularis, G. umbonata, H. baltica, M. barleanum, V. bradyana* and *B. aenariensis.* Some species are rare as or are very few in comparison to another subzones: *H. elegans*, *B. spathulata, U. mediterranea, A. scalaris, G. altiformis, Nodosaridae, B. inflata-costata* and deep infauna .The most visible trends in that subzone are decreased values respectively to other groups such as *U. mediterranea, B. spathulata* and *B. inflata – costata,* and also decreasing percentage values of *C. carinata.*

STBFCZ2a (17.1 – 14.3 cal ka) - In this subzone dominant species are *B. marginata. C. carinata, U. peregrina, U. mediterranea, Miliolidae* and *H. baltica.* Some species are rare as or are very few in comparison to another subzones: *V. brayana*, *B. spathulata, A. scalaris, G. altiformis, B. inflata-costata* and *Globocassidulina* spp.. The most visible trends in that subzone are decreased values respectively to other groups such as *V. brayana*, *B. spathulata, A. scalaris, G. altiformis, B. inflata-costata* and *Globocassidulina* spp., and also decreasing percentage values of *B. marginata.*

STBFCZ1d (14.23- 11 cal ka) - In this subzone on the beginning of ORL1 dominant species are *C. carinata, B. spathulata, U. mediterranea, Miliolida, B. marginata U. peregrina.* and *A. angulosa.* Some species are quite abundant respectively to another subzones: *H. elegans*, *B. spathulata, B. dilatata, B. aenariensis, G. altiformis* and *B. inflata-costata.* The increasing percentage values of *H. elegans*, *B. spathulata, B. dilatata, B. aenariensis, G. altiformis* and *B. inflata-costata* is very characteristic.

STBFCZ1c (11 – 8.7 cal ka) - In this subzone till the end of the ORL1, dominant species are *C. carinata, U. mediterranea, U. peregrina, Miliolidae,* Arenaceous, *H. baltica and B. marginata.* Some species are typically abundant in comparison to the another subzones: *H. elegans*, *B. spathulata, U. mediterranea, A. scalaris, G. altiformis, B. aculeata, B. inflata-costata, B. marginata* and *Globocassidulina* spp. .The most visible trends in that subzone are decreased values almost no *A. angulusa*, *B. dilatata, C. pachyderma, Milioolidae, U. mediterranea a*nd *B. inflata – costata,* and also decreasing percentage values of epiphities, *U. peregrina* and increasing percentage values of *C. crassa*

STBFCZ1b (8.7 – 4.6cal ka) - In this subzone partially corresponding the Sapropel S1, dominant species are *C. carinata, U. mediterranea, U. peregrina, Miliolidae, Arenaceous, H. baltica and B. marginata.* Some species are typically abundant in comparison to the another subzones: *H. elegans*, *B. spathulata, U. mediterranea, A. scalaris, G. altiformis, B. aculeata, B. inflata-costata, B. marginata* and *Globocassidulina* spp. .The most visible trends in that subzone are decreased values almost no *A. angulusa*, *B. dilatata, C. pachyderma, Milioolidae, a*nd *B. inflata – costata,* and also decreasing percentage values of *epiphities, U. peregrina* and increasing percentage values of *C. crassa, U. mediterranea* and *P. ariminiensis.*

STBFCZ1a (4.6 cal ka – present) - In this subzone dominant species are *C. carinata, U. mediterranea, Miliolidae, B. inflata-costata, Globocassidulina* spp.*, B. marginata, H. baltica, C.pachyderma* and *Arenaceous.* Some species are typically abundant in comparison to another subzones: *H. elegans*, *Nodosaridae, G. umbonata, C. crassa, B. alata, B. inflata-costata, B. marginata* and *Globocassidulina* spp.*. T*he most visible trends in that subzone are increasing percentage values of *H. elegans*, *Nodosaridae, G. umbonata, C. crassa, B. alata, B. inflata-costata, B. marginata* and *Globocassidulina* spp..

In core GMS_98-01-C58 three zones were identified:

BFCZ3 (14-10.95 cal ka) – In this subzone dominant species are *C. carinata, Uvigerina spp., Miliolidae, B. spathulata, B. inflata-costata, B. marginata, B. aculeata, G. umbonata and G. altiformis.* Some species are typically abundant in comparison to another subzones: *B. spathulata, G. umbonata* and *G. altiformis*. The most visible trends in that subzone are decreasing percentage values of *B. aculeata*, *C. crassa, B. spathulata* and around 13 ka *Uvigerina* spp..

BFCZ2 (10.95-3.17 cal ka) – In this subzone dominant species are *C. carinata, Uvigerina spp., Miliolidae, C. crassa B. inflata-costata, B. marginata,* Arenaceous*, M. barleanum and Hyalinea baltica. Uvigerina* spp. is even more abundant in comparison to another subzones. The most visible trends in that subzone are decreasing percentage values of *B. spathulata*, *H. elegans* and *B. aculeata* and slightly increasing values of *H. baltica and M. barleanum.*

BFCZ1 (3.17-1.69) - In this subzone dominant species are *C. carinata, Uvigerina spp., Miliolidae, C. crassa, B. inflata-costata, B. marginata,* Arenaceous*, M. barleanum, S. bulloides, Globocassidulina* spp. *and Hyalinea baltica.* The most visible trends in that subzone are increasing percentage values of *B. marginata, B. costata-inflata and S. bulloides* and decreasing percentage values of *B. spathulata* and *B. aculeata,*

In core GMS_98-01-C14 two zones were identified:

BFCZ2 (8.96-7.48 cal ka) – In this subzone dominant species are Arenaceous, *B. aculeata, C. carinata, Uvigerina spp., Miliolidae, B. spathulata, B. inflata-costata* and *B. marginata.* The most visible trends in that subzone are decreasing percentage values of *H. elegans*, *C. crassa* and *B. marginata*.

BFCZ1 (7.48 cal ka – present) - In this subzone dominant species are *C. carinata, Uvigerina spp., Miliolidae, B. spathulata, B. inflata-costata, B. marginata, M. barleanum,* Arenaceous, *Globocassidulina* spp. and *H. baltica..* The most visible trends in that subzone are the strong fluctuations of values around 4.2 ka, decreasing percentage values of *B. aculeata*, *C. crassa, B. spathulata* and *Uvigerina* spp. and also increasing values of *V. bradyana,C. carinata, H. elegans, S. bulloides* and *C. pachyderma.*

6. Discussion

6.1 Relative variation biplots

Relative variation biplots were elaborated for the cores GNS84-C106 and Transect_2017 TR1, for which more samples are available. Within the biplots, the observations were symbolised according to the results of the constrained cluster analysis.

The RVB of Core GNS84-C106 is shown in figure 45. The variability accounted by the first two components is, respectively, 70.12% and 10.10% of total variance, cumulating 80.22% of total variance.

Figure 45 - RVB of planktonic assemblages of Core GNS84-C106. The color of sample points corresponds to the grouping obtained from the zonation of the core (see figure 44).

The pattern of the links connecting column (*taxa*) points highlights, along the first axis, the close relationship (i.e. short links) among warm water *taxa* such as *G. siphonifera, G. ruber, G. sacculifer, O.universa,* all of which are located on the negative side of axis 1. These taxa are contrasted, to cold water *taxa* such as *T. quinqueloba* and *G. scitula* are located on the positive of axis 1. Along the second axis, it can be noted the counterposition between *G. truncatulinoides* and *Neogloboquadrina incompta*, the link between which highlights their high logratio variance. A high logratio variance also can be noted for *G. scitula* and *G. inflata*. By converse, a very low logratio variance can be observed for *G. siphonifera* and *O.universa* or *T. quinqueloba* and *G. glutinata*.

For this core, the RVB appear strongly determined by the contrast between two groups of samples, i.e. last glacial assemblages belonging to Compositional Zones PFCZ4 and Holocene assemblages (Compositional Zones PFCZ1 and PFCZ2). This may hide some source of variability which, however, may be found as important for illustrate the post glacial variability of planktonic assemblages in the Tyrrhenian Sea. The RVB obtained from Core Transect_2017 TR1 (Figure 46) better illustrates the late glacial to Holocene variability of planktonic foraminifera in the Southern Tyrrhenian Sea. For this RVB, the first two components account for a lesser amount of total variability, 35.66% and 23.37%, respectively. This implies that the relationships shown in a 2-dimensional biplot are subjected to a certain degree of approximation and more dimensions would be taken into account to fully describe the dataset. A third component accounts for 8.68% of variance, for a cumulate total of 67.71%b (Figure 46). Within this biplot, it can be clearly seen the strong contrast between *G. truncatulinoides* and *Neogloboquadrina* incompta, which, according to the ecological behaviour of these taxa can be explained in terms of deep mixing/pycnocline vs. shallower pycnocline (shallowing of the top of the LIW). At right angle with the link connecting these species, it can be seen the opposition on two groups of taxa, the first of which represented by *T. quinqueloba, G. glutinata* and *G. scitula,* and the second by warm water species, such as *G. siphonifera, O.universa, G. ruber, G. sacculifer.*
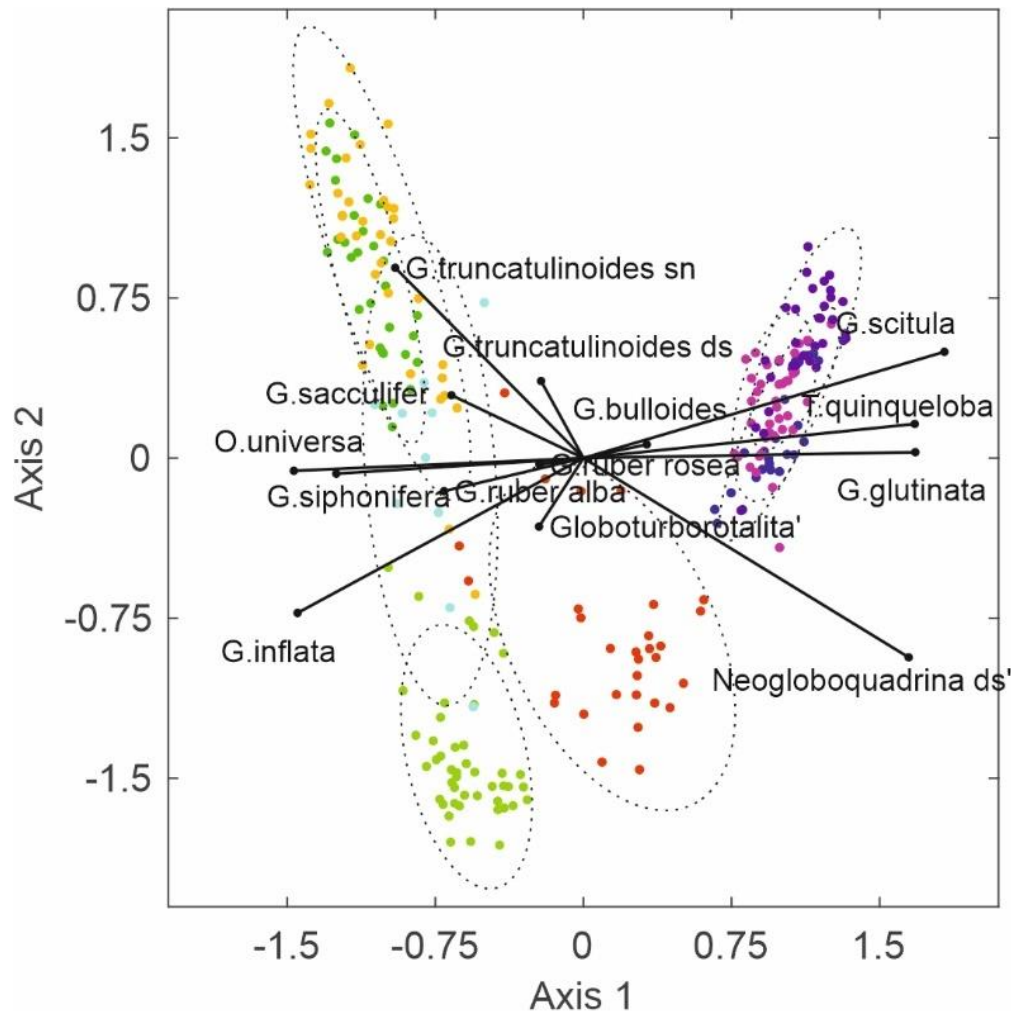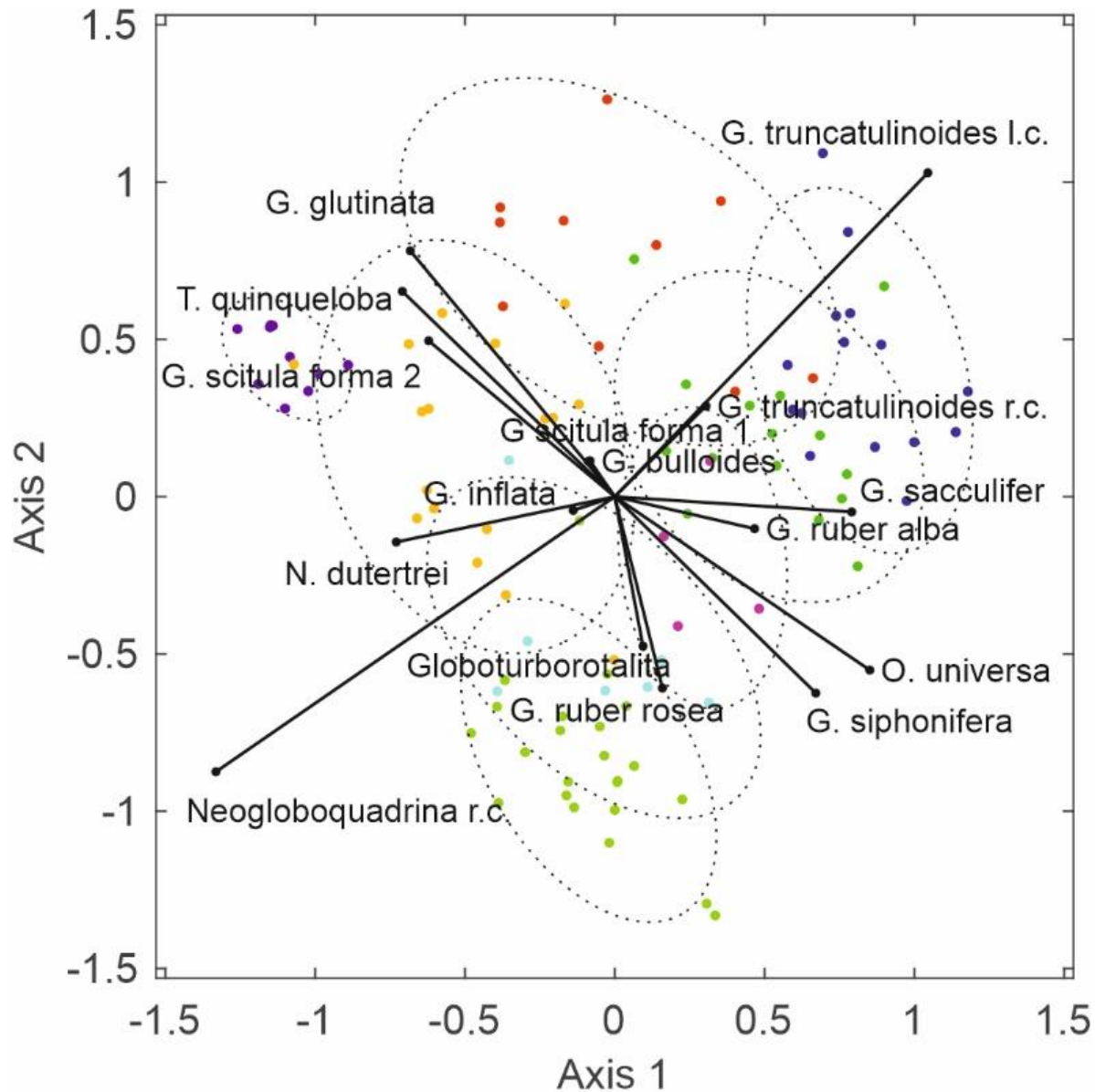
Figure 46 RVB of planktonic assemblages of Core Transect_2017 TR1. The color of sample points corresponds to the grouping obtained from the zonation of the core (see figure 43).

This contrast is clearly related to SST changes. The right angle formed by the links connecting these two groups of taxa indicate a low correlation between the corresponding logratios (Aitchison and Greenacre, 2002), i.e. the logratio between *G. truncatulinoides* and *Neogloboquadrina* r.c. varies independently from the logratios between warm and cold-water taxa. It can be also noted that the *G. sacculifer* column point is located towards the *G. truncatulinoides* column point. This suggest a preference of this species for winter mixing conditions. Besides, at present this species is abundant in the north western Mediterranean (Pujol and Grazzini, 1995), a sector characterised

by higher wind stress and prevailing positive wind stress curl (Pinardi et al., 2015). If a third component is taken into account (Figure 47), it can be seen a relationship with the distribution of *Globoturborotalita* spp. and *G. ruber rosea*. *G. ruber rosea* at present is abundant in the Levantine basin, which is caracterised by higher SST and SSS in comparison with the western Mediterranean. This variety is never abundant in the analysed cores; however, its occurrence may be related to the establishing of warm and salty summer surface layer.
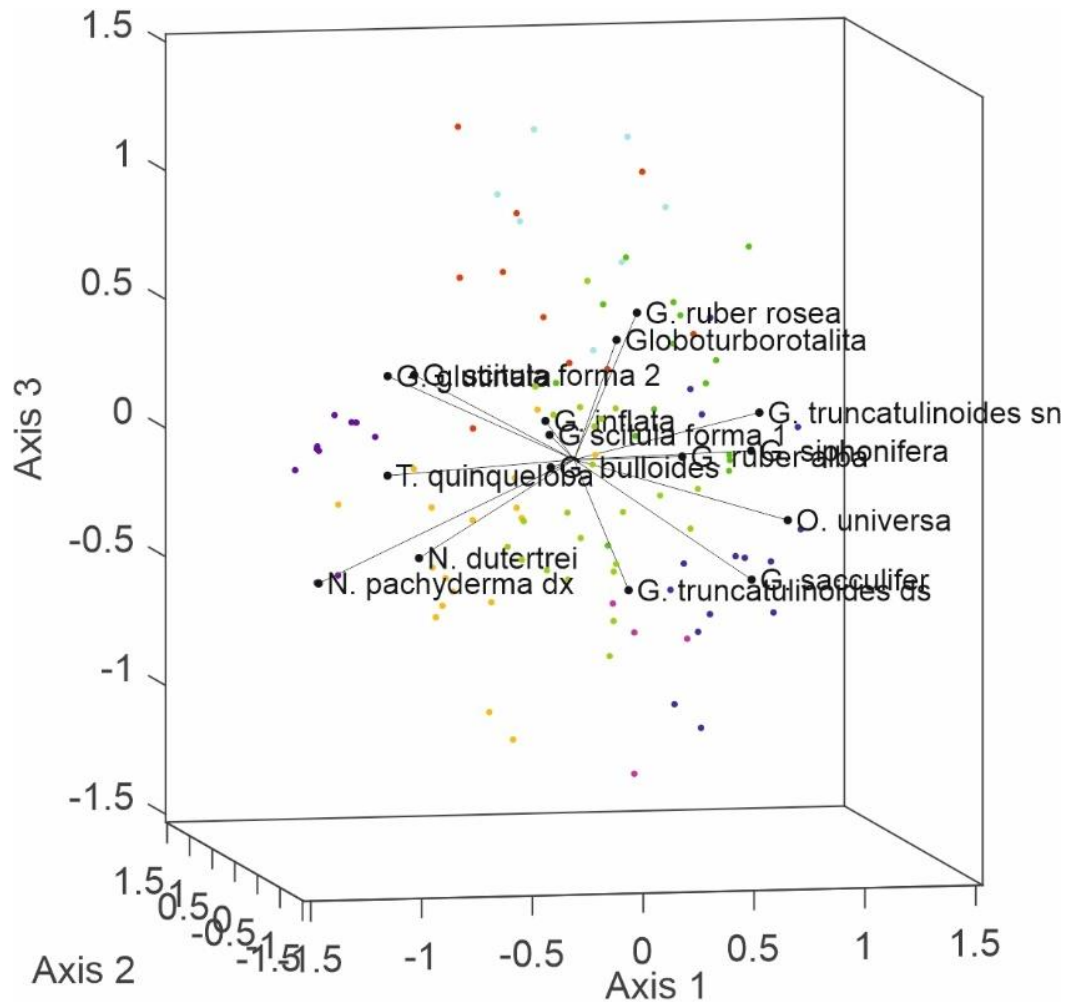
Figure 47 - 3-axes RVB of planktonic assemblages of Core Transect_2017 TR1. The colour of sample points corresponds to the grouping obtained from the zonation of the core (see figure 44).

6.2 Relative variation biplots (benthic foraminifera)

The RVB of Core Transect2017_TR1 is shown in figure 48. The variability accounted by the first two components is, respectively, 24.16% and 15.71% of total variance, cumulating 80.22% of total variance.
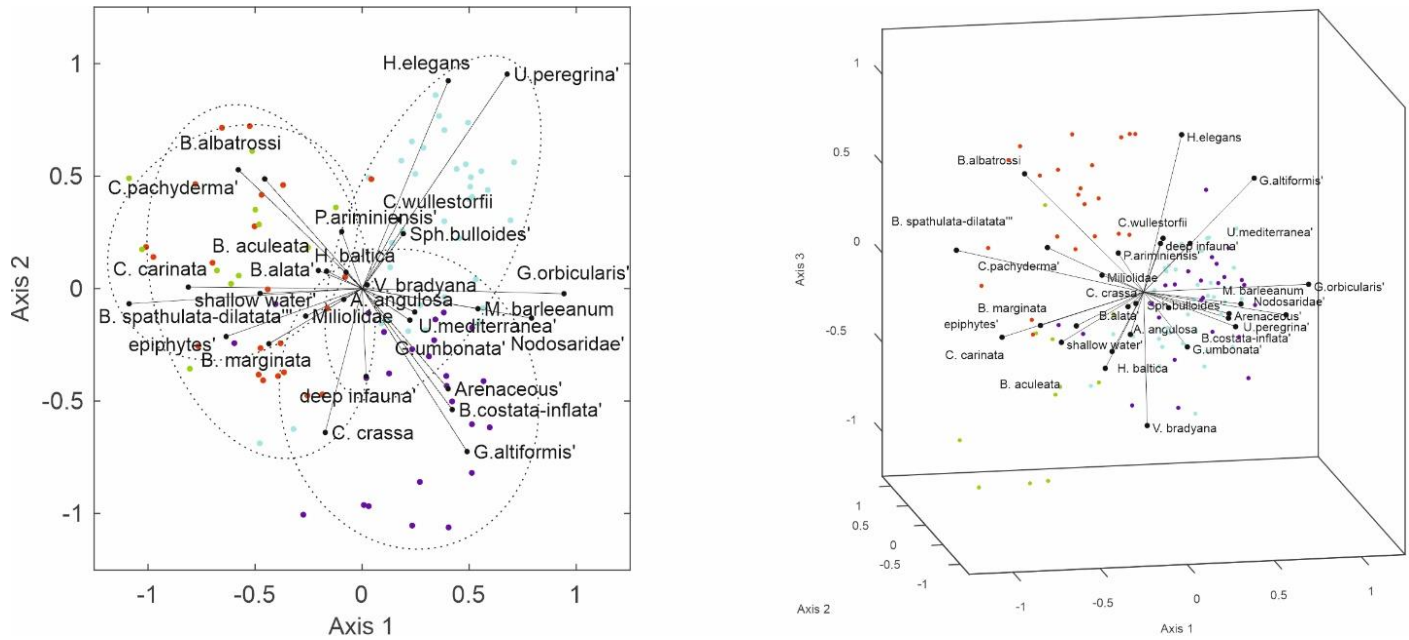
Figure 48 - Relative variation biplot of benthic assemblages of Core Transect2017_TR1. Left: 2 axes; right: 3 axes.

By adding a third component, accounting for 11.56% of total variance, 51.44% of total variance is reached.

The RVB of Core GNS84-C106 is shown in figure 49. The variability accounted by the first two components is, respectively, 43% and 12.6% of total variance, cumulating 55.65% of total variance. By adding a third component, accounting for 5.6% of total variance, 61.3% of total variance is reached.
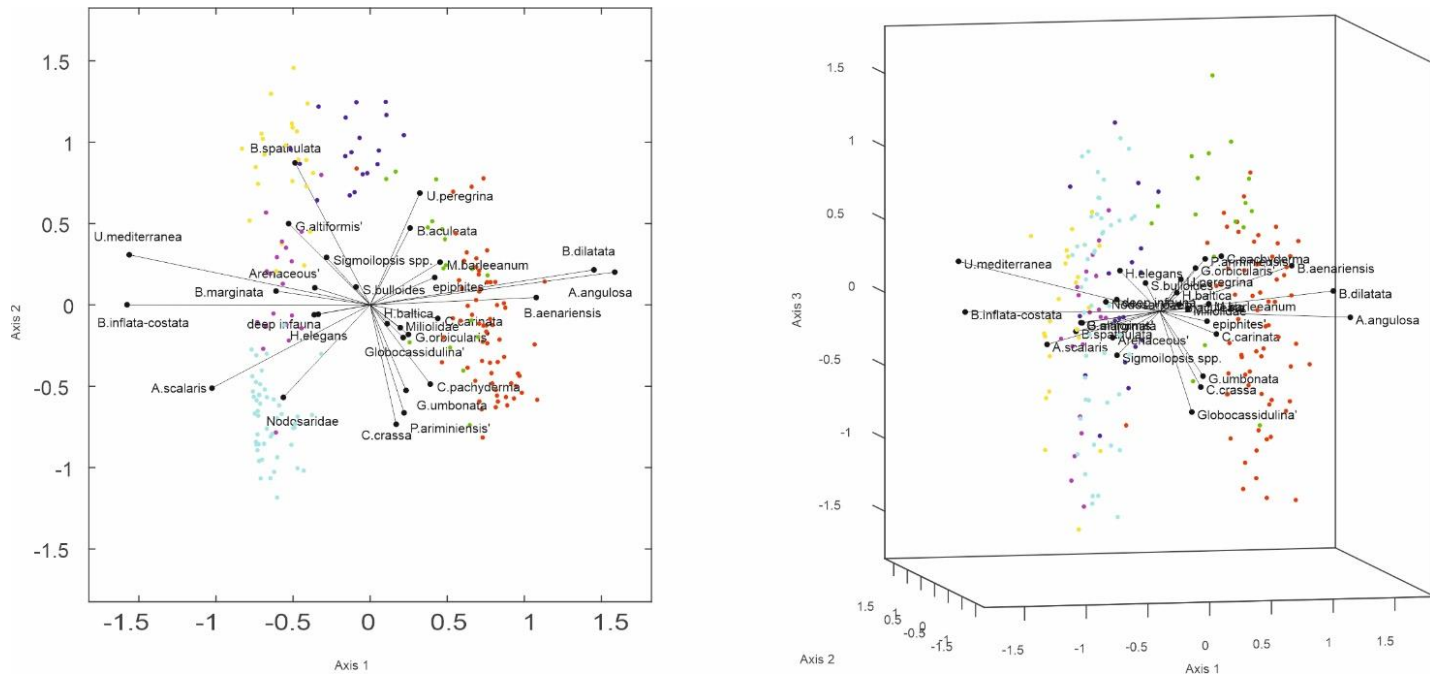
Figure 49 - Relative variation biplot of benthic assemblages of Core GNS84-C106. Left: 2 axes; right: 3 axes.

These results are somewhat poor, since the variance accounted by the first two axis is quite low. This implies a certain degree of approximation on the RVB representation of the multivariate dataset. Moreover, the star-like appearance of biplot rays and the roundness of the cloud of row points indicates the lack of strong relationships between the parts of the compositions. Overall, these results which often arises in RVB of benthic foraminifera assemblages indicate that either a) it is not possible to fully explain the variability of benthic foraminifera in terms of few environmental controlling factors; b) the uniqueness of benthic taxa is high; thus they are characterised by a broad response to the paleoenvironmental control.

By considering more components to be accounted the total variance increases. However, it should be considered that, it may be difficult to relate small variance sources to environmental factor and to distinguish noise effects from true variance sources.

In the RVB of Core GNS84-C106 benthic assemblages, the 1st axis, highlights a logcontrast between *A.angulosa, U.peregrina, B.aenariensis, B. dilatata* versus *Uvigerina mediterranea, Bulimina marginata, Bulimina inflata-costata* group, *Amphicoryna scalaris* (Fig. 49). This axis highlights the main compositional differences between last glacial period (BFCZ2) and Holocene

(BFCZ1a-c) assemblages, located on the positive and negative side of axis 1, respectively. It is not easy to relate it to a single environmental factor. The logcontrasts aligned along this axis carry a palaeodepth signal, since in the Mediterranean *Bulimina inflata-costata* group, *Amphicoryna scalaris* and *Uvigerina mediterranea* are commonly found in the circalittoral bottom, but they become more abundant in bathyal environments (Blanc-Vernet, 1969; Sgarrella and Barra, 1984; Sgarrella and Moncharmont Zei, 1993). Thus, the shift from the positive to the negative side of axis 1 the recorded in the transition from the last glacial period to the Holocene, and the intermediate position of assemblages of late glacial BFCZ1d interval, record the post glacial sea level rise. It can be also noted that assemblages of BFCZ1a and BFCZ2, which cover a time interval characterised by a reduced sea level rise (Lambeck et al., 2014) project on the same position of axis 1. Some of the relationships defined along this axis, however, do not seem to be related to such an environmental factor. *Bolivina dilatatissima* has been reported from Last glacial assemblages of cores recovered in the Gulf of Taranto at depths ranging from 491 to 943 m (Moncharmont-Zei et al., 1984) and *Bolivina aenariensis* is considered a cold climatic marker (Sgarrella, 1992). Their location on the positive side of the 1st axis suggests a relationship with bottom temperatures covarying with paleodepth. As noted in Di Donato et al. (2009), *Uvigerina mediterranea* and *Uvigerina peregrina* show distinct behaviours, as the first became more abundant in the Holocene, while the latter declines. Both species a related to high organic matter fluxes (Fontanier et al., 2002; Mojtahid et al., 2013; Schönfeld and Altenbach, 2005) and not very resistant to low oxygen conditions (Melki et al., 2010; Schmiedl et al., 1997). In the modern Gulf of Salerno (Sgarrella and Barra, 1984) and in the nearby Gulf of Policastro (Sgarrella et al., 1983) the *U. peregrina* has only a scattered occurrence. According to Blanc-Vernet (1969), *Uvigerina peregrina* is rare in the modern Mediterranean sediments, and it could characterise Wurmian sands of the "Detritique du Large". Increased abundances of *Uvigerina mediterranea* from the Last glacial to the Holocene have also been recorded in the Gulf of Taranto (Moncharmont-Zei et al., 1984). Both species are preferentially shallow infaunal (Schmiedl et al., 2000). This *Uvigerina* overturning also occurs at greater depths (see Transect2017_TR1 results) for which a palaeodepth can be ruled out. A bottom temperature effect may instead be considered as controlling factor.

The 2nd axis opposes *Bolivina spathulata, Bulimina aculeata, G. altiformis* to *Cassidulina crassa, Cibicidoides pachyderma, Globocassidulina* spp*., Gyroidina umbonata,* Nodosaridae and *P. ariminiensis* (Fig. 48).

The species of the first group are widespread in circalittoral and bathyal muds. *Bolivina spathulata* is a potential infaunal opportunistic species (Barmawidjaja et al., 1992; Jorissen et al., 1992) and *Bulimina aculeata* is abundant in high productivity areas (Schmiedl et al., 2000; and references therein). Species belonging to *Bolivina, Bulimina* and *Uvigerina* are often combined with dysoxic conditions (Sen Gupta and Machain-Castillo, 1993). Most species located on the negative side of the 2nd axis, namely *Cassidulina crassa, Cibicidoides pachyderma, Gyroidina umbonata*, mainly exhibit an epifaunal or shallow infaunal life-style (e.g. Altenbach et al., 1993; De Stigter et al., 1998; Schmiedl et al., 2000; Fontanier et al., 2008). In the Mediterranean Sea *Cibicidoides pachyderma* and *Cassidulina crassa* are associated with oligotrophic to mesotrophic and well-ventilated conditions (De Rijk et al., 2000; Schmiedl et al., 2000). *P. ariminiensis* is a suspension feeder epifaunal species from elevated substrates, able to obtain the food supply transported by bottom currents (Lutze and Thiel, 1989; Linke and Lutze, 1993; Fontanier et al., 2008). These relationships indicate that the 2nd axis can be interpreted positively related to increased organic flux and slightly reduced bottom ventilation. Noteworthy, samples of BFCZ1c and BFCZ1d, which cover a time interval corresponding to the ORL1, have similar projection on the axis 2 but are shifted along axis 1: they can be related to increased paleoproductivity during a sea level rise. The results obtained for species belonging to the genus *Gyroidina* are somewhat surprising. In general, *Gyroidina altiformis* and *Gyroidina orbicularis* are considered oligotrophic (De Rijk et al., 2000). According to Rasmussen et al. (2002) the *Gyroidina* genus contains some of the few species in the Mediterranean that are able to cope with the extremely oligotrophic lower slopes and abyssal sea floor. In the Core GNS84-C106, as well as in the Core Transect2017_TR1, these species seem to show different behaviours. *Gyroidina altiformis,* as shown by the closeness of its column point to that of *B. spathulata*, seems related to more trophic conditions than *G. orbicularis* and *G. umbonata,* located close to *C. pachyderma* and *P. ariminiensis.* Indeed, this species is more abundant from the second part of the BFCZ1d to the BFCZ1c, during the second half of ORL1, *G. orbicularis* and *G. umbonata* are very rare.

As already emerged in previous analyses of this core (Di Donato et al., 2009), *Hyalinea baltica* and *Sphaeroidina bulloides* column points lie near the origin of the biplot axes (Fig. 48). This suggests for these taxa relative neutrality with respect to the compositional changes explained by the first two axes. Along the third axis, it can be noted the location on the negative side of *G.*

crassa, Globocassidulina spp. and *G. umbonata*, as well as a spread along this axis of BFCZ1a and BFCZ2b assemblages.

6.3 Core Transect2017_TR1

The first axis of the RVB of benthic foraminifera of this deeper core contrast Holocene (BFCZ1, on the positive side) and Late Glacial (BFCZ2, on the negative side) assemblages. As in the case of Core GNS84-C106, *C. pachyderma* and *B. albatrossi* seem to be related one each other, because they are both abundant in the BFCZ2b, and strongly constrasted with *G. altiformis* and *B. costata-inflata,* along both the axes 1 and 2. Along the axis 2 it can be observed the different location of BFCZ1a and BFCZ1b, characterised by, respectively high and low *H. elegans*/*G. altiformis* logratios. As in the case of Core GNS84-C106, *G. altiformis* is more abundant in the second half of ORL1 interval, after which it decreases while *H.elegans* (and *G. orbicularis*) increases. It can be noted also noted the strong contrast of *B. spathulata* and *G. orbicularis* characterised by a very high-variability logratio. On the basis of the benthic record of the Core GNS84-C106 and Transect2017_TR1, *G. orbicularis* seem to be clearly related to oligotrophic conditions, while *G. altiformis* seems to be related to oligo- to mesotrophic conditions with not well ventilated bottom conditions, which, and as highlighted by the contrast of this species with *C. pachyderma.* In the biplot, shallow water and epiphytes seem to be related with *B. spathulata* and *C. carinata* (the latter, even less abundant, shows the same trend as in the Core GNS84-C106). Indeed, these groups are relatively more abundant in the late glacial interval of this core, probably as a consequence of downslope transport and/or currents dispersion of *Posidonia* or other bottom vegetation fragments from the nearby Capri island and Amalfi coast.

6.4 *SST trends in the Southern Tyrrhenian Sea*

The SST obtained with CodaMat and Coda-PLS follow, in general, similar SST trends. However, the last glacial SST reconstructions obtained from Core GNS84-C106 highlight some significant difference. In particular, it can be noted that Coda-PLS provide a quite coherent reconstruction, with GI-1/BA SST values that are intermediate between the last glacial and the Holocene. In particular, CodaMat provides, for this interval quite high values which seem to be typical of full-Holocene conditions. By contrast, the values obtained from CodaMat for the coldest periods, which are correlated with Heinrich event H1 and an interval encompassing H2 and H3 events, are lower in comparison with Coda-PLS. In figure 48 the annual SST reconstructions obtained for Core GNS84-C106 and Transect_2017-TR1 are compared with the alkenone-based SST obtained from the cores BS79-38 and BS79-33 recovered in the southern Tyrrhenian sea (Sbaffi et al., 2001; Marshall et al., 2002). The amplitude of SST changes during the late glacial obtained with Coda-PLS and alkenones is quite similar, while CodaMat provides larger fluctuations. All methods highlight SST maximum in the early Holocene. Afterwards, the quantitative reconstructions points to SST decrease (which is also recorded in the Core BS79-38 alkenone-based SST), which in particular in the results provided by the CodaMAT method seems to be larger. A similar trend was observed in previous reconstructions (i.e. Kallel et al., 1997) and, as observed by Sbaffi et al. (2001) may be partly related to a change in the palaeoceanographic setting, and in particular to a pycnocline shallowing which favoured the development of a DCM and a consequent increase in *Neogloboquadrina pachyderma* l.c., a species which is also abundant in high latitude assemblages. The Mediterranean climate is linked to the North Atlantic regions by means of teleconnections such as the North Atlantic Oscillation (NAO) (see Hurrell et al., 2003 for a review), and in the Late Pleistocene to Holocene record of the Mediterranean basin there are several evidences of teleconnections of this region with Greenland and North Atlantic regions (Cacho et al., 1999; 2000; Di Stefano et al., 2014). It can be noted that the SST record of the southern Tyrrhenian Sea (figure 48), and in particular the SST decrease recorded for a time interval spanning from 7 to 4 ka BP was also recorded in the GISP2 ice core (Alley, 2000, Wanner et al., 2011). This evidence suggests that the SST decrease recorded by CodaMat and Coda-PLS may be explained not only in terms of palaeoceanographic setting change but also in terms of an effective SST decrease.
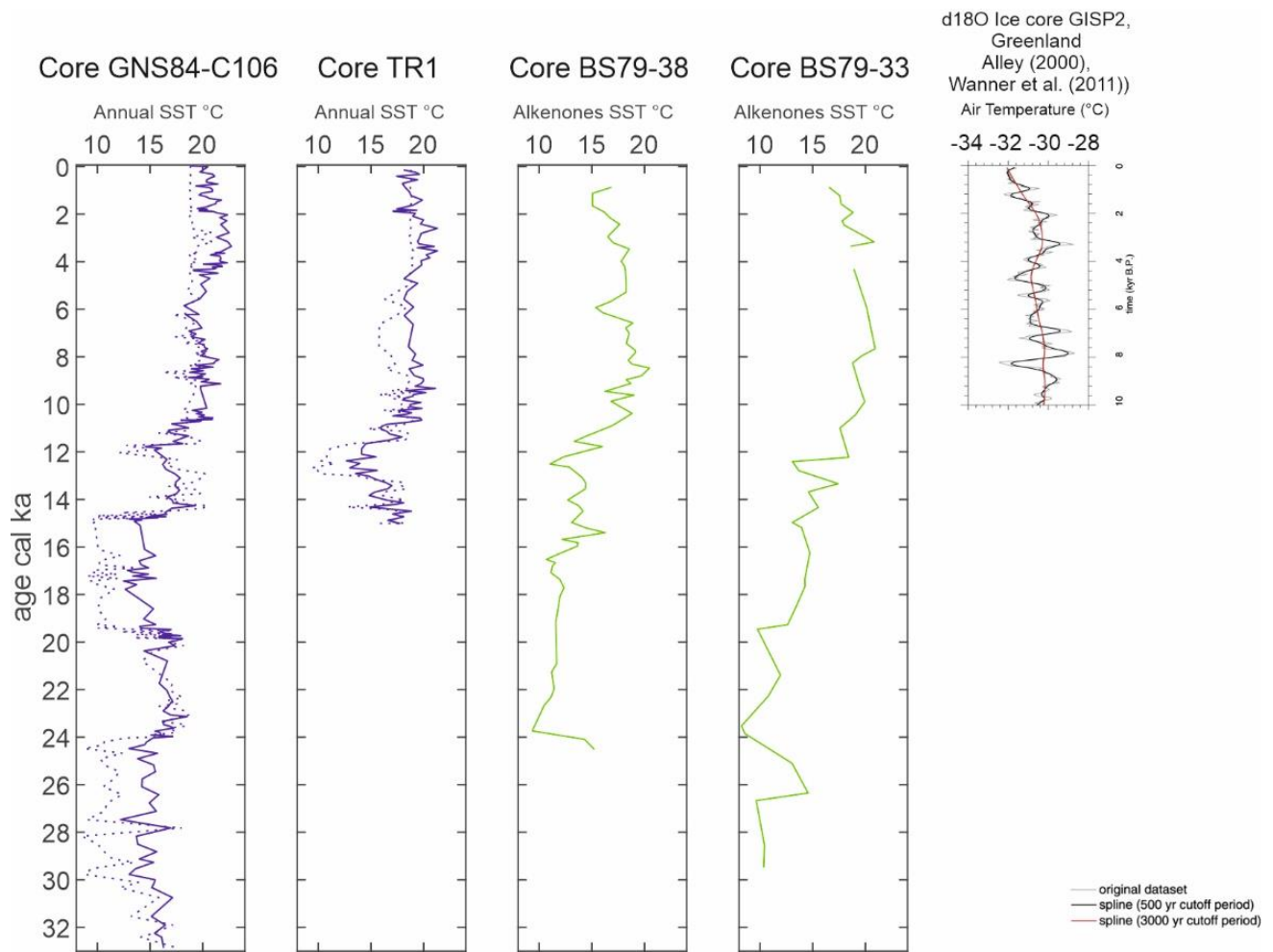
Figure 48 Comparison between Coda-PLS (full line) and Codamat annual SST (dotted line) reconstructions with Alkenones based SST obtained from Cores BS79-33 and BS79-38 and the Greenland GISP Holocene temperature record.

A warm Tyrrhenian Sea around 3 ka BP?

The reconstructed SST by means of CoDa-PLS clearly shows a distinct warming around 3 ka BP, with values higher than present. This episode coincides with the STPFCZ1b (4.0-1.9 cal ka), which is characterised by a peak in G. sacculifer widely recorded in the Mediterraean (Asioli, 1996; Capotondi et al., 1999; Buccheri et al., 2002; Sprovieri et al., 2003; Asioli and Piva, 2006; Margaritelli et al., 2016; among others). In effect, the increase in abundance of G. sacculifer in the Mediterranean late Holocene and during the interstadials MIS11 and 9, has been related to "Climatic Optima" (Piva et al., 2008; Lirer et al., 2013, 2014). The alkenone-based SST

117

reconstructions (Sbaffi et al., 2001) provide somewhat contrasting evidences, as an SST rise is recorded in the Core BS79-33 while it is not evident on the Core BS79-38. The CodaMat record show an SST rise in the Core GNS84 C106 which it is not evident in the Core Transect2017_TR1. It can be noted that the closest modern analogues of samples belonging to STPFCZ1b are mostly found in the western Mediterranean, in core top assemblages in which *G. sacculifer* is not abundant as it is in the STPFCZ1b. This suggests that, for this interval, the CoDaMAt method may be not fully able to capture a peculiar feature of the planktonic foraminifera assemblages.
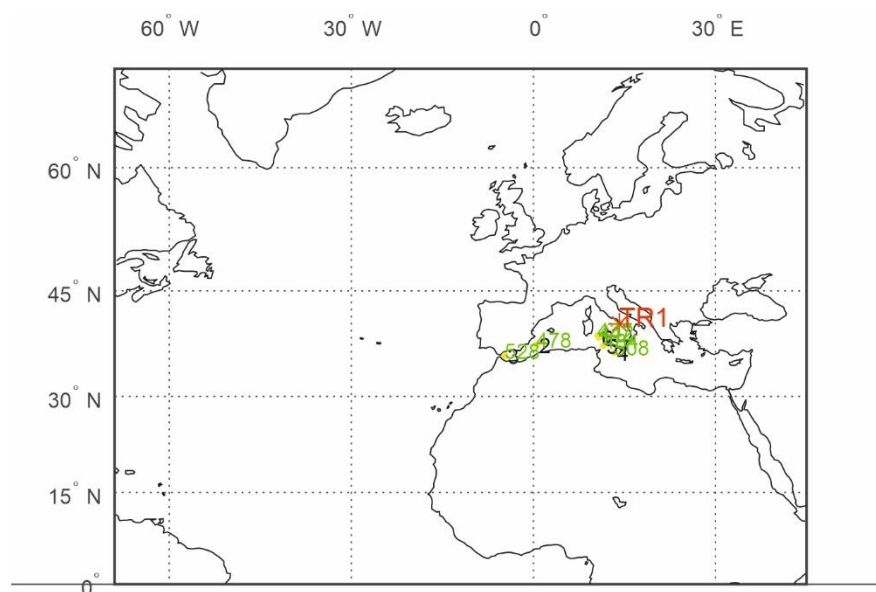
Figure 49 Geographical location of the closest modern analogues for a 3 ka PB sample of the Core Transect2017_TR1

In the model of the Coda-PLS, the *G. sacculifer* load positively to SST estimates, as it is a tropical species, although in the present Mediterranean it is abundant mostly in the north western sectors, which are characterised by relatively lower SST and SSS. As pointed above, the occurrence in sectors in which a positive wind curl stress prevail, may indicate that during this time interval, warm summer conditions were coupled, in winter, with a strong wind stress diffused in large sectors of the Mediterranean, allowing this species to expand in the central-eastern Mediterranean too.

The correspondence of the SST increase recorded around 3 ka with a Greenland air temperature increase, further supports an increasing SST scenario for this interval which immediately follows the 4.2 ka event, which in the reconstructed SST record is characterised by slightly lower values.

6.5 *Climatic evolution and oceanographic setting of the southern Tyrrhenian Sea from the Last Glacial Period to the Holocene.*

The integration of planktonic and benthic foraminifera records obtained from the analysed cores allowed to depict the oceanographic setting of this sector of the southern Tyrrhenian Sea from the Last Glacial Period to the Holocene.

Last Glacial Period

The Last Glacial Period is only represented in the GNS84-C106 Core. Colder conditions in the Gulf of Salerno were reached during two intervals (Fig. 42) the first of which, between 30 and 24 kyr BP, cover a time interval encompassing the Heinrich events H2 and H3 (Heinrich, 1988; Hemming, 2004). The second cold interval, between 18.5 and 14.7 kyr BP corresponds to the Heinrich event H1. As regards the bottom conditions, the combination of low organic carbon values and relatively high carbonate content (Di Donato et al., 2009) suggests a well-oxygenated seafloor in a circalittoral-epibathyal environment. The low total clay component and the scarcity of clay minerals of continental origin indicate limited continental run-off, consistent with the low precipitation in the surrounding areas of Gulf of Salerno (Di Donato et al., 2008), as well as with an open-vegetation pattern in south Italy (Allen et al., 1999). Overall, the benthic assemblages, characterised by the abundance of *C. carinata,* Miliolids, *C. pachyderma* are consistent with oxic conditions and moderate organic fluxes within a lower circalittoral-epibathyal environment. The increase in *C. pachyderma* recorded during the H1 event, event, which was also recorded in the North-western Mediterranean (Melki et al., 2009), indicates enhanced bottom ventilation, coherently with an intensification of termohaline circulation during stadial events (Cacho et al., 1999; Cacho et al., 2000; Cacho et al., 2001, Sprovieri et al., 2012).

Late glacial period (~14.7-11.5 kyr BP)

As shown in chapter 7.1, the negative shift in the 1st axis scores of the benthic foraminifera biplot for Core GNS84-C106 recorded at the beginning of the Late glacial (Fig. 47) highlights a change in bottom conditions which can be related to a first palaeodepth increase during the Meltwater pulse 1a (Fairbanks, 1989; Hanebuth et al., 2000; Weaver et al., 2003). This interval is also marked by the re-entry of *G. inflata,* which, with some diachronism, occurs in the Mediterranean around 15

cal ka (Casford et al., 2002; Pérez-Folgado et al., 2003; Sprovieri et al., 2003; Di Donato et al., 2008; Siani et al., 2010). The present regional distribution of this mesopelagic species follows the path of Atlantic waters and its abundance positively correlates with food availability and winter mixing (Pujol and Vergnaud Grazzini, 1995; Mallo et al., 2017). During the GI-1 with ORL (organic reach layer), increased abundances of *G. inflata* in the Alboran Sea are associated with higher inflow volumes of Atlantic waters and higher SST, and to a deepening of the nutricline and pycnocline, linked to the interference between the Atlantic inflowing waters and the MOW (Pérez-Folgado et al., 2003). A first deepening of the pycnocline is also evidenced by a first increase (though rare) of *G. truncatulinoides,* which is more evident in the deeper Transect2017_TR1 core. The marked and fast SST increase (Figure 44) also correspond to an increase in precipitation highlighted by pollen assemblages (Di Donato et al., 2008). A consequent increase in continental runoff is marked by the increase in the clay component from 10 to 20% with a mean percentage of clay minerals such as kaolinite (8%) followed by illite (6%), smectite (4%) and chlorite (2%) (Naimo et al., 2005). An increase in primary production associated with continental run-off during this interval is consistent with the high Ca values and the first increase in Ba (Di Donato et al., 2009). The productivity increase is also supported by the well recorded in the core GNS84-C106 by the increase in *B. spathulata* and *U. mediterranea* (BFCZ1d), and is clearly identified by the shift in the 2nd axis scores of the benthic foraminifera biplot (Fig. 47), as well as by the increase in benthic foraminifera absolute abundance recorded in both the Core GNS-84-C106 and Core Transect2017_TR1 (fig. 46). An increase in *B. spathulata-dilatata* group (together with *U. mediterranea* and *G. altiformis*) is also recorded in the Core Transect2017_TR1 (BFCZ2a)*,* and testifies for increasing organic matter fluxes, though reduced in comparison with circalittoral-epibatial bottoms, also at depth. As increases in organic matter fluxes at the bottom are often coupled with oxygen depletion, in most cases it is difficult to separate their effects on benthic species (Sen Gupta and Machain-Castillo, 1993). Throughout this interval, the diversity of the benthic assemblages remains quite high, suggesting that only slightly dysoxic conditions may have been established, likely during the summer season.

The cooling phase correlated with the GS1-Younger Dryas recorded in all the studied cores does not seem to cause dramatic changes in bottom conditions. However, it is marked at shallower depth by an increase in Miliolids and, at depth, by a strong increase in *C. pachyderma* which record an increase in bottom ventilation during this stadial.

Overall, the Late glacial geochemical and micropalaeontological proxies reflect a productivity increase, corresponding to the beginning of the ORL1 phase (Rogerson et al., 2008) and of the last Sahara humid phase (Reimer et al., 2010), which can related to nutrient supply from the continent through fluvial inputs and remobilisation of organic matter stocked in previously emerged alluvial plains during this fast sea level rise interval. During this interval the Corg values in the Core GNS84-C106 remain rather low (Fig. 42). Corg content, however, results from several factors, including oxidation processes related to aerobic respiration (Bender and Heggie, 1984). Hence the low Corg content recorded in the Late glacial of core GNS84-C106 may be explained by the persistence of oxic conditions at the bottom, as also testified by the presence of Fe and Mn-hydroxides (Naimo, 2005). Corg values are higher throughout the Core Transect2017_TR1 without highlighting significant changes. Two peaks in the C/N ratio recorded during this interval indicate imputs of organic matter of continental origin.

Early Holocene

The transition to the Holocene is marked a second pycnocline deepening coinciding with the Meltwater pulse 1b. The SST record indicates higher values since around 10 cal ka. Planktonic assemblages (STPFCZ2d) are marked by the re-entry of *G. truncatulinoides* r.c. around 11.5 cal ka, immediately followed by re-entry of *G. truncatulinoides* l.c.. Contemporarily, the abundance of *Neogloboquadrina* r.c. is strongly reduced. In the Atlantic Ocean, *G. truncatulinoides* l.c. prefers warm, nutrient depleted waters such as the center of the subtropical gyre, while the right coiling variety favours the still relatively warm, but more nutrient-rich waters associated with the gyre margins (Renaud and Schmidt, 2003; Ujiié et al., 2010). Moreover, *G. truncatulinoides* l.c., dominates North Atlantic sediments when the permanent thermocline is deep, while the right coiling variety is more abundant when the permanent thermocline is shallow (Feldmeijer et al., 2015). Thus, the record of the Southern Tyrrhenian Sea, highlights a progressive deepening of the thermocline which can be related to a thickening of the MAW layer over a saltier and denser LIW which became progressively isolated from surface processes (Casford et al., 2002; 2003). The deepening of the thermocline prevented the development of DCM, leading to the almost disappearance of *N. incompta* (STPFCZ1b-d). It can be noted that during this time interval, during which OLR1 and Sapropel S1 overlap, this species is also missing in the eastern Mediterranean (Rohling, 1993; among others). The composition of the planktonic foraminifera assemblages does

not provide clear indications on surface salinity, however this interval is characterised by the abundance of *Braarudosphaera bigelowii* among calcareous nannofossils (Esposito and Buccianti, 2004) and *Limacina trochiformis* among pteropods (Buccheri et al., 2002) which indicate reduced surface salinity (Buccheri and Torelli, 1981; Buccheri et al., 1998). A decrease in Tyrrhenian Sea surface salinity during this interval, which corresponds to the last sapropel event in the eastern Mediterranean Sea, was also recorded by Kallel et al. (1997).

In the shallower GNS84-C106 core, the negative shift in the 1st axis scores in benthic foraminifera in the early Holocene (Fig.43) highlights a palaeobathymetric increase corresponding to the melting pulse 1B (Fairbanks, 1989). The positive shift in Corg recorded at the beginning of the Holocene (Fig. 39) together with diagenetic microcrystalline barite and relative increases of barium (Fig. 39), can be related to increasing organic flux at the bottom, which in turn may derive from an increase in land-derived organic matter, as also supported by an increase in the mineralogical clay component, and/or plankton-derived organic matter flux at the bottom (Canfield, 1994). The high absolute abundance of benthic foraminifera (BFCZ1c) is also coherent with meso- to eutrophic conditions which are also indicated by benthic Mollusca and Ostracoda (Di Donato et al., 2009). However, in comparison with the previous interval, there is a reduction in *B. spathulata* to which corresponds an increase in *G. altiformis, U. mediterranea* and *H. baltica.* These assemblages point to a reduction in the organic matter flux to the bottom. At the deeper site, the abundance of *Melonis barleeanum, G. altiformis* benthic foraminifera testify for an intermediate trophic setting. The scarcity of *C. pachyderma* and *P. ariminiensis* (also detected in the Core GNS84-C106) indicates reduced bottom ventilation, however a peak of deep infauna is only recorded at around 9.9 cal ka, followed at 9.7 by peaks of *B. spathulata* and *C. carinata,* likely related to season organic matter pulses.

From 10.5 cal ka, the disappearance of *G. truncatulinoides,* which may indicate a tendency of the stratification in the water column to persist all year around (Kallel et al., 1997), and the progressive increase in *N. pachyderma,* which became more marked from 9.5 cal ka - towards the end of the ORL1 - indicates the progressive shallowing of the pycnocline, and establishing of DCM. This is an important feature of this Holocene interval already recorded in the Tyrrhenian Sea by several authors (Kallel et al., 1997; Sbaffi et al., 2001). This phase is likely related by a progressive shallowing of the LIW in the Tyrrhenian Sea, which is not recorded in the eastern part of the Sicily

Channel until 7.8 ka (Di Donato et al., 2019 in press.) towards the end of the Sapropel S1 event. Today, the LIW is forced to rise passing through the Sicily Channel. The evidences of the Southern Tyrrhenian Sea indicate that, around 10 to 8 cal ka, the top of the LIW settles in the western Mediterranean to a shallower depth in comparison with the eastern Mediterranean. From 10 cal ka the post glacial sea-level rise rate starts to decrease (Stanford et al., 2011). A thickness reduction of the MIW, as a consequence of the progressive reduction of the inflow of Atlantic water in the Mediterranean, which is supported by the progressive decrease in *G. inflata* recorded from 8 cal ka, could have contributed to determining this LIW settlement, to which also contributed differences in the density contrast between LIW and MAW recorded to the two sides of the Sicily Channel.

The time interval between the end of the ORL1 and the end of the S1, is still characterised by high values of Ba and Corg, pointing to persisting eutrophic conditions, as well as by slighty reduced surface salinity, as indicated by the persistence of *Limacina trochiformis*, and *B. bigelowii*, whose abundance, however decreases (Buccheri et al., 2002). Benthic assemblages record a progressive change of bottom conditions during this interval. In the Core GNS84-C106 (BFCZ1b), an increase in *C. pachyderma, H. baltica,* Miliolids, *U. mediterranea* correspond to a decrease in *G. altiformis, C. carinata,* indicating improvement of bottom ventilation and a further reduction in the organic matter flux. In the deeper Core Transect2017_TR1, after a peak around 8.4 ka (BFCZ1b) a decrease in the absolute abundance, the decrease in *Bolivina* and *G. altiformis* and the increase in *G. orbicularis, H. elegans,* points to a transition from oligo/meso- to oligotrophic conditions.

Middle to late Holocene

From about 6.5 kyr BP a major change occurs in the column water and in the bottom environment.

The progressive decrease of *N. pachyerma* r.c. and *G. inflata* (STPFCZ1c) may be related to a further reduction in the water inflow from the Atlantic Ocean related to a further decrease in the sea level rise rate and, contemporary establishing of conditions unfavourable to the development of DCM. At around 4.8-4.6 cal ka (STPFCZ1b) a third pycnocline deepening is recorded by a peak of *G. truncatulinoides* r.c. - already recorded by Capotondi et al., (1999) and in the Sicily Channel by Kuhlmann et al., 2015 - which is followed by an increase in *G. truncatulinoides* l.c., with a compositional change recognised throughout the southern Tyrrhenian Sea (Ariztegui et al., 2000). Differently from the previous pycnocline deepening events, which occurred during periods of sea

level rise, this event occurred during a phase of sea level stabilisation, and is likely related to a deepening of a LIW which became progressively denser as more arid conditions established in the Mediterranean, and in particular in its eastern sectors. In both Cores GNS84-C106 and Transect2017_TR1 a reduction in the absolute abundance of benthic foraminifera indicates the establishment of the oligotrophic conditions which characterise at present the open water system of the Tyrrhenian Sea (Margalef et al., 1966). In the Core GNS84-C106, an increase in *C. pachyderma* with a peak around 3 ka indicate good ventilation at the bottom. This peak coincides with the *G. sacculifer* peak recorded in the Gulf of Gaeta (Di Donato, 2002), Sicily channel (Sprovieri et al., 2003) and Adriatic Sea (Capotondi et al., 1999; Sbaffi et al., 2001).

Palaeoenvironmental reconstructions through compositional data analysis (Article)

Valentino Di Donato[1], Josep Antoni Martín-Fernández[2], Marc Comas-Cufí[2], Joanna Jamka[1]

1. Dipartimento di Scienze della Terra, dell'Ambiente e delle Risorse – Università degli Studi di Napoli "Federico II" – Complesso di Monte Sant'Angelo (Edificio L) Via Cinthia, 21 - 80126, Naples, Italy.

2. Departament d'Informàtica, Matemàtica Aplicada i Estadística, Universitat de Girona – Edifici Politècnica IV, Campus Montilivi, E-17003, Girona, Spain.

Corresponding author: Valentino Di Donato - email address: valedido@unina.it

Abstract

The modern analogue technique has been accordingly revised with compositional data analysis framework. The method adopts the Aitchison distance, obtained from isometric log-ratio coordinates of relative abundances, as a natural measure of similarity among assemblages. The number of analogues from which obtain the estimates was determined through leave-one-out verification of modern assemblages. Mean distances and local outlier factor are considered to evaluate the quality of palaeoestimates. The method has been tested on Atlantic Ocean and Mediterranean planktonic foraminiferal assemblages to reconstruct past sea surface temperatures (SST). In comparison with previous planktonic foraminiferal based reconstructions, the Portugal offshore SST record for the last 210 ka shows a higher coherence with other paleoclimate proxies (i.e. the stable isotope and alkenone records). In comparison with raw data analysis, CoDa-MAT yields lower estimates of the western Mediterranean last glacial period SST.

Keywords: modern analogue technique, Aitchison distance, sea surface temperatures

1. Introduction

Quantitative estimation of past environmental parameters is one of the most challenging engagements of palaeoclimatical and palaeoecological investigations. In palaeoceanographical studies quantitative palaeoclimatic reconstructions can be attained by means of geochemical methods, such as the analysis of long chain alkenones (Brassel *et al.*, 1986) and the Mg/Ca ratio in

foraminifera (Elderfield and Ganssen, 2000), or more strictly paleontological methods based of statistical analysis of census counts of assemblages. These methods, known as transfer function methods, have been introduced to provide quantitative estimates from counts of fossils, including regression-based methods (Imbrie and Kipp, 1971), modern analogue techniques (MAT) (Hutson, 1979; Pflaumann *et al.*, 1996; Waelbroeck *et al.*, 1998) and artificial neural networks (Malmgren *et al.*, 2001). The starting point of these methods is a modern dataset usually consisting of counts of modern assemblages and measured environmental parameters.

One of the main objective of the thesis is to elaborate the methods statistics two different approaches the regression and the CoDaMAT.

The first approach is focused on revising the modern analogue techniques (MAT) according to CoDa principles. The MAT compares fossil assemblages with modern ones using a distance measure or a similarity coefficient. The palaeoenvironmental estimates are obtained from the environmental parameters measured at the location of the most similar modern assemblages. For each fossil samples the nearest modern ones are found by adopting an appropriate distance (d). Then, the palaeoestimate $\hat{p}$ for a fossil is represented by the mean of the environmental parameters p_i measured at the geographical location of the h modern analogues: $\hat{p} = \frac{\sum_{i=1}^{h} p_i}{h}$ where h represents the number of analogues. Following Hutson (1979) and Pfaumann *et al.* (1996), the mean can be weighted on the inverse of the distance ($1/d^{(i)}$), so as increase the influence of the closer analogues on the palaeoestimate:

$$\hat{p} = \frac{\sum_{i=1}^{h}(1/d^{(i)}) \cdot p_i}{\sum_{i=1}^{h}(1/d^{(i)})} \qquad (1)$$

The assessment of the goodness of the method is usually carried out through cross-validation in the reference modern dataset. Following the discussion along the works Telford and Birks (2009, 2011) and Guiot and de Vernal (2011a, 2011b), we assume that in MAT the spatial structure of data has relatively low effect on the calculation of prediction errors. In consequence, in this work we assume no effect of spatial autocorrelation.

MAT mostly differ for the distance measures or similarity indexes used, among which the cosine-theta (Hutson, 1979), the scalar product of the normalized assemblages vectors (Pflaumann *et al.*, 1996), squared chord distance (Waelbroeck *et al.*, 1998) and the Euclidean distance on the logarithm of the species relative abundances in permil (Guiot and de Vernal, 2011a). The

information in a modern and a fossil assemblage is the relative abundance or percentages of species, i.e., they can be considered as compositional data (CoDa) (Aitchison, 1986). That is, the information contained in a vector of counts **x** is the same as in k·**x**, for any real scalar k>0, property known as scale invariance (Aitchison, 1986). That is, any observation **x** is a member of an equivalence class (Barceló-Vidal and Martín-Fernández, 2016). This type of data is common in Earth Sciences when the constituents and compounds are described in terms their concentration (e.g., Buccianti *et al.*, 2006). As with some of the cluster analysis techniques, despite it is also possible to experiment with different distances, we follow Everitt *et al.* (2011, p. 69) recommendation "…the choice of measure will be guided largely by the type of variables being used and the intuition of the investigator". In the particular case of CoDa the Aitchison distance has been proved to be an appropriate measure for the geometry of the sample space (Aitchison *et al.*, 2000). Palarea-Albaladejo *et al.* (2012) present a summary of the properties, advantages and difficulties of several different measures when they are used for CoDa.

The approach proposed on this paper has the aim to develop a MAT in a coherent fashion with the nature of the data, hereafter the CoDa-MAT. In the following section, the basic elements of the log-ratio methodology to CoDa are introduced and the CoDa-MAT is described. Next the method is tested, and its results illustrated using different assemblage datasets. Finally, Section 4 presents some conclusions and final remarks.

In the last decades, several methods were proposed to obtain quantitative estimates of past environmental parameters from counts of fossils assemblages (Imbrie and Kipp, 1971, Hutson, 1979; ter Braak & Juggins, 1993; Pflaumann *et al.*, 1996; Waelbroeck *et al.*, 1998; Malmgren *et al.*, 2001; among others). Most methods are applied to percentage data obtained from counting of specimens. *The peculiar* properties of relative abundance data represent however a key issue to be taken into account when developing transfer functions based of fossil assemblages. Percentage data belong to compositional data (CoDa) (Aitchison, 1986): that is, the information contained in a vector of counts **x** is the same as in k·**x**, for any real scalar k>0, property known as scale invariance which indicates that a composition is an equivalence class (Barceló-Vidal and Martín-Fernández, 2016). This type of data is very common in Earth Sciences when the constituents and compounds are described in terms their concentration (e.g., Buccianti *et al.*, 2006). In a paper recently published (Di Donato et al., 2018) we revised the modern analogues technique (MAT) (Hutson, 1979;

Pflaumann *et al.*, 1996; Waelbroeck *et al.*, 1998) according to the CoDa methodology (Aitchison, 1986).

The second approach is based on regression-based methods, such as Principal Component Regression (PCR) and Partial Least Squares Regression (PLSR). In order to apply PLSR to CoDa, Hinkle and Rayens (1995) proposed logcontrast partial least squares (LCPLS). CoDa refers to vectors of positive components showing the relative weight of a set of parts in a total. Nowadays, there is a general agreement that applying the standard statistical methods to CoDa may yield misleading results (Pawlowsky-Glahn *et al.*, 2015). The log-ratio methodology proposed by Aitchison (1986) and the following developments (i.e. Martín-Fernández and Thió-Henestrosa, 2016a; Martín-Fernández and Thió-Henestrosa, 2016b) represent a powerful set of methods and techniques to apply to CoDa. The approach adopted in this paper follows the principle of working on coordinates (Mateu-Figueras et al., 2011), that is, the standard statistical analysis is conveniently performed after choosing log-ratio coordinates. In particular, we considered to express each D-vector $\mathbf{x} = (x_1, \ldots, x_D)$ of percentages of species as: 1) a D-dimensional vector $\mathbf{z}=(z_1, \ldots, z_D)$ of centred log-ratio coordinates ($\mathbf{z} =$clr($\mathbf{x}$)) (Aitchison, 1986) and 2) a (D−1)-dimensional real vector $\mathbf{y}=(y_1, \ldots, y_{D-1})$ of isometric log-ratio coordinates ($\mathbf{y} =$ilr($\mathbf{x}$)) (Egozcue *et al.*, 2003) (see Appendix 1 in Di Donato et al. (2018) for definitions and details). To develop our approach, the following points were considered: 1) pre-processing techniques; 2) elaboration of regression-based transfer functions 3) evaluation of the results 4) application to fossil assemblages. As case studies, we considered applications based on the estimation of past sea surface temperatures (SST) from planktonic foraminifera assemblages. The analyses were carried out with Matlab codes, except for raw-data analysis which was computed with R package rioja (Juggins, 2017)

2. The CoDa-MAT

CoDa refers to vectors of positive components showing the relative weight of a set of parts in a total. Nowadays, there is a general agreement that applying the standard statistical methods to CoDa may yield misleading results (Pawlowsky-Glahn *et al.*, 2015). The log-ratio methodology proposed by Aitchison (1986) represents a powerful set of methods and techniques to apply to CoDa. During last decades, numerous innovative ideas and strategies to CoDa were presented at the four CoDaWork meetings (e.g., Martín-Fernández and Thió-Henestrosa, 2016a) and collected

in special publications (e.g., Martín-Fernández and Thió-Henestrosa, 2016b). The approach adopted in this paper follows the principle of working on coordinates (Mateu-Figueras *et al.* 2011), that is, the standard statistical analysis is conveniently performed after choosing orthonormal log-ratio coordinates. In particular, we expressed each D-vector $\mathbf{x} = (x_1, \ldots, x_D)$ of percentages of species as a (D−1)-dimensional real vector $\mathbf{y}=(y_1, \ldots, y_{D-1})$ of isometric log-ratio coordinates ($\mathbf{y} =\mathrm{ilr}(\mathbf{x})$) (Egozcue *et al.*, 2003) (see Appendix 1 for definitions and details).

To develop the CoDa-MAT, the following points were considered: 1) pre-processing techniques; 2) choice of the distance measure; 3) number of analogues.

2.1 Data pre-processing: subcomposition, amalgamation and zero replacement

Modern assemblages datasets often include a large number of zeros. As an example, planktonic foraminifera core top datasets include zeros which are partly related to the broadly latitudinal distribution of most species, partly to the fact that there are several rare species whose abundance is often below the detection limit. The zero values present in the data require a pre-processing because the log-ratio methodology needs the data to be strictly positive (Aitchison, 1986). To reduce the number of zero values to be replaced, rarer species can be excluded from the assemblages, by considering a subcomposition of the original assemblages (Aitchison, 1986). Moreover, it is possible to amalgamate species characterised by similar ecological requirements (Aitchison, 1986). The choice of a limited numbers of species is motivated, as pointed out by Bucciati and Esposito (2004), by the necessity to reduce the zero substitutions needed by the log ratio transformations, and to avoid, as much as possible, the generation of extreme clusters of points, corresponding to small values (Tauber, 1999). As pointed out by Kucera *et al.* (2005) the main problem with abundances of rare species is the inevitably low signal to noise ratio. Thus, amalgamation should not involve a reduction in the accuracy of results. About this, it is also worth recalling the subcompositional dominance property of an appropriate distance (Palarea-Albaladejo *et al.*, 2012): distances between observations obtained from subcompositions, are less to equal to those obtained from full compositions.

To manage the zeros occurring in the data, the first step of the analysis is the conversion of species vector of counts $\mathbf{c}$, both for the fossil and modern data, into relative abundance compositional vectors $\mathbf{x}$. If it can be assumed that zero values correspond to count zero, indicating that the

component is absent by a sample size effect, it is possible to replace them by a suitable small value (Martín-Fernández *et al.*, 2015). To do that, we adopted a mixed Bayesian-multiplicative estimation approach, which is recommended when the compositional data arise from counts (Martín-Fernández *et al.*, 2015). This treatment consists on a Bayesian estimation of the zero percentages combined with a multiplicative readjustment (Martín-Fernández *et al.*, 2003) of the non-zero values (see Appendix 1).

After the zero replacement, the ilr-coordinates' vector **y** for the fossil and modern data are obtained. Thus, fossil assemblages are represented by its ilr-coordinates, whereas the modern database is consisting of ilr-coordinates together with the environmental parameters measured at each location (at sea surface for planktonic assemblages core tops).

2.2 Distance measure

The ilr-coordinates are isometric, i.e., an isometry is established between **x** and its real vector **y**. Hence, distances in the sample space of CoDa (the simplex S^D) are associated with distances in R^{D-1}. This property has important consequences for our aims, since distances in the simplex are translated into ordinary ones in the space of coordinates. Thus, the Aitchison distance (d_a) between two compositional vectors **x**, **x*** $\in S^D$ (Aitchison, 2000) is equal to the Euclidean distance (d_e) between their ilr-coordinates vectors y, y* $\in R^{D-1}$, i.e., $d_a(\mathbf{x}, \mathbf{x*})=d_e(y, y*)$ (Palarea-Albaladejo *et al.*, 2012). The Aitchison distance meets the requirements of scale invariance, perturbation invariance and subcompositional dominance that are needed to achieve a meaningful statistical analysis of CoDa (Palarea-Albaladejo *et al.*, 2012). An alternative distance measure that also meets these requirements is the Mahalanobis distance on ilr-coordinates (Palarea-Albaladejo *et al.*, 2012). On the other hand, the distances related to angular measures do not have a compositional coherent behaviour (Palarea-Albaladejo *et al.*, 2012). This narrows it down to just Euclidean or Mahalanobis distance on ilr-coordinates the metrics that can be adopted in the CoDa-MAT.

2.3 How many analogues?

In theory, a *palaeoestimate* for a fossil sample may be obtained from a single very close modern analogue. However, the application on a too restricted number of modern analogues increases the risk of a bad estimate due to presence of anomalous samples in the modern dataset (i.e. arising

from a decoupling of assemblage from the underlying surface conditions, or to taphonomic processes). In consequence, in the application of MAT is essential to determine the optimal number of analogues from which the palaeoestimates are obtained. In the CoDa-MAT this subject is handled by first one evaluating which number of analogues performs better in the modern conditions, by means of sensitivity analysis of leave-one-out cross-validation method (ter Braak and Juggins, 1993; Barrows and Juggins, 2005). Once this number is determined, it is also adopted for palaeoestimates of all fossil assemblages.

The sensitivity analysis to define the optimal number of analogues is based on numerical indices. Indeed, once the environmental estimates are obtained for all the modern samples these are compared with the corresponding measured values, by computing two indices: the Pearson correlation coefficient and the mean squared distances (MSD) (e.g., Martín-Fernández *et al.*, 2003). The MSD is a multivariate index of quality of the estimates of k environmental parameters defined as:

$$MSD = \frac{\sum_{i=1}^{n} d_e^2 \left(\mathbf{P}(i), \hat{\mathbf{P}}(i) \right)^2}{n} \qquad (2)$$

where n is the number of modern samples, $\mathbf{P}$ represents the vector of k measured environmental parameters, and $\hat{\mathbf{P}}$ the corresponding vector of estimated values. This approach is equivalent to analyse the mean of the norm of the residual rows (difference between measured and estimated parameters). The best result of MSD is obtained when $MSD=0$, i.e, all the estimates are equal to the measured values. In consequence, we select as optimal number of analogues the number that produces the minimal MSD value. MSD index is the multivariate generalization of the Mean of Squared Errors (MSE), applied when only one parameter is evaluated. The square root of MSE is the Root Mean Square Error of Prediction (RMSEP), a quality index commonly calculated as a measure of the predictive abilities of the training set (Wallach and Goffmet, 1989; Birks, 1995). The multivariate approach should be applied when there is a set of parameters defining the palaeoclimate, as is usually done in pollen analysis, from which several variables are estimated (i.e. temperature, seasonal or annual precipitation, potential evapo-traspiration). In such a case, the environmental parameters *may be normalized before* the computation of MSD to avoid dominance effects induced by the different measurement units adopted.

Using the standard Pearson correlation index, we can calculate a measure for k environmental parameters. This procedure calculates the Pearson correlation coefficient r between a measured environmental parameter p and its estimates $\hat{p}$ for all the modern analogues. A perfect quality of the estimations will produce a Pearson correlation equal to 1. In a multivariate approach, when one deal with a vector $\mathbf{P}$ of measured environmental parameters (k parameters) and the corresponding vector of estimation $\widehat{\mathbf{P}}$, an index R is defined by

$$R = \sum_{j=1}^{k} r_{P(j)\hat{P}(j)} \Big/ k \qquad (3)$$

where $\mathbf{P}(j)$ and $\widehat{\mathbf{P}}(j)$ respectively represents the jth parameter. In this case, the best value of R corresponds to 1. In consequence, the number of analogues that provides the maximum value of R is selected as optimal. It can be noted that the Pearson correlation coefficient r is used as a similarity index between a measured and an estimated parameter. However, the results with this index could be misleading in some scenarios. For example, when the estimates are closely proportional to the measured values this index will also show a reasonable value (close to one), although the estimations are low-quality estimations because they are systematically biased. By combining R index with MSD index, one completes the information about the quality and avoid these undesirable situations because MSD index measures the goodness of the estimates across the samples

2.4 Application on fossil assemblages

The above-described leave-one-out evaluation provides the basis for the application of CoDa-MAT on fossil assemblages, as best performing number of analogues for the modern conditions was determined by means of MSD and R indexes. In a second step, it can be evaluated if this optimal number of analogues can be adopted to perform palaeoestimates from fossil assemblages.

As in the RAM method (Waelbroeck *et al.*, 1998), the number of analogues may be evaluated for each assemblage, by looking for "jumps", i.e. increases in distance larger than a fraction of the last modern analogue selected. The number of analogues may be also reduced to obtain "*oceanographically coherent*" analogues (in the case of marine assemblages such as planktonic foraminifera - see section 3.2) or to achieve coherence of the vegetational context of the analogues (in the case of continental proxies such as pollens).

2.4.1 No-analogue conditions, outliers and atypicality index.

Probably the most important difficulty of any proxy-based reconstruction is represented by the no-analogue problem, occurring when the palaeoenvironmental conditions represented in the fossil assemblages do not have a correspondence in modern environments. More in general, it is important to define quality indexes of the palaeoestimates. The most obvious ones are represented by the average distance from the fossil assemblages to its nearest modern analogues and by the standard deviation of associated to the estimates. Large mean distances and high standard deviation (often associated with oceanographical incoherence) likely indicate bad estimates. Overpeck *et al.* (1985) indicated threshold values to be adopted with squared chord distance. In the CoDa-MAT the problem of detecting no-analogue conditions is faced by first considering the atypicality index and outlier detection for CoDa sets. In a broad sense, atypicality index (e.g., Aitchison, 1986) represents the probability of a more typical composition (or with a smaller Mahalanobis distance, from the centre of the dataset) than the observed one. In CoDa-MAT, atypicality index is first computed for each modern sample using Mahalanobis distances, to determine critical values of distance for which a sample can be considered a potential outlier. After that, atypicality can be computed for each fossil assemblage to test the hypothesis of a significant difference respect to the population of modern ones. A significant difference may highlight no-analogue conditions. Note that, in CoDa-MAT, this index is based on the Mahalanobis distance applied to ilr real vectors. This strategy is also in the basis of the robust methods to outlier detection for CoDa sets (Filzmoser and Hron, 2008) that are freely available in the R packages *mvoutlier* and *robCompositions* (R Development Core Team, 2011). Robust methods to identify multivariate outliers are based on the robust estimation of the covariance structure (e.g., Peña and Prieto, 2001). In our work, the estimated ilr covariance structure was used to assign a robust Mahalanobis distance to each fossil assemblage indicating how far the sample is from the centre of the modern data cloud.

A second approach to outlier detection has been developed by computing the Local Outlier Factor (LOF) (Breunig *et al.*, 2000) of assemblages. This index is based on a k-distance neighbourhood approach and assigns to each object the degree of being an outlier by determining how isolated the object is with respect to the surrounding neighbourhood. Values much larger than 1 are associated to suspect local outliers. As done for the atypicality, the LOF has been determined on ilr real vectors. The computations were replicated with increasing k values, which yielded quite stable results. The following results are based on a k=10. The relationship between a fossil sample and modern population can be approximately displayed in few

dimensions by means of relative variation biplots (RVB) in which it is also possible to include fossil data as supplementary elements (Daunis-i-Estadella *et al.*, 2011). In this way it is possible to easily visualize the space distribution of fossil samples and their modern counterparts. This may be useful to verify if a fossil sample is located within or at the margin of the surrounding closest modern analogues (see section 3.2). Matlab routines to obtain RVB and perform the CoDa-MAT are provided as supplementary materials.

2.4.2. Evaluation of errors of estimates in relation to hyperspheres radius

This approach provides for each sample an auxiliary tool for evaluating the reliability of the obtained estimates. For each modern sample, the maximum value of the module of the errors of the estimates is computed within hyperspheres with increasing radii centred on the sample itself. The obtained information is applied to fossil assemblages by considering them as laying at the border of *h* hyperspheres, each centred on one of the *h* closest analogues. The highest value of the maximum errors associated to these hyperspheres is recorded as potential estimate error, as a measure of the reliability of the obtained estimates for the fossil assemblages. Confident estimates are obtained when a fossil assemblage is included within the radius of modern assemblages for which errors and standard deviation of the estimates are low. On the contrary, high values suggest considering with caution the reconstructed values or, at the limit, to discard these estimates if the potential error exceeds acceptable values.

3 Testing the method

The performance of CoDa-MAT in the modern conditions was tested on planktonic foraminifera with a modern dataset consisting of 1252 Atlantic and Mediterranean core top assemblages determined on the >150 µm size fraction (Prell *et al.*, 1999; Hayes *et al.*, 2004; Kucera *et al.*, 2004) (Figure 1). Additional Mediterranean Sea core top assemblages were added from available literature datasets and unpublished data. The oceanographical data, consisting of mean annual, caloric summer and caloric winter SST refer to Antonov *et al.* (2010) and Locarnini *et al.* (2010). The SST values at core tops location were computed by means of Ocean Data View 4.7.10 (Schlitzer, 2017). Following Kucera *et al.* (2005), oceanographical data are related to a depth of 10 m. About the modern dataset, it should be noted that the adopted zero substitution approach can't

be directly applied to literature data when the planktonic foraminifera assemblages are reported as percentages without the total of counted specimens. *Although not an ideal solution (the obvious alternative being to exclude these samples),* in few cases the percentages data included in the modern dataset were "reconverted" into counts by assigning a total of 300 specimens to the samples. The adopted modern planktonic foraminiferal assemblage dataset consists of 26 species. With the approach described in Section 2.1 two datasets were generated, consisting of respectively 19 and 15 taxonomical groups (see Appendix 2). The RVB of the planktonic foraminifera assemblages included in the modern dataset is shown in Figure 2. The first two axes accounts for about 63% of total variability (71% if a third axis is added). The pattern of the links connecting column points highlights the close relationship (i.e. short links) among low latitude *taxa* such as *Globigerinoides ruber, Globogerinoides sacculifer* and *Globorotalia menardii-tumida,* all of which are located on the positive side of axis 1. On the contrary the polar *Neobloboquadrina pachyderma* left coiled is characterised by a strong log-ratio variability respect to most of the taxa, except for *Turborotalita quinqueloba.* The location of the samples points in the RVB highlights the well-known broad latitudinal distribution of assemblages.
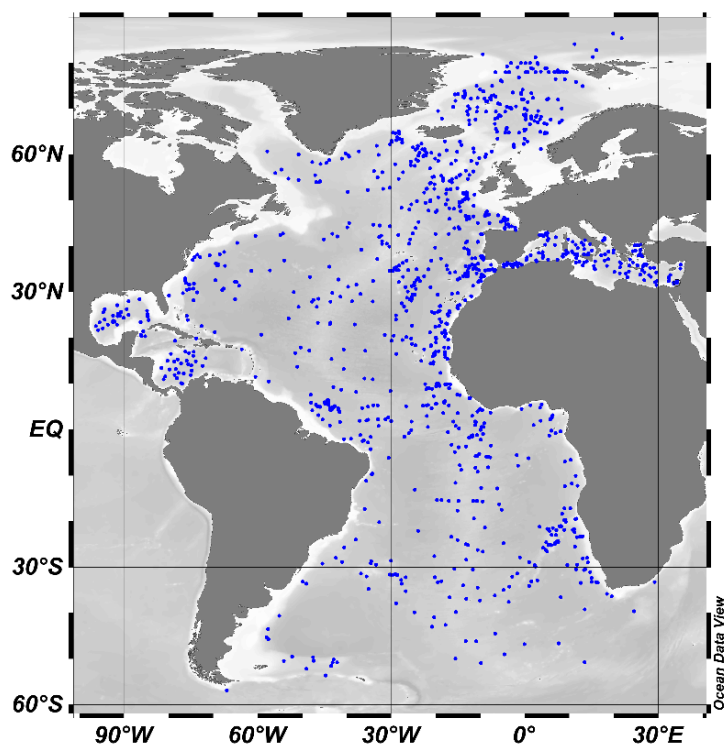
Figure 1. Location of modern planktonic foraminifera core top samples adopted for application of CoDa-MAT. Drawn with Ocean Data View software (Schlitzer 2018).

135
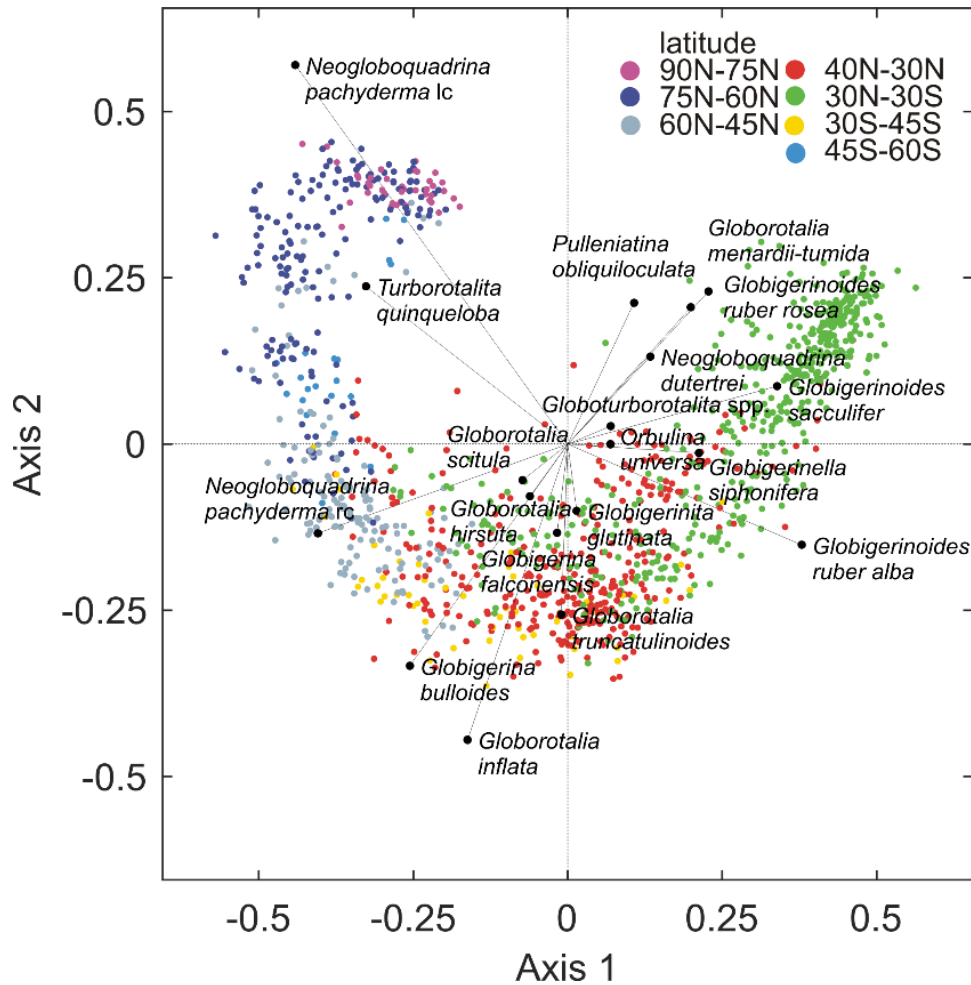
Figure 2. Relative variation biplot of planktonic foraminiferal assemblages included in the modern dataset (19 taxonomical groups). Samples are grouped according to their latitude.

3.1 Leave-one-out verification

The leave-one-out verification (see par. 2.4.1) was carried out on the 15-parts dataset by computing a sensitivity analysis of *MSD* and *R* indexes in relation to the number of analogues (*h*). Both Aitchison and log-ratio Mahalanobis distances were considered. In consideration of the high correlation between annual and seasonal SST, the *MSD* and *R* indexes were only tested with a univariate approach. For this sensitivity analysis a number of analogues *h* in (3) varying from 1 to 30 was considered to obtain the best value of the indexes. For each value of *h* (from 1 to 30) the estimates of the environmental parameter of each modern data sample were calculated using a leave-one-out procedure. As shown in Figure 3, lower *MSD* and higher R values were obtained with 6 to 10 analogues, both for unweighted estimates and estimates weighted on the inverse of the

Aitchison distance. As expected, the weighted estimates were characterised by lower *MSD* values and higher *R* indexes, with peak values for annual SST estimates of 0.993. The annual SST *R* indexes are higher than seasonal ones. Moreover, it can be noted, for both *R* and *MSD* indexes, a rather flat response to the increase in the number of analogues (Figure 3). Although comparable results are obtained from 6 to 10 analogues, the progressive increase in the standard deviation of estimates detected for increasing number of analogues, suggests adopting 6 analogues for the estimates. Figure 4 and Table 1 summarise the relationships between measured seasonal SST and its estimates obtained under these conditions. The maximum mean Aitchison distance between a sample and its closest neighbourhood is about 4.7.

The leave-one-out verification was also tested with the Mahalanobis distance on ilr data. However, in comparison with Aitchison distance, the *MSD* and *standard deviation* values are always higher, and the R indexes lower (Figure 2). Overall, the sensitivity analysis indicates that the Aitchison distance is more performing than the log-ratio Mahalanobis distance. We replicated the sensitivity analysis by testing the 19 parts dataset. The results are quite similar (the correlation coefficient between the annual SST obtained with 19 and 15 parts is 0.999) and are not reported here.

	Mean annual SST	Summer SST	Winter SST
MSD index	0.868	1.344	1.129
R index	0.993	0.989	0.992
Mean std of estimates	0.898	1.062	0.991

Tab. 1 Leave-one-out estimated MSD index, R index and mean std of estimates (6 analogs).
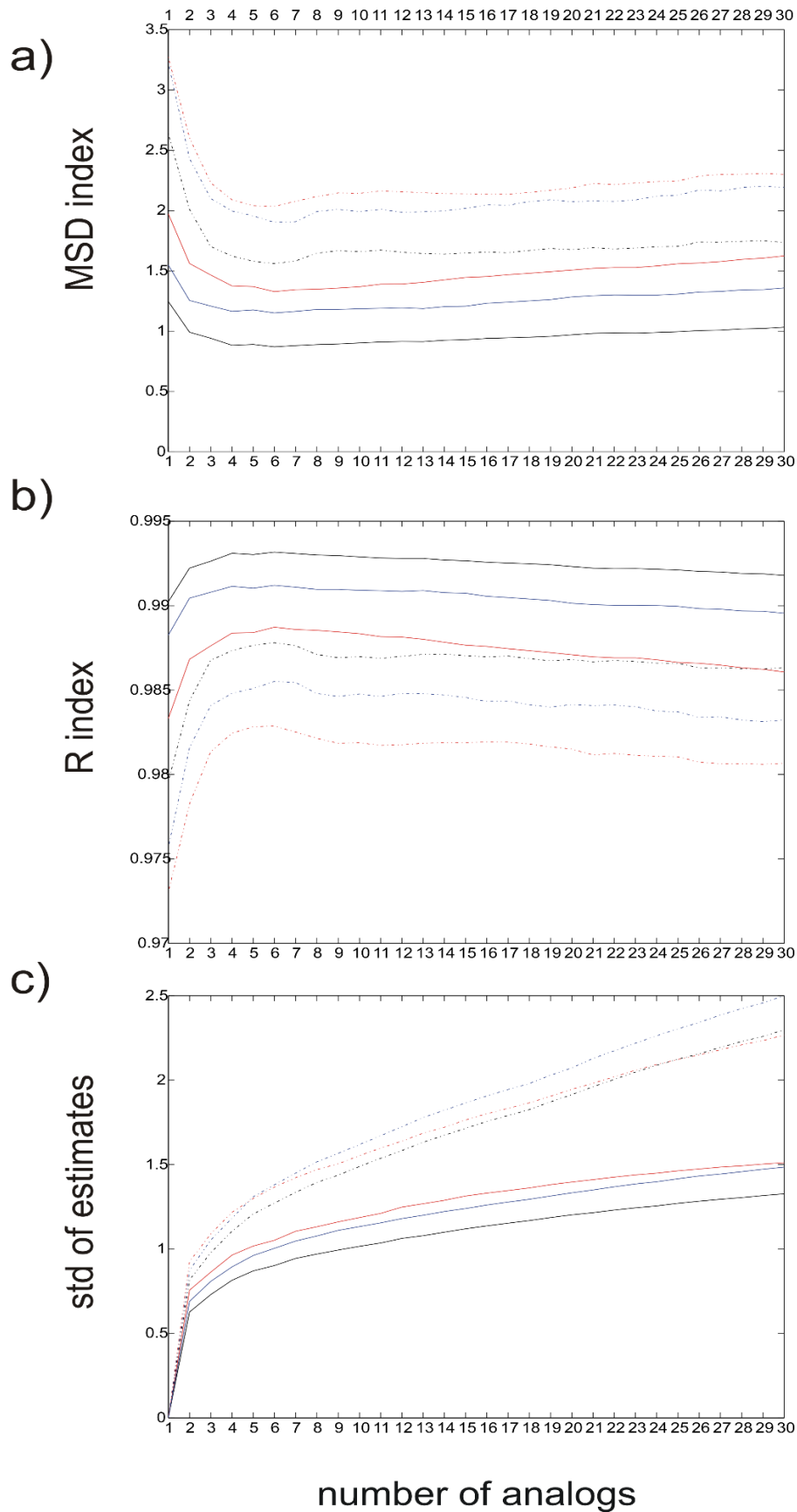
Figure 3. Sensitivity analysis of leave-one-out verification in relation to the number of analogs adopted for the CoDa-MAT estimate of the modern measured seasonal SST. a) MSD index; b) R index; c) mean std of estimates. Black: annual SST; red: summer SST; blue: winter SST. Solid line: ilr-Euclidean (Aitchison) distance; Dashed lines: ilr-Mahalanobis distance.
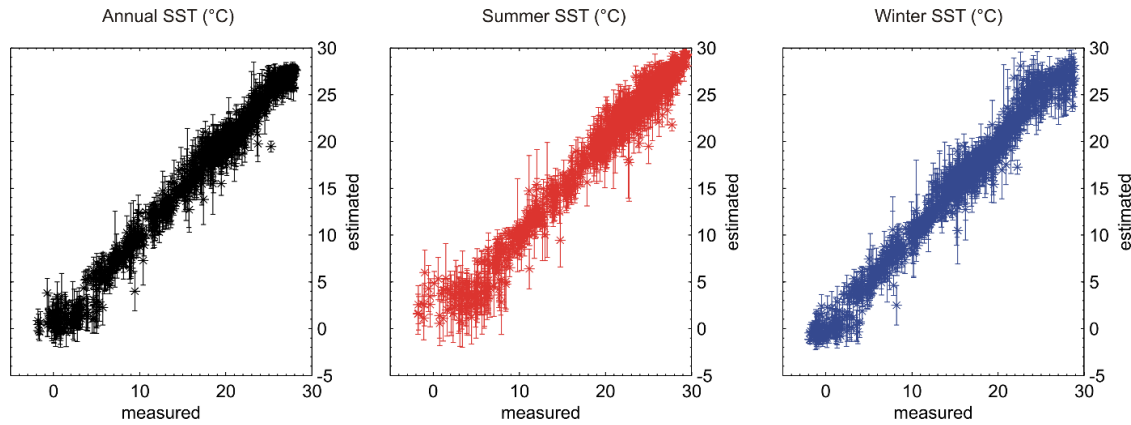
Figure 4. Plots of observed versus estimated SST (annual and seasonal) obtained with 6 analogues. The error bars represent the std of estimates.

3.2 Spatial and geographical relationships.

As discussed above, on the whole dataset, the best leave-one out estimates are obtained with 6 to 10 analogues. Further, the leave-one-out verification was extended to include the whole analogues, by also considering the geographical location of the analogues. In general, the increase in the number of analogues corresponds to an increase in the standard deviation of the estimates. As expected, it can be noted a correspondence between increasing Aitchison and geographical distances (Figure 5). For middle to latitude samples, the sample being tested tends to remain in between the analogues (in terms of both spatial and geographical distribution). With increasing Aitchison distances, farthest away analogues appear, mostly symmetrical with respect to the Equator. However, the behaviour is different for high latitude samples, as the sample being tested get into an *off-center position* as progressively far samples are added. The behaviour is also different for what concern the error of the estimates. For samples located at the border of the cloud of modern data, such as high latitude samples, the increase in the number of analogues corresponds to a progressive increase in the error of the estimates (Figure 5). Instead, for middle and low latitude samples the increase is less marked. Moreover, in several cases, the increase in the number of the analogues (and, consequently, in the Aitchison distances) does not imply further decreasing in the quality of estimates. Likely, this behaviour arises from the fact that the SST differences obtained moving away from the hypersphere's centre in opposite directions tend to compensate each other. These results suggest evaluating, in the application of the method to fossil assemblages, the oceanographical coherency of modern analogues and the spatial relationships between a fossil samples and its modern counterparts. More confident estimates are likely obtained when a fossil

samples is in between its modern analogues, and when the latter are found into a limited geographical region.
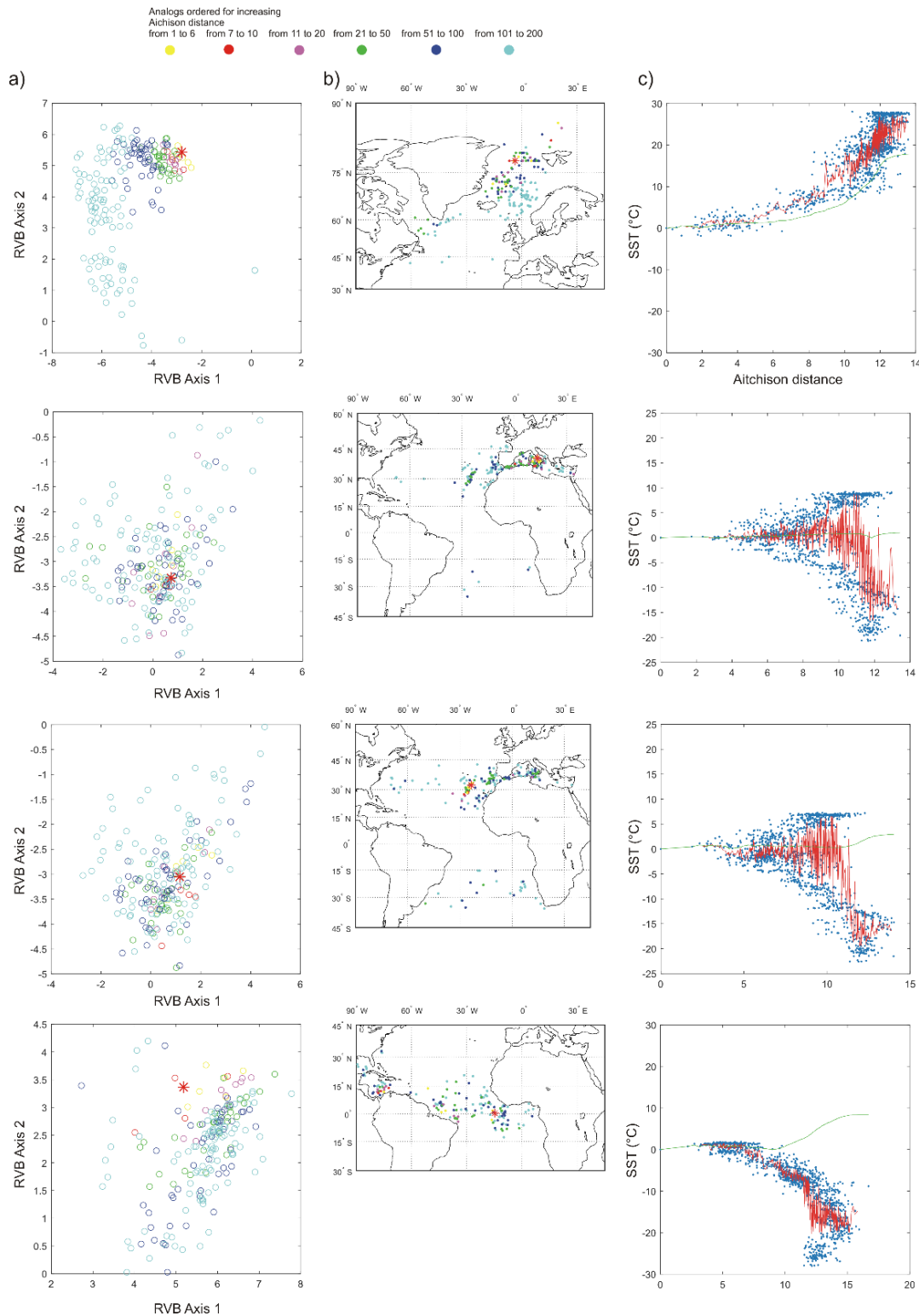
Figure 5. The figure shows, for 4 modern samples located at different latitudes, a) for progressively far analogues, the coordinates on the first 2 axes of the RVB shown in figure 2 and b) their geographical location. The graphs on the left (c) show the differences in SST between a sample and its analogues (blue dots), the SST error for estimates obtained from an increasing number of analogues (green line), and from moving averages of 6 progressively far analogues (red line).

Summing up, threshold distances for evaluating suspect no-analogue conditions can be determined from atypicality index. In addition, confident estimates should fulfil the criteria of: a) closeness and oceanographical/geographical coherence of the analogues, b) reduced standard deviation of the estimates, c) staying in the middle of a fossil samples respect to its modern analogues. These results agree with the findings of Gujot and de Vernal (2011), as geographical closeness among modern analogues appear a prerequisite for obtaining confident estimates.

a)

b)
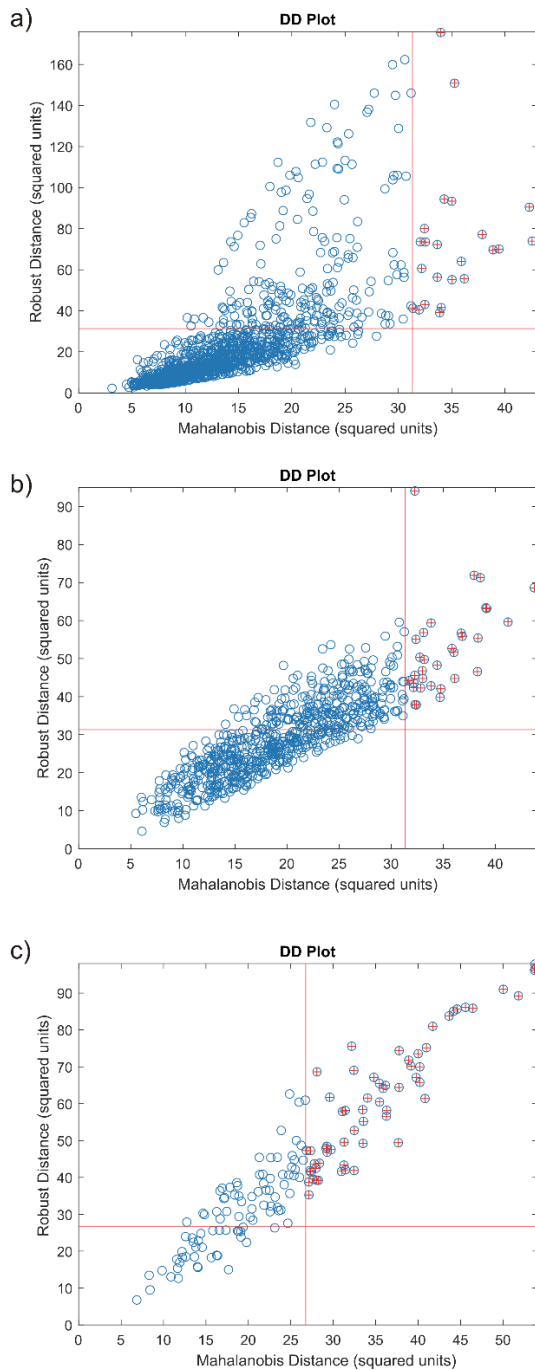
Figure 6. DDplot of squared and robust squared Mahalanobis distances for a) modern data set b) Core MD95-2040 assemblages c) Core GNS84-C106. The red lines represent the 97.5% percentile level, associated to xi-square value.

c)

3.3 Application examples

As an application example, the CoDa-MAT method was applied to two different planktonic foraminifera records. The first one is a literature dataset, consisting of the very detailed record of planktonic foraminifera assemblages of the core MD95-2040 (de Abreu *et al.*, 2003; Voelker and de Abreu, 2011), recovered in the Atlantic Ocean off the Iberian margin, the second is that of GNS84-C106 core recovered in the Tyrrhenian sea (Buccheri et al, 2002; Di Donato *et al.*, 2008; 2009). Both datasets are obtained from >150 μm size fractions. As noted by Di Donato et al. (2015), the drawback represented by the excessive loss of small sized species in this size fraction can be circumvented, at least in part, by means of CoDA methods. The fact remains nevertheless that the unavailability of large modern datasets based on smaller size fractions imposes the choice of the >150 μm one which is not an optimal solution. The atypicality index computed with log-ratio Mahalanobis distances for each sample of the modern database (see section 2.4.1) allowed us to determine a critical value of 26.12 beyond which samples can be considered as outliers. By means of standard and robust atypicality, 91 and 303 outlier samples in the modern database were detected, respectively (Figure 6). These results appear rather restrictive because large part of modern samples is detected as outliers. Note that, by definition, the Mahalanobis distance is a measure of global atypicality, that is, it is affected by the existence of groups in the data. In contrast, using the LOF of modern assemblages, only two samples have values larger than 2, and only 35 samples values higher than 1.4.
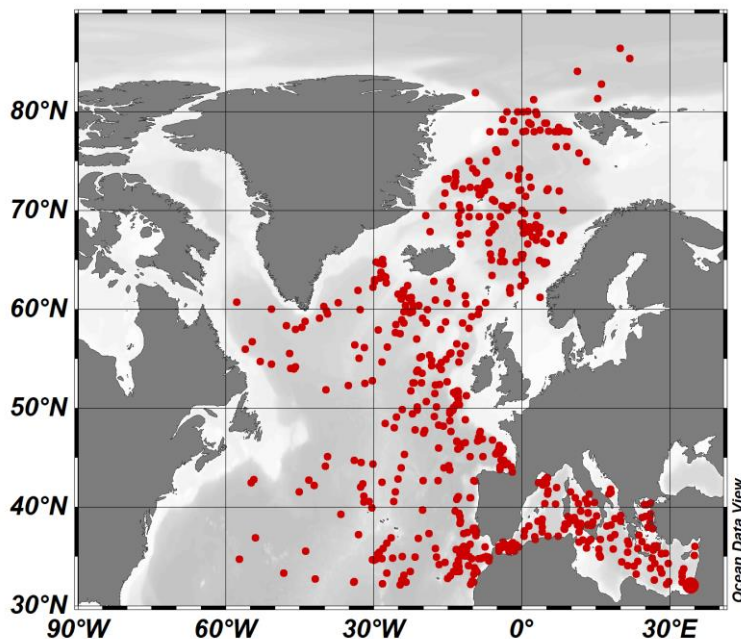
Figure 9. Location of regionalised modern planktonic foraminifera coretop assemblages adopted for application of CoDa-MAT to the Core GNS84-C106. Drawn with Ocean Data View software (Schlitzer 2018).
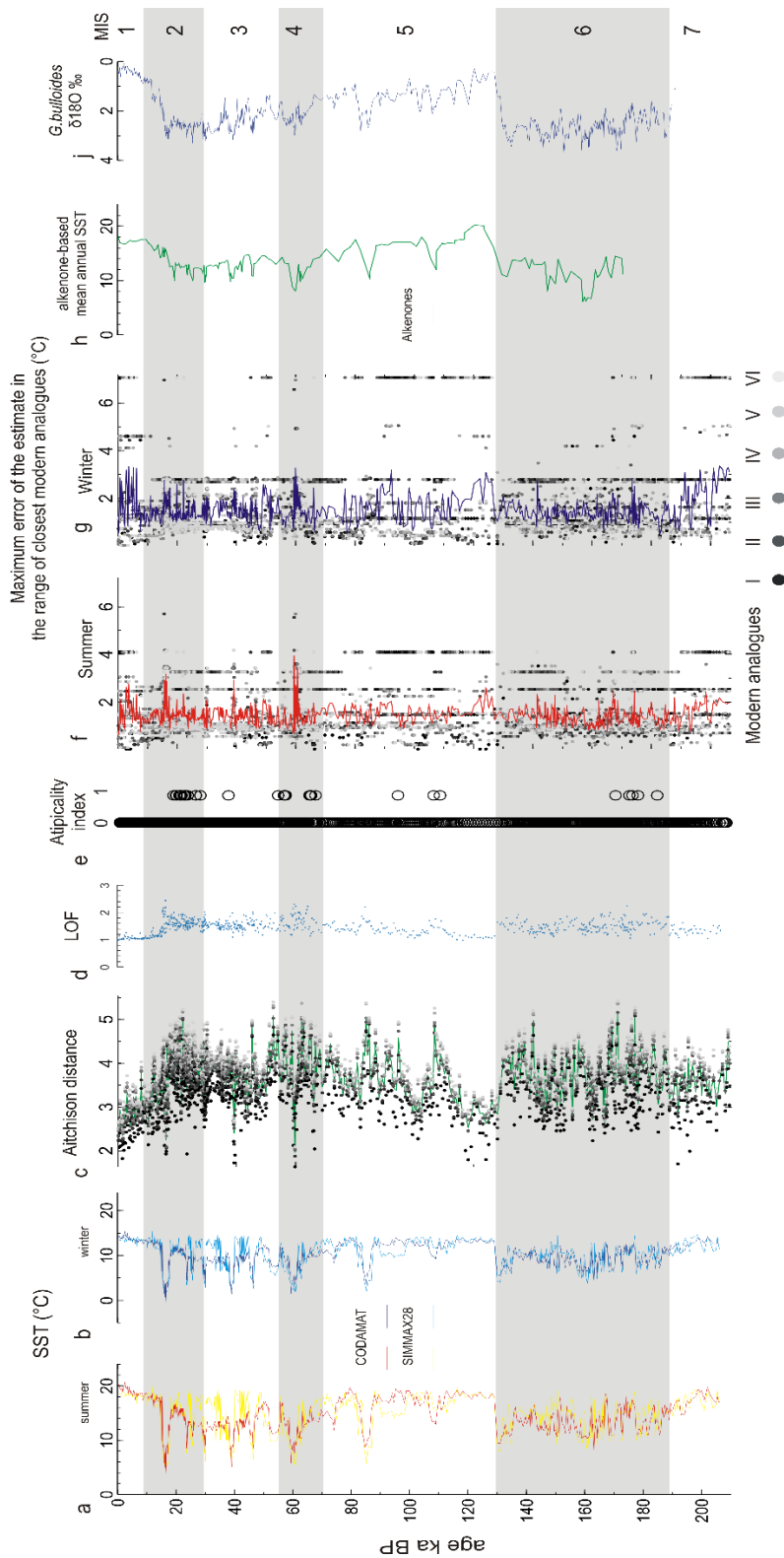
Figure 7. Reconstruction of seasonal SST for the last 210 ka off the Iberian margin from core MD95-2040 and comparison between CoDa-MAT and SIMMAX28 (de Abreu et al., 2003, Voelker and de Abreu, 2011) reconstructed SSTs. a: summer SST. b) winter SST. c) gray-shaded dots: distance of fossil assemblages from each of the 6 closest modern analogues. Full line: mean values. d) LOF values e) atypicality index: 0: not significant; 1: significant f-g) gray-shaded dots: maximum modules of the estimate errors for the closest 6 modern analogues, at radii equal to the measured Aitchison distance. Full line: Mean values. h) Alkenone based SST reconstruction (Pailler and Bard, 2002). j) *Globigerina bulloides* stable isotope record and Marine Isotopic Stages (MIS) (Abreu *et al*., 2003; Schönfeld *et al*., 2003).
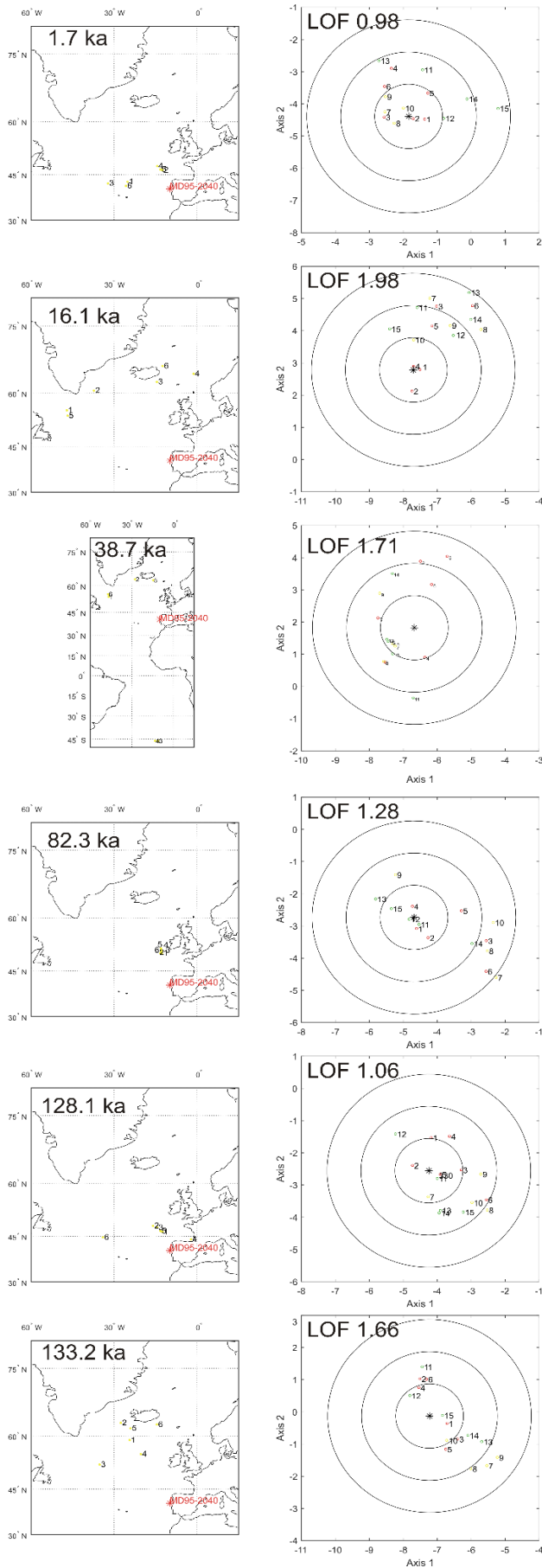
Figure 8. Geographical (left column) and spatial (right column) relationships among selected foraminiferal assemblages of Core MD95-2040 and the modern coretop assemblages. Numbers indicate the ranking of the closest modern analogues.

44

3.2.1 Atlantic Ocean

The foraminiferal record of MD95-2040 core covers the last 210 ka (de Abreu *et al.*, 2003; Voelker, and de Abreu, 2011). Sea surface temperatures for this interval were formerly reconstructed (de Abreu *et al.*, 2003) from planktonic foraminifera with SIMMAX28 method (Pflaumann *et al.*, 1996). As regards the atypicality of assemblages, for about 19% of the samples, the Mahalanobis distances are above the xi-square critical value of 26.11 corresponding to the 97.5 percentile (Figure 6). In relation to the 99.5 percentile, 4% of the samples have Mahalanobis distances are above the xi-square critical value of 31.32. The robust outlier detection is more restrictive, as about 40% of samples lies beyond the critical value. As for the LOF, glacial assemblages are characterised by higher values of up to 2, while most interglacial assemblages have LOF values not exceeding 1.5. Coherently, the mean distance of closest analogues is lower for interglacial periods. However, the expected maximum errors of the estimates are rather stable throughout the core (Figure 7). The comparison with the values reconstructed for summer and winter SST by means of SIMMAX28 (Figure 7) (de Abreu *et al.*, 2003), highlights a same general trend, with decreasing SST around the transition between MIS 7 and MIS 6. From MIS 6 to MIS 4, both methods record colder intervals (around 160 ka, 130 ka, 85 ka and 60 ka BP) which are also evident in the alkenone-based SST reconstructions and in the oxygen stable isotopes record. In addition, CoDa-MAT gives evidence to a negative SST peak around 108 ka BP, which is also evident in the alkenones and $\delta^{18}O$ record. SIMMAX28 and CoDa-MAT reconstructions are quite different for the interval between 50 ka and 20 ka BP. Although the reconstructed values for the most prominent SST decreases (at 40 ka, 30 ka and 16 ka BP) are similar, for this time interval CoDa-MAT provides less fluctuating SST values, which appear more coherent with the alkenone-based SST reconstructions and $\delta^{18}O$ stable isotope record. The spatial and geographical relationships between selected fossil assemblages of the Core MD95-2040 and their closest modern analogues are shown in Figure 8. It can be noted that the modern analogues of some fossil assemblages characterised by higher LOF, are located in the South and North Atlantic Ocean, mostly symmetrical with respect to the Equator.

3.2.2 Tyrrhenian sea (Western Mediterranean Sea)

The Core GNS84-C106 core covers the last 34 ka (Di Donato *et al.,* 2009). Following Kucera *et al.* (2005), the application of the CoDa-MAT was carried out on a regionalised modern dataset represented by Mediterranean and North Atlantic core top assemblages (Figure 9). The amplitude

of SST changes (Figure 10) is of about 10°C, the lower values being recorded between 15 and 17.5 cal ka BP. It can be noted that Holocene samples younger than 6 cal ka BP are characterised by low standard deviation, low mean distances from the closest modern analogues and low LOF. Early Holocene assemblages are characterised by slightly higher mean distances, albeit the low LOF values. On the contrary, the increasing mean distances obtained for late glacial and last glacial period (LGP) assemblages corresponds to an increase in the standard deviation of the estimates. Moreover, the mean distances reach values of up to 5, which are beyond the maximum value obtained for modern assemblages. As regards the atypicality of fossil assemblages, with a critical value of 21.92, several assemblages of this core, in particular from the LGP, can be considered as outliers with respect to the modern dataset (Figure 6). Comparable results are obtained by considering the expected errors of the estimates obtained by means hypersphere radius evaluation (Figure 10). The "expected errors" are below 1°C for the last 5 ka. The higher mean distances recorded in the early Holocene (between 9 and 5 ka BP) corresponds to a first increase in expected errors, with values ranging from 1° to 2°C. Noteworthy this interval is coeval with the eastern Mediterranean sapropel S1 event, during which the Mediterranean oceanographical asset was quite different from today (e.g. Emeis *et al.*, 2000; Ni Fhlaithearta *et al.*, 2010). Higher values, in the order of 2°C were found for the LGP. The spatial and geographical relationships between selected fossil assemblages and their modern counterparts are shown in Figure 11. It can be noted that when the modern analogues are found at higher distances, there are some oceanographic incoherencies. As an example, it can be noted that the closest modern analogues of an LGP assemblage dated at 21.3 cal ka are partly found in the Atlantic Ocean, partly in the Mediterranean Sea. Moreover, in addition to being characterised by high LOF and significant atypicality, in the RVB plot this fossil assemblages seems lying off centre with respect to its modern analogues. A marked oceanographic incoherence also characterises the assemblage dated at 13.5 cal ka. In summary, atypicality of samples and oceanographic incoherency, suggests caution in the interpretation of the reconstructed SST, for the Late Glacial and the LGP intervals of this core, at least for the >150 μm size fraction adopted for the analysis. The results obtained with CoDA-MAT have been compared with those obtained with raw data analysis and squared chord distance adopted as similarity measure (Figure 10). The results appear comparable for the Holocene interval of the core, however for the Late Glacial and Last Glacial Period, the CoDa-MAT reconstructed SST are much lower than those obtained with raw data MAT, which appear even higher than present for the 19-25 cal ka interval.

For this case study, the results are likely influenced by the size fraction commonly adopted for the modern planktonic foraminiferal core top databases, i.e the excessive loss of small sized specimens of *T. quinqueloba* in the >150-micron size fraction (Di Donato *et al.,* 2015). In this respect, it should be noted that are currently not available core top databases of planktonic foraminifera assemblages built with smaller size fractions. However, it is likely that the adoption of smaller size fractions would produce lower SST estimates for the LGP intervals of the GNS84-C106 core.
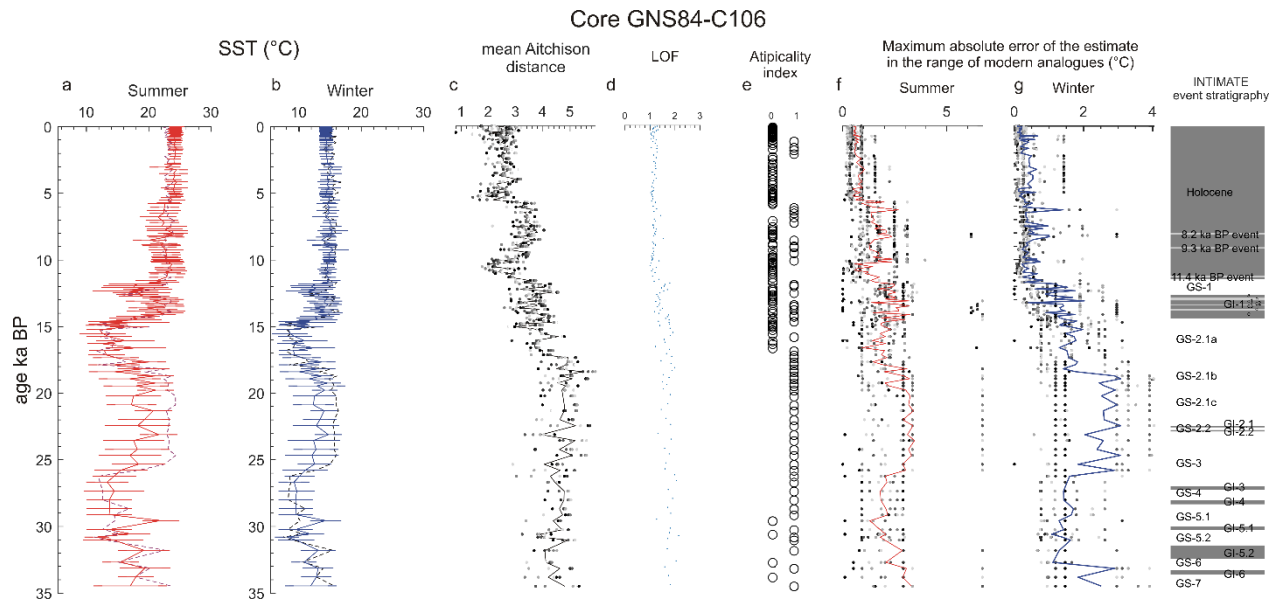
Figure 10. CoDa-MAT reconstruction of seasonal SST obtained from GNS84-C106 Core. a) summer b) winter. The error bars indicate the standard deviation of each reconstructed value. c) gray-shaded dots: distance of fossil assemblages from each of the 6 closest modern analogues. Full line: mean values. d) LOF values e) atypicality index: 0: not significant; 1: significant f-g) gray-shaded dots: maximum modules of the estimate errors for the closest 6 modern analogues, at radii equal to the measured Aitchison distance. Full line: Mean values. The INTIMATE Greenland event stratigraphy is reported from Rasmussen et al. (2014).

4. Conclusive remarks

In general, the leave-one-out cross validation performed on CoDa-MAT with modern data yielded correlations between estimated and measured modern values in the range of methods such as Imbrie and Kipp transfer functions, SIMMAX or RAM if applied to Atlantic Ocean (Waelbroeck *et al.*, 1999). However, as pointed out above, the proposal of a method based on CoDa has not the objective of increase the correlation obtained from previous methods, but rather to develop the method coherently with the nature of data. Up to now, despite the advances in the statistical theory, only a relatively few micropaleontological studies adopted an approach coherent with CoDa principles (Buccianti and Esposito, 2004; Di Donato *et al.*, 2009; Sgarrella *et al.,* 2012; Di Donato

et al., 2018). Apart from these fundamental issues, CoDa-MAT also provides tools for evaluate the reliability of estimates performed on fossil assemblages and the occurrence of atypical fossil assemblages. The application of CoDa-MAT to the examples highlighted a coherent behaviour and, for the Iberian margin, a strong coherence with the stable isotopes record. About the Tyrrhenian sea case study, the caution is suggested regarding LGP SST estimates. However, the CoDA approach seems less subjected to problems related to preparation techniques (i.e. size fraction) than raw data analysis. Although application examples of CoDa-MAT are described in a palaeoceanographic context, this method can be obviously applied to different proxies, i.e. to reconstruct past atmospheric environments, as usually done in palynological studies. Further studies, involving the application of CoDa-MAT to continental proxies will be carried out to evaluate its performing.
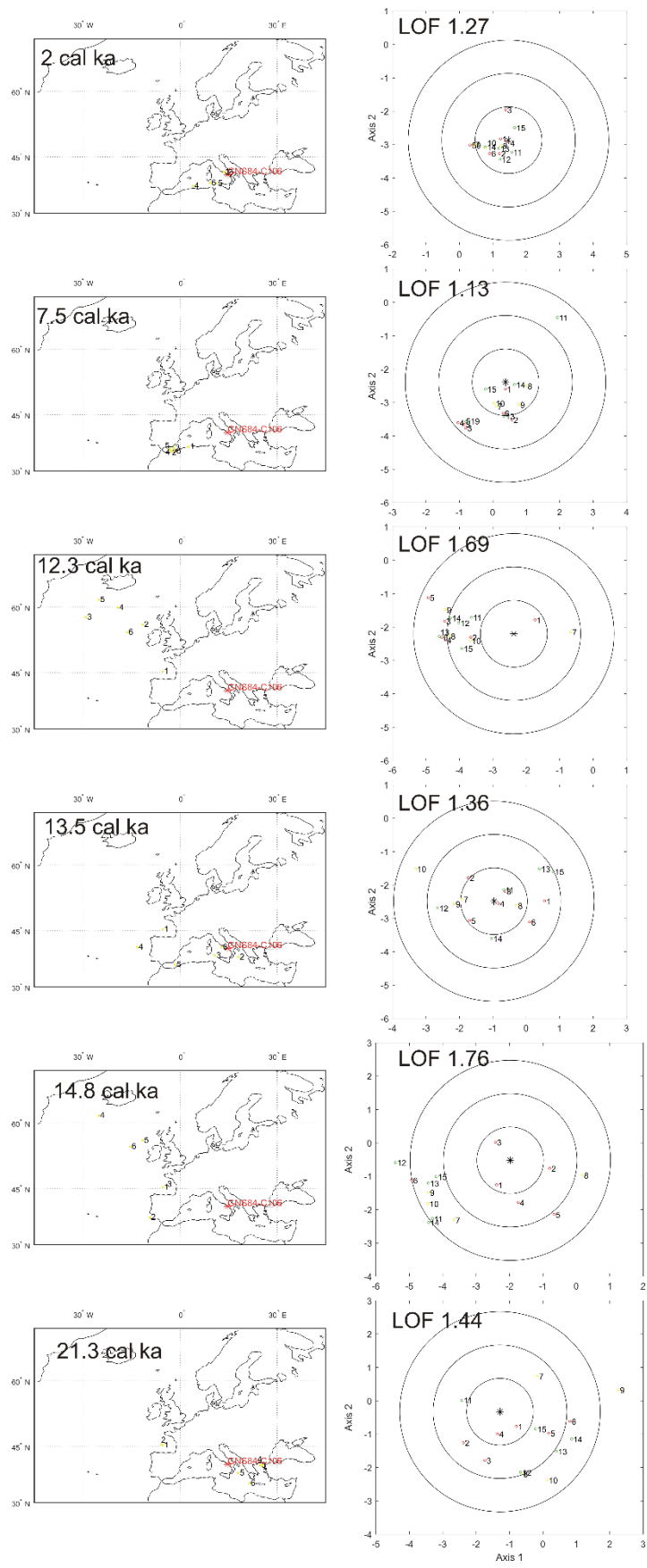
Figure 11. Geographical (left column) and spatial (right column) relationships among selected foraminiferal assemblages of Core GNS84-C106 and the modern coretop assemblages. Numbers indicate the ranking of the closest modern analogues.

Acknowledgements

References

Aitchison, J. (1986) - *The Statistical Analysis of Compositional Data. Monographs on Statistics and Applied Probability*. Chapman and Hall Ltd. (Reprinted 2003 with additional material by The Blackburn Press), London (UK). 416 p.

Aitchison, J., Barceló-Vidal, C., Martín-Fernández, J.A., Pawlowsky-Glahn, V. (2000) - *Logratio analysis and compositional distance*. Mathematical Geology 32 (3), 271-275.

Antonov, J. I., Seidov D., Boyer, T. P., Locarnini R. A., Mishonov A. V., and Garcia H. E. (2010) - *World Ocean Atlas 2009 Volume 2: Salinity.* S. Levitus, Ed., NOAA Atlas NESDIS 69, U.S. Government Printing Office, Washington, D.C., 184 pp.

Barceló-Vidal C, Martín-Fernández J.A. (2016) - *The mathematics of compositional analysis.* Austrian journal of statistics 45(4):57–71

Barrows, T.T, Juggins, S. (2005) - *Sea-surface temperatures around the Australian margin and Indian Ocean during the last glacial maximum.* Quaternary Science Reviews, 24, 1017–1047.

Birks, H.J.B. (1995). *Quantitative palaeoenvironmental reconstructions*. In: Maddy, D., Brew, J.S. (Eds.), Statistical Modelling of Quaternary Science Data. Technical Guide 5. Quaternary Research Association, Cambridge, pp. 116–254.

Brassell, S.C., Eglinton, G., Marlowe, I.T., Pflaumann, U., and Sarnthein, M. (1986) - *Molecular stratigraphy: A new tool for climatic assessment*. Nature, 320 (6058), 129-133.

Breunig M.M., Kriegel H.-P., Ng R.T., Sander J. (2000) - *LOF: identifying density-based local outliers*. In Proceedings of the 2000 ACM SIGMOD international conference on Management of data (SIGMOD '00). ACM, New York, NY, USA, 93-104. DOI=http://dx.doi.org/10.1145/342009.335388

Buccheri, G., Capretto, G., Di Donato, V., Esposito, P., Ferruzza, G., Pescatore, T., Russo Ermolli, E., Senatore, M.R., Sprovieri, M., Bertoldo, M., Carella, D., and Madonna, G. (2002) - *A

high resolution record of the last deglaciation in the southern Tyrrhenian Sea: environmental and climatic evolution. Marine Geology 186, 447-470.

Buccianti, A., Mateu-Figueras, G., Pawlowsky-Glahn, V. (Eds.) (2006) - *Compositional Data Analysis in the Geosciences: From Theory to Practice*. In: Special Publications, vol. 264. Geological Society, London.

Buccianti, A., Esposito, P. (2004) - *Insights on Late Quaternary calcareous nannoplankton assemblages under the theory on statistical analysis for compositional data: an application example*. Palaeogeography, Palaeoclimatology, Palaeoecology, 202, 209–227.

Daunis-i-Estadella J., Thió-Henestrosa S., Mateu-Figueras G. (2011 - *Including supplementary elements in a compositional biplot*. Computers & Geosciences, Volume 37, Issue 5, May 2011, Pages 696 – 701.

de Abreu, L., Shackleton, N.J., Schonfeld, J., Hall M., and Chapman, M. (2003) - *Millennial-scale oceanic climate variability off the Western Iberian margin during the last two glacial periods*. Marine Geology, 196 (1-2), 1-20.

Di Donato, V., Esposito, P., Garilli, V., Naimo, D., Buccheri, G., Caffau, M., Ciampo, G., Greco, A., and Stanzione, D. (2009) - *Surface-bottom relationships in the Gulf of Salerno (Tyrrhenian Sea) over the last 34 kyr: Compositional data analysis of palaeontological proxies and geochemical evidence*. Geobios, 42, 561-579.

Di Donato, V., Esposito, P., Russo Ermolli, E., Scarano, A., and Cheddadi, R. (2008) - *Coupled atmospheric and marine palaeoclimatic reconstruction for the last 35 ka in the Sele Plain-Gulf of Salerno area (southern Italy)*. Quaternary International, 190, 146-157.

Di Donato, V., Insinga, D.D., Iorio, M., Molisso, F., Rumolo, P., Cardines, C. Passaro, S. (2018) - *The palaeoclimatic and palaeoceanographic history of the Gulf of Taranto (Mediterranean Sea) in the last 15 ky*. Global and Planetary Change. 10.1016/j.gloplacha.2018.10.014

Di Donato, V., Martin-Fernandez, J.A., Daunis-i-Estadella, J. & Esposito, P. (2015) - *Size fraction effects on planktonic foraminifera assemblages: a compositional contribution to the golden sieve rush*. Mathematical Geosciences, 47 (4), 455-470.

Egozcue, J.J., Pawlowsky-Glahn, V., Mateu-Figueraz, G., Barceló-Vidal, C. (2003) - *Isometric logratio transformations for compositional data analysis*. Mathematical Geology 35 (3), 279-300.

Egozcue, J.J., and Pawlowsky-Glahn, V. (2011) - *Basic concepts and procedures (Chapter 2)*. In: Pawlowsky-Glahn and Buccianti (2011), pp. 12–28.

Elderfield H., and Ganssen G. (2000) - *Past temperature and d18O of surface ocean waters inferred from foraminiferalMg/Ca ratios.* Nature, 405, 442-445.

Emeis, K.C., Struck, U., Schulz, H.-M., Rosenberg, R., Bernasconi, S., Erlenkeuser, H., Sakamoto, T., and Martinez-Ruiz, F. (2000) - *Temperature and salinity variations of Mediterranean Sea surface waters over the last 16,000 years from records of planktonic stable oxygen isotopes and alkenone unsaturation ratios.* Palaeogeography, Palaeoclimatology, Palaeoecology, 158 (3–4), 259-280. doi 10.1016/S0031-0182(00)00053-5.

Everitt B.S., Landau S., Leese M., Stahl D. (2011) - *Cluster analysis.* John Wiley & Sons, Ltd, Chichester, United Kingdom 5th Edition, 330 pp

Filzmoser, P., and Hron, K. (2008) - *Outlier detection for compositional data using robust methods.* Math. Geosciences, 40, 233-248.

Guiot, J., and de Vernal, A. (2011) - *Is spatial autocorrelation introducing biases in the apparent accuracy of paleoclimatic reconstructions?* Quaternary Science Reviews 30, 1965-1972.

Guiot, J., and de Vernal, A. (2011), *QSR Correspondence "Is spatial autocorrelation introducing biases in the apparent accuracy of palaeoclimatic reconstructions?" Reply to Telford and Birks.* Quaternary Science Reviews 30, 3214–3216.

Hayes, A., Kucera, M., Kallel, N., Sbaffi, L., and Rohling, E. (2004) - *Compilation of planktic foraminifera modern data from the Mediterranean Sea*. Pangaea, doi:10.1594/PANGAEA.227305.

Hutson, W.H. (1979) - *The Agulhas Current during the Late Pleistocene: Analysis of modern faunal analogues.* Science, 207 (1), 64-66.

Imbrie, J. and Kipp, N.G. (1971) - *A new micropaleontological method for paleoclimatology: Application to a Late Pleistocene Caribbean core.* The Late Cenozoic Glacial Ages. New Haven, Yale University Press. 71-181.

Kucera, M., Weinelt, M., Kiefer, T., Pflaumann, U., Hayes, A., Weinelt, M., Chen, M.-T., Mix, A.C., Barrows, T., Cortijo, E., Duprat, J., Juggins, S., and Waelbroeck, C. (2004) - *Compilation of planktic foraminifera census data, modern from the Atlantic Ocean.* Pangaea, doi:10.1594/PANGAEA.227322.

Kucera, M., Rosell-Melé, A., Schneider, R., Waelbroeck, C., Weinelt, M. (2005) - *Multiproxy approach for the reconstruction of the glacial ocean surface (MARGO).* Quaternary Science Reviews, Volume 24 (7-9), 813-819.

Locarnini, R. A., Mishonov, A. V., Antonov, J. I.,Boyer, T. P., and Garcia, H. E. (2010) - *World Ocean Atlas 2009, Volume 1: Temperature*. S. Levitus, Ed., NOAA Atlas NESDIS 68, U.S. Government Printing Office, Washington, D.C., 184 pp.

Malmgren, B. A., Kucera, M., Nyberg, J. and Waelbroeck, C. (2001) - *Comparison of statistical and artificial neural network techniques for estimating past sea surface temperatures from planktonic foraminifer census data*. Paleoceanography, 16 (5), 520–530, doi:10.1029/2000PA000562.

Martín-Fernández, J. A., Barceló-Vidal, C. and Pawlowsky-Glahn, V. (2003) - *Dealing with zeros and missing values in compositional datasets using nonparametric imputation.* Mathematical Geology, 35 (3), 253-278.

Martín-Fernández, J.A., Hron, K., Templ, M., Filzmoser, P,. Palarea-Albaladejo J. (2015) - *Bayesian-multiplicative treatment of count zeros in compositional datasets.* Statistical Modelling, 15(2), 134-158

Martín-Fernández, J.A. and Thió-Henestrosa, S. (eds.) (2016a) - *Compositional Data Analysis: CoDaWork, L'Escala, Spain, June 2015.* Springer Proceedings in Mathematics & Statistics, 187. Springer International Publishing, New York (USA).

Martín-Fernández, J.A. and Thió-Henestrosa, S. (Guest eds.) (2016b) - *Compositional Data Analysis.* Austrian Journal of Statistics, 45(4)

Mateu-Figueras G., Pawlowsky-Glahn V., Egozcue, J.J. (2011) - (Pawlowsky-Glahn V, Buccianti A, eds). John Wiley & *The Principle of Working on Coordinates, in Compositional Data Analysis: Theory and Applications* Sons, Ltd, Chichester, UK: 29–42

Ni Fhlaithearta, S., Reichart, G.J., Jorissen, F.J., Fontanier, C., Rohling, E.J., Thomson, J., and De Lange, G.J. (2010) - *Reconstructing the sea floor environment during sapropel formation using trace metals and sediment composition*. Paleoceanography, 25, PA4225, doi:10.1029/2009PA001869, 2010.

Overpeck, J.T., Webb, T., and Prentice, I.C. (1985) - *Quantitative interpretation of fossil pollen spectra: dissimilarity coefficients and the method of modern analogues*. Quaternary Research, 23, 87-108.

Palarea-Albaladejo, J., Martín-Fernández, J.A. and Soto, J.A. (2012) - *Dealing with Distances and Transformations for Fuzzy C-Means Clustering of Compositional Data.* Journal of Classification 29 (2), 144-169.

Palarea-Albaladejo, J. and Martín-Fernández, J.A. (2015) - *zCompositions - R package for multivariate imputation of nondetects and zeros in compositional datasets.* Chemometrics and Intelligent Laboratory Systems, 143, 85-96.

Pawlowsky-Glahn V, Egozcue J.J., Tolosana-Delgado R. (2015) - *Modeling and analysis of compositional data.* John Wiley & Sons, Chichester, 378 pp

Pawlowsky-Glahn, V., and Buccianti, A. (Eds.) (2011) - *Compositional Data Analysis: Theory and Applications.* John Wiley & Sons, Ltd., Chichester, UK, p. 378.

Peña, D. and Prieto, F. (2001) - *Multivariate outlier detection and robust covariance matrix estimation.* Technometrics, 43 (3), 286-310.

Pflaumann, U., Duprat, J., Pujol, C. and Labeyrie, L.D., 1996. *SIMMAX: a modern analogue technique to deduce Atlantic sea surface temperatures from planktonic foraminifer in deep-sea sediments,* Paleoceanography, 11, 15–36.

Prell, W., Martin, A., Cullen, J., and Trend, M., (1999) - *The Brown University Foraminiferal Data Base.* IGBP PAGES/World Data Center-A for Paleoclimatology Data Contribution Series # 1999–027. NOAA/NGDC Paleoclimatology Program, Boulder, CO, USA.

Rasmussen S.O., Bigler M., Blockley S.P., Blunier T., Buchardt S.L., Clausen H.B., Cvijanovic I., Dahl-Jensen D., Johnsen S.J., Fischer H., Gkinis V., Guillevic M., Hoek W.Z., Lowe J.J., Pedro J.B., Popp T., Seierstad I.K., Peder Steffensen J., Svensson A.M., Vallelonga P., Vinther B.M., Walker M.J.C., Wheatley J.J., Winstrup M. (2014) - *A stratigraphic framework for abrupt climatic changes during the Last Glacial period based on three synchronized Greenland ice-core records: refining and extending the INTIMATE event stratigraphy.* Quaternary Science Reviews, 106, 14-28.

R Development Core Team (2011) - *R: A Language and Environment for Statistical Computing.* R Foundation for Statistical Computing, Vienna, Austria. http://www.r-project.org.

Schlitzer, R. (2018) - *Ocean Data View*, http://odv.awi.de.

Schönfeld, J., Zahn., R., and de Abreu., L. (2003) - *Stable isotope ratios and foraminiferal abundance of sediment cores from the Western Iberian Margin.* doi:10.1594/PANGAEA.733303,
supplement to: **Schönfeld, J.; Zahn, R.; de Abreu, L. (2003):** Surface to deep water response to rapid climate changes at the western Iberian Margin. *Global and Planetary Change, 36(4),* 237-264, doi:10.1016/S0921-8181(02)00197-2.

Sgarrella F., Di Donato, V. and Sprovieri, R. (2012) - *Benthic foraminiferal assemblage turnover during intensification of the Northern Hemisphere glaciation in the Piacenzian Punta Piccola section (Southern Italy).* Palaeogeography, Palaeoclimatology, Palaeoecology, 333-334, 59-74. doi: 10.1016/j.palaeo.2012.03.009

Tauber, F. (1999) - *Spurious clusters in granulometric data caused by logratio transformation.* Mathematical Geology. 31, 491-504.

Telford, R.J., Birks, H.J.B. (2009) - *Evaluation of transfer functions in spatially structured environments.* Quaternary Science Reviews 28, 1309–1316.

Telford, R.J., Birks, H.J.B. (2011) - *Is spatial autocorrelation introducing biases in the apparent accuracy of palaeoclimatic reconstructions?* Quaternary Science Reviews 30, 3210–3213.

ter Braak, C.l.F. Juggins, S. (1993) - *Weighted averaging partial least squares regression (WA-PLS): an improved method for reconstructing environmental variables from species assemblages.* Hydrobiologia. 2691270,485-502.

Voelker, A.H.L., de Abreu, L. (2011) - *A Review of Abrupt Climate Change Events in the Northeastern Atlantic Ocean (Iberian Margin): Latitudinal, Longitudinal and Vertical Gradients.* In: Rashid, H; Polyak, L; Mosley-Thompson, E (eds), Abrupt Climate Change: Mechanisms, Patterns, and Impacts. Geophysical Monograph Series (AGU, Washington D.C.), 193, 15-37, doi:10.1029/2010GM001021.

Waelbroeck, C., Labeyrie, L., Duplessy, J.-C., Guiot, J. and Labracherie, M. (1998) - *Improving past sea surface temperature estimates based on planktonic fossil faunas.* Paleoceanography, 13, 272–283.

Wallach, D., Goffmet, B. (1989) - *Mean squared error of prediction as a criterion for evaluating and comparing system models.* Ecological Modelling, 44,299-306.

Supplementary appendices

Appendix 1: *ilr-coordinates and Bayesian-multiplicative treatment of zeros.*

In our work, each vector represents the composition of species in both fossil and modern data assemblages. Such compositions can be formalised as a vector $\mathbf{x} = [x_1,\ldots,x_D]$ of non-negative elements representing proportions with sum-constraint $x_1+\ldots+ x_D = 1$. Compositions belong to the simplex S^D, the sample space: $S^D=\{\mathbf{x} \in R^D \,/\, x_i>0,\ i=1..D;\ x_1+...+x_D= 1 \}$. Log-ratio coordinates are obtained by one-to-one correspondences between vectors of percentages from CoDa set $\mathbf{X}\in S^D$ and the log-ratio vectors from the coordinates dataset $\mathbf{Y} \in R^{D-1}$ in real space. This correspondence allows the use of standard multivariate techniques on the coordinates dataset $\mathbf{Y}$. Typical log-ratios coordinates are the centered log-ratio coefficients (clr_j):

$$clr(\mathbf{x})= \left(clr_1(\mathbf{x}), \ldots, clr_D(\mathbf{x})\right) \ \text{with} \ clr_j(\mathbf{x})= \ln \frac{x_i}{g(\mathbf{x})},$$

where $g(\mathbf{x})$ is the geometric mean of the composition. Because $\sum_{j=1}^{D} clr_j(\mathbf{x})=0$, then (i.e. the centred log-ratio covariance matrix is singular) the dimension of the clr-space is D-1. One can construct an orthonormal basis in the clr-space to obtain orthonormal log-ratio coordinates. To do this one can calculate the the isometric log-ratio coordinates (ilr) of the percentages of species. The ilr-coordinates' vector is defined by

$$ilr(\mathbf{x}) = \mathbf{y} = [y_1,\ldots, y_{D-1}]\in R^{D-1}, \ \text{where} \qquad \mathbf{y}_i = \frac{1}{\sqrt{i(i+1)}} \ln\left(\frac{\prod_{j=1}^{i} \mathbf{x}_j}{\left(\mathbf{x}_{i+1}\right)^i} \right)$$

From among the log-ratio coefficients, the orthornormal coordinates are preferred because of their advantageous theoretical and practical properties (Pawlowsky-Glahn *et al.*, 2015). The log-ratio coordinates obviously cannot be obtained for CoDa with zero values. Consequently, before proceeding with the log-ratio coordinates, observations with zero values had to be pre-processed with appropriate compositional techniques. The zeros can be present for various reasons in a CoDa set. Martín-Fernández *et al.* (2011) presented a comprehensive description of this difficulty, known in the literature as the *zero problem*, and the several types of zeros and its recommended treatments. In our work we dealt with so-called *count* zeros, i.e. compositional count datasets that contain zero values resulting from insufficiently large samples. We modelled our observations with zero values by a replacement strategy following a *Bayesian-multiplicative* approach (Martín-Fernández *et al.*, 2015). This approach preserves the true total number of counts per row and the ratios between the

observed species. In this way, the distortion of the covariance structure for the observed part of the dataset is minimized. This property, firstly introduced in Martín-Fernández *et al.* (2003), is based on a "readjustment" of the non-zero values in a multiplicative way.

In the Bayesian-multiplicative method we assume that the counts vector **c** of assemblages derives from a multinomial distribution with D categories, i.e., number of different species. Let N be the total count in **c** and let **θ** be the parameter vector of probabilities, where we assume that $\theta_k > 0$. This assumption is crucial because it indicates that the zero values observed in the vector **x**= **c**/N are due the sample size. Note that vector **x** is an estimate of vector **θ**. Using a Bayesian approach, the prior distribution for **θ** is the conjugate distribution of the multinomial: a Dirichlet distribution of parameter vector **α**, where $\alpha_k = st_k$, $k=1,...,$ D. The parameter s is the scalar "strength" of the prior; and vector **t** is the "prior" expectation for **θ**. After one sample is collected, the posterior distribution for **θ** is a Dirichlet distribution of parameter vector **α***, where $\alpha_k{}^* = c_k + st_k$. Here c_k is the observed counts in the category k of vector **c**. Therefore, Bayes theorem gives the posterior estimate for θ_k

For each percentage vector **x** in **X** the replacement of the zeros transforms in a vector **x***=$(x_1^*, ..., x_D^*)$ where

$$x_k^* = \begin{cases} \dfrac{st_k}{N+s} & if\ x_k = 0 \\ x_k\left(1 - \sum_{x_r=0} x_r^*\right) & if\ x_k > 0 \end{cases}. \qquad \hat{q}_k = \frac{c_k + st_k}{N + s}.$$

When one assumes a *prior* non-informative model, the value of t_k is equal to 1/D. s is a parameter that controls for the effect (or weight) that the prior distribution of probability has on the posterior distribution of probability. Note that if $s = 0$, then the posterior is equal to c_k/N and only depends on the observed data in the trial and the prior **t** has no effect on the posterior distribution. Following Palarea-Alabaldejo and Martín-Fernández (2015), in our work we selected the Jeffreys prior (JBZR), where $s = D/2$ and $t_k = 1/D$. Other different priors were checked with no significant differences (Martín-Fernández *et al.*, 2015) because the values of Pearson correlation coefficient between the results provided by different priors were all greater than 0.99.

After the replacement a new dataset **X*** without zeros is available and one could also make the dataset **C*** (pseudo-counts) without zeros if we multiply each row of **X*** by its total count. The ilr-coordinates can be obtained from the new dataset, **X*** or **C***, obtaining the same coordinates dataset **Y**. Because these ilr-coordinates vectors **y** are equivalent to the coordinates of the composition **x*** from a particular orthonormal basis then any typical multivariate technique can be consistently

applied. The unique requirement is that this technique should be invariant under change of orthonormal basis. The CoDa-MAT, based on Aitchison distances, verifies this requirement.

Appendix 2:

Planktonic foraminifera taxonomical groups

19 taxonomical groups dataset

Globigerina bulloides d'Orbigny 1826

Globigerina falconensis Blow, 1959

Globigerinella siphoniphera (d'Orbigny 1839)

Globigerinita glutinata (Egger 1893)

Globigerinoides ruber (d'Orbigny 1839) var. *alba*

Globigerinoides ruber (d'Orbigny 1839) var. *rosea*

Globigerinoides sacculifer (Brady 1877)

Globorotalia hirsuta (d'Orbigny 1839)

Globorotalia inflata (d'Orbigny 1839)

Globorotalia menardi-tumida group

Globorotalia scitula (Brady 1882)

Globorotalia truncatulinoides (d'Orbigny 1839)

Globoturborotalita spp.

Neogloboquadrina dutertrei (d'Orbigny 1839)

Neogloboquadrina pachyderma (Ehremberg 1861) left-coiled

Neogloboquadrina pachyderma (Ehremberg 1861) right-coiled

Orbulina universa d'Orbigny 1839)

Pulleniatina obliquiloculata (Parker & Jones, 1862)

Turborotalita quinqueloba (Natland 1938)

15 taxonomical groups dataset

Globigerina bulloides d'Orbigny 1826

Globigerina falconensis Blow, 1959

Globigerinita glutinata (Egger 1893)

Globigerinoides ruber (d'Orbigny 1839)

Globigerinoides sacculifer (Brady 1877)

Globorotalia hirsuta (d'Orbigny 1839)

Globorotalia inflata (d'Orbigny 1839)

Globorotalia menardi-tumida group

Globorotalia scitula (Brady 1882)

Globorotalia truncatulinoides (d'Orbigny 1839)

Neogloboquadrina dutertrei (d'Orbigny 1839)

Neogloboquadrina pachyderma (Ehremberg 1861) left -coiled

Neogloboquadrina pachyderma (Ehremberg 1861) right-coiled

Turborotalita quinqueloba (Natland 1938)

AWS*: includes *Globigerinella siphoniphera* (d'Orbigny 1839)*; *Globoturborotalita rubescens* (Hofker 1956); *Globoturborotalita tenella* (Parker 1958), *Orbulina universa* d'Orbigny 1839)

Compositional regression-based methods for palaeoenvironmental reconstruction (article)

Compositional regression-based methods for palaeoenvironmental reconstruction

Running title: Palaeoenvironmental CoDa: regression-based methods

Valentino Di Donato[1], Joanna Jamka[1], Josep Antoni Martín-Fernández[2]

Alpine and Mediterranean Quaternary, in press

1. Dipartimento di Scienze della Terra, dell'Ambiente e delle Risorse – Università degli Studi di Napoli "Federico II" – Complesso di Monte Sant'Angelo (Edificio L) Via Cinthia, 21 - 80126, Naples, Italy.
2. Departament d'Informàtica, Matemàtica Aplicada i Estadística, Universitat de Girona – Edifici Politècnica IV, Campus Montilivi, E-17003, Girona, Spain.
Corresponding author: Valentino Di Donato - email address: valedido@unina.it

Abstract

The information in modern or fossil foraminifera assemblages is the relative abundance or percentages of species, i.e., they can be considered as compositional data. In this study we deal with CoDa and regression-based methods as tools to estimate past climatic conditions. We tested standard and robust Partial Least Squares and Principal Component Regression, applied to the log-ratio coordinates of percentage data of Atlantic Ocean and Mediterranean Sea planktonic foraminiferal assemblages. Due to the presence of groups, it was preferred to model separately high latitude and mid to low latitude assemblages. This approach implies the application of cluster analysis, MANOVA and discriminant analysis to the logratio transformed fossil assemblage's compositions. The methods were then applied on marine core assemblages to reconstruct past sea surface temperatures. The obtained results were compared with those formerly obtained by means of compositional modern analogue technique and with the information arising from other paleoclimatic proxies.

1. Introduction

In the last decades, several methods were proposed to obtain quantitative estimates of past environmental parameters from counts of fossils assemblages (Imbrie and Kipp, 1971, Hutson, 1979; ter Braak & Juggins, 1993; Pflaumann *et al.*, 1996; Waelbroeck *et al.*, 1998; Malmgren *et al.*, 2001; among others). Most methods are applied to percentage data obtained from counting of specimens. *The peculiar* properties of relative abundance data represent however a key issue to be taken into account when developing transfer functions based of fossil assemblages. Percentage data belong to compositional data (CoDa) (Aitchison, 1986): that is, the information contained in a vector of counts **x** is the same as in k·**x**, for any real scalar k>0, property known as scale invariance which indicates that a composition is an equivalence class (Barceló-Vidal and Martín-Fernández, 2016). This type of data is very common in Earth Sciences when the constituents and compounds are described in terms their concentration (e.g., Buccianti *et al.*, 2006). In a paper recently published (Di Donato et al., 2018) we revised the modern analogues technique (MAT) (Hutson, 1979; Pflaumann *et al.*, 1996; Waelbroeck *et al.*, 1998) according to the CoDa methodology (Aitchison, 1986). In this study, following the same approach, we deal with regression-based methods, such as Principal Component Regression (PCR) and Partial Least Squares Regression (PLSR). In order to apply PLSR to CoDa, Hinkle and Rayens (1995) proposed logcontrast partial least squares (LCPLS). CoDa refers to vectors of positive components showing the relative weight of a set of parts in a total. Nowadays, there is a general agreement that applying the standard statistical methods to CoDa may yield misleading results (Pawlowsky-Glahn *et al.*, 2015). The log-ratio methodology proposed by Aitchison (1986) and the following developments (i.e. Martín-Fernández and Thió-Henestrosa, 2016a; Martín-

Fernández and Thió-Henestrosa, 2016b) represent a powerful set of methods and techniques to apply to CoDa. The approach adopted in this paper follows the principle of working on coordinates (Mateu-Figueras et al., 2011), that is, the standard statistical analysis is conveniently performed after choosing log-ratio coordinates. In particular, we considered to express each D-vector $\mathbf{x} = (x_1, \ldots, x_D)$ of percentages of species as: 1) a D-dimensional vector $\mathbf{z}=(z_1, \ldots, z_D)$ of centred log-ratio coordinates ($\mathbf{z} =$clr($\mathbf{x}$)) (Aitchison, 1986) and 2) a (D−1)-dimensional real vector $\mathbf{y}=(y_1, \ldots, y_{D-1})$ of isometric log-ratio coordinates ($\mathbf{y} =$ilr($\mathbf{x}$)) (Egozcue *et al.*, 2003) (see Appendix 1 in Di Donato et al. (2018) for definitions and details). To develop our approach, the following points were considered: 1) pre-processing techniques; 2) elaboration of regression-based transfer functions 3) evaluation of the results 4) application to fossil assemblages. As case studies, we considered applications based on the estimation of past sea surface temperatures (SST) from planktonic foraminifera assemblages. The analyses were carried out with Matlab codes, except for raw-data analysis which was computed with R package rioja (Juggins, 2017). MATLAB routines expressly written to perform CoDa-regression and CoDaMAT are provided in the supplementary materials. The Robust Partial Least Squares Regression requires the Rsimpls.m matlab code included in the LIBRA package (Verboven and Hubert, 2004), available at https://github.com/duncombe/matlab/blob/master/LIBRA/rsimpls.m. A workflow of the analysis is shown in Table 1.

2. Approaching the analysis

2.1 The dataset

The dataset on which our applications are computed is represented by a database consisting of 1252 Atlantic and Mediterranean planktonic foraminifera core top assemblages, which represent the regressor variables, determined on the >150 μm size fraction (Prell et al., 1999; Hayes et al., 2004;

Kucera et al., 2004) (Figure 1). In this paper we considered SST as response variables. The oceanographical data, consisting of mean annual and seasonal SST refer to Antonov et al. (2010) and Locarnini et al. (2010). Seasonal temperatures are 3 months averages, i.e. January–March for northern (southern) winter (summer) and July–September for northern (southern) summer (winter). The SST values at core top locations were computed by means of Ocean Data View 4.7.10 (Schlitzer, 2018). Following Kucera et al. (2005), oceanographical data are related to a depth of 10 m.
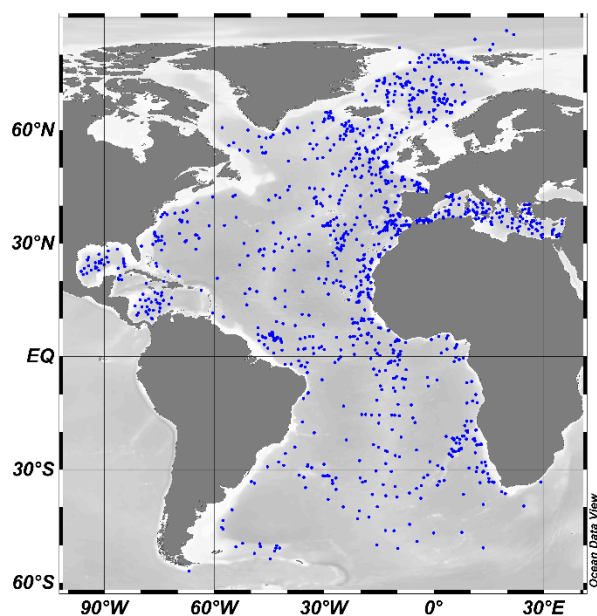
Fig.1 Location of modern planktonic foraminifera coretop samples adopted for application of CoDa-MAT. Drawn with Ocean Data View software (Schlitzer, 2018).

2.2 Data pre-processing: subcomposition, amalgamation and zero replacement

The data pre-processing which is needed to accomplish the analysis is fully explained in Di Donato et al. (2018) and will not be detailed here. In short, our approach requires data to be strictly positive (Aitchison, 1986). To reduce the number of zero values to be replaced, rarer species, which carry inevitably low signal to noise ratios (Kucera et al., 2005) can be excluded from the assemblages, by considering a subcomposition of the original assemblages (Aitchison, 1986). Moreover, an amalgamation of taxa characterised by similar ecological requirements can be also considered (Aitchison, 1986). To manage the zeros occurring in the data, we adopted a mixed Bayesian-multiplicative estimation approach, which is recommended when the compositional data arise from counts (Martín-Fernández et al., 2003; Martín-Fernández et al., 2015) (see also Appendix 1 in Di Donato et al., 2018).

After the zero replacement, the clr- and ilr-coordinates' vectors for the fossil and modern data are obtained. Thus, fossil assemblages are represented by its logratio-coordinates, whereas the modern database is consisting of logratio-coordinates together with the environmental parameters measured at each location. The ilr coordinates can be computed by means of balances (Egozcue et al., 2005). These are logcontrasts obtained by means of a Sequential Binary Partition (SBP) matrix. For each order of the partition, it is possible to define the balance between the two sub-groups formed at that level: if $i_1, i_{2,...}, i_r$ are the r parts of the sub-group coded by +1, and $j_1, j_{2,...}, j_s$ the s parts of the sub-group (coded by -1), a balance is defined as:

$$y = \sqrt{\frac{rs}{r+s}} \ln \frac{(x_{i_1} x_{i_2} ... x_{i_r})^{1/r}}{(x_{j_1} x_{j_2} ... x_{j_r})^{1/s}} \qquad (1)$$

From a D part composition, D-1 balances (ilr-coordinates) can be obtained.

In our case, for the sake of simplicity, we adopted a matrix of the type:

order	x_1	x_2	x_3		x_{D-1}	x_D
1	1	-1	-1	....	-1	-1
2	0	1	-1	....	-1	-1
3	0	0	1	....	-1	-1
....	....	....	....	....	....	....
D-1	0	0	0	....	1	-1

aAs explained in Di Donato et al. (2018), two datasets were generated, consisting of respectively 19 and 15 taxonomical groups (see appendix 2 in Di Donato et al., 2018).

2.3 Multiple regression methods

The PLSR and PCR methods applied to perform the palaeo-estimates are models recommended to predict a response variable when there are a large number of predictor variables highly correlated (Juggins, 2017; ter Braak and Juggins, 1993). Both methods construct new orthogonal, hence not correlated, predictor variables as linear combinations of the original predictor variables. However, while PCR creates components to maximise the observed variability in the predictor variables, without considering the response variable at all, PLSR creates components by maximising the

covariance between predictors and response variables. For PLSR we adopted the SIMPLS algorithm (de Jong, 1993). We also tested a robust PCR (RPCR) and robust PLS (RSIMPLS) (Hubert and Branden, 2003). In order to comply with the CoDa approach, both analyses should be computed on ilr coordinates. It can be noted, however, that clr- and ilr- coordinates, provide the same results for both PCR and PLSR (Filzmoser et al., 2018). Hereafter we denoted with CoDa-PLSR and CoDa-PCR the analysis performed on log-ratio coordinates. The main advantage of clr-coordinates is that they are logcontrast more easily interpretable. However, ilr-coordinates, are advantageous when the analysis requires full rank data, such as discriminant analysis.

In order to evaluate the number of PLS components to be taken into account, we considered, as usual, the percent of variance explained in the response variable and the mean-squared errors (see section 2.4) as a function of the number of components. For CoDa-PCR we considered the percent of total variance of regressor variables.

The Relative variation biplot (RVB) of the planktonic foraminifera assemblages included in the modern dataset is shown in Figure 2. A RVB consists of a standard principal components biplot applied to the clr coordinates of the assemblages. The first two axes accounts for about 63% of total variability (a total of 71% if reached if a third axis is added). The location of the data points in the RVB highlights the well-known broad latitudinal distribution of assemblages. It can be noted that the origin of the RVB corresponds to a low-density area. Moreover, the distribution of data points in the RVB seems to indicate the existence of two groups within the dataset, the first of which is represented by high latitude assemblages. Principal Components Analysis (PCA) is properly defined for homogeneous, normally-distributed data from a single population (Tolosana-Delgado and Mc Kinley, 2016). Separate regional models were considered, among others, in Prell (1995), Ortiz and Miz (1997) and Kucera et al. (2005). For our purposes, a cluster analysis (Ward's method on ilr-coordinates) was applied to the dataset, discarding then some observations that did not belong to either of the two main defined groups. A MANOVA test indicates that the two groups are significantly distinct (with $p\sim0$). Since at high latitude only few planktonic foraminifera species occur, the regression models for the high latitude group was built by considering a sub-composition of the dataset made of only 5 species. The application of this two-step procedure to fossil assemblages requires to first perform a linear discriminant analysis (LDA) in order to classify them into one of the 2 defined groups. Apart from theoretical considerations, the application of LDA to percentage data faces problems related to the singularity of the within groups variance/covariance

matrix. This problem also occurs with clr-coordinates, while ilr-coordinates are not affected by this problem. The LDA misclassification rate provided a leave-one-out cross validation method for the two groups defined in the modern dataset is 0.0085.
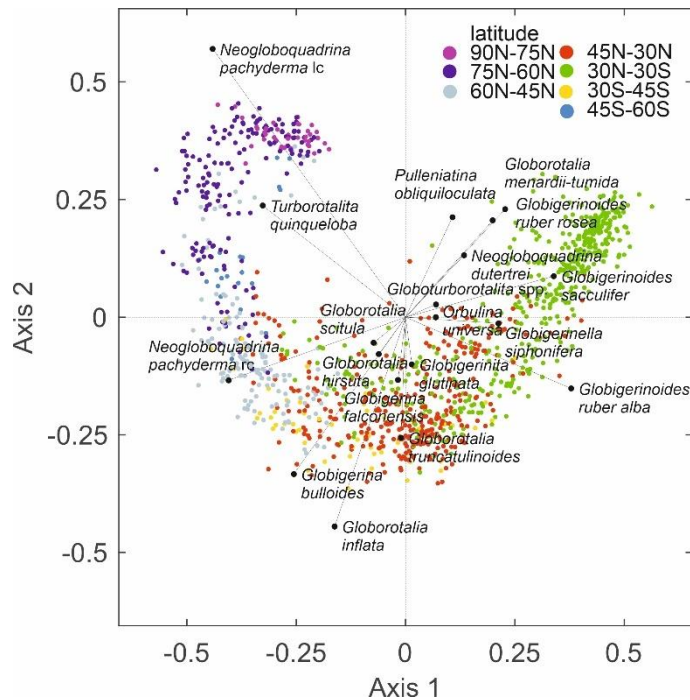
Figure. 2 Relative variation biplot (RVB) of planktonic foraminiferal assemblages included in the modern dataset. Row points are grouped according to their latitude.

2.4 Evaluation of the quality of the estimates

The evaluation of the quality of the estimated results provided by CoDa-PCR and CoDa-PLSR techniques has been carried out by means of sensitivity analysis of leave-one-out cross validation method (ter Braak and Juggins, 1993; Barrows and Juggins, 2005). The indices we took into account were: the Coefficient of determination R2 and the Mean Square Error of Prediction (MSEP) (with its square root, the RMSEP) (Wallach and Goffmet, 1989; Birks, 1995) and as multivariate counterpart, the root of mean squared distances (RMSD) (e.g., Martín-Fernández et al., 2003).

The MSD is a multivariate index of quality of the estimates of k environmental parameters defined as:

where n is the number of modern samples, P represents the vector of k measured environmental parameters, and P^ the corresponding vector of estimated values. This approach is equivalent to analyse the mean of the norm of the residual rows (difference between measured and estimated parameters). The best result of RMSD is obtained when RMSD=0, i.e, all the estimates are equal to the measured values. The multivariate approach may be applied when different paleoclimatic parameters are estimated (i.e. temperature, seasonal or annual precipitation, potential evapo-transpiration, as done in pollen analysis). For the evaluation of the results obtained from grouped assemblages, we considered both a "pooled" R2, i.e. for 2 groups, R2=(SSR gr1+SSR gr2)/(SST gr1+SST gr2), together with the squared correlation coefficient r2 obtained by comparing the overall (both groups) measured and fitted SST values. Squared correlation coefficients are reported in the supplementary table.

2.5 Application on fossil assemblages

Probably the most important difficulty of any proxy-based reconstruction is represented by the no-analogue problem, occurring when the paleoenvironmental conditions represented in the fossil assemblages do not have a correspondence in modern environments (Hutson, 1977). It can be considered that the application of regression methods to no-analogue samples, may be regarded as extrapolation rather than interpolation (Conn et al., 2015). In Di Donato et al. (2018), we adopted atypicality index (e.g., Aitchison, 1986), both standard and robust, and Local Outlier Factor (LOF) (Breunig et al., 2000) of assemblages as tools to detect no-analogue conditions. Details on the computation of atypicality index and robust methods to outlier detection (Peña and Prieto, 2001) for CoDa sets (Filzmoser and Hron, 2008) are reported in Di Donato et al., 2018.

3 Testing the method

3.1 Results

The number of components from which compute the PLS was determined by considering the percent variance explained for the response variables and the MSE of response variable as functions of the number of PLS components (Figure 3) and, for CoDa-PCR, the amount of total variance of regressor variables accounted by the principal components (Figure 4). For both the tested datasets, 4 components seem to provide an adequate CoDa-PLSR model. For CoDa-PCR, we adopted a 6

components model. As regards the two-groups approach, the subcomposition obtained for high latitude assemblages is made of only 6 parts. In the other group, for both CoDa-PLSR and CoDa-PCR, we considered a full-components model.

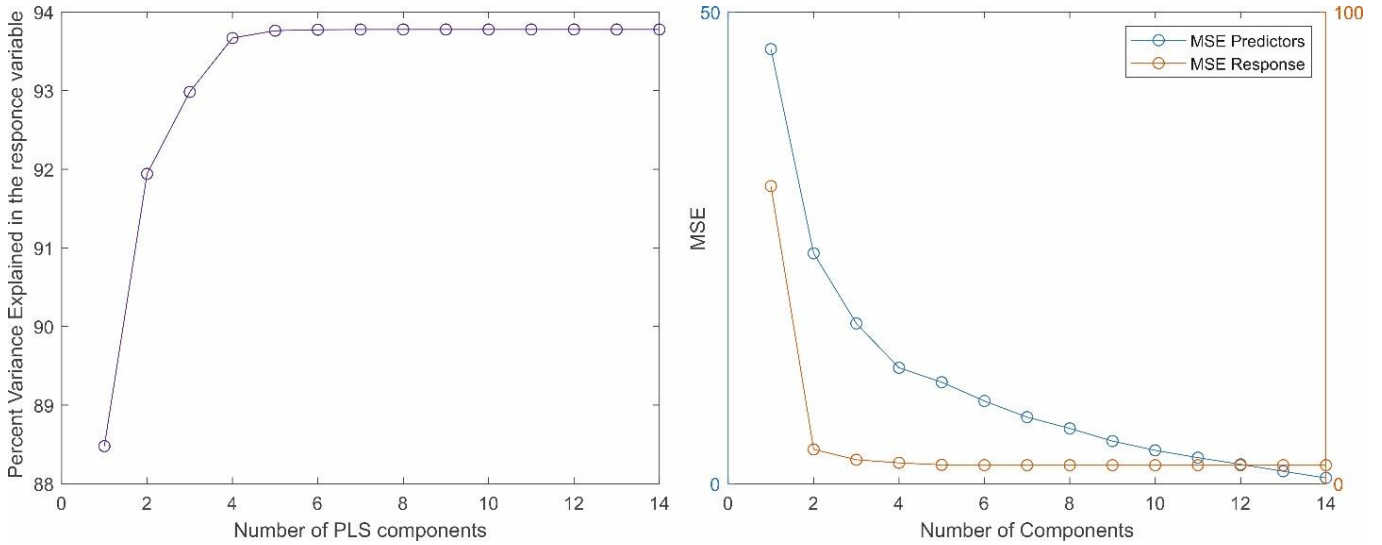**Figure.3** The figure shows for the 15 taxonomic groups dataset plots (from which 14 predictors represented by ilr-variables are obtained) of a) the percent variance explained for a single response variable (annual SST) and b) the MSE of response variable as functions of the number of PLS components.
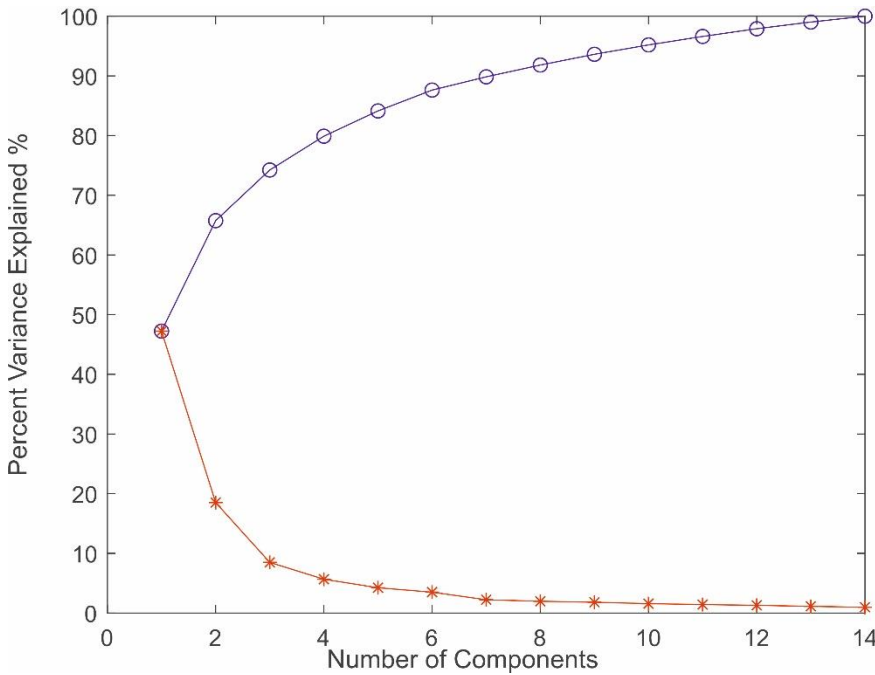
Figure.4 Plot of cumulative percentage accounted (blue line) and variance contribution of each component (red line) in CoDa-PCR.

We tested both annual SST and seasonal SST. Table 1 in supplementary materials summarises the relationships between measured seasonal SST and its estimates obtained with PCR and PLSR, under different conditions. In general, the 15 taxa and 19 taxa datasets provided quite similar results. It can be noted, that, for both CoDa-PCR and CoDa-PLSR, higher squared correlation coefficients and lower RMSEP are obtained with a two-groups analysis. The highest r^2 of 0.9718, with a RMSE of 1.33°C was obtained for mean annual SST with CoDa-PLSR (see supplementary table). Figure 5 shows the relationship between measured and cross-validation-estimated SST for a 1 group and for 2-groups analysis. It can be noted that, the 1-group model, a "plateau" for low SST, which can be also observed, in the Imbrie and Kipp (1971) method and CoDa-MAT validation, and which becomes much less pronounced, with a 2-groups modelling.

For a single group analysis, PLSR performs better than PCR. However, for a 2 groups analysis, PLSR and PCR provided quite similar results. Robust version of CoDa-PLSR and CoDa-PCR did not improve the fitting with respect to standard CoDa-PLSR and CoDa-PCR. In comparison with the CoDa-MAT method, CoDa-PLSR and CoDa-PCR provides slightly lower R^2 and higher RMSEP. A slightly better performance of MAT with respect to a regression method (i.e. the Imbrie and Kipp transfer function) was also found by Ortiz and Mix (1997) by working on raw percentage data. As far as the comparison with raw data regression-based methods, on our dataset, the Imbrie and Kipp (1971) Q-mode regression method yields, with 5 components an $R^2=0.8956$ and an RMSE=2.47°C. The Weighted Averaged Partial Least Squares Method (WAPLS) (ter Braak & Juggins, 1993) yields an $R^2=0.9544$ and an RMSE=1.70°C.
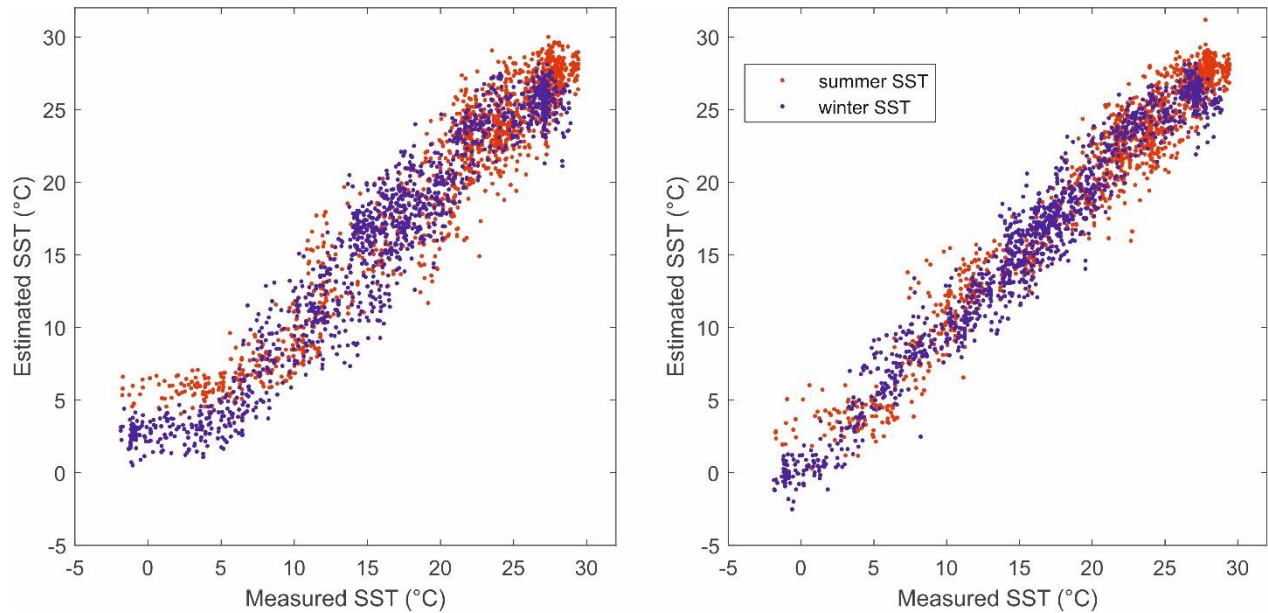
Figure 5. Plots of observed versus estimated SST (annual and seasonal) obtained with a 1-group (left) and a 2-groups CoDa-PLSR modelling.

3.2 Application examples

As an application example, the CoDa-MAT method was applied to planktonic foraminifera records which were also considered to evaluate the performing of CoDa-MAT. The first one is a literature dataset, consisting of the record of planktonic foraminifera assemblages of the core MD95-2040 (de Abreu et al., 2003; Voelker and de Abreu, 2011), recovered in the Atlantic Ocean off the Iberian margin, the second is that of GNS84-C106 core recovered in the Tyrrhenian sea (Buccheri et al, 2002; Di Donato et al., 2008; 2009). For the Mediterranean Sea, we also considered the planktonic foraminiferal record of the Core TEA-C6 (Di Donato et al., 2019), from which an estimate of past SST for the last 15 ka, was obtained with the CoDa-MAT method. All datasets are obtained from >150 μm size fractions. The location of the cores is shown in Figure 6.

A discussion of the possible drawback represented by the excessive loss of small sized species in the >150 μm size fraction can be found in Di Donato et al. (2015). It can be noted that >150 micron and >106 μm datasets, if analysed with CoDa methods, provide the same covariance structure. This suggests that regression-based methods based on CoDa, may be quite robust with respect to treatment changes such as the analysed size fraction.

3.2.1 Atlantic Ocean

The foraminiferal record of MD95-2040 core covers the last 210 ka (de Abreu *et al.*, 2003; Voelker, and de Abreu, 2011). SST for this interval were formerly reconstructed (de Abreu *et al.*, 2003) from planktonic foraminifera with SIMMAX28 method (Pflaumann *et al.*, 1996). The dataset consists of 732 assemblages. As regards the atypicality of assemblages, in relation to the 99.5 percentile only 4% of the samples have Mahalanobis distances are above the xi-square critical value of 31.32 (see Figure 6 in Di Donato et al., 2018). As for the LOF it can be noted that glacial assemblages are characterised by higher values of up to 2, while most interglacial assemblages have LOF values not exceeding 1.5. On the basis of LDA computed on ilr-coordinates, 98 assemblages were classified into the high latitude assemblage group, and 634 assemblages into the low to middle latitude assemblage group. The output of the LDA with the indication of the group to which each assemblage was assigned with the posterior probabilities is provided in the supplementary materials.
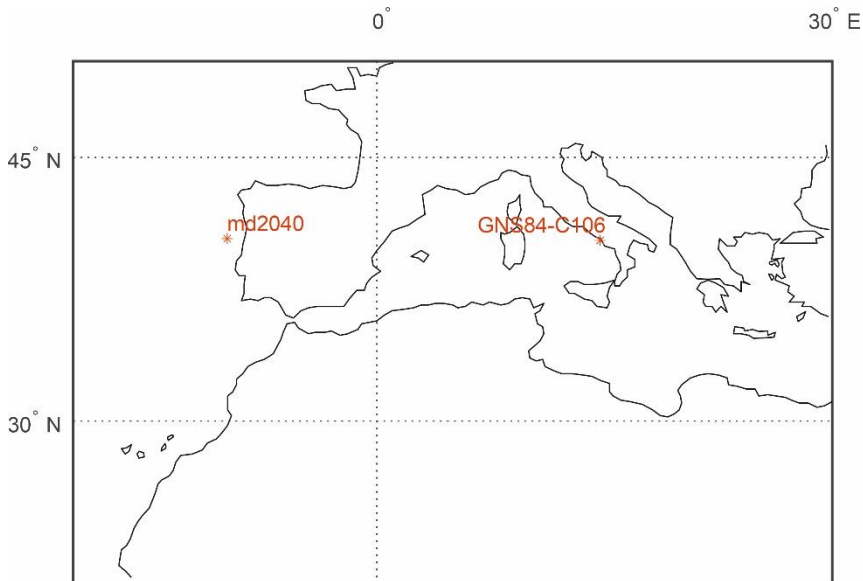
Figure.6 Location of cores considered in this paper.

A comparison between the values reconstructed for summer and winter SST by means of SIMMAX28 (de Abreu *et al.*, 2003), CoDa-MAT, CoDa-PLSR and CoDa-PCR is shown in Figure 7. The stronger coherence of CoDa-MAT reconstruction with Alkenones and the stable isotope record with respect to SIMMAX28 has been already highlighted in Di Donato et al. (2018). Here

we note that CoDa-PLSR and CoDa-PCR reconstruction are largely overlapping and show a same general trend if compared with CoDa-MAT. Several SST minima, which correspond to Heinrich events, are also recorded by CoDa-PLSR and CoDa-PCR with slightly less-deep minima in comparison with CoDa-MAT but more marked in comparison with alkenones record. CoDa-MAT and Regression-based methods also provide different SST reconstructions for the MIS5: the former provides higher SST estimates, while the latter highlight a decreasing trend during the MIS5 which does not appear in the CoDa-MAT reconstruction. The SST reconstructed with the 15 taxa and the 19 taxa datasets, are quite similar, being characterised by a r=0.9865 (r= 0.9868) and by a root mean squared difference of 0.70°C (0.48°C) for summer (winter) SST. The multivariate RMSD between 15 taxa and the 19 taxa reconstructed SST is 0.7177.
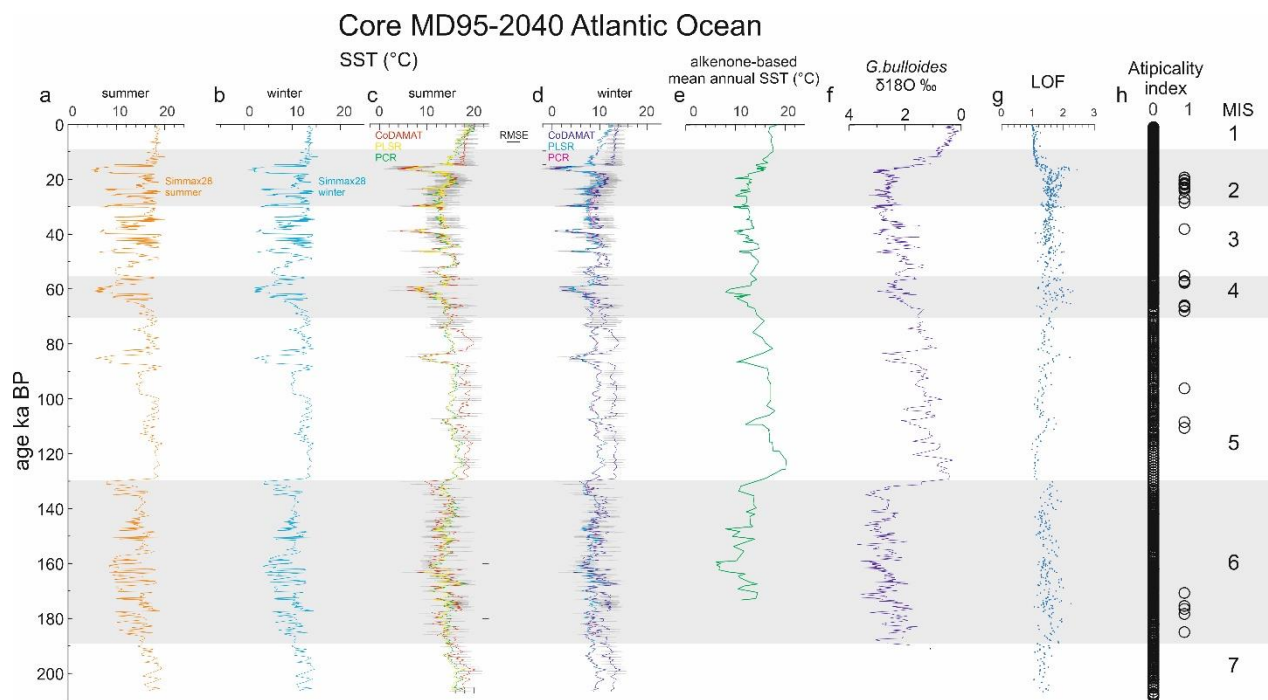
Figure.7 Reconstruction of seasonal SST for the last 210 ka off the Iberian margin from core MD95-2040 and comparison between SIMMAX28 (de Abreu et al., 2003, Voelker and de Abreu, 2011), CoDa-MAT, CoDa-PLSR and CoDa-PCR reconstructed SSTs. a) summer and b) winter SIMMAX28 reconstruction. c) summer and d) winter SST CoDa-based reconstructions. Grey lines indicate the standard deviation of CoDa-MAT estimates e) Alkenone based SST reconstruction (Pailler and Bard, 2002). f) *Globigerina bulloides* stable isotope record and Marine Isotopic Stages (MIS) (Abreu et al., 2003; Schönfeld et al., 2003): grey-shaded dots: distance of fossil assemblages from each of the 6 closest modern analogues. Full line: mean values. g) LOF values (see Di Donato et al., 2018) h) atipicality index: 0: not significant; 1: significant.

3.2.2 Mediterranean Sea

The Core GNS84-C106 recovered in the Gulf of Salerno (Tyrrhenian sea - Western Mediterranean) covers the last 34 ka (Di Donato et al., 2009). This dataset is represented by 228 planktonic foraminiferal assemblages determined on the >150-micron size fraction. The quantitative reconstructions of past climatic conditions for the Mediterranean basin face several problems related to the peculiar hydrological asset of this semi-enclosed basin. Reconstructions became even more problematic for glacial intervals (Sbaffi et al., 2001, among others). As regards the LDA, the whole Core GNS84-C106 dataset was classified into the low to middle latitude group (see supplementary material). However, as shown in Figure 8, a significant atypicality index was found for several planktonic foraminiferal assemblages of the Core GNS84-C106. As in the previous case study, CoDa-PLSR and CoDa-PCR provide quite similar results. For this Core, however, within the same general trend, regression-based methods and CoDa-MAT provide quite different results. In this case study, raw percentage data MAT and, to a lesser degree, CoDa-MAT provided summer SST which seem quite high for the GI-1 interval and for time intervals of the Last Glacial Period (LGP) centred around 24 and 20 ka BP. This problem is likely partly related to the adopted size fraction (Di Donato et al., 2015). Regression based methods seem to provide a more coherent SST trend, i.e. LGP lower than Holocene, and intermediate SST values during the Late Glacial. However, it can be noted that CoDa-PLSR and CoDa-PCR provide higher SST estimates for the colder intervals of the glacial period. As an example, between 15 and 17 ka BP, CoDa-MAT reconstruct winter SST of even 8.5 °C, while CoDa-PLSR and CoDa-PCR indicate lower values of about 10°C. For this core, we do not have, at present alternative proxy-based reconstructions. However, the regression based reconstructed SSTs seem more coherent with alkenone-based reconstructions obtained for the Southern Tyrrhenian Sea (Sbaffi et al, 2001), which provided higher SST values if compared with the MAT reconstructions. During the Holocene, CoDa-MAT, CoDa-PLSR and CoDa-PCR indicate an SST rise around 5 ka BP. However, CoDa-PLSR and CoDa-PCR indicate warmer than present SST for an interval centred around 4 to 3 ka BP, which coincides with a peak in the warm species Globigerinoides sacculifer widely recognized in the Mediterranean Sea (Capotondi et al., 1999; among others) and a decreasing trend afterwards. This trend is quite similar to the alkenones record of the Core BS79-38 recovered in the Southern Tyrrhenian Sea (Sbaffi et al, 2001). However, alkenones provided higher than present SST values for the early to middle Holocene which are not confirmed by planktonic foraminifera.

4. Conclusive remarks

Following out previous paper focused on CoDa and modern analogue technique, in this article we developed a transfer function based on multivariate regression methods in a fashion coherent with a CoDa approach. The main advantages of CoDa-MAT, being a non-parametric method (Guiot and De Vernal, 2011a-b), is its flexibility and the fact that the quality of each single reconstruction can be evaluated by means local outlier factor and mean distances. By contrast, once the model has been built, we must accept the reconstructed SST "as they are". Likely, CoDa-PLSR might be more sensitive than CoDa-MAT to random effects, since limited random effects should not strongly influence the choice of the best modern analogs for a fossil assemblage. However, CoDa-PLSR and CoDa-PCR, may be more robust with respect to treatment changes such as the size fraction adopted for the analysis, which represent a critical point in the analysis of foraminifera assemblages. Whatever the approach, it is important to evaluate the atypicality of the fossil assemblages in comparison with modern ones. In this article we provided application examples for an Atlantic Ocean and a Mediterranean Sea core. CoDa-MAT and regression-based methods seem to provide quite coherent reconstructions for the Atlantic Ocean, while for the Mediterranean Sea, the obtained reconstructions are, as expected, more problematic. Together with CoDa-MAT, CoDa-PLSR and CoDa-PCR provide the basis for more extensive reconstructions which will be the focus of future investigations.
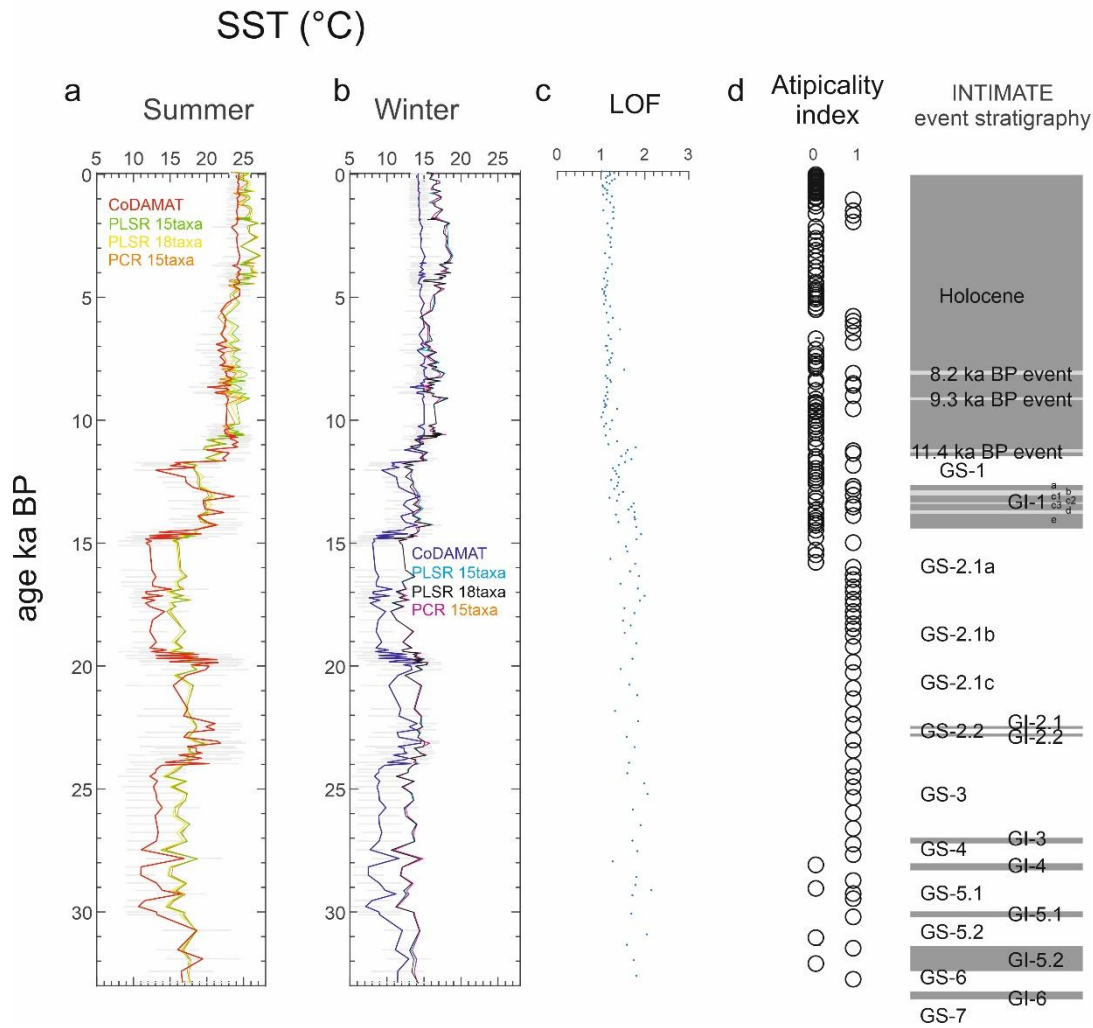
Figure.8 Reconstruction of seasonal SST obtained from GNS84-C106 Core. a) summer b) winter. The grey error bars indicate the standard deviation of each reconstructed value. c) LOF values e) atypicality index: 0: not significant; 1: significant. The INTIMATE Greenland event stratigraphy is reported from Rasmussen et al. (2014).

Acknowledgements

References

Aitchison, J. (1986) - *The Statistical Analysis of Compositional Data. Monographs on Statistics and Applied Probability*. Chapman and Hall Ltd. (Reprinted 2003 with additional material by The Blackburn Press), London (UK). 416 p.

Antonov, J. I., Seidov D., Boyer, T. P., Locarnini R. A., Mishonov A. V., and Garcia H. E. (2010) - *World Ocean Atlas 2009 Volume 2: Salinity.* S. Levitus, Ed., NOAA Atlas NESDIS 69, U.S. Government Printing Office, Washington, D.C., 184 pp.

Barceló-Vidal, C. and Martín-Fernández, J.A. (2016). The mathematics of compositional analysis. Austrian Journal of Statistics, 45(4):57–71.

Barrows, T.T, Juggins, S. (2005) - *Sea-surface temperatures around the Australian margin and Indian Ocean during the last glacial maximum.* Quaternary Science Reviews, 24, 1017–1047.

Birks, H.J.B. (1995). *Quantitative palaeoenvironmental reconstructions*. In: Maddy, D., Brew, J.S. (Eds.), Statistical Modelling of Quaternary Science Data. Technical Guide 5. Quaternary Research Association, Cambridge, pp. 116–254.

Breunig M.M., Kriegel H.-P., Ng R.T., Sander J. (2000) - *LOF: identifying density-based local outliers*. In Proceedings of the 2000 ACM SIGMOD international conference on Management of data (SIGMOD '00). ACM, New York, NY, USA, 93-104. DOI=http://dx.doi.org/10.1145/342009.335388

Buccheri, G., Capretto, G., Di Donato, V., Esposito, P., Ferruzza, G., Pescatore, T., Russo Ermolli, E., Senatore, M.R., Sprovieri, M., Bertoldo, M., Carella, D., and Madonna, G. (2002) - *A high resolution record of the last deglaciation in the southern Tyrrhenian Sea: environmental and climatic evolution.* Marine Geology 186, 447-470.

Buccianti, A., Mateu-Figueras, G., Pawlowsky-Glahn, V. (Eds.) (2006) - *Compositional Data Analysis in the Geosciences: From Theory to Practice*. In: Special Publications, vol. 264. Geological Society, London.

Capotondi, L., Borsetti, A.M., Morigi, C. (1999). *Foraminiferal ecozones, a high resolution proxy for the late quaternary biochronology in the central Mediterranean Sea*. Marine Geology, 153, 253-274.

Conn, P.B., Johnson, D.S., Boveng, P.L. (2015) - *On Extrapolating Past the Range of Observed Data When Making Statistical Predictions in Ecology*. PLoS ONE 10(10): e0141416. doi:10.1371/journal.pone.0141416

de Abreu, L., Shackleton, N.J., Schonfeld, J., Hall M., and Chapman, M. (2003) - *Millennial-scale oceanic climate variability off the Western Iberian margin during the last two glacial periods*. Marine Geology, 196 (1-2), 1-20.

de Jong S. (1993) - *SIMPLS: an alternative approach to partial least squares regression*. Chemometrics Intell. Lab. Syst., 18, 251–263.

Di Donato, V., Esposito, P., Russo Ermolli, E., Scarano, A., and Cheddadi, R. (2008) - *Coupled atmospheric and marine palaeoclimatic reconstruction for the last 35 ka in the Sele Plain-Gulf of Salerno area (southern Italy)*. Quaternary International, 190, 146-157.

Di Donato, V., Esposito, P., Garilli, V., Naimo, D., Buccheri, G., Caffau, M., Ciampo, G., Greco, A., and Stanzione, D. (2009) - *Surface-bottom relationships in the Gulf of Salerno (Tyrrhenian Sea) over the last 34 kyr: Compositional data analysis of palaeontological proxies and geochemical evidence*. Geobios, 42, 561-579.

Di Donato, V., Martin-Fernandez, J.A., Daunis-i-Estadella, J. & Esposito, P. (2015) - *Size fraction effects on planktonic foraminifera assemblages: a compositional contribution to the golden sieve rush*. Mathematical Geosciences, 47 (4), 455-470.

Di Donato V., Martín-Fernández J.A., Comas-Cufí M., Jamka J. (2018) – *Palaeoenvironmental reconstructions through Compositional Data analysis*. Alpine and Mediterranean Quaternary, 31 (1), 59-73.

Di Donato, V., Insinga, D.D., Iorio, M., Molisso, F., Rumolo, P., Cardines, C. Passaro, S. (2019) - *The palaeoclimatic and palaeoceanographic history of the Gulf of Taranto (Mediterranean Sea) in the last 15 ky.* Global and Planetary Change. 10.1016/j.gloplacha.2018.10.014

Egozcue, J.J., Pawlowsky-Glahn, V., Mateu-Figueraz, G., Barceló-Vidal, C. (2003) - *Isometric logratio transformations for compositional data analysis.* Mathematical Geology 35 (3), 279-300.

Egozcue, J. J. and V. Pawlowsky-Glahn (2005). *Groups of parts and their balances in compositional data analysis*. Mathematical Geology 37 (7), 795-828.

Filzmoser, P., Hron, K., Templ, M. (2018) - Applied Compositional Data Analysis. Springer. https://doi.org/10.1007/978-3-319-96422-5

Filzmoser, P., and Hron, K. (2008) - *Outlier detection for compositional data using robust methods.* Math. Geosciences, 40, 233-248.

Guiot, J., and de Vernal, A. (2011a) - *Is spatial autocorrelation introducing biases in the apparent accuracy of paleoclimatic reconstructions?* Quaternary Science Reviews 30, 1965-1972.

Guiot, J., and de Vernal, A. (2011b), *QSR Correspondence "Is spatial autocorrelation introducing biases in the apparent accuracy of palaeoclimatic reconstructions?" Reply to Telford and Birks.* Quaternary Science Reviews 30, 3214–3216.

Hayes, A., Kucera, M., Kallel, N., Sbaffi, L., and Rohling, E. (2004) - *Compilation of planktic foraminifera modern data from the Mediterranean Sea*. Pangaea, doi:10.1594/PANGAEA.227305.

Hinkle, J., Rayens, W. (1995) - *Partial least squares and compositional data: problems and Alternatives*. Chemometrics and Intelligent Laboratory Systems 30 (199.5) 159-172

Hubert, M. and Branden, K. V. (2003), *Robust methods for partial least squares regression*. J. Chemometrics, 17: 537-549. doi:10.1002/cem.822

Hutson, W. H. (1977) - *Transfer functions under no-analog conditions: Experiments with Indian Ocean planktonic foraminifera*, Quaternary Research, 8, 355-367.

Hutson, W.H. (1979) - *The Agulhas Current during the Late Pleistocene: Analysis of modern faunal analogues.* Science, 207 (1), 64-66.

Juggins, S. (2017) *rioja: Analysis of Quaternary Science Data*, R package version (0.9-21). (http://cran.r-project.org/package=rioja)

Imbrie, J. and Kipp, N.G. (1971) - *A new micropaleontological method for paleoclimatology: Application to a Late Pleistocene Caribbean core.* The Late Cenozoic Glacial Ages. New Haven, Yale University Press. 71-181.

Kucera, M., Weinelt, M., Kiefer, T., Pflaumann, U., Hayes, A., Weinelt, M., Chen, M.-T., Mix, A.C., Barrows, T., Cortijo, E., Duprat, J., Juggins, S., and Waelbroeck, C. (2004) - *Compilation of planktic foraminifera census data, modern from the Atlantic Ocean.* Pangaea, doi:10.1594/PANGAEA.227322.

Kucera, M., Weinelt, Mara, Kiefer, T., Pflaumann, U., Hayes, A., Weinelt, Martin, Chen, M.-T., Mix, A.C., Barrows, T.T., Cortijo, E., Duprat, J., Juggins, S., Waelbroeck, C., 2005. *Reconstruction of the glacial Atlantic and Pacific sea-surface temperatures from assemblages of planktonic foraminifera: multi-technique approach based on geographically constrained calibration datasets*. Quaternary Science Reviews, Quaternary Science Reviews, 24, 951–998.

Locarnini, R. A., Mishonov, A. V., Antonov, J. I.,Boyer, T. P., and Garcia, H. E. (2010) - *World Ocean Atlas 2009, Volume 1: Temperature*. S. Levitus, Ed., NOAA Atlas NESDIS 68, U.S. Government Printing Office, Washington, D.C., 184 pp.

Malmgren, B. A., Kucera, M., Nyberg, J. and Waelbroeck, C. (2001) - *Comparison of statistical and artificial neural network techniques for estimating past sea surface temperatures from planktonic foraminifer census data*. Paleoceanography, 16 (5), 520–530, doi:10.1029/2000PA000562.

Martín-Fernández, J. A., Barceló-Vidal, C. and Pawlowsky-Glahn, V. (2003) - *Dealing with zeros and missing values in compositional datasets using nonparametric imputation.* Mathematical Geology, 35 (3), 253-278.

Martín-Fernández, J.A., Hron, K., Templ, M., Filzmoser, P., Palarea-Albaladejo J. (2015) - *Bayesian-multiplicative treatment of count zeros in compositional datasets.* Statistical Modelling, 15(2), 134-158

Martín-Fernández, J.A. and Thió-Henestrosa, S. (eds.) (2016a) - *Compositional Data Analysis: CoDaWork, L'Escala, Spain, June 2015.* Springer Proceedings in Mathematics & Statistics, 187. Springer International Publishing, New York (USA).

Martín-Fernández, J.A. and Thió-Henestrosa, S. (Guest eds.) (2016b) - *Compositional Data Analysis.* Austrian Journal of Statistics, 45(4)

Mateu-Figueras G., Pawlowsky-Glahn V., Egozcue, J.J. (2011) - (Pawlowsky-Glahn V, Buccianti A, eds). John Wiley & *The Principle of Working on Coordinates, in Compositional Data Analysis: Theory and Applications* Sons, Ltd, Chichester, UK: 29–42

Ortiz, J.D., Mix, A.C. (1997). *Comparison of Imbrie-Kipp transfer function and modern analog temperature estimates using sediment trap and core top foraminiferal faunas*. Paleoceanography, 12 (2), 175-190.

Pawlowsky-Glahn V, Egozcue J.J., Tolosana-Delgado R. (2015) - *Modeling and analysis of compositional data.* John Wiley & Sons, Chichester, 378 pp

Peña, D. and Prieto, F. (2001) - *Multivariate outlier detection and robust covariance matrix estimation.* Technometrics, 43 (3), 286-310.

Pflaumann, U., Duprat, J., Pujol, C. and Labeyrie, L.D. (1996) - *SIMMAX: a modern analogue technique to deduce Atlantic sea surface temperatures from planktonic foraminifer in deep-sea sediments,* Paleoceanography, 11, 15–36.

Prell, W.L, (1985) - *The stability of low-latitude sea-surface temperatures: An evaluation of the CLIMAP reconstruction with emphasis on the positive SST anomalies*, Rep. TR025, 60 P., U.S. Dep. of Energy, Washington DC.

Prell, W., Martin, A., Cullen, J., and Trend, M., (1999) - *The Brown University Foraminiferal Data Base*. IGBP PAGES/World Data Center-A for Paleoclimatology Data Contribution Series # 1999–027. NOAA/NGDC Paleoclimatology Program, Boulder, CO, USA.

Rasmussen S.O., Bigler M., Blockley S.P., Blunier T., Buchardt S.L., Clausen H.B., Cvijanovic I., Dahl-Jensen D., Johnsen S.J., Fischer H., Gkinis V., Guillevic M., Hoek W.Z., Lowe J.J., Pedro J.B., Popp T., Seierstad I.K., Peder Steffensen J., Svensson A.M., Vallelonga P., Vinther B.M., Walker M.J.C., Wheatley J.J., Winstrup M. (2014) - *A stratigraphic framework for abrupt climatic changes during the Last Glacial period based on three synchronized Greenland ice-core records: refining and extending the INTIMATE event stratigraphy.* Quaternary Science Reviews, 106, 14-28.

Sbaffi, L., Wezel, F.C., Kallel, N., Paterne. M., Cacho,I., Ziveri, P., Shackleton, N. (2001) - *Response of the pelagic environment to palaeoclimatic changes in the central Mediterranean Sea during the Late Quaternary*, Marine Geology, 178 (1–4), 39-62.

Schlitzer, R. (2018) - *Ocean Data View*, http://odv.awi.de.

Schönfeld, J., Zahn., R., and de Abreu., L. (2003) - *Stable isotope ratios and foraminiferal abundance of sediment cores from the Western Iberian Margin*. doi:10.1594/PANGAEA.733303, supplement to: **Schönfeld, J.; Zahn, R.; de Abreu, L. (2003):** Surface to deep water response to rapid climate changes at the western Iberian Margin. *Global and Planetary Change, 36(4),* 237-264, doi:10.1016/S0921-8181(02)00197-2.

ter Braak, C.l.F. Juggins, S. (1993) - *Weighted averaging partial least squares regression (WA-PLS): an improved method for reconstructing environmental variables from species assemblages.* Hydrobiologia. 2691270,485-502.

Tolosana-Delgado, R. and J. McKinley (2016). *Exploring the joint compositional variability of major components and trace elements in the Tellus soil geochemistry survey (Northern Ireland)*. Applied Geochemistry. DOI: 10.1016/j.apgeochem.2016.05.004

Verboven, S., Hubert, M. 2004. *LIBRA: a MATLAB library for robust analysis.* https://github.com/duncombe/matlab/blob/master/LIBRA/rsimpls.m

Voelker, A.H.L., de Abreu, L. (2011) - *A Review of Abrupt Climate Change Events in the Northeastern Atlantic Ocean (Iberian Margin): Latitudinal, Longitudinal and Vertical Gradients.* In: Rashid, H; Polyak, L; Mosley-Thompson, E (eds), Abrupt Climate Change: Mechanisms, Patterns, and Impacts. Geophysical Monograph Series (AGU, Washington D.C.), 193, 15-37, doi:10.1029/2010GM001021.

Waelbroeck, C., Labeyrie, L., Duplessy, J.-C., Guiot, J. and Labracherie, M. (1998) - *Improving past sea surface temperature estimates based on planktonic fossil faunas.* Paleoceanography, 13, 272–283.

Wallach, D., Goffmet, B. (1989) - *Mean squared error of prediction as a criterion for evaluating and comparing system models.* Ecological Modelling, 44,299-306.

Supplementary materials

		Matlab codes
	Part 1: modelling of modern assemblages	
step 1	Variable selection and (eventually) amalgamation	*Raggruppa*
step 2	Zero replacement (on both modern and fossil assemblages)	*zerorep* (for proportion data); *zeroconteggi* (for count data)
step 3	clr- or ilr- transformation (of both modern and fossil assemblages)	*clr* *ilrprogr* *balances*
	Single group analysis	Multigroup analysis	
step 4	Go to step 6	Classification of modern assemblages, evaluation of groups	*pdist* – linkage* - manova1**
step 5		Extraction of subcompositions (if needed)	
step 6	Partial Least Squares Regression or Principal Components Regression modelling of modern assemblages (single or multigroup)	codatransfer
	Part 2: application to fossil assemblages	
step 7	Detection of no-analog assemblages (atypicality index and local outlier factor, as done in CodaMat)	*mat, LOF***
step 8	Go to step 9	Discriminant analysis of fossil assemblages with modern as training groups (on ilr coordinates)	*classify** (called by codatransfer)
step 9	Application of the model to fossil assemblages	*codatransfer*

*MATLAB toolbox functions   **available at http://dsmi-lab-ntust.github.io/AnomalyDetectionToolbox/

Table 1. Workflow of the analysis

method	R² (squared r-coefficient)	RMSE (°C)	RMSD (°C)
CoDa-PLSR			
15 taxa 2 groups annual	0.9351 (0.9718)	1.3349	
15 taxa 2 groups robust annual	0.9060 (0.9591)	1.7571	
15 taxa 2 groups summer	0.8796 (0.9533)	1.6567	2.3007
15 taxa 2 groups winter	0.9206 (0.9609)	1.5964	
19 taxa 2 groups annual	0.9315 (0.9702)	1.3716	
19 taxa 2 groups summer	0.8741 (0.9512)	1.6945	2.3414
19 taxa 2 groups winter	0.9186 (0.9599)	1.6158	
15 taxa annual	0.9367	1.9985	
15 taxa summer	0.917	2.2054	3.1871
15 taxa winter	0.9188	2.3008	
19 taxa annual	0.9326	2.0625	
CoDa-PCR			
15 taxa 2 groups annual	0.9276 (0.9686)	1.5651	
15 taxa 2 groups summer	0.8678 (0.9487)	1.7364	2.3927
15 taxa 2 groups winter	0.8781 (0.9645)	1.6462	
15 taxa 2 groups robust	0.9262 (0.9685)	1.4103	
15 taxa annual	0.9210	2.2323	
15 taxa summer	0.8933	2.5071	3.4350
15 taxa winter	0.9149	2.3621	
Coda-MAT			
CoDa-MAT annual	0.9857	0.9484	

Supplementary table - Cross-validation results for ilr/clr-PLSR ilr/clr-PCR, obtained under different conditions.

References

Abu-Zied R. H., Rohling E.J., Jorissen F. J., Fontanier C., Casford J.S.L., Cooke S., 2008. Benthic foraminiferal response to changes in bottom-water oxygenation and organic carbon flux in the eastern Mediterranean during LGM to Recent times, Marine Micropaleontology, Volume 67, Issues 1–2, Pages 46-68, ISSN 0377-8398.

Acocella, V. and Funiciello, R. (2006). Transverse systems along the extensional Tyrrhenian margin of central Italy and their influence on volcanism. Tectonics, 25, TC2003. doi:10.1029/2005TC001845

AGIP, 1977. Temperature Sotterranee. Segrate, Milano. 1390 pp.

Aiello, G., Budillon, F., Cristofalo, G., D'Argenio, B., de Alteriis, G., De Lauro, M., Ferraro, L., Marsella, E., Pelosi, N., Sacchi, M., Tonielli, R., 2001. Marine geology and morphobathymetry in the Bay of Naples (south-eastern Tyrrhenian Sea, Italy. In: Faranda, F.M., Guglielmo, L., Spezie, G. (Eds.), Mediterranean Ecosystems: Structures and Processes. Springer-Verlag, Italia, pp. 1 –8.

Aitchison, J. and Greenacre, M. (2002) Biplots of Compositional Data. Applied Statistics, 51, 375-392.

Aitchison, J., 1986. The Statistical Analysis of Compositional Data. Monographs on Statistics and Applied Probability. Chapman and Hall Ltd. (Reprinted 2003 with additional material by The Blackburn Press), London (UK). 416 p.

Allen, J., Brandt, U., Brauer, A. et al. Rapid environmental changes in southern Europe during the last glacial period. Nature 400, 740–743 (1999) doi:10.1038/23432

Alley, R.B., 2000. The Younger Dryas cold interval as viewed from central Greenland. Quaternary Sci. Rev. 19, 213-226.

Almogi-Labin A., 1984. Population dynamics of planktic Foraminifera and Pteropoda—Gulf of Aqaba, Red Sea. Proc K Ned Akad Van Wet Ser B Palaeontol Geol Phys Chem 87:481–511

Altenbach A., Heeger T., Linke P, Spindler M., Thies A, 1993. Miliolinella subrotunda (Montagu), a miliolid foraminifer building large detritic tubes for a temporary epibenthic lifestyle. Marine Micropaleontology. 20. 293-301. 10.1016/0377-8398(93)90038-Y.

Altenbach, A.V., Pflaumann, U., Schiebel, R., Thies, A., Timm, S., Trauth, M., 1999. Scaling percentages and distributional patterns of benthic foraminifera with flux rates of organic carbon. Journal of Foraminiferal Research 29, 173–185.

Amore, F. O., Caffau, M., Massa, B., Morabito, S., 2004. Late Pleistocene–Holocene paleoclimate and related paleoenvironmental changes as recorded by calcareous nannofossils and planktonic foraminifera assemblages in the southern Tyrrhenian Sea (Cape Palinuro, Italy). Marine Micropaleontology 52, 255–276.

André A., 2013. Taxonomies moléculaire et morphologique chez les foraminifères planctoniques: Élaboration d'un référentiel et cas particuliers de Globigerinoides sacculifer et Neogloboquadrina pachyderma. PhD Thesis, University of Lyon.

Antonov, J. I., Seidov D., Boyer, T. P., Locarnini R. A., Mishonov A. V., and Garcia H. E., 2010. World Ocean Atlas 2009 Volume 2: Salinity. S. Levitus, Ed., NOAA Atlas NESDIS 69, U.S. Government Printing Office, Washington, D.C., 184 pp.

Ariztegui D., Asioli A., Lowe J. J., Trincardi F., Vigliotti L., Tamburini F., Chondrogianni C., Accorsi C. A., Bandini Mazzanti, M., Mercuri A. M., Van der Kaars S., McKenzie J. A., Oldfield F., 2000. Paleoclimate and the formation of sapropel S1: inferences from Late Quaternary lacustrine and marine sequences in the central Mediterranean region. Palaeogeogr. Palaeoclimatol. Palaeoecol. 158, 215-240.

Asioli, A. and Piva, A., 2006: Il ruolo dei foraminiferi nelle ricostruzioni paleoceanografiche e paleoclimatiche: esempi dal Mediterraneo Centrale (Adriatico) per il tardo Olocene attraverso un approccio multidisciplinare. Informatore Botanico Italiano 38, 14—24.

Asioli, A., 1996. High resolution foraminifera biostratigraphy in the Central Adriatic basin during the last deglaciation: a contribution to the PALICLAS Project. In: Oldfield, F., Guilizzoni P. (Eds.), Palaeoenvironmental Analysis of Italian Crater Lake and Adriatic Sediments. Memorie dell'Istituto Italiano di Idrobiologia 55, 197-218.

Asioli, A., Trincardi, F., Lowe, J. J., Ariztegui, D., Langone, L., Oldfield, F., 2001. Submillennial scale climatic oscillations in the central Adriatic during the Lateglacial. Paleoceanographic implications. Quarter. Sci. Rev., 20, 1201-1221.

Astraldi M, Gasparini G.P., Sparnocchia S., Moretti M., Sansone E., 1996. The characteristics of the water masses and the water transport in the Sicily Channel at long time scales. Bull. Instit. Oceanogr., 17: 95-116.

Astraldi M., Gasparini G.P., Vetrano A., Vignudelli S., 2002. Hydrographic characteristics and interannual variability of water masses in the central Mediterranean: a sensitivity test for long-term changes in the Mediterranean Sea. Deep-Sea Res. Pt. I, 49: 661-680.

Auras-Schudnagies A, Kroon D, Ganssen G, Hemleben C, van Hinte JE., 1989. Distributional pattern of planktonic foraminifers and pteropods in surface waters and top core sediments of the Red Sea, and adjacent areas controlled by the monsoonal regime and other ecological factors. Deep-Sea Res I 36:1515–1533.

Avnaim-Katav S., Almogi-Labin A., Sandler A., Sivan D., 2013. Benthic foraminifera as palaeoenvironmental indicators during the last million years in the eastern Mediterranean inner shelf, Palaeogeography, Palaeoclimatology, Palaeoecology, Volume 386, Pages 512-530, ISSN 0031-0182.

Barceló Vidal C., Martín Fernández J.A., Fdez-Henestrosa S. T., 2019. Statistical Analysis of Compositional Data – CoDa course material from CoDa course week 1-5 July, 2019.

Barmawidjaja DM, Jorissen FJ, Puskaric S, Van der Zwaan GJ, 1992. Microhabitat selection by benthic foraminifera in the Northern Adriatic Sea. J Foram Res 22:297–317.

Barra, D., Bonaduce, G., Brancaccio, L., Cinque, A., Ortolani, F., Pagliuca, S., Russo, F., 1989. Evoluzione geologica olocenica della piana costiera del Fiume Sarno (Campania). Mem. Soc. Geol. Ital. 42, 255– 267.

Bartole, R., Savelli, D., Tramontana, M., Wezel, F.C., 1984. Structural and sedimentary features in the Tyrrhenian margin off Campania, Southern Italy. Mar. Geol. 55, 163– 180.

Baumfalk YA, Troelstra SR, Ganssen G, van Zanen MJL., 1987. Phenotypic variation of Globorotalia scitula (Foraminiferida) as a response to Pleistocene climatic fluctuations. Mar Geol 75:231–240.

Bé A.W.H., 1960. Ecology of recent planktonic foraminifera: Part2: Bathymetric and seasonal distributions in the Sargasso Sea off Bermuda. Micropaleontology 6 (4),373–392.

Bé, A. W. H., 1977. An ecological, zoogeographic and taxonomic review of recent planktonic foraminifera. In Ramsey, A.T.S., Ed., Oceanic Micropalaeontology. London: Academic Press,1-100.

Bé A.W.H., Ericson D.B., 1963. Aspects of calcification in planktonic foraminifera (Sarcodina). Ann.NYAcad.Sci.109(1),65–81.

Bé A. W. H., Harrison SM, Lott L., 1973. Orbulina universa (d'Orbigny) in the Indian Ocean. Micropaleontology 19:150–192.

Bé, A. W. H. and Tolderlund, D. S., 1971. Distribution and ecology of living planktonic foraminifera in surface waters of the Atlantic and Indian Oceans. In (Funnell, B.M. and Riedel, W.R., eds), The Micropalaeontology of Oceans, 105-149. Cambridge University Press.

Bé, A. W.H., Bishop, J. K. B., Sverdlove, M. S. and Gardner, W. D., 1985. Standing stock, vertical distribution and flux of planktonic foraminifera in the Panama Basin. Mar. Micropalaeontol., 9, 307-333.

Bemis BE, Spero HJ, Bijma J, Lea DW., 1998. Reevaluation of the oxygen isotopic composition of planktonic foraminifera: experimental results and revised paleotemperature equations. Paleoceanography 13:150–160.

Bergami C, Capotondi L, Langone L, Giglio F, Ravaioli M., 2009. Distribution of living planktonic foraminifera in the Ross Sea and the Pacific sector of the Southern Ocean (Antarctica). Mar Micropaleontol 73:37–48.

Bergamin L., Romano E., Celia Magno M., Ausili A., Gabellini M., 2005. Pollution monitoring of Bagnoli Bay (Tyrrhenian Sea, Naples, Italy), a sedimentological, chemical and ecological approach, Aquatic Ecosystem Health & Management, 8:3, 293-302, DOI: 10.1080/14634980500220866.

Bernhard J.M. 1986, Characteristic assemblages and morphologies of benthic foraminifera from anoxic, organic-rich deposits: Jurassic through Holocene. Journal of Foraminiferal Research 16, 207-15.

Berrino, G., Corrado, G., and Riccardi, U.,2008. Sea gravity data in the Gulf of Naples. A contribution to delineating the structural pattern of the Phlegraean volcanic district. Journal of Volcanology and Geothermal Research, 175(3), 241–252.

Béthoux, J. P., 1979. Budgets of the Mediterranean Sea. Their dependence on local climate and on characteristics of the Atlantic water. Oceanologica Acta, 2, 157-163.

Béthoux, J. P., Morin, P., Chaumery, C., Connan, O., Gentili B. and Ruiz-Pino, D., 1997. Nutrients in the Mediterranean Sea, mass balance and statistical analysis of concentrations with respect to environmental change. Marine Chemistry, 63: 155-169.

Bijma J., Erez J., Hemleben C. (1990a) Lunar and semi-lunar reproductive cycles in some spinose planktonic foraminifers. J Foraminifer Res 20:117–127

Bijma J., Faber W.W., Hemleben C.(1990b) Temperature and salinity limits for growth and survival of some planktonic foraminifers in laboratory cultures. J Foraminifer Res 20:95–116.

Bishop, J.K.B., 1988. The barite–opal–organic carbon association in oceanic particulate matter. Nature 33, 341–343. INTIMATE members, Björck, S., Walker, M.J.C., Cwynar, L.C., Johnsen, S., Knudsen, K.-L., Lowe, J.J., Wohlfarth, B., 1998. An event stratigraphy for the Last Termination in the North Atlantic region based on the Greenland ice-core record: a proposal by the INTIMATE group. Journal of Quaternary Science 13, 283–292.

Blanc-Vernet, L., 1969. Contribution à l'étude des foraminifères de Méditerranée. Thèse de Doctorat Etat. Travaux de la Station Marine d'Endoume, Marseille, 281 pp.

Blanc-Vernet, L., Sgarrella, F., Acquaviva, M., 1984. Evènements climatiques, hydrologie et foraminifèrs en Mèditerranè e au Quaternaire rècent. Bull. Soc. Ge´ol. Fr. 26, 1235–1243.

Brancaccio, L., Cinque, A., Romano, P., Russo, F., Santangelo, N. Santo, A., 1991. Geomorphology and neotectonic evolution of asector of the Tyrrhenian flank of the southern Apennines (Region of Naples Italy). Z. Geomorphol. 82, 47– 58.

Brocchini, D., Principe, C., Castradori, D., Laurenzi, M.A., Gorla, L., 2001. Quaternary evolution of the southern sector of the Campanian Plain and early Somma–Vesuvius activity: insights from the Trecase 1 well. Mineral. Petrol. 73, 67–92.

Brummer GJA, Hemleben C, Spindler M., 1987. Ontogeny of extant spinose planktonic foraminifera (Globigerinidae): a concept exemplified by Globigerinoides sacculifer (Brady) and G. ruber (d'Orbigny). Mar Micropaleontol 12:357–381.

Brummer, G. J. A. and Kroon, D., 1988. Genetically controlled planktonic foraminiferal coiling ratios as tracers of past ocean dynamics. In: G.J. Brummer and D. Kroon (Editors), Planktonic Foraminifers as Tracers of Ocean-climate history. Free Univ. Press, Amsterdam, pp. 293-298.

Bruno, P.P.G., Rapolla, A., Di Fiore, V., 2003. Structural setting of the Bay of Naples (Italy) seismic reflection data: implications for Campanian volcanism. Tectonophysics 372, 193-213.

Bryden, H. L. and Kinder, T. H., 1991. Steady two-layer exchange through the Strait of Gibraltar. Deep-Sea Research, 38, 445-463.

Buccheri G., Ferretti O., Agate M., Bertoldo M., Immordino F., Lucido M., 1998. Valutazioni stratigrafiche, sedimentologiche e paleoclimatiche sui sedimenti tardopleistocenici-Olocenici del Golfo di Castellammare (Sicilia Nordoccidentale): indagini sulle carote PaCa2 e PaCa3. Bollettino della Società Geologica Italiana 117, 219–248.

Buccheri, G., Capretto, G., Di Donato, V., Esposito, P., Ferruzza, G., Pescatore, T., Russo Ermolli, E., Senatore, M.R., Sprovieri, M., Bertoldo, M., Carella, D., Madonna, G., 2002. A high resolution record of the last deglaciation in the southern Tyrrhenian Sea: environmental and climatic evolution. Mar. Geol. 186, 447–470.

Buccheri, G., Torelli, L., 1981. Stratigraphy and Paleoclimatic evaluations of the cores BS77-15 and BS77-33 (Sardinia Basin, Western Tyrrhenian Sea) by means of Pteropods assemblages. Ateneo Parmense Acta Naturalia 17, 73–94.

Buccianti, A. and Esposito, P., 2004. Insights on Late Quaternary calcareous nannoplankton assemblages under the theory on statistical analysis for compositional data: an application example. Palaeogeography, Palaeoclimatology, Palaeoecology, 202, 209–227.

Buccianti, A. and V. Pawlowsky-Glahn (2005). New perspectives on water chemistry and compositional data analysis. Mathematical Geology 37 (7), 703–727.

Budillon G., Gasparini G.P., Schroeder K., 2009. Persistence of an Eddy Signature in the Central Tyrrhenian Basin. Deep Sea Research, Part II, 56: 713-724.

Budillon, F., Pescatore, T., Senatore, M.R., 1994. Cicli deposizionali del Pleistocene Superiore–Olocene sulla piattaforma continentale del Golfo di Salerno (Tirreno Meridionale). Boll. Soc. Geol. Ital. 113, 303–316.

Budillon, F., Violante, C., Conforti, A., Esposito, E., Insinga, D., Iorio, M., Porfido, S., 2005. Event beds in the recent prodelta stratigraphic record of the small flood-prone Bonea stream (Amalfi Coast, Southern Italy). Mar. Geol. 222–223, 419–441.

Buongiorno Nardelli, B., and Salusti E., 2000. On dense water formation criteria and their application to the Mediterranean Sea. Deep-Sea Research I, 47, 193-221.

Cacho I., Grimalt J. O., Sierro F. J., Shackleton N. J. and Canals M., 2000. Evidence for enhanced Mediterranean thermohaline circulation during rapid climatic coolings, Earth Planetary Science Letters, 183, 417– 429.

Cacho I., Grimalt J.O., M.Canals M., 2002. Response of the Western Mediterranean Sea to rapid climatic variability during the last 50,000 years: a molecular biomarker approach. Journal of Marine Systems Volumes 33–34, Pages 253-272.

Cacho I., Grimalt J.O., Pelejero C., et al. Dansgaard-Oeschger and Heinrich event imprints in Alboran Sea paleotemperatures. Paleoceanography 1999; 14: 698-705. [8]

Cacho, I., Grimalt, J. O., Canals, M., Sbaffi, L., Shackleton, N. J., Schònfeld, J.,Zahn, R., 2001. Variability of the western Mediterranean Sea surface temperature during the last 25,000 years and its connection with the Northern Hemisphere climatic changes. Paleoceanography 16,40-52.

Canfield D.E., 1994. Factors influencing organic carbon preservation in marine sediments. Chemical Geology 114, 315-329.

Capotondi L., Borsetti A., Morigi C., 1999. Foraminiferal ecozones, a high resolution proxy for the late Quaternary biochronology in the central Mediterranean Sea. Marine Geology 153, 253– 274.

Capotondi L., Girone A., Lirer F., Bergami C., Verducci M., Vallefuoco M., Afferri A., Ferraro L., Pelosi N., De Lange G.J., 2016. Central Mediterranean Mid-Pleistocene paleoclimatic variability and its association with global climate, Palaeogeography, Palaeoclimatology, Palaeoecology, Volume 442, 72-83.

Capotondi L., Morigi C., Turi B. and Brilli M., 2000. Biological and oxygen isotope records in LateQuaternary sediments from the Eastern Mediterranean Sea. Rendiconti Lincei. Scienze fisiche e naturali. 134. 169-183.

Caron M. and Homewood P. 1983, Evolution of Early Planktic Foraminifers. Marine Micropaleontology 7, 453-462.

Carrada G. C., Hopkins T. S., Bonaduce G., Ianora A., Marino D., Modigh M., Ribera d'Alcalà M., Scotto di Carlo B., 1980. Variability in the hydrographic and biological features of the Gulf of Naples: P. S. Z. N. I.: Marine Ecology, 1: 105-120.

Carstens J, Hebbeln D, Wefer G., 1997. Distribution of planktic Foraminifera at the ice margin in the Arctic (Fram Strait). Mar Micropaleontol 29:257–269.

Carstens J, Wefer G., 1992. Recent distribution of planktonic foraminifera in the Nansen Basin, Arctic Ocean. Deep-Sea Res I 39:507–524.

Casford J.S.L., Rohling E.J., Abu-Zied R., Cooke S., Fontanier C., Leng M., Lykousis V., 2002. Circulation changes and nutrient concentrations in the late Quaternary Aegean Sea: A nonsteady state concept for sapropel formation. PALEOCEANOGRAPHY, VOL. 17, NO. 2, 1024, 10.1029/2000PA000601

Casford, J.S.L., Rohling, E.J., Abu-Zied, R.H., Fontanier, C., Jorissen, F.J., Leng, M., Schmiedl, G., Thomson, J., 2003. A dynamic concept for eastern Mediterranean circulation and oxygenation during sapropel formation. Palaeogeography, Palaeoclimatology, Palaeoecology 190, 103–119.

Chapman MR., 2010. Seasonal production patterns of planktonic foraminifera in the NE Atlantic Ocean: implications for paleotemperature and hydrographic reconstructions. Paleoceanography.

Ciampo, G., 2003. Reconstruction of Late Pleistocene-Holocene palaeobathymetries from Ostracoda on the Tyrrhenian continental shelf. Geobios 36, 1–11.

Cimerman F. and Langer MR., 1991. Mediterranean Foraminifera. Academia Scientiarum et Artium Slovenica, Ljubljana 30:1–118

Cinque, A., 1999. La trasgressione versiliana nella Piana del Sarno (Campania). Geogr. Fis. Din. Quat. 14, 63– 71.

Cinque, A., Augelli, P.P.C., Brancaccio, L., Mele, R., Milia, A., Robustelli, P., Romano, P., Russo, F., Santangelo, N., Sgambati, D., 1997. Volcanism, tectonics and recent geomorphological change in the Bay of Napoli. Suppl. Geogr. Fis. Din. Quat. 3, 123– 141.

Cita, M. B., Vergnaud-Grazzini, C., Robert, C., Chamley, H., Ciaranfi, N. and d'Onofrio, S., 1977. Palaeoclimatic record of a long deep sea core from the eastern Mediterranean. Quat Res., 8, 205-235.

Cléroux C, Cortijo E, Anand P, Labeyrie L, Bassinot F, Caillon N, Duplessy J., 2008. Mg/Ca and Sr/Ca ratios in planktonic foraminifera: proxies for upper water column temperature econstruction. Paleoceanography.

Cléroux C, Cortijo E, Duplessy JC, Zahn R., 2007. Deep-dwelling Foraminifera as thermocline temperature recorders. Geochem Geophys Geosystems.

Cléroux C, Lynch-Stieglitz J, Schmidt MW, Cortijo E, Duplessy JC., 2009. Evidence for calcification depth change of Globorotalia truncatulinoides between deglaciation and Holocene in the western Atlantic Ocean. Mar Micropaleontol 73:57–61.

Compositional Data Analysis.
Conan SMH, Brummer GJA., 2000. Fluxes of planktic Foraminifera in response to monsoonal upwelling on the Somalia Basin margin. Deep-Sea Res II 47: 2207–2227.

Conforti, A., 2003. Stratigrafia integrata della sequenza Tardo-Quaternaria del settore settentrionale del Golfo di Salerno e di quello meridionale del Golfo di Napoli. PhD thesis, University of Naples Federico II, 144 pp.

Coppa MG, Di Tuoro A., 1995. Preliminary data on the Holocene foraminifera of the Cilento continental shelf (Tyrrhenian Sea). Rev Esp Paleont 10(2):161–174.

Coppa MG, Russo B, Siani G., 1994. The Holocene foraminiferal assemblages of the continental margin between Agropoli and Capo Palinuro (Tyrrhenian Sea). In: Matteucci R (ed) Studies on ecology and paleoecology of benthic communities. Boll Soc Paleont Ital 2:67–91.

Corliss B.H. and Emerson S. 1990, Distribution of Rose Bengal stained deep-sea benthic foraminifera from the Nova Scotia continental margin and Gulf of Maine. Deep-sea Research 37, 589-605.

Corliss B.H., (1991). Morphology and microhabitat preferences of benthic foraminifera from the Northwest Atlantic Ocean. Mar. Micropal., Vol. 17, 195-236.

Corliss B.H., 1985. Microhabitats of benthic foraminifera within deep-sea sediments. Nature vol. 314, p. 435–438.

Culver Sj and Buzas Ma (1986) Distribution of recent benthic foraminiferal off the North America Pacific coast from California to Baja. Smithsonian Contributions Mar Sci 28:1–634

D'Orbigny AD (1826) Tableau méthodique de la classe des Céphalopodes. Ann Sci Nat 1:245–314.

D'Argenio, B., Aiello, G., de Alteriis, G., Milia, A., Sacchi, M., Tonielli, R., Budillon, F., Chiocci, F.L., Conforti, A., De Lauro, M., Di Martino, G., D'Isanto, C., Esposito, E., Ferraro, L., Innangi, S., Insinga, D., Iorio, M., Marsella, E., Molisso, F., Morra, V., Passaro, S., Pelosi, N., Porfido, S., Raspini, A., Ruggieri, S., Sarnacchiaro, G., Terranova, C., Vilardo, G., Violante, C., 2004. Digital elevation model of the Naples Bay and adjacent areas, eastern Tyrrhenian Sea. In: Pasquarè, G., Venturini, C. (Eds.), Mapping Geology in Italy. APAT (Agenzia per la Protezione dell'Ambiente e per i Servizi Tecnici)-National Geological Survey of Italy Spec. Vol., S.E.L.C.A., Florence, pp. 22–28.

Darling KF, Kucera M, Pudsey CJ, Wade CM., 2004. Molecular evidence links cryptic diversification in polar planktonic protists to Quaternary climate dynamics. Proc Natl Acad Sci USA 101:7657–7662

Darling KF, Wade CM, Stewart IA, Kroon D, Dingle R, Brown AJL., 2000. Molecular evidence for genetic mixing of Arctic and Antarctic subpolar populations of planktonic foraminifers. Nature 405:43–47.

Darling KF, Wade CM., 2008. The genetic diversity of planktic Foraminifera and the global distribution of ribosomal RNA genotypes. Mar Micropaleontol 67:216–238.

Davidsson S. 2014. The Distribution of the Benthic Foraminiferal Fauna in the Gullmar Fjord Deep Basin, at Station AE73142B: A Comparison with Hydrographic Parameters and the North Atlantic Oscillation. Bachelor of Science thesis, Faculty of Science, University of Gothenburg.

De Maio, A., 1959. Annali Ist. Univ. Nav., XXVIII, 1-16.

De Maio, A.; Moretti, 1973. Contributo a un progetto di studio delle correnti del Golfo di Napoli: Fondazione Politecnica per il Mezzogiorno d'Italia - Quaderno n.71. Ed. Giannini, Napoli.

De Maio, A.; Moretti, M.; Sansone, E.; Spezie, G.; Vultaggio, M., 1978-1979a. Annali Ist. Univ. Nav., XLVII-XLVIII, 201-213.

De Maio, A.; Moretti, M.; Sansone, E.; Spezie, G.; Vultaggio, M., 1978-1979b. Annali Ist. Univ. Nav., XLVII-XLVIII, 215-231.

De Maio, A.; Moretti, M.; Sansone, E.; Spezie, G.; Vultaggio, M., 1980-1981. Annali Ist. Univ. Nav., IL-L, 1-305.

De Maio, A.; Moretti, M.; Sansone, E.; Spezie, G.; Vultaggio, M., 1983. Annali Ist. Univ. Nav., LI, 1-58.

De Pippo, T., Di Cara, A., Guida, M., Pescatore, T., Renda, P. (1984). Contributi allo studio del Golfo di Pozzuoli. Lineamenti di geomorfologia. Memorie Società Geologica Italiana, 7, 151–159.

De Rijk, S., Jorissen, F.J., Rohling, E.J., Troelstra, S.R., 2000. Organic flux control on bathymetric zonation of Mediterranean benthic foraminifera. Marine Micropaleontology. 400: 151-166.

de Ruggiero P., 2013. PhD thesis "High-resolution model studies of the circulation in coastal areas of the Tyrrhenian Sea (including the Gulf of Naples)". Universitá degli studi di napoli "federico ii" scuola di dottorato in scienze della terra "giuseppe de lorenzo" with: universitá degli studi di napoli "Parthenope" Seconda Universitá di Napoli In collaboration with: Istituto per l'Ambiente Marino Costiero - C. N. R. Stazione Zoologica Anton Dohrn.

De Stigter, H.C., Jorissen, F.J., Van der Zwaan, G.J., 1998. Bathymetric distribution and microhabitat partitioning of live (Rose Bengal stained) benthic foraminifera along a shelf to bathyal transect in the Southern Adriatic Sea. J. Foraminiferal Res. 28, 40–65.

De Vargas C, Norris R, Zaninetti L, Gibb SW, Pawlowski J., 1999. Molecular evidence of cryptic speciation in planktonic foraminifers and their relation to oceanic provinces. Proc Natl Acad Sci 96: 2864–2868.

De Vargas C, Renaud S, Hilbrecht H, Pawlowski J., 2001. Pleistocene adaptive radiation in Globorotalia truncatulinoides: Genetic, morphologic, and environmental evidence. Paleobiology 27:104–125.

Deino, A.L., Orsi, G., de Vita, S., Piochi, M., 2004. The age of the Neapolitan Yellow Tuff caldera-forming eruption (Campi Flegrei caldera-Italy) assessed by 40Ar/39Ar dating method. J. Volcanol. Geotherm. Res. 133, 157– 170.

deMenocal P. B., Ortiz J. D., Guilderson T. P., Adkins J., Sarnthein M., Baker L.; Yarusinsky M., 2000. Abrupt onset and termination of the African Humid Period: rapid climate responses to gradual insolation forcing. Quaternary Science Reviews, 19(1-5), 347-361,

Deuser WG, Muller-Karger FE, Hemleben C. 1988. Temporal variations of particle fluxes in the deep subtropical and tropical North Atlantic: Eulerian versus Lagrangian effects. J Geophys Res Oceans 1978– 2012(93):6857–6862.

Deuser WG, Ross EH, Hemleben C, Spindler M., 1981. Seasonal changes in species composition, numbers, mass, size, and isotopic composition of planktonic foraminifera settling into the deep Sargasso Sea. Palaeogeogr Palaeoclimatol Palaeoecol 33:103–127.

Di Donato V., 2002. Effects of Late Pleistocene–Holocene climatic changes on the planktonic foraminifera in the Gulf of Gaeta (Tyrrhenian sea, Italy), Il Quaternario 15 (2), 251–257.

Di Donato V., Martín-Fernández J.A., Comas-Cufí M., Jamka J., 2018. *Palaeoenvironmental reconstructions through Compositional Data analysis*. Alpine and Mediterranean Quaternary, 31 (1), 59-73.

Di Donato, V., Esposito, P., Garilli, V., Naimo, D., Buccheri, G., Caffau, M., Ciampo, G., Greco, A., and Stanzione, D. (2009) - Surface-bottom relationships in the Gulf of Salerno (Tyrrhenian Sea) over the last 34 kyr: Compositional data analysis of palaeontological proxies and geochemical evidence. Geobios, 42, 561-579.

Di Donato, V., Esposito, P., Russo Ermolli, E., Scarano, A., and Cheddadi, R., 2008. Coupled atmospheric and marine palaeoclimatic reconstruction for the last 35 ka in the Sele Plain-Gulf of Salerno area (southern Italy). Quaternary International, 190, 146-157.

Di Donato, V., Insinga, D.D., Iorio, M., Molisso, F., Rumolo, P., Cardines, C. Passaro, S., 2018. The palaeoclimatic and palaeoceanographic history of the Gulf of Taranto (Mediterranean Sea) in the last 15 ky. Global and Planetary Change. 10.1016/j.gloplacha.2018.10.014

Di Donato, V., Martín-Fernández, J.A., 2008. CODAMAT: a modern analogue technique for compositional data. In: Daunis-i-Estadella, J., Martín-Fernández, J.A. (Eds.), Proceedings of CODAWORK'08, The 3rd Compositional Data Analysis Workshop, May 27-30. University of Girona, Girona (Spain).

Di Donato, V., Martin-Fernandez, J.A., Daunis-i-Estadella, J. & Esposito, P., 2015. Size fraction effects on planktonic foraminifera assemblages: a compositional contribution to the golden sieve rush. Mathematical Geosciences, 47 (4), 455-470.

Di Stefano E., Incarbona A., Sprovieri R., Ferraro S., 2014. Ten Years of Paleoceanographic Studies at ODP Site 963 (Central Mediterranean Sea). Open Paleontology Journal, 2014, 5, 10-19

Di Vito, M. A., Lirer, L., Mastrolorenzo, G., & Rolandi, G. (1987). The 1538 Monte Nuovo eruption (Campi Flegrei, Italy). Bulletin of Volcanology, 49, 608–615.

Dieci, G. 1959: I foraminiferi tortoniani di Montegibbio e Castel Vetro. – Palaeontographia Italica, LIV (n. ser. vol. XXIV), 1–113, Pisa.

Droser M.J. and Bottjer D.J., 1991. Trace fossils and ichnofabric in Leg 119 cores. Proc. Ocean Drill. Program Sci. Results 119, 635–641.

Düing, W., 1965. Strömungsverhältnisse im Golf con Neapel: Pubbl. Staz. Zool. Napoli 34, 256-316.

Eggins S, De Dekker P, Marshall J., 2003. Mg/Ca variation in planktonic foraminifera tests: implications for reconstructing palaeo-seawater temperature and habitat migration. Earth Planet Sci Lett 212:291–306

Egozcue J. J. and Pawlowsky-Glahn V., 2005. Groups of parts and their balances in compositional data analysis. Mathematical Geology 37 (7), 795-828.

Egozcue J.J., Pawlowsky-Glahn V., Mateu-Figueraz, G., Barceló-Vidal, C., 2003. - Isometric logratio transformations for compositional data analysis. Mathematical Geology 35 (3), 279-300.

Erez J, Almogi-Labin A, Avraham S., 1991. On the life history of planktonic foraminifera: lunar reproduction cycle in Globigerinoides sacculifer (Brady). Paleoceanography 6:295–306

Fairbanks, R. G, 1989. 17,000-year glacio-eustatic sea level record: influence of glacial melting rates on the Younger Dryas event and deep-ocean circulation. Nature 342, 637–642, doi:10.1038/342637a0.

Fairbanks, R. G., Sverdlove, M., Free, R., Wiebe, P. H. and Bé, A. W. H., 1982. Vertical distribution of living planktonic foraminifera from the Panama Basin. Nature, 298, 841-844.

Fairbanks R.G., Wiebe P.H., 1980. Foraminifera and chlorophyll maximum: Vertical distribution, seasonal succession and paleoceanographic significance. Science 209,1524–1526.

Feldmeijer W., Metcalfe B., Brummer G.-J. A. and Ganssen G. M., 2015. Reconstructing the depth of the permanent thermocline through the morphology and geochemistry of the deep dwelling planktonic foraminifer Globorotalia truncatulinoides. Paleoceanography, 30, 1–22, doi:10.1002/ 2014PA002687.

Ferraro L, Lirer F., 2006. Morphological variations of benthonic foraminiferal tests from Holocene sediments of the Punta Campanella Shelf (south Tyrrhenian Sea). In: Coccioni R, Marsili A (eds) Proceedings of the second and third Italian meetings on environmental micropaleontology. Grzybowski Foundation Special Publication, vol 11, pp 45–59

Ferraro L, Pescatore T, Russo B, Senatore MR, Vecchione C, Coppa MG, Di Tuoro A, 1997. Studi di geologia marina del margine tirrenico: la piattaforma continentale tra Punta Licosa e Capo Palinuro (Tirreno Meridionale). Boll Soc Geol It 116:473–485.

Ferraro L. and Molisso F., 2000. Sedimentological and paleontological features of sea floor sediments of Penta Palummo and Miseno volcanic highs, Gulf of Naples (South-eastern Tyrrhenian Sea). Rendiconti Lincei, 11(1), 59–67.

Finetti, I., Morelli, C., 1974. Esplorazione sismica a riflessione dei golfi di Napoli e Pozzuoli. Boll. Geofis. Teor. Appl. 16, 175–222.

Fischer G, Wefer G., 1999. Use of proxies in paleoceanography: examples from the South Atlantic. Springer, Berlin.

Flores, J. A., Sierro, F. J., Francès, G., Vasquez, A., Zamarreno, I., 1997. The last 100,000 years in the western Mediterranean: sea surface water and frontal dynamics as revealed by coccolithophores. Mar. Micropaleontol. 29, 351–366.

Folk R.L., Ward W.C., 1957. Brazos river bar: a study in the significance of grain-size parameters. J. Sediment. Petrol. 27, 3–26.

Fontanier C., Jorissen F., Geslin E., Zaragosi S., Duchemin G., Laversin M., Gaultier M. ,2008. Live and dead foraminiferal faunas from Saint-Tropez Canyon (Bay of Fréjus): Observations based on situ and incubated cores. Journal of Foraminiferal Research 38(2), 137-156.

Fontanier, C., Jorissen, F.J., Licari, L., Alexandre, A., Anschultz, P., Carbonel, P., 2002. Live benthic foraminiferal faunas from the Bay of Biscay: faunal density, composition, and microhabitats. Deep Sea Research 49, 751–785.

Frezza V, Carboni MG, 2009. Distribution of recent foraminiferal assemblages near the Ombrone River mouth (Northern Tyrrhenian Sea, Italy). Rev Micropaleontol 52:43–66

Friedrich O, Schiebel R, Wilson PA, Weldeab S, Beer CJ, Cooper MJ, Fiebig J., 2012. Influence of test size, water depth, and ecology on Mg/Ca, Sr/Ca, d18O and d13C in nine modern species of planktic foraminifers. Earth Planet Sci Lett 319–320:133–145.

Fusco, G., Manzella, G. M. R., Cruzado, A., Gačić, M., Gasparini, G. P., Kovačević, V., Millot, C., Tziavos, C., Velasquez, Z. R., Walne, A., Zervakis, V., and Zodiatis, G., 2003. Variability of mesoscale features in the Mediterranean Sea from XBT data analysis. Ann. Geophys., 21: 21-32.

Fusi, N., Mirabile, L., Camerlenghi, A., Ranieri, G., 1991. Marine geophysical survey of the Gulf of Naples (Italy): relationships between submarine volcanic activity and sedimentation. Mem. Soc. Geol. Ital. 47, 95–114.

Ganssen, G and Troelstra, S. R., 1987. palaeoenvironmental changes from stable isotopes in planktonic foraminifera from eastern Mediterranean sapropels. Marine Geology, 75, 221-230.

Gasse F. and Van Campo E., 1994. Abrupt post-glacial climate events in West Asia and North Africa monsoon domains, Earth and Planetary Science Letters, Volume 126, Issue 4, Pages 435-456, ISSN 0012-821X.

Georgopoulos, D., Theocharis, A., and Zodiatis, G., 1989. Intermediate Water Formation in the Cretan Sea (S. Aegean Sea), Oceanologica Acta, 12, 353-359.

Geraga M., Tsaila-Monopolis S., Ioakim C., Papatheodorou G., Ferentinos G., 2005. Short-term climate changes in the southern Aegean Sea over the last 48,000 years. Palaeogeography, Palaeoclimatology, Palaeoecology 220, 311– 332.

Geslin E., Heinz P., Jorissen F.J., Hemleben C., 2004. Migratory responses of deep-sea benthic foraminifera to variable oxygen conditions: laboratory investigations, Marine Micropaleontology, Volume 53, Issues 3–4, Pages 227-243.

Gooday A.J., 1994. The biology of deep-sea foraminifera: a review of some advances and their applications in paleoceanography. Palois, Vol. 9, 14-31.

Gooday, A. J. 2003, Benthic foraminifera (Protista) as tools in deep-water paleoceanography: environmental influences on faunal characteristics. Advances in Marines Biology 46, 3-90.

Gravili D., Napolitano E., Pierini S., 2001. Barotropic aspects of the dynamics of the Gulf of Naples (Tyrrhenian Sea). Continental Shelf Research, 21, 455-471.

Gray K.R. and Biddlestone A.J., 1973. Composting - process parameters. The Chemical Engineer. Feb. pp 71-76.

Greenacre, M. J. (1984) Theory and Applications of Correspondence Analysis. London: Academic Press.

Grieco L., Tremblay L.-B., Zambianchi E., 2005. A hybrid approach to transport processes in the Gulf of Naples: an application to phytoplankton and zooplankton population dynamics. Continental Shelf Research, 25, 711-728.

Grimm E.C. 1987, CONISS: a FORTRAN 77 program for stratigraphically constrained cluster analysis by the method of incremental sum of squares, Computers & Geosciences 13, 13-35.

Guptha MVS, Curry WB, Ittekkot V, Muralinath AS., 1997. Seasonal variation in the flux of planktic Foraminifera; sediment trap results from the Bay of Bengal, northern Indian Ocean. J Foraminifer Res 27:5–19.

Hanebuth T., Stattegger K. and Grootes P., 2000. Rapid Flooding of the Sunda Shelf: A Late-Glacial Sea-Level Record. Science (New York, N.Y.). 288. 1033-5. 10.1126/science.288.5468.1033.

Hapgood, H.W., 1960. Hydrographic observations in the Bay of Naples (golfo di Napoli). January 1957-1958 (Stations list): Pubbl. Staz. Zool. Napoli, 31, 337-371.

Hayes A., Kucera M., Kallel N., Sbaffi L. and Rohling E., 2004. Compilation of planktic foraminifera modern data from the Mediterranean Sea. Pangaea, doi:10.1594/PANGAEA.227305.

Hayes, A., 1999. Late Quaternary palaeoclimatic and palaeoecological changes in the Mediterranean Sea. University of Southampton, Faculty of Science, Department of Oceanography, PhD Thesis pp.139.

Heburn, G. W. and La Violette, P. E., 1990. Variations in the structure of the anticyclonic gyres found in the Alboran Sea. J. Geophys. Res., 92, 2901-2906.

Heinrich H., 1988. "Origin and consequences of cyclic ice rafting in the northeast Atlantic Ocean during the past 130,000 years". Quaternary Res. **29** (2): 142–152.

Hemleben C, Bé AWH, Anderson OR, Tuntivate S., 1977. Test morphology, organic layers and chamber formation of the planktonic foraminifer Globorotalia menardii (d'Orbigny). J Foraminifer Res 7:1–25.

Hemleben C, Spindler M, Breitinger I, Deuser WG., 1985. Field and laboratory studies on the ontogeny and ecology of some globorotaliid species from the Sargasso Sea off Bermuda. J Foraminifer Res 15:254–272.

Hemleben C, Spindler M., 1983. Recent advances in research on living planktonic foraminifera. Utrecht Micropaleontol Bull 30:141–170.

Hemleben C., Spindler M., Anderson O.R. 1989. Modern Planktonic foraminifera, Springer – Verlag, 1-363.

Hemming, S.R., 2004. Heinrich events: Massive late Pleistocene detritus layers of the North Atlantic and their global climate imprint. Reviews of Geophysics. 42 (1): RG1005.

Hilbrecht H., 1996. Extant planktic Foraminifera and the physical environment in the Atlantic and Indian Oceans: an atlas based on Climap and Levitus, 1982. In: Mitteilungen aus dem Geologischen Institut der Eidgen. Technischen Hochschule und der Universität Zürich. Zürich, 93 pp.

Hillaire-Marcel C, de Vernal A (2007) Proxies in Late Cenozoic paleoceanography. Elsevier, New York.

Hopkins, T. S., Battilotti, M., De Lauro, M., Monassi, M., Ribera d'Alcalà, M., Saggiomo, V., Tramontano, M. A., Zangaglia, A. Atti AIOL, 1994, 10, 375-387.

Hutson WH., 1977. Transfer functions under no-analog conditions: experiments with Indian Ocean planktonic foraminifera. Quat Res 8:355–367.

Insinga, D., 2003. Tefrostratigrafia dei depositi tardo-quaternari della fascia costiera campana. PhD thesis, University of Naples Federico II, 202 pp.

Insinga, D., Calvert, A.T., Lanphere, M.A., Morra, V., Perrotta, A., Sacchi, M., Scarpati, C., Saburomaru, J., Fedele, L., 2006. The Late-Holocene evolution of theMiseno area (southwestern Campi Flegrei) as inferred by stratigraphy, petrochemistry and 40Ar/39Ar geochronology. In: De Vivo, B. (Ed.), Volcanism

in the Campania Plain: Vesuvius, Campi Flegrei and Ignimbrites. Developments in Volcanology Series. Elsevier B.V., pp. 97–125.

Insinga, D., Molisso, F., Lubritto, C., Sacchi, M., Passariello, I., Morra, V. 2008. The proximal marine record of Somma–Vesuvius volcanic activity in the Naples and Salerno bays (eastern Tyrrhenian Sea) during the last 3 kyrs. Journal of Volcanology and Geothermal Research, 177, 170–186.

Iorio, M., Sagnotti, L., Angelino, A., Budillon, F., D'Argenio, B., Dinares Turell, J., Macrı , P., Marsella, E., 2004. High-resolution petrophysical and paleomagnetic study of late- Holocene shelf sediments, Salerno Gulf, Tyrrhenian Sea. Holocene 14 (3), 433–442.

Ippolito, F., Ortolani, F., Russo, M., 1973. Struttura marginale tirrenica dell'Appennino campano: reinterpretazioni di dati di antiche ricerche di idrocarburi. Mem. Soc. Geol. Ital. 12, 227– 250.

Itou M, Ono T, Oba T, Noriki S., 2001. Isotopic composition and morphology of living Globorotalia scitula: a new proxy of sub-intermediate ocean carbonate chemistry? Mar Micropaleontol 42:189–210.

Ivanova E, Conan SMH, Peeters FJ, Troelstra SR., 1999. Living Neogloboquadrina pachyderma sin and its distribution in the sediments from Oman and Somalia upwelling areas. Mar Micropaleontol 36:91–107.

Ivanova EM, Schiebel R, Singh AD, Schmiedl G, Niebler HS, Hemleben C., 2003. Primary production in the Arabian Sea during the last 135,000 years. Palaeogeogr Palaeoclimatol Palaeoecol 197:61–82.

Jonkers L, Brummer GJA, Peeters FJC, van Aken HM, de Jong MF., 2010. Seasonal stratification, shell flux, and oxygen isotope dynamics of left-coiling N. pachyderma and T. quinqueloba in the western subpolar North Atlantic. Paleoceanography.

Jorissen F. J, Asioli A., Borsetti A. M., Capotondi L., de Visser J.P., Hilgen F.J., Rohling E. J., van de Borg K., Vergnaud-Grazzini C., Zachariasse W.J., 1993. Age determination of sediment core BS78-12. PANGAEA Late Quaternary central Mediterranean biochronology. Marine Micropaleontology, 21(1-3), 169-189.

Jorissen F.J., 1987. The distribution of benthic foraminifera in the Adriatic Sea. Mar Micropaleontol 12:21–48.

Jorissen F.J., 1988. Benthic foraminifera from the Adriatic Sea: principles of phenotypic variation. Utrecht Micropaleontological Bulletins 37.

Jorissen F.J., Barmawidjaja D. M,, Puskaric S., Van der Zwaan G.J., 1992. Vertical distribution of benthic foraminifera in the northern Adriatica Sea: the relation with organic flux. Mar Micropaleontol 19:131–146.

Jorissen F.J., De Stinger H.C., Widmark J.G.V. 1995, A conceptual model explaining benthic foraminiferal microhabits. Marine Micropaleontology 26, 3-15.

Jorissen F.J., Wittling I., Peypouquet J.P., Rabouille C., Relexans J.C., 1998. Live benthic foraminiferal faunas off Cape Blanc, NW-Africa: Community structure and microhabitats, Deep Sea Research Part I: Oceanographic Research Papers, Volume 45, Issue 12, Pages 2157-2188.

Kaiho K. 1994, Benthic foraminiferal dissolved-oxygen index and dissolved-oxygen levels in the modern ocean. Geology 22, 719-722.

Kallel, N., Paterne, M., Labeyrie, L., Duplessy, C., Arnold, M., 1997. Temperature and salinity records of the Tyrrhenian Sea during the last 18,000 years. Palaeogeogr. Palaeoclimatol. Palaeoecol. 135, 97–108.

Kemle-von Mücke S, Oberhänsli H., 1999. The distribution of living planktic Foraminifera in relation to southeast Atlantic oceanography. In: Fischer G, Wefer G (eds) Use of proxies in paleoceanography. Springer, Berlin, pp 91–115.

Kemle-von-Mücke S, Hemleben C, 1999. Planktic Foraminifera. In: Boltovskoy E (ed) South Atlantic zooplankton. Backhuys Publishers, Leiden, pp 43–67.

Krom M.D, Brenner S., Kress N., Gordon L.I., 1991. Phosphorus limitation of primary productivity in the Eastern Mediterranean Sea. Limnology and Oceanography, Vol.36, Is.3, P.: 424-432.

Kroon D, Ganssen G., 1988. Northern Indian Ocean upwelling cells and the stable isotope composition of living planktic Foraminifera. In: Brummer GJA, Kroon D (eds) Planktonic foraminifers as tracers of ocean-climate history. Free University Press, Amsterdam, pp 219–238.

Krumbein W.C., 1938. Size frequency distributions of sediments and the normal phi curve. J. Sediment. Petrol. 8, 84–90.

Kucera, M., Rosell-Melé, A., Schneider, R., Waelbroeck, C., Weinelt, M., 2005. Multiproxy approach for the reconstruction of the glacial ocean surface (MARGO). Quaternary Science Reviews, Volume 24 (7-9), 813-819.

Kucera, M., Weinelt, M., Kiefer, T., Pflaumann, U., Hayes, A., Weinelt, M., Chen, M.-T., Mix, A.C., Barrows, T., Cortijo, E., Duprat, J., Juggins, S., and Waelbroeck, C., 2004. Compilation of planktic foraminifera census data, modern from the Atlantic Ocean. Pangaea, doi:10.1594/PANGAEA.227322.

Kuhlmann J., Asioli A., Trincardi F., Klügel A., Huhn K., 2015. Sedimentary response to Milankovitch-type climatic oscillations and formation of sediment undulations: Evidence from a shallow-shelf setting at Gela Basin on the Sicilian continental margin. Quaternary Science Reviews 108:76-94.

Lambeck K., Rouby H., Purcell A., Sun Y., Sambridge M., 2014. Sea level and global ice volumes from the Last Glacial Maximum to the Holocene. Proceedings of the National Academy of Sciences of the United States of America. 111. 10.1073/pnas.1411762111.

Lascaratos, A., 1993. Estimation of deep and intermediate water mass formation rates in the Mediterranean Sea. Deep Sea Res. II. 40, 1327-1332.

Leckie M.R. 1987, Paleoecology of Mid-Cretaceous Planktonic foraminifera: A Comparison of Open Ocean and Epicontinental Sea Assemblages. Micropaleontology 33, 164-176.

Linke P. and Lutze G.F., 1993. Microhabitats preferences of benthic foraminifera — a static concept or a dynamic adaptation to optimise food acquisition? In: Langer, M.R. (Ed.), Foraminiferal Microhabitats: Marine Micropaleontology, 20, pp. 215–234.

Lirer, F., Sprovieri, M., Ferraro, L., Vallefuoco, M., Capotondi, L., Cascella, A., Petrosino, P., Insinga, D., Pelosi, N., Tamburrino, S., Lubritto, C., 2013. Integrated stratigraphy for the Late Quaternary in the eastern Tyrrhenian Sea. Quat. Int. 292, 71–85.

Lirer, F., Sprovieri, M., Vallefuoco, M., Ferraro, L., Pelosi, N., Giordano, L., Capotondi, L., 2014. Planktonic foraminifera as bio-indicators for monitoring the climatic changes occurred during the last 2000 years in the SE Tyrrhenian Sea. Integrative Zool. J. 9, 542–554

Locarnini R. A., Mishonov A. V., Antonov J. I., Boyer T. P., and Garcia, H. E., 2010. World Ocean Atlas 2009, Volume 1: Temperature. S. Levitus, Ed., NOAA Atlas NESDIS 68, U.S. Government Printing Office, Washington, D.C., 184 pp.

Lohmann GP, Malmgren BA., 1983. Equatorward migration of Globorotalia truncatulinoides ecophenotypes through the late Pleistocene: gradual evolution or ocean change? Paleobiology 9:414–421.

Lohmann GP., 1995. A model for variation in the chemistry of planktonic foraminifera due to secondary calcification and selective dissolution. Paleoceanography 10:445–457.

Lombard F, Erez J, Michel E, Labeyrie L., 2009. Temperature effect on respiration and photosynthesis of the symbiont-bearing planktonic foraminifera.

Lončarić N, Peeters FJC, Kroon D, Brummer GJA., 2006. Oxygen isotope ecology of Recent planktic Foraminifera at the central Walvis Ridge (SE Atlantic). Paleoceanography.

Lončarić N, van Iperen J, Kroon D, Brummer GJA., 2007. Seasonal export and sediment preservation of diatomaceous, foraminiferal and organic matter mass fluxes in a trophic gradient across the SE Atlantic. Prog Oceanogr 73:27–59.

Loubere P. and Fariduddin M., 1999. Benthic Foraminifera and the flux of organic carbon to the seabed. In: Modern Foraminifera. Springer, Dordrecht.

Lutze G.F. and Coulbourn W.T., 1984. Recent benthic foraminifera from the continental margin of northwest Africa: Community structure and distribution, Marine Micropaleontology, Volume 8, Issue 5, Pages 361-401.

Lutze, G.F., Thiel, H., 1989. Epibenthic foraminifera from elevated microhabitats: Cibicidoides wuellerstorfi and Planulina ariminensis. Journal of Foraminiferal Research 19, 153–158.

Malanotte-Rizzoli P., 2001. In Encyclopedia of Ocean Sciences; Steele, J.; Thorpe, S.; Turekian, K. (Eds.); Academic Press: London; pp 605-612.

Malanotte-Rizzoli, P., and Hecht A., 1988. Large-scale properties of the eastern Mediterranean: a review. Oceanologica Acta, 11, 323-335.

Mallo M., Ziveri P., Mortyn P.G., Schiebel R., Grelaud M., 2017. Low planktic foraminiferal diversity and abundance observed in a spring 2013 west–east Mediterranean Sea plankton tow transect. Biogeosciences, 14, 2245–2266.

Marchant M, Hebbeln D, Giglio S, Coloma C, González HE., 2004. Seasonal and interannual variability in the flux of planktic Foraminifera in the Humboldt Current System off central Chile (30°S). Deep-Sea Res II 51:2441–2455.

Marchant M, Hebbeln D, Wefer G., 1998. Seasonal flux patterns of planktic Foraminifera in the Peru-Chile Current. Deep-Sea Res I 45:1161–1185.

Margalef, R., Herrera, J., Steyaert, M., Steyaert, J., 1966. Distribution et charactéristiques des communautés phytoplanctoniques dans le basin Tyrrhenien de la Méditerranée en function des facteurs ambiants et à la fin de la stratification estivale de l'année. Bulletin de l'Institut Royal des Sciences Naturelles de Belgique 42, 1-56.

Margaritelli G., Vallefuoco M., Di Rita F., Capotondi L., Bellucci L.G., Insinga D.D., Petrosino P., Bonomo S., Cacho I., Cascella A., Ferraro L., Florindo F., Lubritto C., Lurcock P.C., Magri D., Pelosi N., Rettori R., Lirer F., 2016. Marine response to climate changes during the last five millennia in the central Mediterranean Sea, Global and Planetary Change, Volume 142, 53-72.

Mariani, M., Prato, R., 1988. I bacini neogenici costieri del margine tirrenico: approccio sismo-stratigrafico. Mem. Soc. Geol. Ital. 41, 519–531.

Marino G., 2008. Palaeoceanography of the interglacial eastern Mediterranean Sea. PhD Thesis, ISBN 978-90-393-4762-1 NSG publication No. 2008 02 21 LPP Contributions Series No. 24.

McDermott F., Frisia S., Huang Y., Longinelli A., Spiro B., Heaton T.H.E., Hawkesworth C.J., Borsato A., Keppens E., Fairchild I.J., van der Borg K., Verheyden S., Selmo E., 1999. Holocene climate variability in Europe: evidence from d18O and textural variations in speleothems. Quaternary Science Reviews 18, 1021–1038.

Melki, T., Kallel, N., Fontugne, M., 2010. The nature of transitions from dry to wet condition during sapropel events in the Eastern Mediterranean Sea. Palaeogeography, Palaeoclimatology, Palaeoecology 291, 267–285.

Melki, T., Kallel, N., Jorissen, F.J., Guichard, F., Dennielou, B., Berné, S., Labeyrie, L., Fontugne, M., 2009. Abrupt climate change, sea surface salinity and paleoproductivity in the western Mediterranean Sea (Gulf of Lion) during the last 28 kyr. Palaeogeography, Palaeoclimatology, Palaeoecology 279, 96–113.

Milia, A. and Torrente, M. M. 1999. Tectonics and stratigraphic architecture of a peri-Tyrrhenian halfgraben (Bay of Naples, Italy). Tectonophysics, 315, 297–314.

Milia, A., 1996. Evoluzione tettono-stratigrafica di un bacino peritirrenico: il Golfo di Napoli. PhD thesis, University of Naples Federico II,Q 184 pp.

Milia, A., 1999a. Aggrading and prograding infill of a peri-Tyrrhenian basin (Naples Bay,Italy). Geo Mar. Lett. 19, 73–88.

Milia, A., 1999b. The geomorphology of Naples Bay continental shelf (Italy). Geogr. Fis. Din. Quat. 22, 73–88.

Milia, A., 2010. The stratigraphic signature of volcanism off Campi Flegrei (Bay of Naples, Italy). Geological Society of America Special Papers, 464, 155–170.

Milia, A., Mirabile, L., Torrente, M.M., Dvorak, J.J., 1998. Volcanism offshore of Vesuvius volcano in Naples Bay. Bull. Volcanol. 59, 404– 413.

Milia, A., Torrente, M. M., & Bellucci, F. (2012). A possible link between faulting, cryptodomes and lateral collapses at Vesuvius volcano (Italy). Global and Planetary Change, 90–91, 121–134.

Milia, A., Torrente, M.M., 2000. Fold uplift and syn-kinematic stratal architectures in a region of active transtensional tectonics and volcanism, Easter Tyrrhenian Sea. Geol. Soc. Amer. Bull. 112, 1531– 1542.

Milia, A., Torrente, M.M., 2003. Late-Quaternary volcanism and transtensional tectonics at the Campania continental margin, Bay of Naples, Italy. Min. Pet. 79, 33– 47.

Milia, A., Torrente, M.M., Zuppetta, A., 2003b. Offshore debris avalanches at Somma–Vesuvius volcano (Italy): implications for hazard evaluation. J. Geol. Soc. (Lond.) 160, 309–317.

Miller K. G. and Lohmann G. P. 1982. Environmental distribution of Recent benthic foraminifera on the northeast United States continental slope. GSA Bulletin ; 93 (3): 200–206.

Milliman, J. D., 1992. Sea-level rise response to climatic change and tectonics in the Mediterranean Sea. In L. Jeftic, J. D. Milliman, & G. Sestini. Climate change in the Mediterranean pp. 45–56. (London).

Millot C., 1987. Circulation in the Western Mediterranean Sea. Oceanologica Acta, 10: 143-149.

Millot C., 1999. Circulation in the Western Mediterranean Sea. J. Mar. Syst., 20: 423-442.

Mojtahid M, Jorissen F, Lansard B, Fontanier C, Bombled B, Rabouille C., 2009. Spatial distribution of live benthic foraminifera in the Rhoˆne prodelta: faunal response to a continental-marine organic matter gradient. Mar Micropaleontol 70:177–200.

Mojtahid, M., Jorissen, F. et al. 2013. High-resolution Holocene record in the southeastern Bay of Biscay: Global versus regional climate signals. Palaeogeography, Palaeoclimatology, Palaeoecology, 377, 28–44.

Moncharmont-Zei, M., Russo, B., Sgarrella, F., Bonaduce, G., Mascellaro, P., 1984. Paleoclimatic record from 4 cores (Gulf of Taranto, Ionian Sea). Evidence from Foraminifera and Ostracoda. Bollettino della Società Paleontologica Italiana 23 (1), 21-51.

Morigi C., 2001. Benthic foraminiferal faunas in surface sediments off nw africa: relationship with organic flux to the ocean floor. Journal of Foraminiferal Research - J FORAMIN RES. 31. 350-368.

Mulitza S, Dürkoop A, Hale W, Wefer G, Niebler HS., 1997. Planktonic foraminifera as recorders of past surface-water stratification. Geology 25:335–338.

Munsell Soil Color Charts, 1994. MacBeth Division of Kollmorgen Instruments Corp, 1994 edition. New Windsor, NY.

Murray JW., 2006. Ecology and applications of benthic foraminifera. Cambridge University Press, Cambridge 426.

Naidu PD, Malmgren BA., 1996a. A high-resolution record of late Quaternary upwelling along the Oman Margin, Arabian Sea based on planktonic foraminifera. Paleoceanography 11:129–140.

Naimo, D., Adamo, P., Imperato, M., Stanzione, D., 2005. Mineralogy and geochemistry of a marine sequence, Gulf of Salerno, Italy. Quaternary International 140/141, 53–63.

Nederbragt A.J., Erlich, R.N. Fouke, B.W. Ganssen, G.M., 1998. Palaeoecology of the biserial planktonic foraminifer Heterohelix moremani (Cushman) in the late Albian to middle Turonian Circum-North Atlantic. Palaeogeography, Palaeoclimatology, Palaeoecology 144, 115-133.

Norris RD and de Vargas C., 2000. Evolution all at sea. Nature 405:23–24.

Orsi, G., Di Vito, M. A., Isaia, R., 2004. Volcanic hazard assessment at the restless Campi Flegrei caldera. Bulletin of Volcanology, 66, 514–530.

Otero, N., R. Tolosana-Delgado, A. Soler, V. Pawlowsky-Glahn, and A. Canals (2005). Relative vs. absolute statistical analysis of compositions: a comparative study of surface waters of a mediterranean river. Water Research Vol 39 (7), 1404–1414.

Ottens JJ (1992) Planktic Foraminifera as indicators of ocean environments in the northeast Atlantic. PhD Thesis, Free University, Amsterdam.

Parker FL, 1958. Eastern Mediterranean Foraminifera, sediment cores from the Mediterranean Sea and Red Sea. Rep Swed Deep-Sea Exped 1947–1948(8): 219–285.

Parker FL, 1962. Planktonic foraminiferal species in Pacific sediments. Micropaleontology 8:219–254.

Parrilla, G., Kinder, T. H. and Preller, R. H., 1986. Deep and intermediate Mediterranean water in the western Alboran Sea. Deep-Sea Research, 33, 55-88.

Passaro S., Tamburrino S., Vallefuoco M., Gherardi S., Sacchi M., Ventura G., 2016. High-resolution morpho-bathymetry of the Gulf of Naples, Eastern Tyrrhenian Sea. Journal of maps, vol. 12, no. S1, 203–210.

Pawlowsky-Glahn V., Egozcue J. J., Tolosana-Delgado R., 2007. Lecture Notes On Compositional Data Analysis.

Pawlowsky-Glahn V., Egozcue J.J. and Tolosana-Delgado R., 2011. Lecture Notes on On Compositional Data Analysis.

Pawlowsky-Glahn, V. and J. Egozcue (2006). Anisis de datos composicionales con el coda-dendrograma. In J. Sicilia-Rodr´ıguez, C. Gonzalez-Martın, M. A. Gonzalez-Sierra, and D. Alcaide (Eds.), Actas del XXIX Congreso de la Sociedad de Estad´ıstica e Investigaci´on Operativa (SEIO'06), pp. 39–40. Sociedad de Estadıstica e Investigaci´on Operativa, Tenerife (ES), CD-ROM.

Pawlowsky-Glahn, V., and Buccianti, A. (Eds.) (2011) - Compositional Data Analysis: Theory and Applications. John Wiley & Sons, Ltd., Chichester, UK, p. 378. Pérez-Folgado, M., Sierro, F. J., Flores, J. A., Grimalt, J.O., Zahn, R., 2004. Paleoclimatic variations in foraminifer assemblages from the Alboran Sea (Western Mediterranean) during the last 150 ka in ODP Site 977. Marine Geology 212, 113–131.

Peeters F, Ivanova E, Conan S, Brummer GJA, Ganssen G, Troelstra S, van Hinte J., 1999. A size analysis of planktic Foraminifera from the Arabian Sea. Mar Micropaleontol 36:31–63.
Pérez-Folgado, M., Sierro, F. J., Flores, J. A., Cacho, I., Grimalt, J. O., Zahn, R., Shackleton, N. 2003. Western Mediterranean planktonic foraminifera events and millennial climatic variability during the last 70 kyr. Marine Micropaleontology, 48, 1-2, 49-70.

Peryt D. Alegret L., Molina E. 2003, Otwornice bentosowe a granica kreda/paleogen (K/P) w profilu Ain Settara, Tunezja. Przegląd geologiczny 51, 1069-1074.

Petrizzo M.R. 2002, Paleoceanographic and palaeoclimatic interferences from Late Cretaceous planktonic foraminiferal assemblages from the Exmouth Plateau (ODP Sites 762 and 763, eastern Indian Ocean). Marine Micropaleontology 45, 117-150.

Petrosino P., Insinga D. D., Molisso F., Sacchi M., 2018. Tephra markers as a tool for the timing of the morphotectonic dynamics in the Campi Flegrei caldera. Poster INQUA–INTAV International Field Conference and Workshop Crossing New Frontiers-Tephra Huntin Transylvania 24-29 June2018 in Romania, Europe.

Pinardi, N. and Masetti, E., 2000. Variability of the large scale general circulation of the Mediterranean Sea from observations and modeling: a review. Paleogeography, Paleoclimatology, Paleoecology, 158, 153-173.

Pinardi, N., Zavatarelli, M., Adani, M., Coppini, G., Fratianni, C., Oddo, P., Simoncelli, S., Tonani, M., Lyubartsev, V., and Dobricic, S, 2015. The Mediterranean Sea large scale low frequency ocean

variability from 1987 to 2007: a retrospective analysis, Progress in Oceanography., 132, 318–332, doi:10.1016/j.pocean.2013.11.003.

Piva, A., Asioli, A., Trincardi, F., Schneider, R.R., Vigliotti, L., 2008. Late-Holocene climate variability in the Adriatic Sea (Central Mediterranean). The Holocene 18 (1), 153–167

Poulain PM. and Zambianchi E., 2007. Near surface circulation in the central Mediterranean Sea as deduced from Lagrangian drifters in the1990s. Cont. Shelf Res., 27: 981-1001.

Prell W., Martin A., Cullen J. and Trend M., 1999. The Brown University Foraminiferal Data Base. IGBP PAGES/World Data Center-A for Paleoclimatology Data Contribution Series # 1999–027. NOAA/NGDC Paleoclimatology Program, Boulder, CO, USA.

Premoli Silva I., Slitter W.V. 1995, Cretaceous planktonic foraminiferal biostratigraphy and evolutionary trends from the Bottaccione Section, Gubbio, Italy. Paleontolographia Italica 82, 1-89.

Principato M. S., Giunta S., Corselli C., Negri A., 2003. Late Pleistocene-Holocene planktonic assemblages in three box-cores from the Mediterranean Ridge area (west-southwest of Crete): palaeoecological and palaeoceanographic reconstruction of sapropel S1 interval. Palaeogeography, Palaeoclimatology, Palaeoecology 190, 61-77.

Pujol C. and Vergnaud-Grazzini C., 1995: Distribution patterns of live planktic foraminifera as related to regional hydrography and productive systems of the Mediterranean Sea. Marine. Micropaleontology 25, 187–217.

Rasmussen, T.L., Thomsen, E., Troelstra, S.R., Kuijpers, A., Prins, M.A., 2002. Millennial-scale glacial variability versus Holocene stability: changes in planktic and benthic foraminifera faunas and ocean circulation in the North Atlantic during the last 60000 years. Marine Micropaleontology 47, 143-176.

Rathburn, A. E. and Corliss, B. H., 1994. The ecology of living (stained) deep-sea benthic foraminifera from the Sulu Sea. Paleoceanography, 9, 87-150.

Ravelo AC, Fairbanks RG, Philander SGH., 1990. Reconstructing tropical Atlantic hydrography using planktontic Foraminifera and an ocean model. Paleoceanography 5:409–431.

Renaud S. and Schmidt D.N., 2003. Habitat tracking as a response of the planktic foraminifer Globorotalia truncatulinoides to environmental fluctuations during the last 140 kyr. Mar Micropaleontol 49:97–122

Retailleau S, Eynaud F, Mary Y, Abdallah V, Schiebel R, Howa H., 2012. Canyon heads and river plumes: How might they influence neritic planktonic foraminifera communities in the SE Bay of Biscay? J Foraminifer Res 42:257–269.

Retailleau S, Schiebel R, Howa H., 2011. Population dynamics of living planktic foraminifers in the hemipelagic southeastern Bay of Biscay. Mar Micropaleontol 80:89–100.

Reynolds L., Thunell R.C.., 1985. Seasonal succession of planktonic foraminifera in the subpolar North Pacific. J Foraminifer Res 15:282–301.

Richez, C. and Gascard, J. C., 1986. Mediterranean water flows when approaching the Strait of Gibraltar. Deep Sea Research, 135-137.

Rigual-Hernández AS, Sierro FJ, Bárcena MA, Flores JA, Heussner S., 2012. Seasonal and interannual changes of planktic foraminiferal fluxes in the Gulf of Lions (NW Mediterranean) and their implications for paleoceanographic studies: two 12-year sediment trap records. Deep-Sea Res I 66:26–40.

Rinaldi E., Buongiorno Nardelli B., Volpe G., Santoleri R., 2014. Chlorophyll distribution and variability in the Sicily Channel (Mediterranean Sea) as seen by remote sensing data, Continental Shelf Research, Volume 77, Pages 61-68.

Robinson A. R., Leslie W. G., Theocharis A., Lascaratos A., 2001. In Encyclopedia of Ocean Sciences; Steele, J.; Thorpe, S.; Turekian, K. (Eds.); Academic Press: London; pp 1689-1706.

Robinson A.R., Golnaraghi M., 1994. The Physical and Dynamical Oceanography of the Mediterranean Sea. In: Malanotte-Rizzoli P., Robinson A.R. (eds) Ocean Processes in Climate Dynamics: Global and Mediterranean Examples. NATO ASI Series (Series C: Mathematical and Physical Sciences), vol 419. Springer, Dordrecht.

Rogerson M., Cacho I., Jimenez-Espejo F., Reguera M.I., Sierro F. J., Martinez-Ruiz F., Frigola J., Canals M., 2008. A dynamic explanation for the origin of the western Mediterranean organic-rich layers. Geochem. Geophys. Geosyst.9, Q07U01.

Rögl, F., 1998. Palaeogeographic considerations for Mediterranean and Paratethys seaways (Oligocene to Miocene). Annalen des Natur-historischen Museums in Wien, 99A: 279-310.

Rohling E.J., Jorissen F.J., Vergnaud Grazzini C. and Zachariasse W.J., 1993. Northern Levantine and Adriatic Quaternary planktic foraminifera; Reconstruction of paleoenvironmental gradients. Mar. Micropaleontol., 21 : 191-218.

Rohling EJ, Sprovieri M, Cane T, Casford JSL, Cooke S, Bouloubassi I, Emeis KC, Schiebel R, Rogerson M, Hayes A, Jorissen FJ, Kroon D., 2004. Reconstructing past planktic foraminiferal habitats using stable isotope data: a case history for Mediterranean sapropel S5. Mar Micropaleontol 50:89–123. doi:10.1016/S0377-8398(03)00068-9.

Rohling, E. J., 2001. The dark secret of the Mediterranean - a case history in past environmental reconstruction. http://www.noc.soton.ac.uk/soes/staff/ejr/DarkMed/ref-cond.html.

Rohling, E. J., Hayes, A., De Rijk, S., Kroon, D., Zachariasse, W. J. and Eisma, D., 1998. Abrupt cold spells in the northwest Mediterranean, Paleoceanography, 13: 316-322.

Rohling, E. J., Jorissen, F. J., de Stigter, H. C., 1997. 200 year interruption of Holocene sapropel formation in the Adriatic Sea. J. Micropaleontol. 16, 97–108.

Rohling, E. J., Mayewski, P. A., Hayes, A., Abu-Zied, R. H., and Casford, J. S. L., 2002a, Holocene atmosphere-ocean interactions: records from Greenland and the Aegean Sea. Climate Dynamics, 18: 587-593.

Rohling, E.J., Abu-Zied, R., Casford, J.S.L., Hayes, A., and Hoogakker, B.A.A, 2008. The Mediterranean Sea: Present and Past. Oxford University Press.

Rossignol-Strick M., 1985. Mediterranean Quaternary sapropels, an immediate response of the African monsoon to variation of insolation, Palaeogeography, Palaeoclimatology, Palaeoecology, Volume 49, Issues 3–4, Pages 237-263, ISSN 0031-0182.

Rossignol-Strick M., 1999. The Holocene climatic optimum and pollen records of sapropel 1 in the eastern Mediterranean, 9000–6000BP, Quaternary Science Reviews, Volume 18, Issues 4–5, 1999, Pages 515-530, ISSN 0277-3791.

Sacchi, M., Infuso, S., Marsella, E., 1994. Late Pliocene–Early Pleistocene compressional tectonics in offshore Campania (eastern Tyrrhenian Sea). Boll. Geofis. Teor. Appl. 36, 141–144.

Sacchi, M., Insinga, D., Milia, A., Molisso, F., Raspini, A., Torrente, M.M., Conforti, A., 2005. Stratigraphic signature of the Vesuvius 79 AD event off the Sarno prodelta system, Naples Bay. Mar. Geol. 222–223, 443–469.

Sacchi, M., Pepe, F., Corradino, M., Insinga, D. D., Molisso, F., Lubritto, C. (2014). The Neapolitan Yellow Tuff caldera offshore the Campi Flegrei: Stratal architecture and kinematic reconstruction during the last 15ky. Marine Geology, 354, 15–33.

Santacroce, R. (Ed.), 1987. Somma–Vesuvius. Cons. Naz. Ric, Quaderni de bLa Ricerca ScientificaQ. 133 pp.

Santacroce, R., Sbrana, A. (Eds.), 2003. Geological Map of Vesuvius. Dipartimento di Scienze della Terra Universita` di Pisa. SELCA, Firenze.

Santacroce, R., Sulpizio, R., Zanchetta, G., Cioni, R., Marianelli, P., Sbrana, A., Donahue, D.J., Joron, J.L., 2008. Age and whole rocks-glass composition of proximal pyroclastics from the major explosive eruptions of Vesuvius: a review as a tool for distal tephrostratigraphy. J. Volcanol. Geotherm. Res. 177, 1–8 (this issue).

Sautter LR, Sancetta C., 1992. Seasonal associations of phytoplankton and planktic Foraminifera in an upwelling region and their contribution to the seafloor. Mar Micropaleontol 18:263–278

Sautter LR, Thunell RC., 1989. Seasonal succession of planktonic foraminifera; results from a four-year time-series sediment trap experiment in the Northeast Pacific. J Foraminifer Res 19:253–267.

Sautter LR, Thunell RC., 1991. Seasonal variability in the d18O and d13C of planktonic foraminifera from an upwelling environment: sediment trap results from the San Pedro Basin, Southern California Bight. Paleoceanography 6:307–334.

Sbaffi, L., Wezel, F. C., Curzi, G., Zoppi, U., 2004. Millennial- to centennial-scale palaeoclimatic variations during Termination I and the Holocene in the central Mediterranean Sea. Global and Planetary Change 40, 201–217.

Sbaffi, L., Wezel, F.C., Kallel, N., Paterne. M., Cacho,I., Ziveri, P., Shackleton, N., 2001. Response of the pelagic environment to palaeoclimatic changes in the central Mediterranean Sea during the Late Quaternary, Marine Geology, 178 (1–4), 39-62.

Schiebel R, Waniek J, Zeltner A, Alves M., 2002. Impact of the Azores Front on the distribution of planktic foraminifers, shelled gastropods, and coccolithophorids. Deep-Sea Res II 49:4035–4050.

Schiebel R, Zeltner A, Treppke UF, Waniek JJ, Bollmann J, Rixen T, Hemleben C., 2004. Distribution of diatoms, coccolithophores and planktic foraminifers along a trophic gradient during SW monsoon in the Arabian Sea. Mar Micropaleontol 51:345–371.

Schiebel R., 2002. Planktic foraminiferal sedimentation and the marine calcite budget. Glob Biogeochem Cycles.

Schiebel R., 2005. Modern Planktic Foraminifera. Paläontologische Zeitschrift 79(1):135-148.

Schiebel R., Bijma J., Hemleben C., 1997. Population dynamics of the planktic foraminifer Globigerina bulloides from the eastern North Atlantic. Deep-Sea Res Part Oceanogr Res Pap 44:1701–1713.

Schiebel R., Hemleben C., 2000. Interannual variability of planktic foraminiferal populations and test flux in the eastern North Atlantic Ocean (JGOFS). Deep-Sea Res II 47:1809–1852.

Schiebel R., Hiller B., Hemleben C., 1995. Impacts of storms on Recent planktic foraminiferal test production and CaCO3 flux in the North Atlantic at 47°N, 20° W (JGOFS). Mar Micropaleontol 26:115–129.

Schiebel R., Waniek J., Bork M., Hemleben C., 2001. Planktic foraminiferal production stimulated by chlorophyll redistribution and entrainment of nutrients. Deep-Sea Res I 48:721–740.

Schilman, B., Almogi-Labin, A., Bar-Matthews, M., Labeyrie, L., Paterne M. and Luz, B., 2001. Long- and short-term carbon fluctuations in the Eastern. Mediterranean during the late Holocene. Geology 29, 1099–1102.

Schlitzer, R. (2018) - Ocean Data View, http://odv.awi.de.

Schlitzer, R., Roether, W., Oster, H., Junghaus, H. G., Hausmann, M., Johannesen, J., Michelato, A., 1991. Chlorofluoro methane and oxygen in the Eastern Mediterranean. Deep Sea Research 38, 1531–1551.

Schmidt DN, Renaud S, Bollmann J, Schiebel R, Thierstein HR., 2004. Size distribution of Holocene planktic foraminifer assemblages: Biogeography, ecology and adaptation. Mar Micropaleontol 50:319–338

Schmiedl G, de Bove EF, Buscail R, Charrie´re B, Hemleben Ch, Medernach L, Picon P., 2000. Trophic control of benthic foraminiferal abundance and microhabitat in the bathyal Gulf of Lions, western Mediterranean Sea. Mar Micropaleontol 40:167–188.

Schmiedl G., Mackensen A., Miiller P.J., 1997. Recent benthic foraminifera from the eastern South Atlantic Ocean: dependence on food supply and water masses. Marine Micropaleontology 32, 239–287.

Schmuker B. and Schiebel R., 2002. Planktic foraminifers and hydrography of the eastern and northern Caribbean Sea. Mar Micropaleontol 46:387–403.

Schmuker B., 2000. Recent planktic Foraminifera in the Caribbean Sea: distribution, ecology and taphonomy. PhD Thesis, ETH Zürich

Schönfeld J. and Altenbach A.V., 2005. Late Glacial to Recent distribution pattern of deep-water Uvigerina species in the north-eastern Atlantic. Marine Micropaleontology, Volume 57, Issues 1–2, Pages 1-24.

Seears HA, Darling KF, Wade CM (2012) Ecological partitioning and diversity in tropical planktonic foraminifera. BMC Evol Biol 12:54. doi:10.1186/ 1471-2148-12-54.

Semeniuk TA, 2000. Spatial variability in epiphytic foraminifera from micro- to regional scale. J Foram Res 30:99–109.

Sen Gupta B.K., Machain-Castillo M.L., 1993. Benthic foraminifera in oxygen-poor habitats. Marine Micropaleontology 20, 183–201.

Sen Gupta BK., 2003. Modern Foraminifera. Kluwer Academic Publishers, Dordrecht.\

Sen Gupta, B.K., Smith, L.E., and Machain-Castillo, M.L. 2009b. Foraminifera of the Gulf of Mexico, p. 87-129. In Felder, D.L. and Camp, D.K. (eds.), Gulf of Mexico. Origins, Waters, and Biota Biodiversity. Texas A&M University Press, College Station, Texas.

Sgarrella F., "Interpretazione paleoclimatica di due carote profonde del Tirreno", Bollettino della Società Paleontologica Italiana, 27(01), 1988, pp. 33-55

Sgarrella F, Barra D, Improta A., 1983. The benthic foraminifers of the Gulf of Policastro (Southern Tyrrhenian Sea, Italy). Boll Soc Nat Napoli 92:77–114.

Sgarrella F. and Barra D., 1984. Distribuzione dei foraminiferi bentonici nel Golfo di Salerno (Basso Tirreno, Italia). Boll Soc Nat Napoli 93:51–110.

Sgarrella F., 1992. Revision of Brizalina aenariensis Costa, 1856 (Foraminiferida). Bollettino della Società Paleontologica Italiana 31 (3), 317-323.

Sgarrella, F. and Moncharmont Zei, M., 1993. Benthic foraminifera of the Gulf of Naples (Italy): systematic and autoecology. Bollettino della Societa`paleontologica Italiana 32, 145– 264.

Shepard F.P., 1954. Nomenclature Based on Sand-Silt-Clay Ratios. Journal of Sedimentary Petrology, 24, 151-158.

Siani G., Colin Ch., Michel E., Carel M., Richter T., Kissel C. and Dewilde F., 2010. Late Glacial to Holocene terrigenous sediment record in the Northern Patagonian margin: Paleoclimate implications. Palaeogeography, Palaeoclimatology, Palaeoecology. 297. 26-36. 10.1016/j.palaeo.2010.07.011.

Sohn Y.K.and Cough S.K., 1989. Depositional processes of the Suwolbong tuff ring, Cheju Island (Korea). Sedimentology 36, 837–855.

Sparnocchia S., Gasparini G.P., Astraldi M., Borghini M., Pistek P., 1999. Dynamics and mixing of the Eastern Mediterranean outflow in the Tyrrhenian Basin. J. Mar. Syst. 20, 301–317.

Spero HJ, Bijma J, Lea DW, Bemis BE., 1997. Effect of seawater carbonate concentration on foraminiferal carbon and oxygen isotopes. Nature 390:497–500.

Spero HJ, DeNiro MJ, 1987. The influence of symbiont photosynthesis on the d18O and d13C values of planktonic foraminiferal shell calcite. Symbiosis 4:213–228.

Spero HJ, Lea DW.,1993. Intraspecific stable isotope variability in the planktic Foraminifera Globigerinoides sacculifer: results from laboratory experiments. Mar Micropaleontol 22:221–234.

Spero HJ, Parker SL., 1985. Photosynthesis in the symbiotic planktonic foraminifer Orbulina universa, and its potential contribution to oceanic primary productivity. J Foraminifer Res 15:273–281.

Spindler M, Dieckmann G.S., 1986. Distribution and abundance of the planktic foraminifer Neogloboquadrina pachyderma in sea ice of the Weddell Sea (Antarctica). Polar Biol 5:185–191.

Sprovieri R., Di Stefano E., Incarbona A., Gargano M. E., 2003. A high-resolution of the last deglaciation in the Sicily Channel based on foraminiferal and calcareous nannofossil quantitative distribution. Palaeogeography, Palaeoclimatology, Palaeoecology 202, 119-142.

Sprovieri M., Di Stefano E., Incarbona A., Salvagio Manta D., Pelosi N., Ribera d'Alcalà M., Sprovieri R., 2012. Centennial- to millennial-scale climate oscillations in the Central-Eastern Mediterranean Sea between 20,000 and 70,000 years ago: evidence from a high-resolution geochemical and micropaleontological record, Quaternary Science Reviews, Vol. 46, P. 126-135.

Sprovieri R., Sprovieri M., Caruso A., Pelosi N., Bonomo S., Ferraro L., 2006. Astronomic forcing on the planktonic foraminifera assemblage in the Piacenzian Punta Piccola section (southern Italy). Paleoceanography. 21 PA4204.

Stanford J.D., Rohling E.J., Bacon S., Holliday N.P., 2011. A review of the deep and surface currents around Eirik Drift, south of Greenland: Comparison of the past with the present, Global and Planetary Change, Volume 79, Issues 3–4, Pages 244-254.

Stefanelli S., 2004, Cyclic changes in oxygenation based on foraminifera microhabitats: Early-Middle Pleistocene, Lucania Basin (southern Italy): Journal of Micropaleontology, 23, 81–95.

Steig Eric J., 1999. Mid-Holocene Climate Change. sci. 286. 1485-1487.

Steinhardt J, de Nooijer LLJ, Brummer G-J, Reichart G-J., 2015. Profiling planktonic foraminiferal crust formation. Geochem Geophys Geosystems.

Storz D, Schulz H, Waniek JJ, Schulz-Bull DE, Kučera M., 2009. Seasonal and interannual variability of the planktic foraminiferal flux in the vicinity of the Azores Current. Deep-Sea Res I 56:107–124.

Stuiver M. and Reime, P. J., 1993. Extended 14C data base and revised CALIB 3.0 14C Age calibration program. Radiocarbon 35(1), 215-230.

Tang, C. M. and Stott, L. D., 1993. Seasonal salinity changes during Mediterranean sapropel deposition 9000 years BP.: evidence from isotopic analyses of individual planktonic foraminifera. Paleoceanography, 8, 473-493.

Terrasi F., Rogalla D., De Cesare N., D'Onofrio A., Lubritto C., Marzaioli F., Passariello I., Rubino M., Sabbarese C., Casa G., Palmieri A., Gialanella L., Imbriani G., Roca V., Romano M., Sundquist M., Loger R., 2007. A new AMS facility in Caserta/Italy. AMS 10 Conferences, Radiocarbon.

Thiede J., 1975. Distribution of Foraminifera in surface waters of a coastal upwelling area. Nature 253:712–714.

Thunell RC, Reynolds LA., 1984. Sedimentation of planktonic foraminifera: seasonal changes in species flux in the Panama Basin. Micropaleontology 30:243–262.

Thunell, R. C and Williams, D. F., 1983. Paleotemperature and paleosalinity history of the eastern Mediterranean during the Late Quaternary. Palaeogeogr., Palaeoclimatol., Palaeoecol., 44, 23-39.

Thunell, R. C., 1978. Distribution of recent planktonic foraminifera in surface sediments of the Mediterranean Sea. Mar Micropaleontol., 3: 147-173.

Tolderlund, D. S. and Bé, A. W. H., 1971. Seasonal distribution of planktonic foraminifera in the western North Atlantic. Micropalaeontology, 17, 297-329.

Tsimplis, M. N., Zervakis, V., Josey, S., Peeneva, E., Struglia, M. V., Stanev, E., Lionello, P., Malanotte-Rizzoli, P., Artale, V., Theocharis, A., Tragou, E. and Oguz, T., 2006. Changes in the oceanography of the Mediterranean Sea and their link to climate variability. In: P. Lionello, P. Malanotte-Rizzoli & R. Boscolo (Eds), Mediterranean Climate Variability, Amsterdam, Elsevier, pp. 227-282.

Turley C. M., Bianchi M., Christaki U., Conan P., Harris JRW., Psarra S., Ruddy G., Stutt ED.,

Tselepides A., Van Wambeke F., 2000. Relationship between primary producers and bacteria in an oligotrophic sea - The Mediterranean and biogeochemical implications. Marine Ecology Progress Series 193:11-18.

Ufkes E, Jansen JHF, Brummer GJA., 1998. Living planktonic foraminifera in the eastern South Atlantic during spring: Indicators of water masses, upwelling and the Congo (Zaire) River plume. Mar Micropaleontol 33:27–53.

Ufkes E, Zachariasse WJ., 1993. Origin of coiling differences in living neogloboquadrinids in the Walvis Bay region, off Namibia, southwest Africa. Micropaleontology 39:283–287.
Use R!, DOI 10.1007/978-3-642-36809-7 2, Springer-Verlag Berlin Heidelberg.

Vallefuoco M., 2008. "Planktonic foraminiferal events and climatic variability in sediment of Southern Tyrrhenian Sea during the last 80 Kyr". PhD thesis.

Van der Zwaan G.J., 1982. Paleoecology of Late Miocene foraminifera. Utrecht Micropalentological Bulletin, Vol. 25, 202 pp.

van den Boogaart K.G. and Tolosana-Delgado R., 2013. Analyzing Compositional Data with R.

Van Der Zwaan G.J. 1999, Benthic foraminifers: proxies or problems? A review of paleocological concepts. Earth-Science Reviews 46, 213-236.

Van der Zwaan, G., Jorissen, F., 1991. Biofacial patterns inriver-induced shelf anoxia. In: Tyson, R.V., Pearson, T.H (Eds.), Modern and Ancient Continental Shelf Anoxia. Geological Society Special Publication.

Van Leeuwen RJW., 1989. Sea-floor distribution and late quaternary faunal patterns of planktonic and benthic foraminifers in the Angola Basin. Utrecht Micropal, Bull 38, pp 288.

Van Morkhoven, F. P. C. M., Berggren, W. A., And Edwards, A. S., 1986. Cenozoic cosmopolitan deep-water benthic foraminifera. Bulletin Centre Research Exploration et Production, Elf-Aquitaine, Memoire 11, 421 pp.

Verardo D. J, Froelich I. N., Mcintyre A., Deep-Sea Res., Part A, 1990, 37, 157–165.

Vergnaud-Grazzini, C., Borsetti, A. M., Cati, F., Colantoni, P., Siesser, W. G., Saliege, J. F., Sartori, R., Tampieri, R., 1988. Paleoceanographic record of the last deglaciation in the Strait of Sicily. Mar. Micropaleontol. 13, 1– 21.

Vergnaud-Grazzini, C., Glaçon, G., Pierre, C., Pujol, C. and Urrutiaguer, M. J., 1986. Foraminiferes planctoniques de Méditerranée en fin d'été. Relations avec les structures hydrologiques. Mem. Soc. Geol. Ital., 36, 175-188.

Vezzoli, L. (Ed.)., 1988. The island of Ischia. CNR Quaderni de "La Ricerca Scientifica" 114(10), 1–122.

Vincent E and Berger WH., 1981. Planktonic foraminifera and their use in paleoceanography. Ocean Lithosphere Sea 7:1025–1119.

Violanti, D., Parisi, E., Erba, E., 1987. Fluttuazioni climatiche durante il Quaternario nel Mar Tirreno, Mediterraneo Occidentale (Carota PC-19 BAN 80). Riv. Ital. Paleontol. Stratigr. 92, 515–570.

Volkmann R., 2000a. Planktic foraminifer ecology and stable isotope geochemistry in the Arctic Ocean: implications from water column and sediment surface studies for quantitative reconstructions of oceanic parameters. Reports on Polar Research. PhD Thesis, AWI Bremerhaven

Volkmann R., 2000b. Planktic foraminifers in the outer Laptev Sea and the Fram Strait-modern distribution and ecology. J Foraminifer Res 30:157–176.

Wang L., 2000. Isotopic signals in two morphotypes of Globigerinoides ruber (white) from the South China Sea: Implications for monsoon climate change during the last glacial cycle. Palaeogeogr Palaeoclimatol Palaeoecol 161:381–394.

Wang M., Albanese S., Lima A., Cannatelli C, Cosenza A., Lu W., Sacchi M., Doherty A., De Vivo B., 2015. Compositional analysis and pollution impact assessment: A case study in the Gulfs of Naples and Salerno. Estuarine, Coastal and Shelf Science 160, 22-32.

Wanner H., Solomina O., Grosjean M., Ritz S. P., and Jetel M., 2011. Structure and origin of Holocene cold events, Quaternary Sci. Rev., 30, 3109–3123.

Weaver, A. J., O. A. Saenko, P. U. Clark, and J. X. Mitrovica (2003), Meltwater pulse 1° from Antarctica as a trigger of the Bølling-Allerød warm interval, Science, 299, 1709 –1713.

Wenger, W. F. 1987: Die Foraminiferen des Miozäns der bayerischen Molasse und ihre stratigraphische sowie paläogeographische Auswertung. – Zitteliana, 16, 173–340, München.

Wentworth C.K., 1922. A scale of grade and class terms for clastic sediments. J. Geol. 30 (5), 377–392.

Weyl PK., 1978. Micropaleontology and ocean surface climate. Science 202:475–481.

Wilkin R.T., Barnes H.L., Brantley S.L. 1996, The size distribution of framboidal pyrite in modern sediments: an indicator of redox conditions. Geochim. Cosmochim. Acta, 60, 3897–3912.

Wüst, G., 1961. On the vertical circulation of the Mediterranean Sea. J. Geophys. Res., 66, 3261-3271.